# BIOLOGICALLY ACTIVE ASSEMBLIES THAT ATTENUATE THROMBOSIS ON BLOOD-CONTACTING SURFACES

A Dissertation
Presented to
The Academic Faculty

by

Zheng Qu

In Partial Fulfillment
of the Requirements for the Degree
Doctor of Philosophy in Bioengineering

Georgia Institute of Technology
December 2012

**BIOLOGICALLY ACTIVE ASSEMBLIES THAT ATTENUATE THROMBOSIS**

**ON BLOOD-CONTACTING SURFACES**

Approved by:


Dr. Elliot L. Chaikof, Advisor
The Wallace H. Coulter Department of
Biomedical Engineering
*Georgia Institute of Technology*
Department of Surgery
*Beth Israel Deaconess Medical Center*

Dr. Larry V. McIntire
The Wallace H. Coulter Department of
Biomedical Engineering
*Georgia Institute of Technology*

Dr. Julia E. Babensee
The Wallace H.Coulter Department of
Biomedical Engineering
*Georgia Institute of Technology*

Dr. W. Robert Taylor
Division of Cardiology
*Emory University School of Medicine*

Dr. Stephen R. Hanson
Department of Biomedical Engineering
*Oregon Health and Science University*


Date Approved: November 2, 2012

Dedicated to my parents,

for their unconditional love.

## ACKNOWLEDGEMENTS

The progress and advances made in this research were enabled by contributions from many colleagues and peers, as well as support from family and friends. It is these relationships that were forged during the course of my career that I cherish the most.

First and foremost, I want to express my sincerest gratitude for Dr. Elliot Chaikof, for guiding me through the many challenges of scientific research with innovative ideas and patient advice, and above all, by always keeping the "big picture" in perspective. Dr. Chaikof has taken the time to personally support every step along the way of my career as a PhD candidate despite his huge commitments to the clinic. He has fostered my growth as an independent scientist, and facilitated many of the exciting collaborations that were instrumental in shaping the development of this dissertation. It has been an honor to be mentored by a towering figure in both the field of vascular surgery and biomedical engineering. Dr. Chaikof's enthusiasm and drive to achieve tangible impact, through translating innovative science to clinically effective therapies that improve patient care, has fired me with a vision that will shape my professional growth for years to come.

I want to thank my committee members, Dr. Julia Babensee, Dr. W. Robert Taylor, Dr. Larry McIntire, and Dr. Stephen Hanson, for their multidisciplinary guidance, insight, and support. As a chemical engineer by training, I sincerely appreciate the time and assistance from leaders in the fields of material science, thrombosis, and cardiovascular biology to steer my ventures into the field of biomaterial blood-compatibility. In particular, the collaborative efforts with Dr. Hanson and his talented group of engineers and surgeons at the Oregon Primate Research Center to develop non-human primate models of thrombosis were essential in the testing and validation of the

research presented here. I want to thank Ms. Ulla Marzec, Mr. Sawan Hurst, and Dr. Monica Hinds for their creativity, patience, and rigor in the iterative development and testing of clinically relevant animal models. I wish all the best for Dr. Hanson, as well as Dr. McIntire, in their retirement! I also would like to thank Dr. Abraham Stroock and Dr. Mario Cabodi from Cornell University, who instilled in me a passion for scientific discovery by taking me on as an undergraduate research assistant to apply principles of transport phenomena from the classroom in the development of new medical therapies.

Every member of the Chaikof Lab has been involved in my dissertation in some form, and they have made my graduate school life much more enjoyable beyond the bench experience. I will fondly remember the many classes we have taken together, the group outings, and the birthday celebrations. I am forever indebted to Dr. Carolyn Haller, who has taught me nearly every assay and protocol needed to complete this work since the day I joined the lab. By drawing on her extensive background, Dr. Haller has provided me countless detailed and candid feedback which helped me gain the skills and intuition for experimental design and implementation. I would also like to acknowledge Dr. John Wilson, whose scientific rigor and enthusiasm for high impact research have forever influenced my approach towards science. It has been an honor working with Dr. Wilson in the field of pancreatic islet transplantation. Moreover, I appreciate the collaborative learning environment fostered through working with Dr. Sumanas Jordan, Dr. Murali Urlam, Dr. Sharmila Muthukrishnan, Dr. Venkat Krishnamurthy, Dr. Wookhyun Kim, Dr. Wanxing Cui, Dr. Adam Martinez, Dr. Jeff Caves, and Dr. Vivek Kumar, who contributed time, materials, and advice from drawing on their unique expertise and skills.

Since the Chaikof Lab transition to Boston, I had the fortunate opportunity to build an ongoing collaboration with Dr. David Liu's lab at the Department of Chemistry and Chemical Biology at Harvard. A major portion of this dissertation would not have been possible without reagents provided by Mr. Brent Dorr, a graduate student in Dr. Liu's lab. This collaboration will undoubtedly influence the long term approach by both the Chaikof and Liu labs to achieve their research missions. Beyond the exchange of scientific ideas and reagents, the contagious enthusiasm, optimism, and passion for new discovery from Brent and the Liu lab members were equally important in shaping the concluding years of my thesis. I want to also highlight Dr. Erbin Dai's patience and skill in operating on small animal models to validate my designs. Dr. Dai's can-do attitude, combined with his rare expertise in replicating the most complex clinical procedures in small animals, will undoubtedly be a key driver in the development of new therapies from the Chaikof Lab in the future. It has been fortunate that the list of colleagues in the Georgia Tech, Emory, Cornell, and Harvard academic and hospital communities, the Wyss Institute, and Genzyme, as well as friends from Ithaca, Atlanta, and Boston, is too long to list individually here, and I express my sincerest thanks for their time and contributions to my personal and professional growth. I am also indebted to the National Institute of Health, Georgia Tech, as well as Medtronic, for their financial aid during my research career.

Above all else, I'm forever grateful to my parents, who were always willing to lend an ear to my troubles, encourage me when everything seems hopeless, and cheer me on when I succeed. I could not have made it this far without their unconditional love and support.

## TABLE OF CONTENTS

## LIST OF TABLES

Page

## LIST OF FIGURES

Page

## LIST OF SYMBOLS AND ABBREVIATIONS

| | |
|---|---|
| 5’ SrtA | Pentamutant sortase A |
| AHA | Azidohomoalanine |
| ADH | Adipic dihydrazide |
| ADP | Adenosine diphosphate |
| Alg-CHO | Oxidized alginate aldehyde |
| aPC | Activated protein C |
| APC | Antigen presenting cells |
| CVD | Chemical vapor deposition |
| DBCO | Dibenzylcyclooctyne |
| DC | Dendritic cell |
| EPCR | Endothelial protein C receptor |
| ePTFE | Expanded poly(tetrafluoroethylene) |
| EtO | Ethylene oxide |
| FITC | Fluorescein isothiocyanate |
| FLAG | Asp-Tyr-Lys-Asp-Asp-Asp-Asp-Lys |
| GGG | Triglycine peptide |
| HDI | Hexamethylene diisocyanate |
| HSPG | Heparan sulfate proteoglycans |
| id | Inner diameter |
| IV | Intravenous |
| LPXTG | Leucine-proline-X-threonine-glycine (X = any amino acid) |

| | |
|---|---|
| PAGE | Polyacrylamide gel electrophoresis |
| PBS | Phosphate buffered saline |
| PEG | Poly(ethylene glycol) |
| PEI | Poly(ethylenimine) |
| PEM | Polyelectrolyte multilayer |
| PFP | Pentafluorophenyl |
| $PGI_2$ | Prostaglandin $I_2$ |
| PLL | Poly(L-lysine) |
| PU | Polyurethane |
| Rh-$N_3$ | Rhodamine-azide |
| SDS | Sodium dodecyl sulfate |
| SEM | Scanning electron microscopy |
| SrtA | Sortase A |
| TBS | Tris buffered saline |
| TEA | Triethylamine |
| TF | Tissue factor |
| TLR | Toll-like receptor |
| TM | Thrombomodulin |
| TPP | Triphenylphosphine |
| TxA2 | Thromboxane 2 |
| v/v | Fraction volume/volume basis |
| w/v | Fraction weight/volume basis |
| WT | Wild type |

## SUMMARY

All artificial organ systems and medical devices that operate in direct contact with blood elicit activation of coagulation and platelets, and their long-term use often necessitates antithrombotic therapies that carry significant cost and bleeding risk. Since the clinical inception of fabric grafts in 1952, none of the existing synthetic arterial substitutes perform comparably to autologous conduits in small-caliber (< 6 mm id) revascularization, a cornerstone in the fields of cardiac, vascular, and plastic surgery. Two key factors behind this status quo are the mechanical mismatch between the native vasculature and synthetic conduits, as well as acute occlusion resulting from elaboration of undesired thrombotic reactions initiated at the blood-material interface.

Although major advances in tissue engineering approaches have yielded biomaterials that mimic the bulk biomechanical properties of native tissue, many of which have been translated to clinical use, there is still no generally acceptable blood compatible material. Moreover, it is increasingly recognized that long term failure of synthetic vascular grafts is largely driven by incomplete reendothelialization decades after implantation due to a persistent foreign body response at the blood-material interface that impairs healing, which may be elicited or augmented by interfacial activation of thrombotic cascades. The combination of ongoing efforts to develop biofunctional materials that induce spontaneous endothelialization, as well as attenuation of acute thrombotic activation cascades, could ultimately improve the long term performance of these materials in blood contacting applications.

Molecular engineering of the blood-material interface to actively control the evolution of the healing response subsequent to implantation is a central paradigm in the development of new blood-compatible materials. The production of thrombin downstream of coagulation activation cascades elicited by implanted materials may be a key driver behind maladaptive host responses, due to the multifaceted activity of thrombin to crosslink fibrin, activate platelets, and induce the onset and elaboration of inflammatory responses, which, in the context of small-diameter revascularization, contributes to acute thrombotic occlusion and possibly impaired reendothelialization in the long term. Therefore, optimal attenuation of acute thrombotic activation cascades on synthetic materials could hinge on surface engineering strategies that inhibit thrombin and its production.

In this dissertation, we developed surface engineering platforms inspired by natural mechanisms contained in the endothelial lining of the circulatory system that attenuate thrombosis. Thrombomodulin (TM) is an endogenous inhibitor of thrombin production localized on the endothelial cell surface. We developed covalent chemical coupling strategies to immobilize TM on blood-contacting interfaces, and validated their capacity to inhibit platelet deposition in a clinically relevant animal model of thrombosis. Moreover, we further demonstrated a reversible chemoenzymatic approach to regenerate depleted surface activity by rapid removal and "recharging" of surfaces using a mutant transpeptidase, the *S. Aureus* sortase A, which exhibited dramatically enhanced catalytic activity.

Following a brief overview of the research in the first chapter, chapter 2 of this dissertation provides an extensive background review of current synthetic materials used

in construction of artificial blood vessels, the interplay between platelets, coagulation, and inflammation, as well as the surface engineering strategies that have been explored to date in an effort to fulfill the blood compatibility gap in the design of implantable devices and artificial organ systems. We then discuss in chapter 3 our initial efforts to develop conformal coatings through layer-by-layer assembly of polyelectrolyte multilayer films on solid supports, as a means to generate chemically reactive anchor sites for immobilizing bioactive molecules. This system provides a facile method to modify medical device materials with a conformal coating, whose properties may be engineered by selection or modification of appropriate polyelectrolyte components.

In chapter 4, we detail our first surface engineering platform to functionalize the luminal surface of commercial 4 mm i.d. ePTFE vascular grafts with azide-tagged recombinant human TM, by site-specific Staudinger Ligation reaction with immobilized triphenylphosphine anchors. This single-point immobilization approach would maximize the bioactivity of the surface enzyme assembly by minimizing undesirable modification of residues contained near the catalytically active site. Significantly, the TM modified grafts generated through this strategy reduced the level of platelet deposition in an arteriovenous (A-V) shunt model in nonhuman primates. To our knowledge, this is the first study reporting *in vivo* therapeutic function of a site-specifically immobilized anticoagulant enzyme on clinically relevant medical device surfaces since the development of end-point attachment methods for heparin.

We discuss in Chapter 5 our efforts to optimize the production of azide-tagged TM, as well as surface chemistry schemes that would enable the site-specific immobilization of TM in a manner that facilitates terminal sterilization of medical device

surfaces. Through this process we developed a general method to conjugate a single azide motif to the C-terminus of TM using the bacteria transpeptidase Sortase A. This approach facilitates expression of TM without the use of non-natural azido-tagged amino acid analogues, and is compatible with eukaryotic expression systems typically used in the biopharmaceutical industry. Moreover, we developed a surface modification strategy whereby sterically strained cyclooctyne motifs covalently immobilized on the luminal surface of 4 mm i.d. ePTFE grafts retained their capacity undergo [3+2] cycloaddition with azide-tagged TM after ethylene oxide sterilization, the current industry standard used in sterilization of synthetic vascular grafts. We demonstrated for the first time the superior efficacy of TM to reduce the level of local platelet deposition than commercial heparin modified grafts using a novel A-V shunt model in nonhuman primates, which more closely mimics the thrombotic stresses encountered during and immediately after surgical implantation.

On the basis of these results, we detail in Chapter 6 our discovery of a reversible surface engineering approach that could extend the lifetime of TM activity on surfaces, using a bioorthogonal covalent chemistry scheme that facilitates removal of activity-depleted TM and regenerating the surface with fresh bioactive TM. We hypothesized that sortase A (SrtA), a house-keeping calcium-dependent cysteine transpeptidase used to anchor cell surface proteins in *S. Aureus*, may enable the regeneration of TM activity on modified surfaces. Although these efforts were limited by the low catalytic activity of wild-type SrtA, we demonstrated that a mutant SrtA which exhibited 140-fold higher catalytic activity enabled the rapid and repeatable recharging of TM surfaces *in vitro*. Significantly, we were able to demonstrate the *in vivo* application of this approach to

modify catheters deployed in the mice. To our knowledge, these results are the first to demonstrate a covalent chemistry approach to repeatably regenerate the activity of enzyme surface assemblies by a rapid 2-step strip/recharge cycle. The capacity to recharge solid surfaces *in situ* under a range of environmental conditions would prolong the lifetime of medical device, diagnostics, and artificial organ system designs, as well as solid supported enzymes in industrial bioprocess applications.

# CHAPTER 1

# INTRODUCTION

## 1.1. Significance

All artificial organ systems and medical devices that operate in direct contact with blood elicit activation of coagulation and platelets, and their long-term use often necessitates antithrombotic therapies that carry significant cost and bleeding risk [1, 2]. Since the clinical inception of fabric grafts in 1952, none of the existing synthetic arterial substitutes perform comparably to autologous conduits in small-caliber (< 6 mm id) revascularization procedures central to the field of cardiac, vascular, and plastic surgery [3]. Poor clinical outcomes are driven by blood-material and tissue-material interactions that include rapid thrombotic occlusion, restenosis due to biomechanical mismatch, as well as impaired reendothelialization due to a persistent foreign body response to synthetic materials many years after implantation [4]. Despite advances in tissue engineering approaches that have yielded biomaterials that mimic the bulk properties of native tissue and promote healing [5-7], a generally accepted blood compatible material does not exist [8].

In this dissertation, we developed site-specific approaches to covalently attach thrombomodulin (TM), a major endogenous inhibitor of blood coagulation localized on the endothelial cell surface, on the luminal surface of commercial vascular grafts using bioorthogonal chemistry that was compatible with ethylene oxide sterilization. Notably, we demonstrated the superior efficacy of TM to reduce platelet deposition compared with commercial heparin modified grafts using a non-human primate model of acute graft

thrombosis. Finally, we optimized a novel reversible chemistry to rapidly and repeatedly regenerate immobilized TM, with the potential to significantly extend the lifetime of biologically active films. Significantly, the modular nature and broad applicability of the approaches described herein could provide a general strategy to engineer biological active synthetic materials, which optimize the evolution of host responses at the blood-material and tissue-material interfaces to promote healing and regeneration.

### 1.2. Rationale

Physiological onset of thrombosis hinges on the generation of thrombin, a central mediator that amplifies the intrinsic coagulation cascade, crosslinks fibrin, and activates platelets [9, 10]. Surface engineering approaches that mimic the natural mechanism of endothelial cells to attenuate thrombin production such as heparin and thrombomodulin have yielded promising results [8, 11, 12]. First demonstrated in 1963 [13], heparin immobilization has been hypothesized to mimic the antithrombin activity of cell surface heparan sulfate proteglycans (HSPG) expressed by the endothelium [14]. The physiological role of heparin, produced primarily by mast cells, in hemostasis remains unclear [15] as the majority of anticoagulantly active HSPG is not in direct contact with flowing blood [16] and knock-out mice lacking the specific pentasaccharide sequence that inhibits thrombin do not exhibit a procoagulant phenotype [17]. In contrast, thrombomodulin (TM) is a major vasculoprotective molecule localized on the endothelial cell surface, and overwhelming evidence indicates that defects therein increase the risk of inflammatory disorders and thromboembolism [18]. TM sequesters thrombin's prothrombotic activity and accelerates thrombin's ability to activate protein C (APC) by 1000-fold, which inhibits upstream proteases necessary for amplifying thrombin

production and represents the primary physiological mechanism by the endothelium to regulate hemostasis [19]. Therefore, the reconstitution of TM activity on blood-contacting surfaces would mimic endogenous mechanisms contained in the endothelial surface to actively attenuate thrombin production, and consequently reduce the acute thrombotic activation cascades.

### 1.3. Central Hypothesis and Specific Aims

Our overall objective is to develop a new generation of clinically durable synthetic materials that actively and sustainably attenuate thrombus formation elicited at the blood-contacting interface. The central hypothesis of this research is that the assembly of biologically active thrombomodulin at the blood-contacting interface to attenuate thrombin production will abrogate thrombotic activation cascades. Our overall approach to test this hypothesis is to optimize bioorthogonal chemistry and protein engineering approaches to develop a surface engineering platform that maximizes the bioactivity of immobilized TM, facilitates sterilization for off-the-shelf availability, and sustains TM activity over clinically relevant time scales. The specific aims of this work were: (i) generate a biologically active TM surface assembly by covalent site-specific immobilization, (ii) enable clinical translation by optimizing the scalability of TM production, maximizing the functional capacity of TM films to inhibit thrombosis, and validating a surface coupling chemistry that is compatible with industrial sterilization processes, (iii) demonstrate the capacity to repeatably regenerate surfaces with fresh TM in an effort to sustain the bioactivity of permanently implanted materials.

The outcomes of this research are expected to define general surface engineering strategies to control the evolution of the biological response at host-material interfaces, a

key paradigm in the future design of clinically durable implantable devices, artificial organs, and extracorporeal metabolic support systems.

# CHAPTER 2

# BACKGROUND

In this Chapter, we provide an extensive background review of current synthetic materials used in construction of artificial blood vessels, the interplay between platelets, coagulation, and inflammation, as well as the surface engineering strategies that have been explored to date in an effort to bridge the blood compatibility gap in the design of implantable devices and artificial organ systems.

## 2.1. Current Synthetic Arterial Substitutes

Progressive arterial occlusion by atherosclerosis is the leading cause of mortality and morbidity in the United States [20]. Despite advances in minimally invasive techniques, the traditional practice of surgical bypass or reconstruction of diseased vessels has endured as the standard of care in a number of clinical settings [3, 21]. Lack of suitable autologous conduits, as well as associated risks involved with graft harvest were significant drivers behind development of an artificial vascular prosthesis. Synthetic conduits in modern arterial reconstructive surgery were introduced by Voorhees and colleagues in 1952 with the development of a vascular graft woven from Vinyon-N™ fibers, a polyamide related to nylon-6,6 [22]. Despite successful early clinical outcomes, prostheses formulated from Vinyon-N™ lacked long-term durability. Within five years, graft dilation and aneurysmal degeneration was frequent with an 80% loss in tensile strength [23, 24]. A variety of candidate materials for synthetic arterial conduits were examined throughout the 1950s, including solid rigid metals, glass, and silk. Their failure led to the supposition that porosity and resistance to thrombosis were

critical features for an arterial substitute. Innovations in polymer science and engineering in the period surrounding World War II led to the synthesis of poly(tetrafluoroethylene) (PTFE, GoreTex™) in 1938 and poly(ethylene terephthalate) (PET, Dacron™) in 1941. Both polymers, when engineered as fibers or as a non-woven fabric, proved to be more durable and biocompatible than nylon and have remained commercial standards in modern vascular surgery.

The performance of these materials, while adequate in large diameter formats, is unacceptable for small-diameter (< 6mm) applications such as coronary and peripheral arterial reconstruction or bypass, due in part to activation of the coagulation cascade and platelets on the graft surface whose deleterious impact on graft patency is accentuated in small-diameter configurations [25, 26]. Prospective randomized clinical studies have confirmed that Dacron and expanded PTFE (ePTFE) grafts differ little in their long-term performance characteristics when used in the infrainguinal position [27]. The inherent thrombogenicity of available polymeric materials and the presence of a chronic injury site at the anastomosis due, in part, to a compliance mismatch between the prosthesis and host artery, are contributing features for late graft occlusion. These failure modes manifest whether a synthetic conduit is used for lower extremity revascularization or for arteriovenous hemodialysis access, even when the prosthesis has an inner diameter of 6 mm or larger. Despite significant effort by industrial and academic research groups over the past half-century, a durable, synthetic small diameter vascular graft does not exist.

### 2.1.1. Dacron Prosthesis

Dacron™ is the DuPont trademark for poly(ethylene terephthalate), a highly durable polyester thermoplastic polymer that can be processed into synthetic fibers.

DeBakey introduced the first knitted Dacron prosthesis in 1957, which was used extensively in arterial reconstruction of the thoracic and abdominal aorta, as well as proximal peripheral vessels [28]. This pioneering work, combined with developmental and clinical studies by Szylagyi, Wesolowski, Sauvage, and Cooley contributed to the popularization of Dacron grafts in the early era of artificial blood vessels.

Historically, weaving and knitting have been the two common techniques to fabricate Dacron fibers into a tubular conduit. The knit structure involves looping fibers in an interlocking chain, which yields a soft and stretchable fabric. In contrast, a woven structure assembles the yarn in an over-and-under pattern in the lengthwise and circumferential directions. Woven grafts are stronger and less porous than knitted grafts, but are less compliant and may fray when cut. Typically, highly porous knitted Dacron grafts required "preclotting," a process which involved exposing the graft to an aliquot of the patient's blood prior to heparinization. Currently, most commercial knitted grafts are impregnated with gelatin [29], collagen [30], or albumin [31]. Despite some evidence that coated grafts may induce a greater inflammatory response compared to preclotted grafts [32, 33], both display similar patency rates [34, 35].

Characteristically, knitted grafts incorporate a velour finish, which orients the loops of yarn upward, perpendicular to the fabric surface, thereby increasing available surface area and enhancing the anchorage of fibrin and cells to promote tissue integration. The preference for a velour finish has been primarily motivated by improved handling characteristics with little data demonstrating that internal, external, or double velour grafts exhibit greater patency rates [36]. Dacron grafts are often crimped longitudinally

to increase flexibility, elasticity, and kink resistance. However, these properties are lost soon after implantation, as a consequence of tissue in-growth.

Recently, several modifications of Dacron grafts have been approved for clinical use. To reduce surface thrombogenicity, grafts coated with bioactive heparin or passivated with fluoropolymers have been developed [37]. A silver coated Dacron graft has also been introduced to decrease the occurrence of graft infection. Long-term follow-up studies will be required to determine if these modifications improve outcomes. Early versions of knitted grafts were susceptible to dilatation over time with a 10% to 20% increase in graft size immediately following implantation [38], followed by slow expansion [39]. Nonetheless, correlation of graft dilation and structural failure has not been established [40]. All told, the structural integrity of Dacron grafts has been reported to be extremely durable. In 1997, the FDA disclosed a total of 68 cases of structural failure occurring at an average of 7.4 years after implantation [41]. A recent single center review noted a 0.2% structural failure rate at a mean follow-up of 12 years [42].

### 2.1.2. ePTFE Prosthesis

Poly(tetrafluoroethylene), or PTFE, is a fluoropolymer that was trademarked as Teflon™ by Dupont in the late 1930's. It is chemically inert, hydrophobic, and mechanically durable. PTFE was initially used as a fiber in textile based grafts, but today is predominantly processed into expanded PTFE (ePTFE) tubes by extruding the polymer resin through a die. ePTFE grafts were first implanted in animals in 1972 [43], and Campbell and colleagues reported their first clinical use in 1976 [44].

Macroscopically, the ePTFE surface is smoother than Dacron, and the grafts are soft and pliable. On a microscopic scale, the extrusion process results in a porous morphology consisting of solid islands or nodes linked by fibrils. This node-fibril structure occupies about 20% of the total volume of the expanded polymer, and results in a higher ratio of pores to material than in Dacron grafts. However, the void space in ePTFE grafts is considerably smaller than voids in woven or knitted materials. Further, the inherent hydrophobic nature of the fluoropolymer establishes a natural barrier to water that prevents permeation of blood. Despite the chemical inertness of ePTFE, plasma proteins and platelets adhere to the surface and the host response is similar to Dacron [45].

In standard ePTFE grafts, the fibril length measures about 30 μm, though there have been experimental variants with a larger fibril length of 60 μm, which in animal models facilitated luminal endothelialization [46]. However, these observations have not been replicated in clinical studies. Thin walled ePTFE has a wall thickness of 200 to 300 μm, compared to a standard wall thickness of 400 to 600 μm. This increases the compliance of the graft and improves handling, but with some loss of suture retention strength and an inability to use the prosthesis for repeated dialysis access. Clinical performance of thin and standard walled ePTFE is otherwise similar [47]. Stretch ePTFE is a modification of standard ePTFE where a micro-crimping process is applied to compress the fibrils. This allows the graft to extend longitudinally as the fibrils are stretched to their full length, which provides some improvement in handling characteristics. Kink resistance of ePTFE grafts has been improved by the application of external plastic rings. A recognized limitation of ePTFE grafts is their relative stiffness,

which leads to a compliance mismatch between the prosthesis and host artery that may contribute to anastomotic intimal hyperplasia. In addition, since ePTFE does not display self-sealing characteristics, early access for hemodialysis is precluded due to bleeding at the puncture site.

Despite some evidence that suggests that platelet deposition [48-50] and complement activation [51] are lower on ePTFE than Dacron prostheses, the patency rates of Dacron and ePTFE grafts are similar [27]. Recently, heparin and carbon coated ePTFE prostheses have become commercially available, but little data exists that confirms increased patency rates compared to unmodified grafts. It has been suggested that intimal hyperplasia may be related to adverse local hemodynamic effects. This has led to the use of a vein cuff at the distal anastomosis with reports of improved three-year patency for below knee femoral-popliteal bypasses (45% vs. 19%) [52]. A recent clinical study has demonstrated that grafts, which incorporate a distal PTFE cuff have similar patency rates to those with a vein cuff [53].

### 2.1.3. Polyurethane Prosthesis

The development of a polyurethane vascular prosthesis was largely motivated by a desire to reduce compliance mismatch. Polyurethane is more elastomeric than Dacron or ePTFE, and has been used as a polymeric coating for pacemaker leads, breast implants [54], and barrier films for dermal wounds [55]. Polyurethane is a copolymer that consists of three different monomer types: a diisocyanate hard domain, a chain extender, and a diol soft domain. At physiological temperatures, the soft domains provide flexibility while the hard domains impart strength. The most common medical grade polyurethanes are based on soft domains made from polyester, polyether, or polycarbonate. By varying

the composition of the monomer repeat units, the mechanical properties of polyurethane prostheses can be tuned.

Polyester based soft domains were used in the earliest generation of polyurethane vascular grafts. Good biocompatibility was observed *in vivo*, but the hydrolytic susceptibility of the ester linkage led to chemical deterioration [56, 57]. In a small clinical study of below-knee bypass grafts, more than half occluded within one year [58]. Biodegradation is also a concern, since some degradation products may be carcinogenic. The FDA terminated the use of polyurethane foam in breast implants in 1991 due to the release of 2,4-toluene diamine, which caused liver cancer in animals [59]. However, most polyurethanes studied today incorporate a different monomeric diamine subunit.

A more hydrolytically stable polyether based polyurethane graft was later developed, but the ether linkage remains susceptible to oxidative degradation *in vivo* [57]. Vectra™ (Bard, Inc.) is the only commercially available graft based on polyetherurethane and is used solely for hemodialysis access [60]. It may be punctured within 24 hours of implantation due to self-sealing characteristics. A second polyurethane graft, known as the Aria™ graft (Thoratec, Inc.) had been subject to clinical study but is not longer being produced [61].

The latest generation of polycarbonate based polyurethanes is inert to both hydrolysis and oxidation in both *in vitro* and animal studies [62-64]. The Corvita™ graft (Corvita, Corp.), a composite polyurethane and Dacron prosthesis, did not dilate in dogs after a one year implantation period, but is no longer in development [65]. The Expedial™ graft (LeMaitre, Inc.) was a polycarbonate based polyurethane graft

impregnated with heparin. This prosthesis underwent evaluation for hemodialysis applications, but is no longer under development [66].

A summary of current commercially available vascular grafts is summarized in Table 2.1. Activation of platelets and the coagulation cascade at the blood-contacting interface of these grafts is a major cause underlying the acute thrombotic occlusion which has precluded their use in small caliber (< 6 mm i.d.) applications, and the crosstalk between thrombosis and inflammation may be a contributing factor to the characteristic maladaptive healing response that results in poor long-term outcomes in synthetic arterial substitutes. Improvements upon existing synthetic vascular grafts, as well as the development of durable small-diameter conduits, will hinge on increasing our understanding of the mechanisms behind the onset of these detrimental host reactions, as elaborated in the next section.

**Table 2.1.** Vascular grafts commercially available in the United States

| Material type | Company | Product | Description |
|---|---|---|---|
| *Standard* | | | |
| ePTFE | Angiotech / Edwards Life Sci | Lifespan | Reinforced |
| | Atrium | Advanta VXT | Softwrap technology |
| | | Advanta SST | Trilaminate, allows pulsation |
| | | Advanta VS | 60/20 µm thru-pore design |
| | | Flixene | Laminated with biomaterial film |
| | Bard | Impra CenterFlex | Unmodified |
| | Boston Scientific | Exxcel Soft Vascular Graft | Unmodified |
| | Braun | VascuGraft | Unmodified |
| | Vascutek | Maxiflo Ultrathin | Thin wall, external ePTFE wrap |
| | | Maxiflo Wrap | Regular wall, external ePTFE wrap |
| | WL Gore & Assoc. | Gore-Tex | Unmodified |
| | | Gore-Tex Stretch | Stretch |
| | | Gore Intering | Unibody, intrawall radially supported |
| Dacron | Braun | Protegraft | Knitted, double velour |
| | InterVascular | InterGard Ultrathin | Unmodified |
| | Vascutek | VP1200K | Unmodified |
| *Sealed* | | | |
| ePTFE | Vascutek | SealPTFE Ultrathin | Gelatin sealed, thin wall |
| | | SealPTFE Wrap | Gelatin sealed, regular wall |
| | | Taperflo | Gelatin sealed, tapered |
| Dacron | Atrium | Ultramax | Knitted, gelatin sealed, double velour |
| | Bard | Vasculour II | Knitted, albumin sealed |
| | Boston Scientific | Hemashield Gold Microvel | Knitted, collagen sealed, double velour |
| | | Hemashield Platinum | Woven, collagen sealed |
| | Braun | UniGraft | Woven, gelatin sealed, single/double velour |
| | InterVascular | InterGard Woven | Woven, collagen coated |
| | | InterGard Knitted | Knitted, collagen coated |
| | Vascutek | Gelseal | Knitted, gelatin sealed |
| | | Gelsoft | Knitted, gelatin sealed |
| | | Gelsoft Plus | Köper knitted, gelatin sealed |
| *Heparin modified* | | | |
| ePTFE | WL Gore & Assoc. | Propaten | Carmeda Bioactive heparin coating |
| Dacron | InterVascular | InterGard Heparin | Knitted, collagen coated |
| *Carbon modified* | | | |
| ePTFE | Bard | Impra Carboflo | Carbon coated |
| | | Distaflo | Preformed cuff at distal end |
| | | Dynaflo | Preformed cuff at distal end |
| *Silver modified* | | | |
| Dacron | Braun | SilverGraft | Antibacterial |
| | InterVascular | InterGard Silver | Antibacterial |
| *Others* | | | |
| Collagen-based | Artegraft | Artegraft | Crosslinked bovine carotid artery |

## 2.2. Interface between Thrombosis and Inflammation

Hemostasis is an exquisite orchestration of physical and biochemical forces to arrest bleeding. Trauma initiates local vasoconstriction and enhanced extravasation of blood to the surrounding tissue. The endothelium lining the luminal surface of blood vessels can be "activated" or physically denuded by injury to generate a highly prothrombotic interface. As a consequence, circulating platelets bind and activate on the injured site, while coagulation is triggered by exposed tissue factor (TF). These two systems are independent but highly complementary. Platelet phospholipid membrane is an optimal substrate to amplify the coagulation cascade, which generates thrombin that enables fibrin crosslinking to firmly bind platelet clusters culminating in hemostatic plug formation. Thrombin, in turn, is a powerful physiological activator of platelets, leading to the release of molecular mediators that promote hemostatic reactions and initiate an inflammatory response.

Tantamount to pathogen recognition, "danger" signals elicited by inflammation are obligatory for activation of antigen presenting cells (APCs) to direct the maturation of naïve precursor T and B lymphocytes. In the absence of danger cues, quiescent "semi-mature" APCs maintain peripheral tolerance to self antigens [67]. A growing body of evidence suggests that hemostasis, in this regard, tips the balance towards the onset of adaptive immunity. Thrombin's ability to activate inflammatory mediators, particularly protease activated receptors (PAR), as well as osteopontin and chemerin, has emerged as a new molecular mechanism contributing to the pathogenesis of a number of immune disorders. In collaboration, platelets express and secrete a complex set of pro-inflammatory mediators such as serotonin, platelet factor 4, P-selectin, as well as CD154

(CD40 ligand), an indispensible co-stimulatory molecule for activation of naïve lymphocytes. A number of recent observations in vivo implicate platelet derived CD154 in enhancing germinal center formation, protecting against infection, and inducing allograft rejection. This review will summarize and interpret recently accumulated evidence that substantiates a previously underappreciated role by hemostatic components as adjuvants in the initiation and development of host immune responses.

### 2.2.1. Platelets and Coagulation in the Pas de Deux of Hemostasis

Current understanding of hemostatic mechanisms is largely based on *in vitro* studies, and their functional significance *in vivo* remains a topic of ongoing investigation [10, 68]. The physiologically important soluble activators of platelets include thromboxane A2 (TxA2), adenosine diphosphate (ADP), and thrombin. Alternatively, exposed collagen at sites of vascular injury facilitates site-specific platelet adhesion and activation. Physiological initiation of the coagulation cascade occurs when sub-endothelial tissue factor (TF) binds factor VIIa, the enzymatically active form of factor VII. The VIIa/TF "tenase" complex converts factor X to Xa, which assembles with cofactor Va and $Ca^{2+}$ on the platelet phospholipid membrane to form a "prothrombinase" complex that cleaves prothrombin into active thrombin. Secondary to VIIa/TF-induced onset of coagulation, thrombin production is sustained by an alternate tenase, the complex of VIIIa and IXa, and amplified through positive feedback by thrombin's activation of VIIIa and Va, as well as XIa required for IX activation. Ultimately, thrombin cleaves fibrinogen and activates factor XIII to enable fibrin crosslinking. Activated platelets further augment hemostasis by secreting their granular cargo consisting of TxA2, ADP, thrombin, fibrinogen, as well as factor V. As a result, small

amounts of thrombin can trigger coagulation and platelet activation which rapidly intensify in magnitude to generate a hemostatic plug (Figure 2.1).

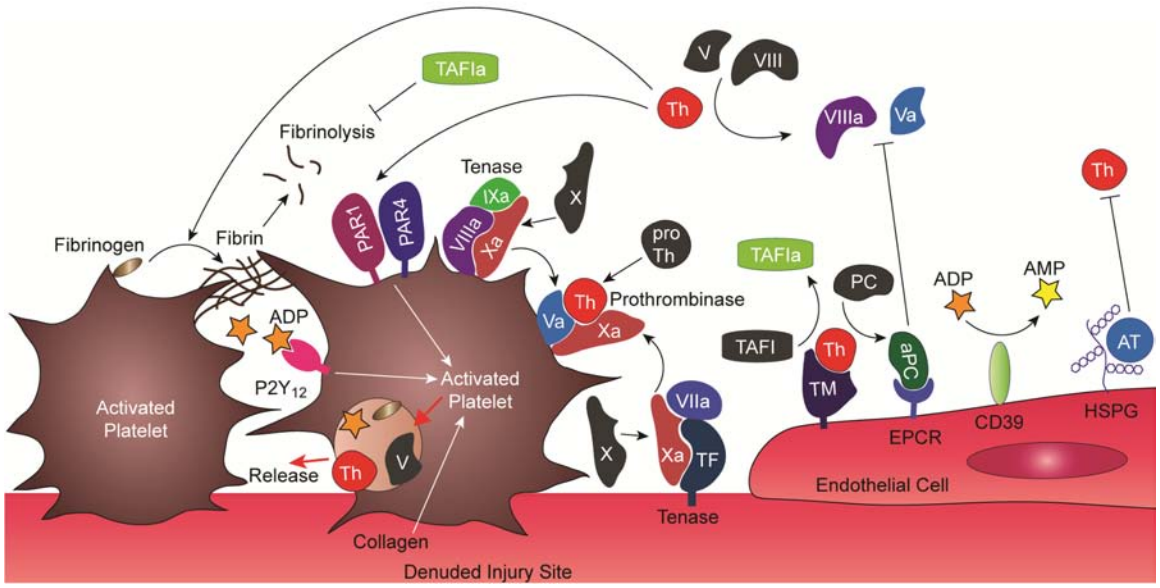


**Figure 2.1**. Physiological elaboration of coagulation and platelet activation are quarantined by quiescent endothelial cells. Generation of thrombin (Th) from the coagulation cascade facilitates fibrin crosslinking to form a hemostatic plug, and is intimately linked to activation of platelets through PAR1/PAR4 heterodimers. Self-reinforcing feedback systems amplify production of Th through its activation of factor VIII and V, as well as platelet activation which release agonists such as Th, factor V, and ADP. Endogenous regulators of coagulation in the endothelium include heparan sulfate proteoglycans (HSPG) that catalyze the inactivation of Th by antithrombin III (AT), as well as thrombomodulin (TM), a cofactor for Th that reverses its prothrombotic activity to accelerate the generation of activated protein C (aPC) which disrupts formation of tenase and prothrombinase complexes. The TM–Th complex also catalyzes formation of thrombin-activatable fibrinolysis inhibitor (TAFI) which stabilizes crosslinked fibrin. In concert, platelet activation is abrogated by endothelial regulators, such as CD39 that hydrolyze ADP to AMP. Mediators of hemostasis are increasingly associated with establishing a state of inflammation that is linked to the initiation and development of adaptive immunity. Abbreviation: TF, tissue factor.

Multiple regulatory mechanisms are present in the vascular endothelium to establish an activation threshold for hemostasis. The endothelium synthesizes prostacyclin (prostaglandin $I_2$, $PGI_2$) which limits platelet response to TxA2, nitric oxide (NO) that decreases intracellular $Ca^{2+}$ to suppress αIIbβ3 binding with fibrinogen, and expresses ecto-diphosphohydrolase (CD39) to hydrolyze ADP (reviewed in [68]). Notably, $PGI_2$ and NO are vasodilators which enhance the convective efflux of hemostatic mediators, thus limiting their participation in surface reactions. Circulating antithrombin III irreversibly inactivates thrombin in a process catalyzed by heparan sulfate proteoglycans, a constituent of the endothelium. Thrombomodulin (TM), expressed in quiescent endothelial cells, forms a 1:1 complex with thrombin, reversing its procoagulant activity to accelerate production of activated protein C (aPC) that suppresses coagulation through inactivation of cofactors Va and VIIIa to destabilize formation of tenase and prothrombinase complexes. In this role, aPC bound to endothelial protein C receptors (EPCR) appears more important than soluble aPC for factor Va inactivation. Furthermore, factor Va associated with the with prothrombinase complex on platelets is drastically more resistant to aPC inactivation than factor Va bound to the endothelium [69]. The TM-thrombin complex also catalyzes activation of thrombin-activatable fibrinolysis inhibitor (TAFI) that stabilizes crosslinked fibrin. Hence, rather than competitively inhibiting hemostasis after its onset, physiological regulatory mechanisms within the endothelium "cordon off" injury sites where hemostasis is elaborated, thereby limiting deleterious systemic thrombosis.

### 2.2.2. Protease Activated Receptors at the Nexus between Coagulation and Inflammation

Coagulation serine proteases engage cell surface PARs, an emerging signaling paradigm affecting the onset of adaptive immunity. Of the four known PARs, PAR1 can be activated by the transient VIIa/TF/Xa complex, thrombin, as well as EPCR-bound aPC (see review [69, 70]). Thrombin's potent capacity to activate platelets via PAR1 underscores the intricate ties between the cellular and plasma compartments of hemostasis (reviewed in [71]). Both plasmacytoid and myeloid DCs express PAR1, and can be stimulated by thrombin to produce monocyte chemotactic protein-1 (MCP-1), IL-10, and IL-12 [72]. Thrombin activation of PAR1 in mature DCs can also induce expression of CCL18, a potent chemoattractant for immature DCs and T lymphocytes [73]. In a xenotransplantation model, proinflammatory MCP-1 cytokine production by activated donor endothelial cells required PAR1 engagement [74]. These studies suggest that, immediately following tissue injury, the thrombin/PAR1 signaling pathway aids in homing and activation of APCs to maximize antigen presentation. In support of this view, PAR1 knockout protected mice against carbon tetrachloride induced liver fibrosis, concomitant with a reduction in T cell infiltration [75]. The VIIa/TF/Xa complex can additionally activate PAR2. DC activation and migration to the lymph nodes as well as T cell activation were dependent on the engagement of PAR2 in mice [76]. PAR2 and toll-like receptor (TLR4) have synergistic effects in NFκB induction, a possible mechanism for augmenting DC response to "danger" signals [77]. However, it does not appear that human DCs express PAR2 [73].

Activation of platelet PAR1 by thrombin and consequent activation of sphingosine kinase leads to production and release of sphingosine 1-phosphate (S1P), an essential regulator of vascular permeability as well as immune cell trafficking and

differentiation (reviewed in [78, 79]). Notably, S1P appears to shift the phenotype of effector T cells towards Th2 and Th17 while hampering Th1 type responses [78]. S1P's signaling capacity is partially transmitted through a family of five S1P receptors (S1PR) which exhibit differential constitutive and inducible tissue expression. The S1P receptor 1 (S1PR1) is abundantly expressed in endothelial cells, and both S1PR1 and S1PR3 are highly expressed in the lymphoid organs. S1PR1 signaling was recently shown to be critical in maintaining basal vascular integrity and blunting lethal responses to leak-inducing agents in mice [80]. Immature DCs preferentially express S1PR1, but upregulate S1PR3 upon maturation. Consistent with this observation, thrombin stimulation of DCs induced S1P production which activates S1PR3, leading to an autocrine amplification of coagulation and inflammation through increased tissue factor and IL-1β production [81]. Engagement of lymphocyte S1PR1 was instrumental in promoting T cell retention in peripheral tissues in response to inflammation which increase S1P levels [82]. S1PR1 also appears responsible for suppressing regulatory T cell development and function through activation of the Akt-mTOR pathway [83].

Downstream PAR1 signaling pathways from activation by thrombin and aPC, two opposing forces in the coagulation cascade, exert opposite effects on inflammation. Thrombin-PAR1 signaling increased inflammation-induced vascular leakage that is dependent on activation of S1PR3, while aPC/EPCR-PAR1 signaling and transactivation of S1PR1 produced the opposite effect in LPS challenged mice [84]. While aPC could mediate this effect *in vivo* by blocking thrombin generation, it was demonstrated that aPC's PAR signaling activity was more significant than its anticoagulant function in reducing mortality in this model [85]. In addition to the divergent downstream S1P

receptor signaling pathways of PAR1, the barrier-protective effects of aPC/EPCR also requires the trans-activation of endothelial PAR2 [86]. This is consistent with other studies that demonstrate PAR3 heterodimerization with PAR1 to allosterically modulate thrombin-mediated PAR1 activation in endothelial cells [87]. Likewise, the PAR4 heterodimerizes with PAR1 on platelets and enables their activation by thrombin [88]. It is increasingly clear that both heterodimerization of PARs and divergent S1PR engagement influence the signaling outcome of PAR1 activation.

### 2.2.3. Coagulation-activated Mediators in Inflammatory Disorders

Osteopontin (Opn), a phosphorylated glycoprotein, is traditionally tied to its physiological roles in bone and tissue remodeling. Proteolytic cleavage of Opn by thrombin exposes hidden α4β1 integrin (also known as VLA4) and CD44 binding domains to enable migration of antigen-specific T cells to sites of inflammation. Conversely, TAFI renders thrombin-cleaved Opn inactive to suppress inflammation [89]. Considerable evidence were compiled recently using several disease models which reveal Opn's role in augmenting Th1 and Th17 mediated immune responses [90]. Antigen-specific CD4+ and CD8+ memory T cells secreted Opn upon activation and steered effector T cells towards a Th1 phenotype by down-modulating their IL-4 production in murine models of chronic allergic contact dermatitis (ACD) [91]. Likewise, during the sensitization stage of ACD, autocrine Opn production was a vital component for DC migration to the skin-draining lymph nodes [92]. In experimental autoimmune encephalomyelitis (EAE), Opn was abundantly expressed in mouse DCs, which induced IL-17 and IFN-γ production by T cells in a process mediated by integrins, while diminishing IL-10 production through CD44 engagement [93]. Further, engagement of

type I interferon receptors on DCs suppressed production of Opn and inhibited IL-17 secretion [94]. In agreement with these observations, interferon β, a standard treatment for relapsing forms of multiple sclerosis (MS), decreased Opn and IL-17 production, as well as T cell migration [95]. Opn induced NF-κB activation, inhibited pro-apoptotic FOXO3A activity, and altered Bim, Bak, and Bax expression, which collectively prolonged survival of stimulated CD4+ and CD8+ T cells to exacerbate EAE relapse and progression [96]. In light of these discoveries, Opn is increasingly recognized as a central mediator of relapsing MS (reviewed in [97]).

Highlighting the growing importance of bioinformatics in the field of immunology, a proteomic analysis of human MS lesions identified tissue factor and protein C inhibitor unique to chronic acute plaques. Respective inhibition of the physiological activity of these target molecules with hirudin and aPC significantly ameliorated EAE in mice. aPC exerted these effects by suppressing IL-17 production and NF-κB signaling by activated T cells [98]. A potential route by which aPC mediated this effect is through attenuating thrombin-mediated activation of Opn. These results also raise the possibility that aPC can directly modulate the functional behavior of immune cells, though the extent of this influence remains unexplored. Indeed, it was demonstrated that on leukocytes where EPCR expression is low, the integrin CD11b/CD18 could play a bigger role in mediating aPC-PAR1 signaling [99]. Our understanding of aPC as an anti-inflammatory mediator is far from complete, and their binding partners and signaling pathways in cellular compartment of immunity should present exciting new areas of research.

Chemerin is a recently characterized chemoattractant that is increasingly studied for its role in regulating inflammation. Similar to Opn, chemerin circulates as an inactive precursor that can be activated by serine proteases involved in coagulation and fibrinolysis, the most potent of which are factor XIIa and plasmin, and to a lesser extent factor VIIa. Additionally, thrombin-stimulated platelets appear to release partially cleaved chemerin [100]. Chemerin signaling via its cognate receptor ChemR23 (CMKLR1) may be involved in the accumulation of DC in lesions from patients with psoriasis [101] as well as oral lichen planus [102]. Emerging evidence also implicate chemerin in the development of EAE [103]. Sequential cleavage of chemerin by plasmin and TAFI *in vitro* synergistically enhanced the activity of chemerin to affect plasmacytoid DC migration through ChemR23 [100]. The significance of this observation *in vivo* is unclear, as TAFI inhibits plasmin generation. Surprisingly, chemerin can reduce the production of proinflammatory mediators and macrophage activation through ChemR23 but requires additional C-terminal processing by cysteine proteases [104]. This suggests an intriguing link with the secretion of cysteine proteases by *Staphylococcus aureus* that could inhibit effective host defense to clear infections [105]. In view of these observations, chemerin exhibits incredible plasticity to transform into ligands that exert opposite effects on inflammation through the same receptor, a process that deserves further study.

### 2.2.4. Platelet Activation Strengthens Antigen Presentation

Platelet activation is increasingly implicated in a number of chronic adaptive immune diseases, including inflammatory bowel disease (IBD), atherosclerosis, infections, and transplant rejection. In a mouse model of IBD, depletion of platelets by

thrombocytopenia commensurately reduced leukocyte adhesion in the inflamed colonic venules [106]. Antibody blockade of TF function significantly blunted colonic inflammation induced by dextran sodium sulfate (DSS) in mice. Remarkably, the treatment nearly abolished both leukocyte and platelet recruitment to the venules of inflamed colons [107]. Genetic deletion of CD39 significantly exacerbated IBD in mice, and lower CD39 expression in humans was correlated with increased susceptibility to Crohn's disease [108]. Activated platelets, which express P-selectin (CD62P), appear to directly interact with DCs. Following initial contact between CD62P and PSGL-1 expressed on DCs, junctional adhesion molecule C (JAM-C) and Mac-1 mediated firm DC adherence to platelets *in vitro* [109]. JAM-C deficient mice showed decreased persistence of specific circulating IgG titers and impaired germinal center formation [110]. Elevated soluble CD62P levels, a marker for platelet activation, is associated with an increased risk for atherosclerosis in $ApoE^{-/-}$ mice [111].

Despite their considerable importance as a neurotransmitter, serotonin (5-HT) is increasingly known for its role as an inflammatory mediator. Platelets sequester 5-HT in their dense granules and release them upon activation. Human monocytes treated with 5-HT exhibited enhanced capacity to stimulate allogenic T cells *in vitro* and reduced susceptibility to Fas-FasL mediated apoptosis [112]. Exogenous 5-HT induced activation of ERK1/2 and NFκB as well as endogenous production of 5-HT in naïve T cells, contributing to their activation and proliferation [113]. Interestingly, in a murine model of noncytopathic lymphocytic choriomeningitis viral infection, platelet-derived 5-HT delayed activated virus-specific CD8+ T cell infiltration but prolonged their persistence in the liver primarily through altering the sinusoidal microcirculation [114]. Hence, 5-HT

appears to exert proinflammatory effects through physical and biochemical enhancement of T cell activation and survival.

Platelet-derived CD154 appears to be an important component in directing the process of antigen presentation so as to optimize the maturation of naïve adaptive immune precursors. A number of recent observations *in vivo* implicate platelet derived CD154 in enhancing germinal center formation, protecting against infection, and inducing allograft rejection. TLR-4 engagement on platelets induced release of soluble CD154, implicating platelet activation in immune response to infections [115]. DCs adherent to platelets were able to stimulate lymphocyte proliferation only in the presence of CD154 [109]. Platelet-derived membrane vesicles were capable of delivering CD154 to sites distant from location of activation to stimulate antigen-specific IgG production and to enhance CD4+ T cell mediated germinal center formation [116]. Platelet CD154 secretion correlated with B lymphocyte activation and IgG production [117], and augmented cytotoxic T cell response to Listeria challenge [118]. Activation of platelets was required for virus-specific cytotoxic T lymphocyte response, a process that depended on CD154 [119]. Soluble CD154 induced rejection 30 days following allogeneic cardiac transplantation in mice, while platelet infusion had no effect [120]. Thus, i*n vivo* activation of platelets from surgical trauma at the time of transplantation could serve as the sole exogenous source of CD154 to instigate allograft rejection. Both CD40-/- and CD154-/- mice were significantly protected from DSS induced colitis, concomitant with a reduction in inflammatory angiogenesis [121]. Hyperinsulinemia and hyperglycemia induced greater circulating levels of CD154+ platelets, as well as tissue factor

procoagulant activity, leading to a prothrombotic state that could be linked to the greater incidence of atherosclerosis in patients with type 2 diabetes [122, 123].

### 2.2.5. Clinical Perspectives

The link between adaptive immunity and hemostasis has long been suspected through observations by transplant surgeons associating acute allograft rejection with significant thrombosis. Despite recent progress, therapeutic targeting of the hemostatic system and its related signaling pathways to treat disorders of adaptive immunity has not been well defined. Clinical trials in the last decade have revealed benefits of anticoagulants, such as aPC (Xigris®) to treat severe sepsis. Undesirable bleeding risks associated with these formulations may be overcome by engineering newer aPC variants with impaired anticoagulant activity but intact PAR signaling capacity [69]. Alternatively, thrombomodulin exhibits thrombin-dependent, "on-demand" generation of aPC and TAFI, whose anti-inflammatory downstream pathways are only beginning to be uncovered. Our laboratory showed exogenous TM infusion enhanced long-term engraftment in an allogeneic murine model of intraportal islet transplantation, substantially suppressing the hallmark endogenous "danger" signals IL-1β and TNF-α in the liver [124]. Risks of bleeding and dosage requirement can be further reduced through recombinant TM fusion proteins with targeting moieties for TF [125], as well as techniques to site-specifically tether TM to tissue surfaces [126].

Two decades after their initial discovery, the PAR and downstream S1P signaling pathway has emerged as a new paradigm linking inflammation and a plethora of adaptive immune disorders. Phase III clinical trials showed fingolimod (Gilenia®), a synthetic S1P analogue, significantly reduced relapse rates in MS patients compared with placebo and

IFN β-1a therapy [127, 128]. Fingolimod is an agonist of four of the five S1P receptors and influences lymphocyte trafficking, though its immune-modulatory mechanisms are currently not fully characterized. In 2010, a US Food and Drug Administration advisory panel unanimously recognized the safety and effectiveness of fingolimod, and overwhelmingly recommended its approval as a first-line treatment for relapsing MS. Therapeutic intervention with a specific inhibitor of sphingosine kinase-1 has also been demonstrated to inhibit production of proinflammatory cytokines in a mouse model of sepsis [129]. These encouraging developments have demarcated the lipid metabolic and signaling pathways as a new frontier in the quest to create a unified model of inflammation onset and resolution.

In conclusion, recent research substantiates an elegant system whereby activation of coagulation and platelets in response to trauma contributes to a state of inflammation that is central to the development of an effective host defense response as well as numerous adaptive immune disorders (Figure 2.2). In this regard, the generation of thrombin by physiological activation of hemostasis on in injured tissue at the proximal anastomosis further exacerbates deleterious thrombotic reactions occurring downstream on the surface of synthetic vascular grafts, and may contribute to a prolong state of inflammatory response on the surface of synthetic vascular grafts, which do not completely re-endothelialize many years after implantation. We anticipate that the evolution of bioinformatics, as well as *in vitro* and *in vivo* models of immune dysfunction will further expand our understanding of the molecular networks through which hemostatic reactions affect the onset of adaptive immunity, as well as our repertoire of available drug targets that provide new opportunities to modulate this process.

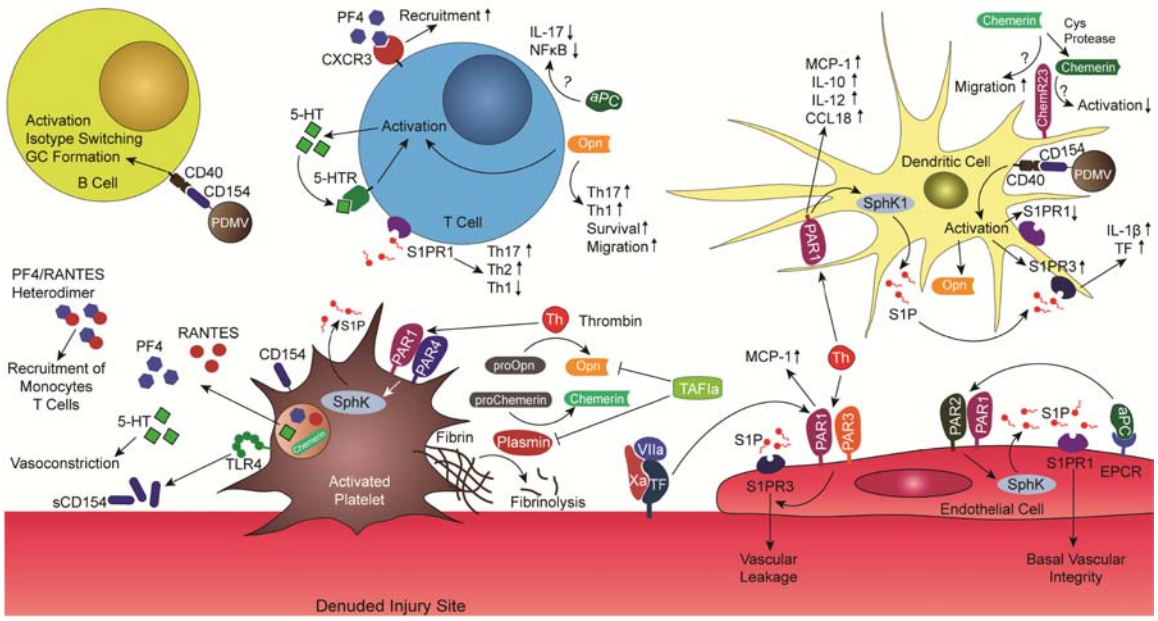


**Figure 2.2.** Interface between hemostasis and adaptive immunity. Thrombin activation of PARs and pro-osteopontin (proOpn), in concert with platelet derived CD154, serotonin (5-HT), platelet factor 4 (PF4), and RANTES, have now been discovered to optimize the process of antigen presentation to initiate and possibly steer the phenotype of subsequent adaptive immune responses. Platelets express CD154 which can be secreted by TLR4 induction or remotely delivered by platelet derived microvesicles (PDMV) to augment both dendritic and B cell activation. In a similar capacity, 5-HT can activate T cells and induce further production 5-HT to amplify this process. PF4 directly interacts with CXCR3 to increase T cell recruitment, or forms dimers with RANTES that recruits monocytes and T cells. Activation of PAR1 on dendritic cells (DC) enhanced the production of proinflammatory and prothrombotic mediators, a potential feedback system to amplify antigen presentation. A critical signaling pathway downstream of PAR engagement is activation of sphingosine kinase (SphK) to activate sphingosine-1 phosphate (S1P) that act on S1P receptors (S1PR). Extravasation of inflammatory cells through the endothelium is enhanced by thrombin (Th) activation of the S1PR3 pathway, while activated protein C (aPC) maintains the endothelial barrier through S1PR1. Engagement of S1PR1 is responsible for steering T helper cells away from Th1 phenotype towards a Th2 type response. aPC attenuates Th17 responses and downregulate T cell activation. Osteopontin (Opn) has been implicated in prolonging of T cell survival and driving a Th17 response. Chemerin depends on precise protease processing to either enhance or attenuate inflammation through the same receptor ChemR23. Activated thrombin-activatable fibrinolysis inhibitor (TAFIa) deactivates Opn and inhibits chemerin cleavage by plasmin, which yields a proinflammatory ligand for ChemR23. Substantial crosstalk between the hemostatic and adaptive immune compartments is therefore an indispensible component in the onset of effective host defense as well as immune dysfunction. Abbreviations: TF, tissue factor; MCP-1, monocyte chemotactic protein-1.

## 2.3. Passive Thromboresistant Surface Engineering Strategies

Adsorption and unfolding of plasma proteins on blood-contacting surfaces is the fundamental process underlying platelet adhesion and activation of coagulation factors to elicit a thrombotic response. Generally, electrostatic and hydrophobic interactions dictate the binding and subsequent folding of proteins, a thermodynamically favorable process whereby surface bound water molecules are displaced the by adsorbed species. Although this process may never be completely eliminated, these effects may be reduced by a number of surface modification strategies such as PEG, pyrolytic carbon, album, phosphorylcholine, as well as ECM based proteins such as elastin.

### 2.3.1. Poly(ethylene glycol)

In the early 1970s, it was observed that PEG passively adsorbed onto glass surfaces prevented the adsorption of viruses, platelets, and thrombin and subsequent studies have demonstrated that PEG has among the lowest levels of protein or cellular adsorption of any known polymer. This property was attributed to the presence of a hydrophilic ether oxygen in its structural repeat unit, $[CH_2\text{-}CH_2\text{-}O]_n$, which leads to a water-solvated structure that is capable of forming a “liquid-like” surface with highly mobile molecular chains that exhibit no systematic molecular order. Unlike other hydrophilic polymers, such as poly(hydroxyethyl methacrylate) and polyacrylamide, the absence of surface charges and the presence of only small hydrophobic methylene groups in the structural repeat unit was thought to provide few other sites for protein or cellular binding [130]. Surface modification with PEG has been attempted by several methods, including bulk modification, covalent grafting, and physical adsorption. In most cases, investigators have been able to demonstrate resistance to protein binding *in vitro*,

however, *in vivo* results have been inconsistent and clinical studies of a PEG modified stent or graft have yet to be performed. A comprehensive review of the blood compatibility of PEG by Lee and colleagues is available elsewhere [131].

### 2.3.2. Albumin Coating

Albumin as an inert, thromboresistant coating has been pursued since early studies of platelet interactions with various adsorbed proteins on artificial surfaces established that albumin induced significantly less platelet adhesion compared to other plasma proteins, including fibrinogen and gamma-globulin [132-135]. Some groups have covalently grafted albumin to surfaces [136-138] while others have modified surfaces with long aliphatic chains (C8-C18) or PEG-tethered warfarin to increase selective affinity for endogenous albumin [139-144]. Guidoin et al developed a glutaraldehyde-crosslinked albumin coating later manufactured by Bard, Inc [145, 146]. The Bard albumin-coated Dacron prosthesis was evaluated by Kotte-Marchant et al. and displayed reduced platelet and leukocyte adhesion and aggregation, as well as fibrin production *in vitro* [147]. In a thoracoabdominal bypass model in dogs, however, only small differences were observed between coated and uncoated grafts[148]. In clinical studies, Al Khaffaf [149] and Kudo et al [150] have evaluated this prosthesis in the aortic position with performance characteristics that are similar to other non-coated vascular prostheses.

### 2.3.3. Carbon Coating

Pyrolytic, or graphitic, carbon coating of implantable materials has been investigated for a variety of blood-contacting devices, including vascular grafts, heart valves, and stents [151-153]. In brief, pyrolytic carbon films are produced by chemical vapor deposition (CVD) in which a hydrocarbon, such as methane, is heated to its

decomposition temperature and the graphitic layer allowed crystallize as a highly ordered layer of carbon atoms. Early animal studies of carbon-coated vascular prostheses demonstrated improved patency rates compared to uncoated controls [154, 155]. However, surface irregularities on carbon-lined ePTFE grafts have contributed to poor performance in other investigations [156, 157]. More recently, 15 month implant studies in sheep documented reduced platelet adhesion and spreading on carbon-coated polyester grafts, but these observations did not affect overall histologic outcomes or patency rates [158]. Furthermore, in a prospective, randomized multicenter study conducted in Germany, 283 patients received either 6-mm carbon-coated (Carboflow™, Bard, Inc.) or uncoated ePTFE grafts (Bard, Inc.) for femoral-anterior tibial artery bypass. At three-year follow-up, no significant differences were observed between the two groups with respect to patency or limb salvage [159].

### 2.3.4. Phosphorylcholine Coating

Planar-supported bilayers of phosphatidylcholine (PC), the predominant glycerophospholipid found in animal cell membranes, have been shown to reduce protein and cell adhesion *in vitro* [160-164]. It has been proposed that this phenomenon is due to the zwitterionic nature of the phosphorylcholine head group that while carrying both positive and negative charges is electrically neutral at physiologic pH. Applications of supported lipid films as coatings for implantable devices has been limited by the inherent instability of a coating that is formed by individual molecules, which "self-assemble" as a monolayer or bilayer film through relatively weak hydrophobic van der Waal interactions [165]. Consequently, methods have been to create stable "membrane-mimetic" films through protein anchors [166, 167], heat stabilization [168], and *in situ* polymerization of

synthetically modified polymerizable phospholipids [169-174]. In all studies, the protein and cell resistant properties of the exposed PC layer were retained. Since 1984, a variety of polymethacrylate and polyurethane based polymers have been synthesized that incorporate the phosphorylcholine head group within the polymer backbone [175, 176]. For example, Yoneyama and colleagues demonstrated excellent in vivo blood compatibility of a segmented poly(etherurethane)/2-methacryloyloxyethyl phosphorylcholine (MPC) polymer blend processed as a coating for Dacron prostheses [177-179]. Chen et al. evaluated a 4 mm diameter ePTFE grafts coated with a copolymer of MPC and laurylmethacrylate (LM) in a canine femoral arteriovenous shunt. Significantly reduced platelet deposition was demonstrated, as well as limited neointimal hyperplasia at anastomotic sites [180, 181]. Similarly, UV polymerizable acrylate-modified phospholipids assembled on the lumen of an ePTFE graft ($d$ = 4 mm) reduced platelet adhesion in an *ex vivo* baboon femoral arteriovenous shunt model [182]. Direct chemical grafting of phospholipids on Dacron and ePTFE have been reported to reduce fibrinogen and platelet adhesion *in vitro* [183] and polyurethane based grafts ($d$ = 2mm) modified with PC prevented thrombus formation after 8 weeks in a rabbit model [179].

### 2.3.5. Elastin-inspired Surfaces

Elastin is a constituent structural protein in the vascular wall and elicits minimal platelet adhesion and aggregation [184, 185]. Dacron grafts coated with elastin inhibited SMC migration, suggesting elastin may also inhibit neointimal hyperplasia [186]. However, the intrinsic insolubility of elastin makes purification and processing from tissue difficult. This has largely been overcome by the identification of consensus sequences involved in the molecular assembly of elastin, which are used to construct a

variety of elastin-mimetic protein polymers [187-192].

Covalent immobilization of poly(VPGVG) on silicone reduced fibrinogen and immunoglobulin adsorption, and inhibited the secretion of proinflammatory cytokines from monocytes *in vitro* [193]. In a later study, the passive adsorption of recombinant elastin peptides onto polyurethane catheters decreased fibrin deposition and increased patency in a rabbit model [194]. Recently, ePTFE grafts ($d$ = 4 mm) were coated with a thin film of a recombinant amphiphilic elastin-mimetic protein polymer that inhibited platelet deposition in an acute primate *ex vivo* shunt model [195].

## 2.4. Inhibition of Thrombin and Fibrin Formation

The endothelial cell presents and releases a number of biologically active constituents that limit thrombotic responses which can lead to catastrophic graft failure . As such, seeding or otherwise reconstituting endothelial cells on a prosthetic surface has been actively pursued as a strategy for generating thromboresistant vascular substitutes. However, this approach poses its own challenges related to cell sourcing, stability, viability, and function [196-198]. Alternatively, promising results have been achieved through biologically-inspired or 'biomimetic' design, in which antithrombogeneic features of the endothelial cell surface are selectively mimicked by introducing bioactive molecules, such as heparin, thrombomodulin, or urokinase [199-204] onto the surface of synthetic materials.

### 2.4.1. Heparin

The first report of a heparinized surface was published in 1963 by Gott and colleagues who demonstrated significantly prolonged *in vitro* and *in vivo* clotting times on graphite-coated surfaces ionically bonded with heparin [152]. Since then, heparin-

coating technologies have been developed for a number of blood-contacting devices and used most extensively in cardiopulmonary bypass circuits [205, 206]. The literature on heparin immobilization is extensive and has been reviewed elsewhere [207-209]. Briefly, techniques to immobilize heparin include, but are not limited to, electrostatic self-assembly via heparin's negatively-charged sulfate groups [210, 211], covalent grafting often via a spacer arm [212-216], integration into a hydrogel network [217], and loading into a bulk polymer for controlled release [218]. One technique, which has been successfully translated to the clinic, is end-point immobilization, in which the reducing end of the linear heparin chain is depolymerized to yield a single reactive aldehyde group that can then be conjugated to a primary amine on the graft or stent surface [219-221].

Several heparin bonded vascular grafts have been recently assessed in clinical trials. A prospective randomized multicenter study compared the Intergard™ heparin-bonded Dacron (HBD) grafts to standard ePTFE for femoropopliteal bypass. The patency of HBD grafts was superior to ePTFE at three years, but a significant difference was not observed at five years [222]. Recently, a randomized multi-center prospective study found that HBD grafts displayed a five years patency rate in the femoropopliteal position that was similar to previously reported performance for standard ePTFE and Dacron [223]. A heparin modified ePTFE graft, marketed as Propaten™ (W.L. Gore, Inc.), received FDA approval in 2006. Several nonrandomized clinical trials using Propaten™ have reported 1 and 2 year patency rates for femoral-popliteal bypass that are similar to those previously noted for unmodified grafts [224-226].

### 2.4.2. Thrombomodulin

Several investigators have immobilized thrombomodulin (TM) onto polymeric surfaces in order to generate surfaces that actively limit the local generation of thrombin through the production of activated protein C (APC) rather than inactivate thrombin after it has already been produced. Specifically, APC inactivates factors Va and VIIIa, thereby limiting Xa and thrombin production. Kishida and colleagues conjugated recombinant human TM to both aminated and carboxylated surfaces, including poly(vinyl amine) and poly(acrylic acid) surface-grafted polyethylene and a surface-hydrolyzed poly(ether urethaneurea) [227-229]. Similarly, Vasilets et al. reported binding TM onto poly(acrylic acid) surface-grafted PTFE [230]. As an alternate approach, Cutler and colleagues physically adsorbed and crosslinked soluble human TM onto small caliber ePTFE grafts and reported promising short term results *in vivo* [231]. Other investigators, such as Sperling et al [232, 233] and Han et al [234] have tethered TM to surfaces via a PEG spacer. A disadvantage of all of the above strategies is the inherent reduction in bioactivity that is associated with immobilization schemes that involve reactions to any freely available amino or carboxyl functionality on the protein surface, including those near or within the catalytic site of the protein.

Recently, genetically directed synthesis has been used to create a recombinant TM construct comprised of the catalytically active site along with a C-terminal synthetic, non-natural amino acid, azido($N_3$)-methionine. The azido-functionalized TM construct can be coupled to surfaces directly through the C-terminus using highly selective reaction schemes with full retention of bioactivity [235, 236]. As an additional strategy, TM-containing membrane-mimetic surface assemblies have been produced that display

prolonged stability and activity in high shear environments [237, 238]. The ability of surface bound TM to dramatically reduce tissue factor-induced thrombin production has been characterized under both simulated venous and arterial flow conditions [237].

### 2.4.3. Direct Thrombin Inhibitors and Fibrinolytic Agents

Direct thrombin inhibitors, such as recombinant hirudin (rHir) and argatroban, have been used as an additional strategy to produce thromboresistant surfaces. Seifert et al [239] crosslinked hirudin to poly(D,L-lactide-co-glycolide) with glutaraldehyde, and LoGerfo and coworkers have grafted rHir to polyurethane and Dacron via a crosslinker modified albumin basecoat [240-244]. Several groups have also reported the immobilization of urokinase on surfaces to confer local fibrinolytic activity [199-202].

## 2.5. Inhibition of Platelet Adsorption

The capacity of aspirin to reduce thrombosis of ePTFE vascular prostheses has been noted in a number of randomized trials [245]. However, prolonged systemic administration of all antiplatelet drugs significantly increases the risk of bleeding and gastrointestinal complications. This has motivated the development of materials that locally inhibit platelet activity by surface immobilization of antiplatelet molecules, such as prostacylin, or local delivery of antiplatelet agents, including nitric oxide (NO).

### 2.5.1. Antiplatelet Drugs

Direct surface immobilization of antiplatelet agents has been extensively studied. Prostacyclin ($PGI_2$) and prostaglandin ($PGE_1$) have been immobilized on albumin covered surfaces [246, 247]. Likewise, Dacron and ePTFE grafts have been coated with collagen or laminin for covalent conjugation of $PGI_2$ and $PGE_1$ [183]. Dipyridamole has also been conjugated to polyurethane vascular grafts with improved patency rates

reported in a sheep model [248-250]. Aspirin eluting coatings for sustained release has been explored by several groups [251-254] and applied to Dacron grafts with reduced platelet deposition in a canine *ex vivo* shunt model [255]. Similarly, ePTFE grafts have been impregnated with alginate containing the prostacyclin analog, Iloprost™, with reduced thrombus formation *in vitro* [256].

### 2.5.2. Nitric Oxide

Nitric oxide (NO) inhibits platelet aggregation and prevents smooth muscle cell proliferation [257, 258]. Two types of NO donors, diazeniumdiolates ($[N(O)NO]^-$) and S-nitrosothiols, have been extensively studied in graft modifications to release and generate NO. Diazeniumdiolate ions are stable solids that readily release NO in physiological conditions [259]. The earliest studies involved loading the pores of ePTFE grafts with polyethylenimine microspheres that incorporated diazeniumdiolate ions [260, 261]. The capacity for NO to reduce platelet deposition on grafts was confirmed in a baboon ex vivo shunt model. Diazeniumdiolate has also been conjugated to polyurethane grafts that released NO over two months [262, 263]. A major limitation of diazeniumdiolate polymers is the leaching of diamine precursors that form carcinogenic nitrosamines [264]. This has led to the design of leach-resistant lipophilic diazeniumdiolate formulations [265-267].

S-nitrosothiols are a stable form of NO that is present in circulating blood and may act as an NO donor [268, 269]. S-nitrosothiols have been covalently bound on synthetic surfaces with satisfactory *in vitro* bioactivity [270]. However, S-nitrosothiols may act as an endogenous reservoir of NO that can be activated by copper (II)-based

catalysts [271, 272], cysteine modified polymers [273, 274], and organoditelluride [275] incorporated into polymers.

## 2.6. Biohybrid Vascular Grafts

A guiding principle of graft design since the 1950s has been the notion that the presence of an intact, quiescent endothelial lining on the prosthetic graft surface would reduce the risk of thrombosis and neointimal hyperplasia. However, it is now well understood that prosthetic grafts do not facilitate reendothelialization many years after implantation. Efforts to overcome this challenge have included both *in vitro* seeding with autologous endothelial cells and surface engineering schemes to induce *in vivo* endothelialization of the graft surface.

### 2.6.1 Endothelial Cell Seeding

In 1978, Herring and coworkers introduced a single-stage technique whereby venous endothelial cells were seeded onto grafts with enhanced patency in a canine model [276]. While a promising concept, translating these results to the clinic has been challenging. Zilla et al. noted in an early clinical report the absence of a confluent endothelial cell lining 14 weeks after bypass grafting [277]. A subsequent clinical study revealed that at 30 months the patency of single-stage endothelial cell seeded ePTFE grafts in the femoropopliteal position was significantly worse when compared to vein bypass (38% vs. 92%) [278]. Similarly, endothelial cell seeded Dacron aortobifurcated grafts did not demonstrate improved late outcome [279]. These disappointing outcomes were attributed to insufficient initial cell density, poor adhesion under flow, and failure to achieve confluence.

Cell density was increased using a two-stage technique [280, 281] and a three to four week culture period. The two-stage technique has yielded encouraging clinical results with a randomized study reporting that seeded grafts had greater patency than non-seeded grafts at 32 month (85% vs 55%) [282]. In a follow-up report, nine year patency was 65% for cell seeded as compared to 16% for non-seeded grafts [283]. In a subsequent report, similar primary patency rates were observed for 153 seeded ePTFE grafts [284]. A total of 14 patients have received cell seeded 4 mm ePTFE grafts for coronary bypass with 91% patency rates noted at 28 months [285].

Adhesive proteins, such as fibronectin, collagen, and fibrin [286-295], as well as adhesive peptide sequences [296-298] have been investigated as coatings to increase cell anchorage, but the most appropriate coating for clinical studies is unclear [299]. Other techniques, such as electrostatic seeding [300, 301] and shear conditioning [302, 303] may also increase cell adhesion. Phenotypic modulation of cells through genetic engineering has been pursued to increase expression of antithrombotic proteins such as tissue plasminogen activator [304] and nitric oxide synthase [305]. Endothelial progenitor cells (EPC) from either the bone marrow [306, 307] or peripheral blood [308], as well as the microvasculature in the omentum or subcutaneous fat have been highlighted as potential sources for endothelial cells [309-312].

### 2.6.2. Promoting *In Vivo* Reendothelialization

A more recent approach to improve the blood compatibility of implanted materials is functionalizing the blood contacting surface with active domains that promote natural regenerative processes involved in the healing of damaged endothelium. To illustrate, ePTFE grafts have been impregnated with fibrin glue containing fibroblast

growth factor-1 (FGF-1) and heparin, which in a dog model promoted transmural endothelialization, as well as the proliferation of smooth muscle cells [313-315]. Polyurethane based grafts coated with heparin and fibroblast growth factor-2 (FGF-2) have accelerated transmural endothelialization [316]. ePTFE grafts coated with an anti-CD34 antibody to capture circulating EPCs increased the rate of endothelialization in pigs [317].

## 2.7. Summary

Despite advances in surgical technique and antithrombotic pharmaceutical therapy, there remains a need for synthetic small diameter (< 6mm) conduits that perform comparably to autologous grafts in the fields of cardiac, vascular, and plastic surgery. Efforts to improve the blood compatibility have involved surface engineering techniques that incorporate passive mechanisms that inhibit adhesion of proteins and cells, as well as active domains that attenuate the platelet and coagulation activation cascades. While endothelial seeding of grafts has achieved encouraging outcomes in the clinic, the associated technical complexity remains a significant limitation to the widespread use of this approach. Currently, both heparin and carbon coated grafts have been commercialized for clinical use, but more long term evidence is needed to conclusively demonstrate their improvement in patency when compared to standard grafts. Multifunctional surface modification schemes involving bioactive enzymes, such as thrombomodulin and S-nitrosothiols are promising areas of current research. Despite efforts to coat graft surfaces with therapeutics, two key limitations remain: the finite reservoir and physiological degradation of immobilized therapeutics that limit the

duration of bioactivity, as well as sterilization requirements that may reduce the activity of immobilized biomolecules.

# CHAPTER 3

# LAYER-BY-LAYER ASSEMBLY OF POLYELETROLYTE MULTILAYERS AS SUBSTRATE FOR COVALENT IMMOBILIZATION OF BIOMOLECULES

This Chapter details our initial efforts to develop conformal coatings through layer-by-layer assembly of polyelectrolyte multilayer films on solid supports, as a means to generate chemically reactive anchor sites for immobilizing bioactive molecules. This system provides a facile method to modify medical device materials with a conformal coating, whose properties may be engineered by selection or modification of appropriate polyelectrolyte components.

## 3.1. Introduction

Layer-by-layer (LbL) deposition of alternating polyelectrolytes has emerged as a highly versatile and universal strategy to generate uniform films of controlled thickness and structural properties on substrates manifesting a net surface charge. This simple process entails the immersion of the substrate in a charged polymer species followed by rinsing to remove non-electrostatically bound polymers and incubation in the oppositely charged species. The universality of this approach is underscored by its applicability to any charged molecular species ranging from DNA to proteins, thus facilitating the construction of films with diverse architecture and functionality [318]. In particular, PEM films have been investigated as protein adsorption resistance on medical device surfaces. PEM films consisting of hyaluronic acid and chitosan were assembled on the surface of endovascular stents [319] as well as damaged blood vessels [320] to prevent platelet adhesion, which was further enhanced by the additional incorporation of charged

nitric oxide donors into the film. Poly(ethylenimine) and heparin PEMs were similarly assembled on stainless steel and prevented platelet adhesion [321, 322]. In an alternative approach, the deposition of fibrinogen and platelets were significantly reduced on polyurethane surfaces coated with PEM films comprising chitosan and dextran sulfate. Importantly, the authors showed that this inhibition property depends on the presence of the anionic polyelectrolyte as the outermost layer [323]. Similarly, chitosan/alginate microcapsules resist the deposition of fibrinogen but requires that a net negative charge be present on the surface [324]. Since our laboratory has observed that PLL is significantly cytotoxic [325], a rational approach is generating a PEM film containing the anionic polyelectrolyte as the outermost layer. However, it has been demonstrated that positively charged plasma proteins will preferentially deposit on this surface [326], but the enhanced adsorption was attenuated by incorporation of PEG as a diblock copolymer as the cationic species [327]. Additionally, the choice of anionic polyelectrolyte may also play a role, as hyaluronic acid was more effective than PEG and heparin modified polyurethane in limiting protein adsorption and platelet adhesion [328]. A rigorous assay to determine the extent of protein adsorption on PEM films upon exposure to plasma will be required to screen optimal film architectures that minimize these interactions.

The stability of PEM films can be further improved by crosslinking the polyelectrolyte layers with multifunctional linkers. Oxidation of alginate using sodium periodate generates reactive aldehydes that can be used to form stable covalent linkages with hydrazides [329, 330]. Hydrogels generated by crosslinking periodate oxidized alginate using bis-hydrazide linkers dramatically improved their stability [331]. The degree of crosslinking can be further tailored by incorporating linkers with multiple

hydrazide motifs to yield much higher stability than bifunctional linkers [332]. In a similar capacity, cationic constituents in PEM films have been crosslinked with glutaraldehyde [333]. Others have studied the direct covalent layer-by-layer assembly of azide and alkyne functionalized polyelectrolytes, which yielded selectively permeable membranes and facilitated further post-functionalization with azide modified probes [334]. Recently, we have demonstrated the ability to modify both living and nonliving substrates with a PEM film that enables covalent immobilization of biomolecules. Specifically, we grafted terminally functionalized PEG chains onto PLL to yield a surface reactive cationic constituent that formed PEMs with alginate on the surface pancreatic islets as well as glass surfaces [335]. The versatility of this approach was illustrated by the capacity to generate azide, hydrazide, and biotin anchor sites with the PEM architecture that facilitated conjugation of cyclooctyne, aldehyde, and streptavidin labeled probes. Further, it was demonstrated that a PLL-*g*-PEG-azide can be covalently immobilized on amine-reactive surfaces to facilitate covalent conjugation of cyclooctyne functionalized IKVAV peptide at highly controlled densities. Moreover, immobilization by copper-free [3 + 2] cycloaddition was highly efficient, evident by observations indicating peptide binding to the surface within 15 minutes [336]. Thus, both cationic and anionic constituents of PEM films can be derivatized to generate functional motifs on the film surface to facilitate immobilization of biomolecules. Moreover, covalent crosslinking using bifunctional linkers would not only improve the stability of films, but the incorporation of PEG may further enhance the film's capacity to resist protein adsorption. Given the broad substrate compatibility of PEM film formation, our proposed studies will serve as a starting point to demonstrate the feasibility of depositing

conformal PEM films on blood-contacting surfaces that also facilitate functionalization of active enzymes to limit the onset and elaboration of thrombotic reactions. In this regard, optimal PEM film architectures may electrostatically incorporate heparin and other charged therapeutic drugs such as NO donors, antimicrobial polypeptides [337, 338], and DNA [339], or facilitate covalent immobilization of bioenzymes.

In this report, we showed the exponential growth characteristics of PEM films comprising PLL and periodate oxidized alginate, covalent crosslinking of these PEM films by hydrazone bond formation using a dihydrazide crosslinker which improved film stability, and the formation of PEM films that incorporate heparin on commercial ePTFE vascular graft materials. These outcomes provide a starting point for generating a stable PEM film that display a high surface density of chemical anchor motifs for immobilizing biologically active molecules which resist thrombosis on the blood-contacting surface of implantable medical devices.

## 3.2. Results and Discussion

### 3.2.1. Assembly of PEM Films on Quartz

Oxidized sodium alginate was generated by reaction with sodium metaperiodate, which selectively opens sacchaide rings between vicinal diols and leaves two aldehydes groups. In these reactions, molar equivalents of periodate was added to oxidize 1 %, 5 %, 20 %, and 40 % of the total molar quantity of alginate sugar monomers. In preliminary studies, PEM films were generated by LbL deposition of PLL labeled with FITC (PLL-FITC) and 40 % oxidized alginate (Alg-CHO (40)) on transparent quartz substrates and monitored by UV-vis spectroscopy, as illustrated in Figure 3.1A. The PEM film exhibited exponential growth behavior, and was visibly yellow under ambient light.

Notably, after the $10^{th}$ bilayer of PLL-FITC/Alg-CHO (40), PEM films appeared opaque, as evident by substantial increase in absorbance in the visible region (600 nm) in Figure 3.1B. At the surface densities achieved after the $10^{th}$ bilayer, PLL and alginate may be undergoing a coacervation process that contributes to the exponential accumulation of polyelectrolytes.

Next, PEM films containing 10 bilayers of PLL-FITC and 40% alginate were covalently crosslinked by reaction with excess adipic dihydrazide (ADH), which forms stable hydrazone bonds with the aldehydes generated by alginate oxidation. This crosslinking reaction exhibits a characteristic increase in the UV absorption intensity near 240 nm (Figure 3.2). As expected, no change in the PLL content was observed during the crosslinking reaction. Overnight incubation in high ionic strength buffer (5 M NaCl) did not substantially remove the crosslinked PEM film deposited on quartz slides, as opposed to the immediate and complete desorption observed for noncrosslinked films comprising PLL-FITC and non-oxidized alginate.

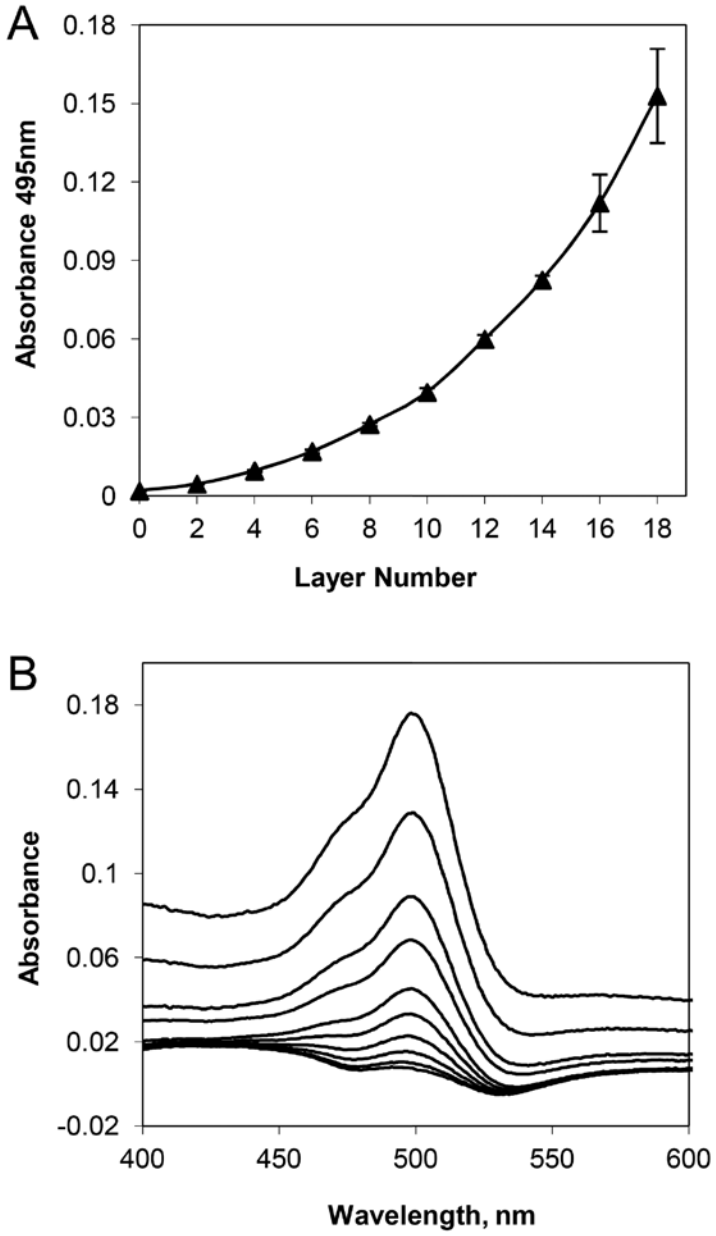


**Figure 3.1.** Evaluation of layer-by-layer assembly of fluorescein labeled poly(lysine) and periodate oxidized alginate (40% oxidation) on quartz surfaces. (A) Maximal absorbance of fluorescein at 495 nm was used to determine growth profile of films. Absorbance expressed as average of 2 independent substrates. (B) Typical UV spectra of films as measured after every 2 bilayers of polyelectrolytes were deposited.

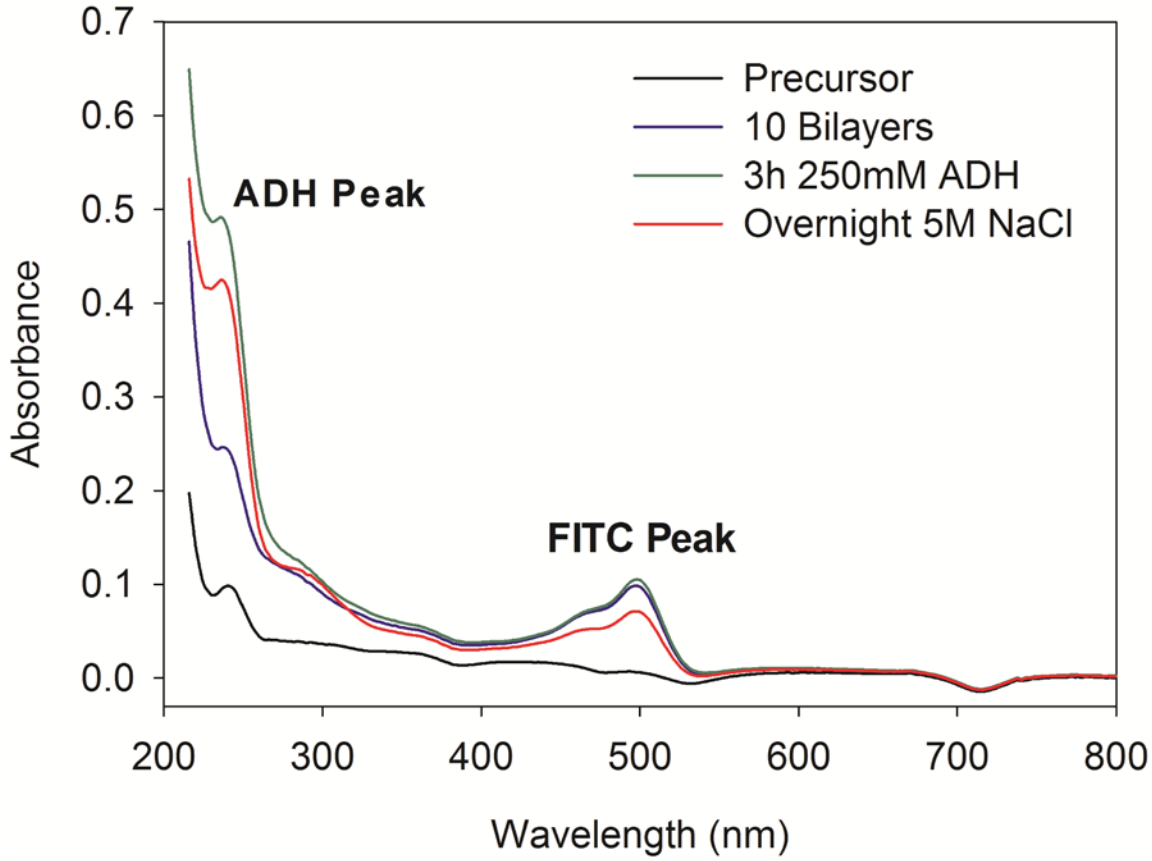


**Figure 3.2.** Evaluation of crosslinked polyelectrolyte multilayer (PEM) films assembled on quartz substrates. A distinct adipic dihydrazide (ADH) peak at 240 nm was observed following crosslinking of PEM films comprising fluorescently labeled poly(L-lysine) (PLL-FITC) and 40 % oxidized alginate (Alg-CHO (40)).

Interestingly, the film growth characteristics and film stability as measured by exposure to high ionic stress environments (5M NaCl) following ADH crosslinking appears to depend on the extent of alginate oxidation. As shown in Figure 3.3, film growth increased in proportion to the extent of alginate oxidation up to 20%, but the trend was reversed for 40% oxidized alginate (Alg-CHO (40)) as evident by the reduced film thickness. These observations may be attributable to the oxidative cleavage of the polysaccharide rings of alginate, which resulted in greater polymer chain flexibility to improve the growth of PEM films. However, these results also suggest a critical threshold may exist at 40% oxidation, where the increased polymer flexibility may result in electrostatic repulsion that decreases the quantity of adsorbed alginate per layer. In contrast, film stability appears to be maximal following ADH crosslinking for the 40% oxidized alginate. Stability decreased in a manner commensurate with the reduction in extent of alginate oxidation, with 5% oxidized alginate films being the least stable as summarized in Table 3.1. These results strongly suggest that while film growth may be impaired by loss in structural integrity of the polysaccharide chain, the increase in aldehydes motifs in the high oxidation variants afforded greater film stability due to increased covalent crosslinking with ADH.

**Table 3.1.** Stability of adipic dihydrazide crosslinked PEM films containing PLL-FITC and oxidized alginate with varying degrees of oxidation

| | % of 10 bilayer FITC signal ($Abs_{495\ nm}$) following overnight 5M NaCl exposure |
|---|---|
| PLL-FITC + Alg-CHO (5) | 37.8 |
| PLL-FITC + Alg-CHO (10) | 57.5 |
| PLL-FITC + Alg-CHO (20) | 65.5 |
| PLL-FITC + Alg-CHO (40) | 97.9 |

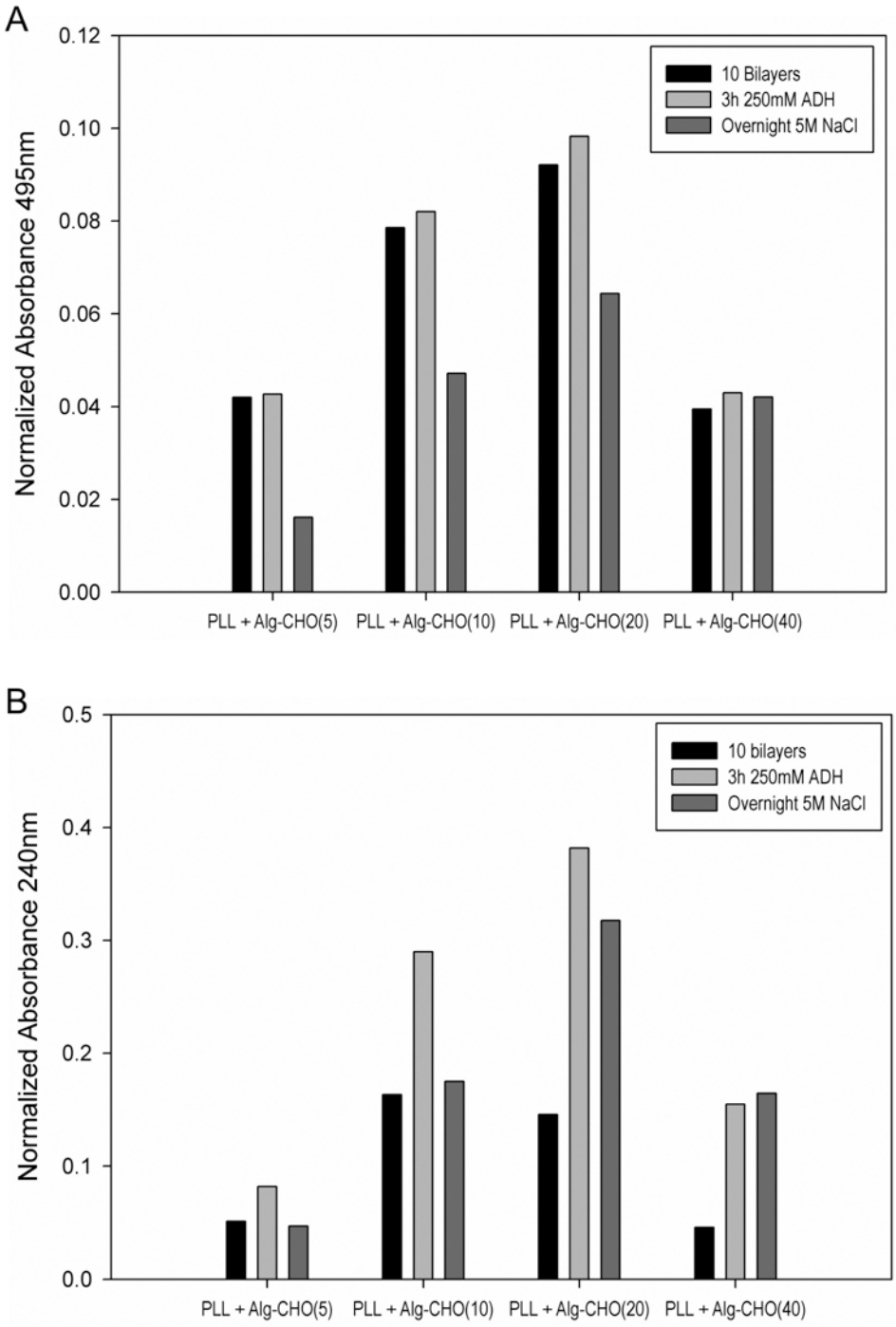


**Figure 3.3.** Layer-by-layer deposition of PLL-FITC and 5%, 10%, 20%, and 40% oxidized alginate was monitored by UV-vis absorption. Films were crosslinked by 250mM ADH for 3 hours and subsequently exposed to 5 M NaCl overnight. (A) Signal at the FITC absorption peak of 495 nm (B) Signal at the ADH absorption peak of 240 nm.

We also observed that PEM films containing oxidized alginate were more resistant to degradation under high ionic conditions, even in the absence of ADH crosslinking. Measurement of film integrity by UV spectroscopy over time suggests that with a 30 minute exposure time in 5 M NaCl, PEM films fabricated from PLL and 40% oxidized alginate (Alg-CHO (40)) was more resistant to degradation than PLL and non-oxidized alginate, as shown in Figure 3.4.

These observations indicate that the aldehydes generated from alginate oxidation, which undergoes Schiff Base formation with primary amines on PLL, may have improved the stability of the PEM films. However, due to the inherent instability of Schiff Base forming reactions due to hydrolysis, crosslinking by ADH was required to sustain the stability of PLL/Alg-CHO films beyond 2 hours. In addition, we observed that oxidized alginate yielded greater film growth as evident by higher PLL-FITC incorporation than non-oxidized alginate in Figure 3.4, which is likely a result of the greater polymer chain flexibility of oxidized alginate that enables greater deposition of polymers on the solid substrates.

The exponential growth of PEM on quartz slides may afford a surface modification strategy to yield high density of reactive anchor sites for biomolecule immobilization. Moreover, studies performed on quartz substrates indicate covalent crosslinking may be a feasible strategy to influence film stability as well as growth profiles.

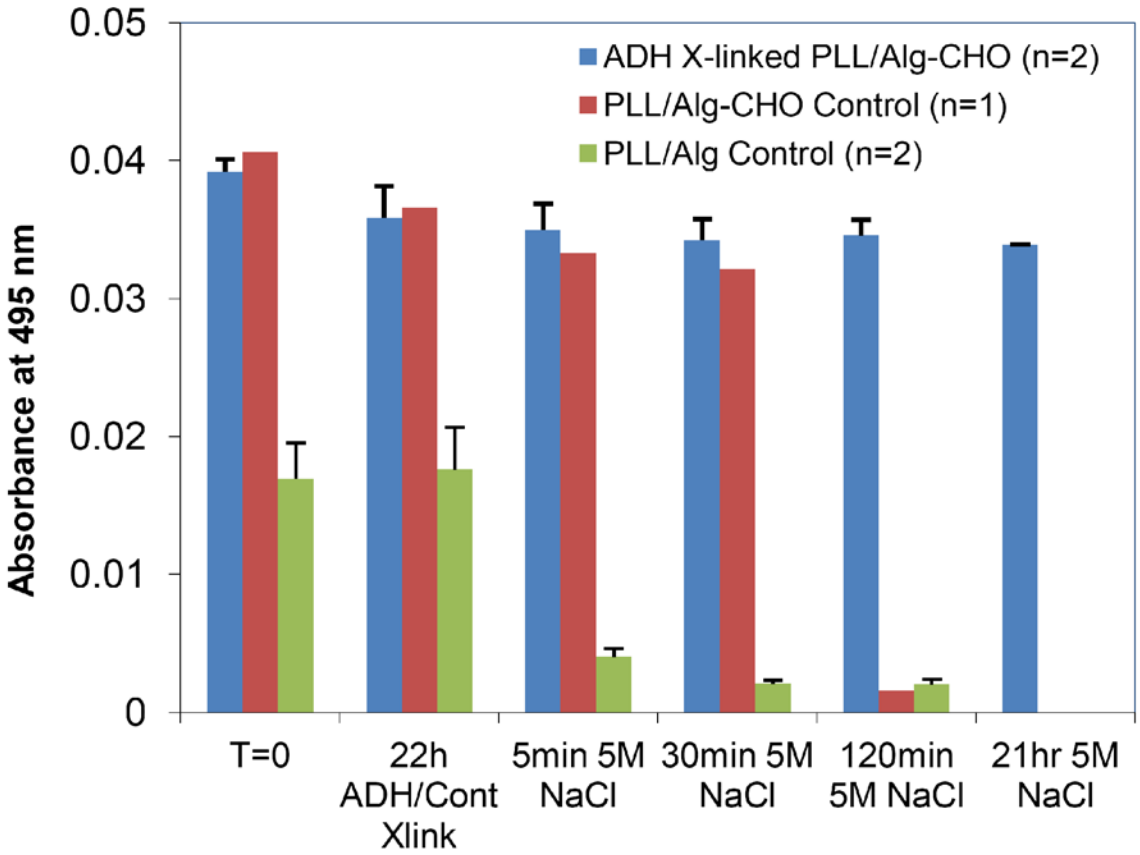


**Figure 3.4.** Evaluation of crosslinked polyelectrolyte multilayer films assembled on quartz substrates. ADH crosslinked films were substantially more robust to degradation by 5 M NaCl, and PLL-FITC/Alg-CHO films incorporated more PLL-FITC than PLL-FITC/Alginate films.

### 3.2.2. Assembly of PEM Films on ePTFE Grafts

As a step towards translating these findings as a viable surface engineering strategy to modify the blood contacting interface of implantable medical devices, we assessed the PEM assembly on the lumen of commercial expanded poly(tetrafluoroethylene) (ePTFE) vascular grafts. Fluorescently labeled poly(ethylenimine) (PEI) served as the precursor layer and polycation in our efforts to generate PEM films, which incorporated heparin as the polyanionic component as illustrated in Figure 3.5. Detection of surface modification was carried out by UV illumination and *en face* imaging.

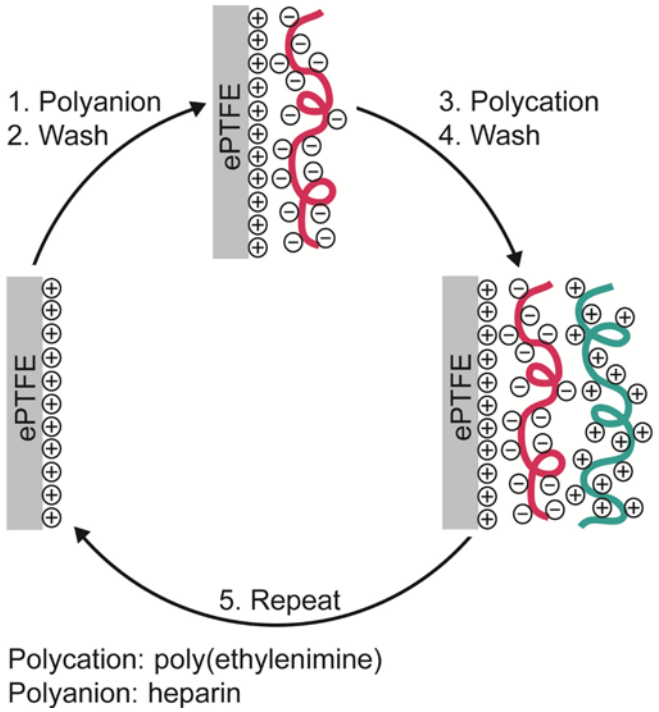


**Figure 3.5.** Layer-by-layer assembly of alternating polycations and polyanions on ePTFE vascular grafts.

Using an automated dip-coating system, which incubates samples in a solution of polyeletrolytes followed by incubation in multiple wash reservoirs, 8 or 16 bilayers of alternating FITC labeled PEI and heparin were assembled on the luminal surface of ePTFE grafts. In agreement with results from PEM film formation on quartz slides, the quantity of polymer deposited as PEM was substantially higher for 16-bilayer films than 8-bilayer (Figure 3.6). As expected, PEM films did not form in the absence of the one of the polyelectrolyte components, in this case the polyanionic heparin. Cumulative layer-by-layer deposition yielded a visually yellow and highly wettable film on the surface of the ePTFE graft, as illustrated in Figure 3.7. Moreover, the PEM films assembled using this approach were susceptible to degradation in 5M NaCl, further supporting the PEM nature of these films (Figure 3.7). These results suggest that a uniform PEM film containing heparin could be assembled on ePTFE surfaces.

Mechanical stability of PEM films was evaluated by subjecting coated ePTFE graft segments to 1000 $s^{-1}$ shear at 37 ºC for 24 h. These conditions were generated by connecting the graft segment in line with a perfusion loop housed in an incubation chamber. DPBS was circulated through the graft segment to mimic the physiological pH. Fluorescent imaging of the luminal surface of graft samples (Figure 3.8) provided qualitative evidence that the PEM film was mechanically stable under the shear stresses generated by this system. Further enhancement of film stability could be achieved by generating PEM films comprising PEI and oxidized heparin, however, it is unclear whether the oxidation of heparin using the current protocols will affect antithrombotic activity.

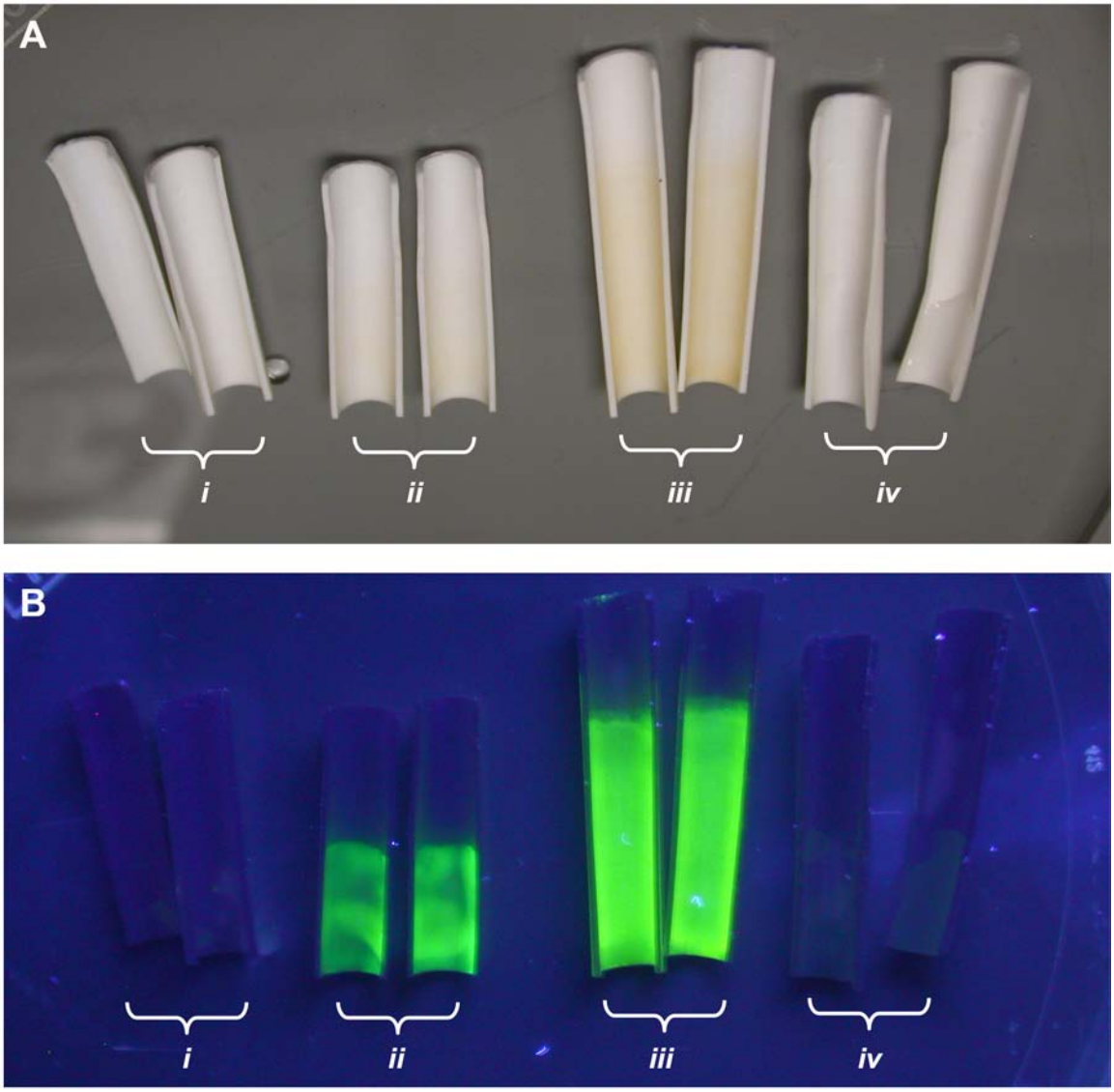


**Figure 3.6.** (**A)** En face and **(B)** fluorescent imaging of polyelectrolyte film coating on the luminal surface of 4 mm i.d. ePTFE grafts. (i) Control film fabricated by deposition of 8 layers of fluorescein labeled poly(ethylenimine) (FITC-PEI); (ii) alternating deposition of 8 bi-layers of FITC-PEI and heparin; (iii) alternating deposition of 16 bi-layers of FITC-PEI and heparin; and (iv) control films fabricated by deposition of 16 layers of FITC-PEI.

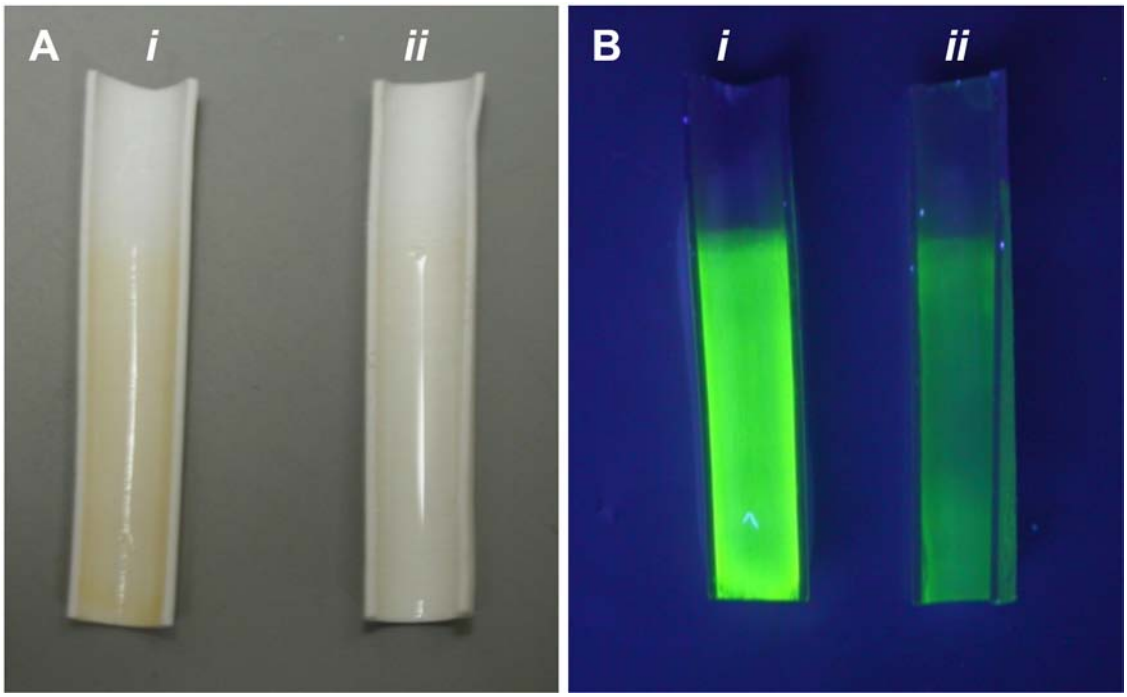


**Figure 3.7.** (**A)** En face and **(B)** fluorescent imaging of polyelectrolyte film coating on the luminal surface of 4 mm i.d. ePTFE grafts fabricated by alternating deposition of 16 bi-layers of fluorescein labeled poly(ethyleneimine) (PEI) and heparin (i) and after exposing film to 5 M NaCl for 20 minutes(ii).

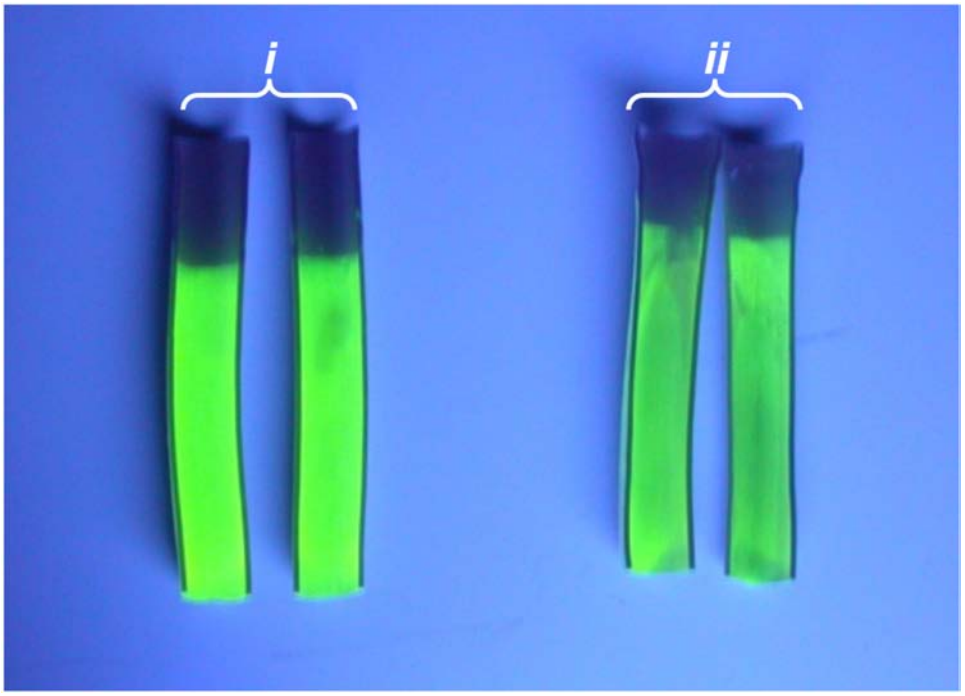


**Figure 3.8.** Fluorescent imaging of 16-bilayer PEI/heaprin films on the luminal surface of 4 mm i.d. ePTFE vascular grafts before (i) and after (ii) mechanical shear stress at 1000 $s^{-1}$ at 37 ºC for 24 h.

## 3.3. Conclusion

The exponential growth PEM film assembly on solid supports may be a strategy to maximize the density of surface anchor sites for covalent immobilization of biomolecules. We show that PEM films comprising alternating PLL and periodate oxidized alginate can be stabilized by covalent crosslinking through hydrazone bond formation using a dihydrazide linker. Formation of PEM films that incorporate heparin may be translated to modify commercial ePTFE vascular graft materials, and preliminary results show that these films could withstand the mechanical shear stresses encountered in the arterial vasculature. These outcomes support the future investigation of PEM films as a general strategy to provide a base coating for immobilizing biologically active molecules.

## 3.4. Methods

### 3.4.1. Synthesis and Characterization of Oxidized Alginate

Sodium metaperiodate (Pierce) oxidation of sodium alginate was carried out using reaction conditions previously reported [165, 186]. Briefly, sodium alginate (NovaMatrix, 75 – 220 kD) was dissolved at 1% w/v in deionized water, and sodium metaperiodate was added to yield final molar equivalents of 1 %, 5 %, 20 %, and 40 % with respect to the total moles of sugar residues, and stirred in the dark at room temperature for 24 hours. An equimolar amount of ethylene glycol (Sigma) was added to quench excess periodate for 1 hour, and the solution was placed in Slide-A-Lyzer dialysis cassettes (Pierce) with a molecular weight cutoff of 3.5 kD, and dialyzed against double deionized water for 3 days. Dialysis buffer was exchanged twice a day. Subsequently, oxidized alginate variants were snap frozen in liquid nitrogen and lyophilized to yield a

white product. The degree of alginate oxidation generate reactive aldehydes was determined by quantifying the number of aldehydes using t-butyl carbazate (Sigma) as reported elsewhere [165]. Briefly, excess carbazate was added to oxidized aldehyde allowed to react overnight. Unreacted carbazate was determined using a TNBS solution (Sigma) and measuring the absorbance of the trinitrophenyl derivatives that forms at 334nm. Aqueous formalin solutions were used to generate standard curves correlating aldehyde concentration with TNBS signal.

### 3.4.2. Synthesis and Characterization of FITC Labeled PLL and PEI

To facilitate characterization of the layer-by-layer assembly of polyelectrolytes, PLL and PEI (Sigma) were labeled with FITC (Pierce Biotechnology) according to manufacturer's instructions. A stock solution of FITC in DMSO was added at a stoichiometric ratio corresponding to 1% (0.01 molar equivalents) of the primary amine repeats in PLL or PEI (1 : 2 : 1 ratio of primary : secondary : tertiary amines) dissolved in PBS buffer (pH 7.4), and reacted in the dark for 24 h at RT. The unreacted FITC was removed by dialysis using Slide-A-Lyzer Dialysis Cassettes with a 3.5 kD MWCO (Pierce Biotechnology), and the final FITC-PLL or FITC-PEI was lyophilized to yield 92 % and 97 % product, respectively.

The extent of labeling of PLL or PEI with FITC was determined using a standard curve of correlating the absorbance intensity at 494nm of FITC versus known solution concentrations of FITC. The final extent of labeling of PLL labeling was 0.65 % and the final extent of labeling of PEI primary amine labeling was 0.52 %. A typical regression equation for FITC is:

$$\left[FITC\,\frac{mg}{ml}\right] = 0.0086 \times A_{494nm} + 0.000096$$

### 3.4.3. Assembly of PEM Films on Quartz and ePTFE

Fluorescein labeled PLL (PLL-FITC, Sigma, 12kD) and 40% oxidized alginate (Alg-CHO) was used in initial studies to evaluate PEM film growth on quartz. Quartz slides (Chemglass, 1mm thick) were cut into 2.5cm x 1cm substrates and cleaned using Piranha solution to oxidize the surface. Briefly, slides were incubated in an ammonium hydroxide/hydrogen peroxide/water (1:1:5 volume ratio) mixture at 80C for 10 minutes, followed by incubation in a sulfuric acid and hydrogen peroxide (7:3 volume ratio) mixture at 80C for 10 minutes. Slides were thoroughly rinsed with deionized water following each step, and as a final step rinsed in 200 proof ethanol before drying under a stream of argon. Prior to PEM assembly, slides were treated with a precursor bilayer of poly(diallyldimethylammonium chloride) (PDDA, Sigma, 200 – 350kD) for 30 minutes, rinsed in deionized water, and incubated in 0.15% sodium alginate in phosphate buffered saline for 20 minutes to generate a negatively charged surface. For ePTFE graft modification, 4 mm i.d. ePTFE grafts (Bard) were cut into ~2 – 3cm segments and directly mounted on the automated coating system without any pre-treatment.

Substrates were coated with PEM assemblies using a custom-built automated slide coater assembled using two BiSlide assemblies and stepper motors (Velmex Inc, Bloomfield NY). The coater comprises two linear, screw driven actuators combined to allow horizontal and vertical translation of substrates, which are mounted vertically on a lever using customized clips. Substrates were immersed in and removed from polymer and wash solutions at a rate of 1.3 cm/s using the vertical actuator, and translated horizontally between solution reservoirs at a rate of 5.1 cm/s. Programming of substrate coating procedures was carried out using COSMOS software per manufacturer's

instructions (Velmex Inc). PLL-FITC or PEI-FITC at 1mg/ml and 40% oxidized Alg-CHO (2.5mg/ml), non-oxidized alginate (2.5 mg/ml), or heparin (2.5mg/ml), were deposited on quartz substrates by alternating incubations for 5 minutes. Between each layer, substrates were rinsed by four 1 minute incubations in fresh PBS.

Film growth on quartz was monitored every 2 bilayers in a UV-spectrometer (Cary 50, Varian Inc) using a custom jig that allows absorbance measurement of quartz slides submerged in a solution of PBS. PLL/Alg-CHO films show an exponential growth profile as determined by the maximal adsorption of FITC at 495 nm. Film growth on ePTFE grafts after assembly of PEM was measured by first cutting the graft segment lengthwise in two halves to expose the luminal surface. A short-wave UV lamp was used to illuminate the PEI-FITC component for imaging.

### 3.4.4. PEM Film Stability and Crosslinking

Oxidized alginate films were crosslinked by incubating films in 250 mM adipic dihydrazide (ADH, Sigma) in PBS (pH 7.4). Stability of films was evaluated by incubation in 5 M NaCl solution for up to 21 hours. ADH incorporation into the film was evaluated by measuring the absorbance at 240 nm. Mechanical stability of PEM films assembled on the luminal surface of ePTFE grafts was determined by connecting a segment of modified graft in-line with a peristaltic pump (Variable Flow Chemical Pump, VWR) that maintained a 400 ml/min flow rate, as well as a ~300 ml reservoir of DPBS. The setup was placed in an incubator at 37 ºC and the graft was perfused for 24 hours.

# CHAPTER 4

# A BIOLOGICALLY ACTIVE SURFACE ENZYME ASSEMBLY THAT ATTENUATES THROMBUS FORMATION

Activation of hemostatic pathways by blood-contacting materials remains a major hurdle in the development of clinically durable artificial organs and implantable devices. We postulate that surface-induced thrombosis may be attenuated by the reconstitution onto blood contacting surfaces of bioactive enzymes that regulate the production of thrombin, a central mediator of both clotting and platelet activation cascades. Thrombomodulin (TM), a transmembrane protein expressed by endothelial cells, is an established negative regulator of thrombin generation in the circulatory system. Traditional techniques to covalently immobilize enzymes on solid supports may modify residues contained within or near the catalytic site, thus reducing the bioactivity of surface enzyme assemblies. In this report, we present a molecular engineering and bioorthogonal chemistry approach to site-specifically immobilize a biologically active recombinant human TM fragment onto the luminal surface of small diameter prosthetic vascular grafts. Bioactivity and biostability of TM modified grafts is confirmed *in vitro* and the capacity of modified grafts to reduce platelet activation is demonstrated using a non-human primate model. These studies indicate that molecularly engineered interfaces that display TM actively limit surface-induced thrombus formation.

## 4.1. Introduction

The molecular engineering of biologically active surface assemblies that control host reactions at tissue-material interfaces may be an important step in the development

of clinically durable artificial organs and implantable devices [340, 341]. In this regard, pathological thrombus formation on materials in direct contact with blood has precluded development of a clinically durable small-diameter (< 6 mm inner diameter) arterial prosthesis critical to the fields of cardiac, vascular, and plastic surgery, and has necessitated adjunctive antithrombotic therapies that increase bleeding risk and healthcare costs for numerous cardiovascular procedures [8, 342]. The onset and amplification of thrombogenesis on blood-contacting materials involves concomitant activation of platelets and elaboration of the coagulation cascade to generate thrombin and fibrin, culminating in hemostatic plug formation [343]. Thrombin serves as a central initiator, amplifier, and effector molecule at the nexus of these pathways by crosslinking fibrin, directly triggering platelet activation that lead to a local burst of thrombin production,[344] and eliciting inflammatory reactions [345] that influence long-term healing characteristics of implanted materials [346]. Therefore, a rational approach to improve blood compatibility and long-term durability of blood-contacting materials may entail the incorporation of endogenous regulators of thrombin production, normally active within the endothelial cell membrane, onto synthetic molecularly engineered surfaces.

Heparan sulfate proteoglycans (HSPG) in the arterial wall accelerates thrombin inactivation by antithrombin III, a mechanism Gott and coworkers first replicated on artificial surfaces by heparin immobilization in 1963 [347]. However, the physiological significance of HSPG remains poorly understood, since the majority of anticoagulantly active HSPG is not in direct contact with flowing blood [348], and thrombin becomes resistant to inhibition by the heparin-antithrombin III complex upon binding to fibrin

[349]. Alternatively, surface-bound direct thrombin inhibitors, such as hirudin [239, 240, 350, 351] and its analogues [352], as well as argatroban [353, 354], and benzamidine [355] quench the activity of locally produced thrombin. However, a potential constraint of these approaches is the inability to generate a continuous surface reservoir of direct thrombin inhibitors that would be required to curtail self-reinforcing thrombin generation cascades which are rapidly amplified upon initiation. Hemostatic occlusion in the arterial circulation is actively regulated by the protein C (PC) pathway, whereby activated protein C (aPC) inactivates precursors requisite for amplification of coagulation and thrombin formation [356]. Endothelial cells that line the vascular system express thrombomodulin (TM), a transmembrane protein that binds thrombin as a 1:1 stoichiometric complex. In the process of sequestering thrombin, TM limits its capacity to activate platelets or to otherwise serve as a prothrombotic factor. More importantly, TM accelerates thrombin's ability to produce aPC by 1000-fold [19]. Hence, we postulate that engineering blood-contacting surfaces, which display biologically active TM assemblies would locally generate aPC "on demand", thereby, inhibiting thrombin generation.

Traditional techniques to immobilize active enzymes on solid supports, such as passive adsorption or covalent ligation via free amino or carboxyl residues[357] have been reported to generate surfaces modified with TM [228, 230-233, 358-360]. However, these covalent ligation approaches randomly orient immobilized enzymes and potentially modify residues contained within or near the catalytic site [361], consequently reducing optimal surface activity that could otherwise be achieved by these enzyme assemblies. Emerging advances in bioorthogonal chemistry and molecular engineering

provides an opportunity to site-specifically tether large enzymes onto surfaces. The azide ($-N_3$) group is absent from biological systems and was first explored as a bioorthogonal handle with Staudinger Ligation [362]. Further application of this chemistry to immobilize proteins containing an azide-modified C terminus has been performed on glass surfaces modified with triphenylphosphine [363, 364], but thiol reagents used in expressed protein ligation to generate the azide moiety may perturb the folding and catalytic activity of bioenzymes rich in disulfide bonds [365], including TM [366]. An alternative strategy that first converted a single lysine residue to azide facilitated immobilization of an active enzyme by traceless Staudinger Ligation on glass, which maximized its bioactivity relative to random coupling via amine residues [367]. However, a possible limitation of this approach is the lack of site-specificity when multiple lysines are present in larger biomolecules, such as TM.

Our laboratory has generated a truncated 15 kDa human TM fragment containing the soluble extracellular epidermal growth factor-like domains 4 through 6 ($EGF_{4–6}$) [235], which displays the requisite binding sites for thrombin and protein C necessary to catalyze production of aPC [368]. Using site-specific incorporation of the non-canonical methionine surrogate azidohomoalanine [369] we have generated a TM variant expressing a single C-terminal azide moiety (TM-$N_3$). In this report, we immobilize recombinant TM-$N_3$ by Staudinger Ligation onto the luminal surface of polyurethane coated expanded poly(tetrafluoro-ethylene) (ePTFE) vascular grafts (Figure 4.1). Further, we demonstrate the capacity of these surfaces to generate aPC and confirm the stability of TM surface assemblies *in vitro*. The ability of TM modified grafts to inhibit thrombosis *in vivo* was demonstrated using a non-human primate model.

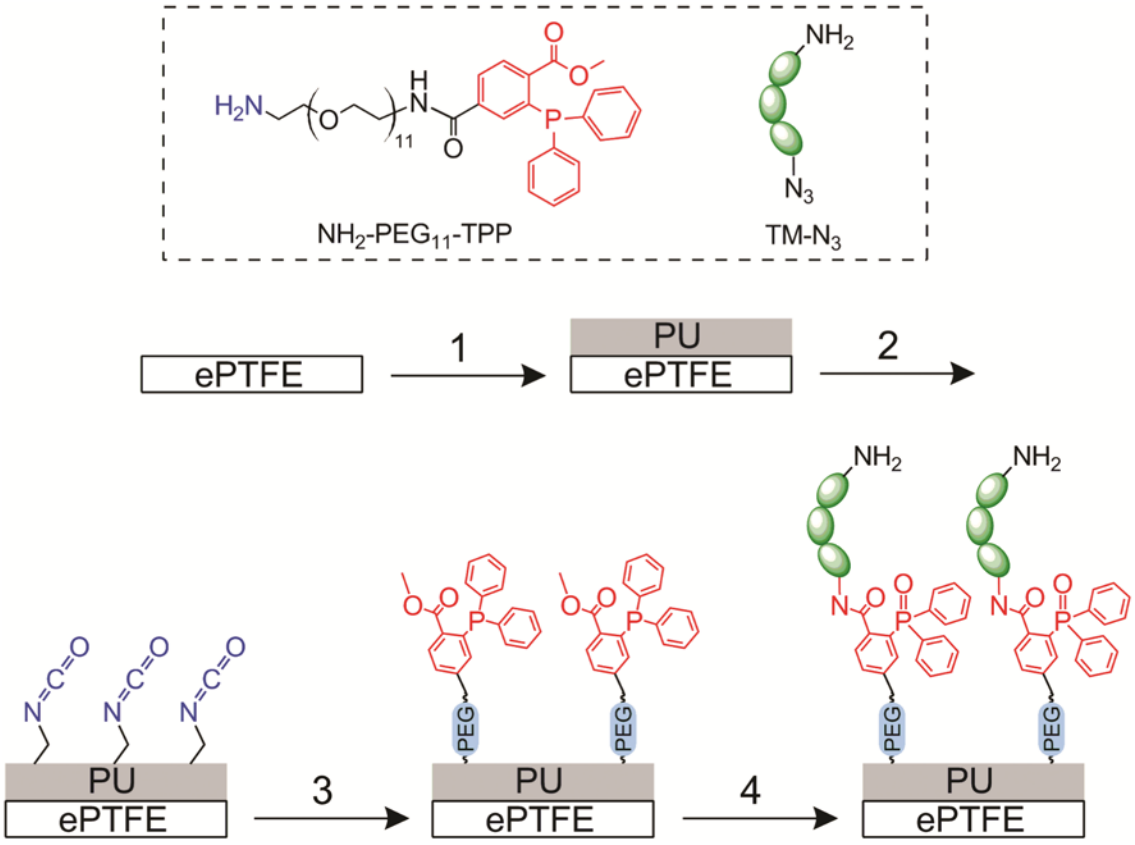


**Figure 4.1.** Reaction sequence to covalently immobilize recombinant human thrombomodulin (TM) onto the luminal surface of expanded poly(tetrafluoroethylene) (ePTFE) grafts: (1) generation of polyurethane (PU) coating on ePTFE graft lumen; (2) isocyanate activation of PU with hexamethylene diisocyanate; (3) immobilization of amino-$PEG_{11}$-triphenylphosphine ($NH_2$–$PEG_{11}$–TPP) linker; (4) Staudinger Ligation of recombinant TM expressing a single C-terminal azide moiety (TM-$N_3$) to TPP.

## 4.2. Results and Discussion

### 4.2.1. Coating of ePTFE Grafts with a Polyurethane Film

Although inert PTFE surfaces may be modified by high energy radiation to generate reactive chemical handles [370], translation of these techniques to ePTFE vascular prostheses on clinically relevant length scales has been difficult. Therefore, an extrusion method was used to deposit a thin coating of medical grade Elasthane 80A polyurethane (PU) onto the luminal surface of ePTFE grafts that could then be readily modified by chemical techniques [371]. Scanning electron microscopy (SEM) confirmed deposition of a smooth, uniform ~50 μm PU film that penetrated the porous node-fibril architecture of ePTFE **(**Figure 4.2**)**.

As expected, PU coating thickness was proportional to the quantity of material deposited and uniform along the length of the prosthesis (Figure 4.3). Attenuated total reflectance IR (ATR-IR) spectroscopy was performed on PU coatings on ePTFE (Figure 4.4a), as well as model thin films generated by solvent casting of PU onto glass substrates (Figure 4.4b). A hydrogen-bonded urethane N–H peak at 3320 $cm^{-1}$ that is characteristic of PU was observed, as were peaks at 2885 and 1535 $cm^{-1}$ corresponding to C–H stretching and C–H–N bending, respectively. Additional PU peaks were detected at 1591 $cm^{-1}$ (C=C, aromatic ring), 1110 $cm^{-1}$ (C–O–C, stretch), 1730 $cm^{-1}$ (urethane C=O, free from hydrogen bonding), and 1710 $cm^{-1}$ (urethane C=O, hydrogen bonded), consistent with prior reports [372].

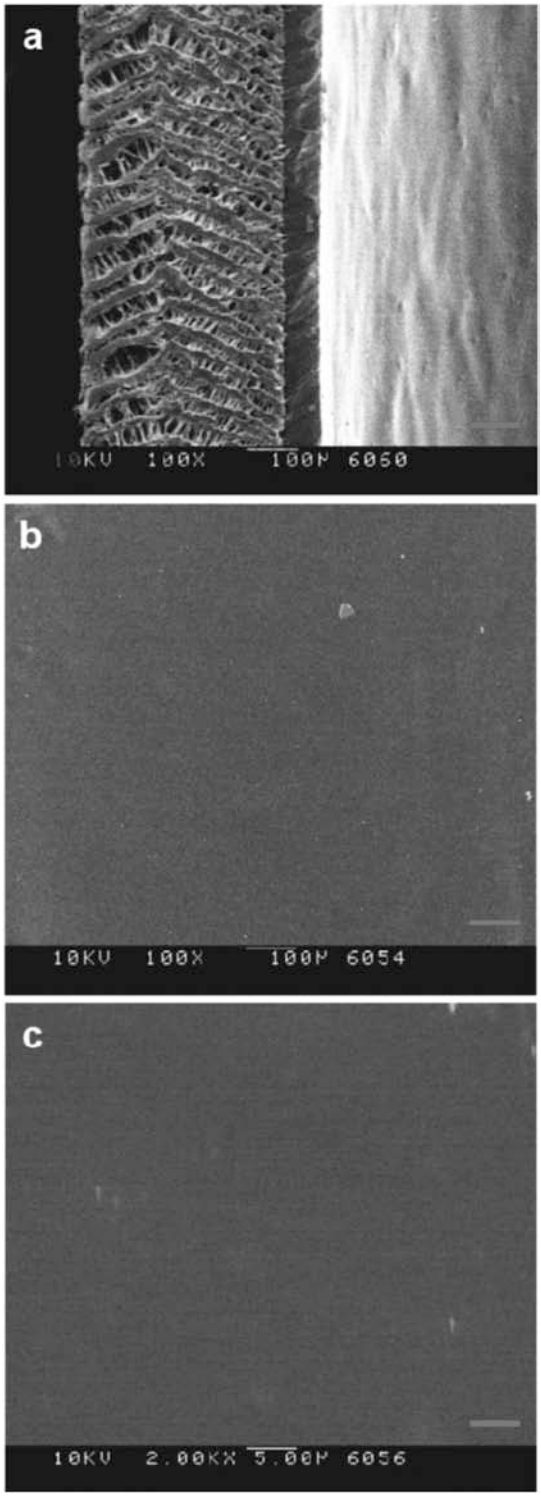


**Figure 4.2.** Scanning electron microscopy of polyurethane (PU) coating on (a) the edge of ePTFE graft at 100x, and on (b) the luminal surface at 100x and (c) 2000x. Scale bars: (a and b) 100 µm; (c) 5 µm.

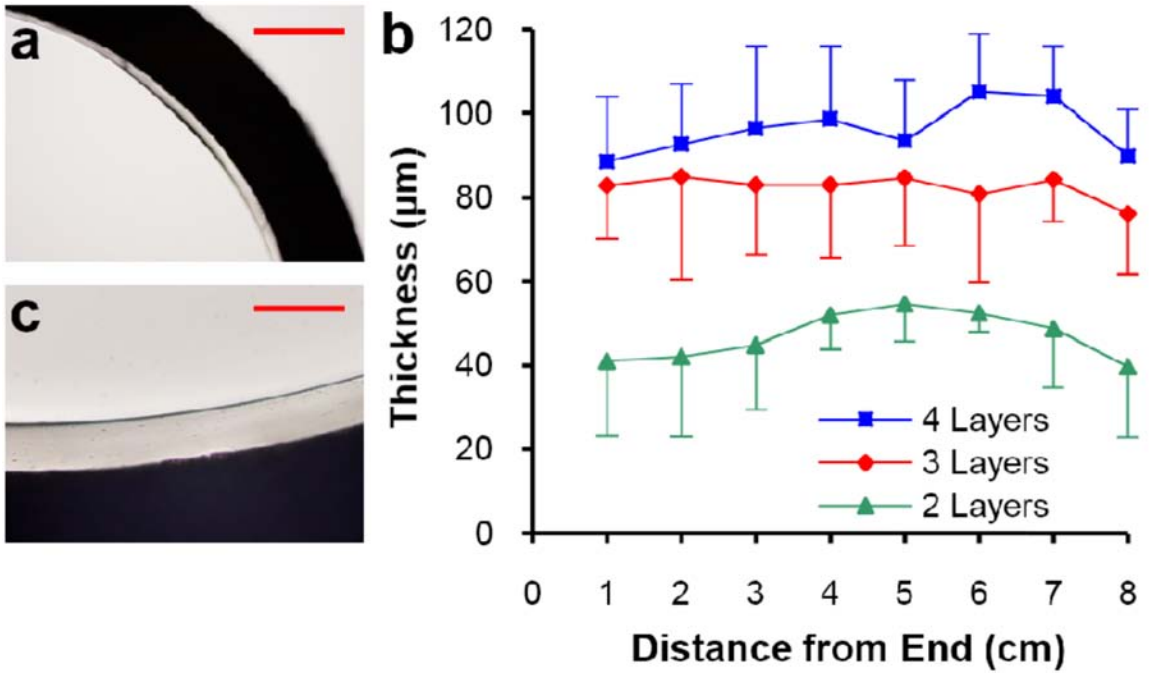


**Figure 4.3.** Light microscopy of thin cross sections of polyurethane (PU) coated ePTFE grafts. (a) Interface between opaque ePTFE graft wall and transparent 2-layer PU lining observed at 4x. (b) Mean ± standard deviation of PU thickness measured at 4 positions per cross section and 1cm intervals along 8cm ePTFE graft segment coated with 2, 3, and 4 deposited layers of PU on top of a base extruded layer. (c) Interface between opaque ePTFE graft wall and transparent 4 layer PU lining observed at 20x. Scale bars: (a) 500 µm; (c) 100 µm.

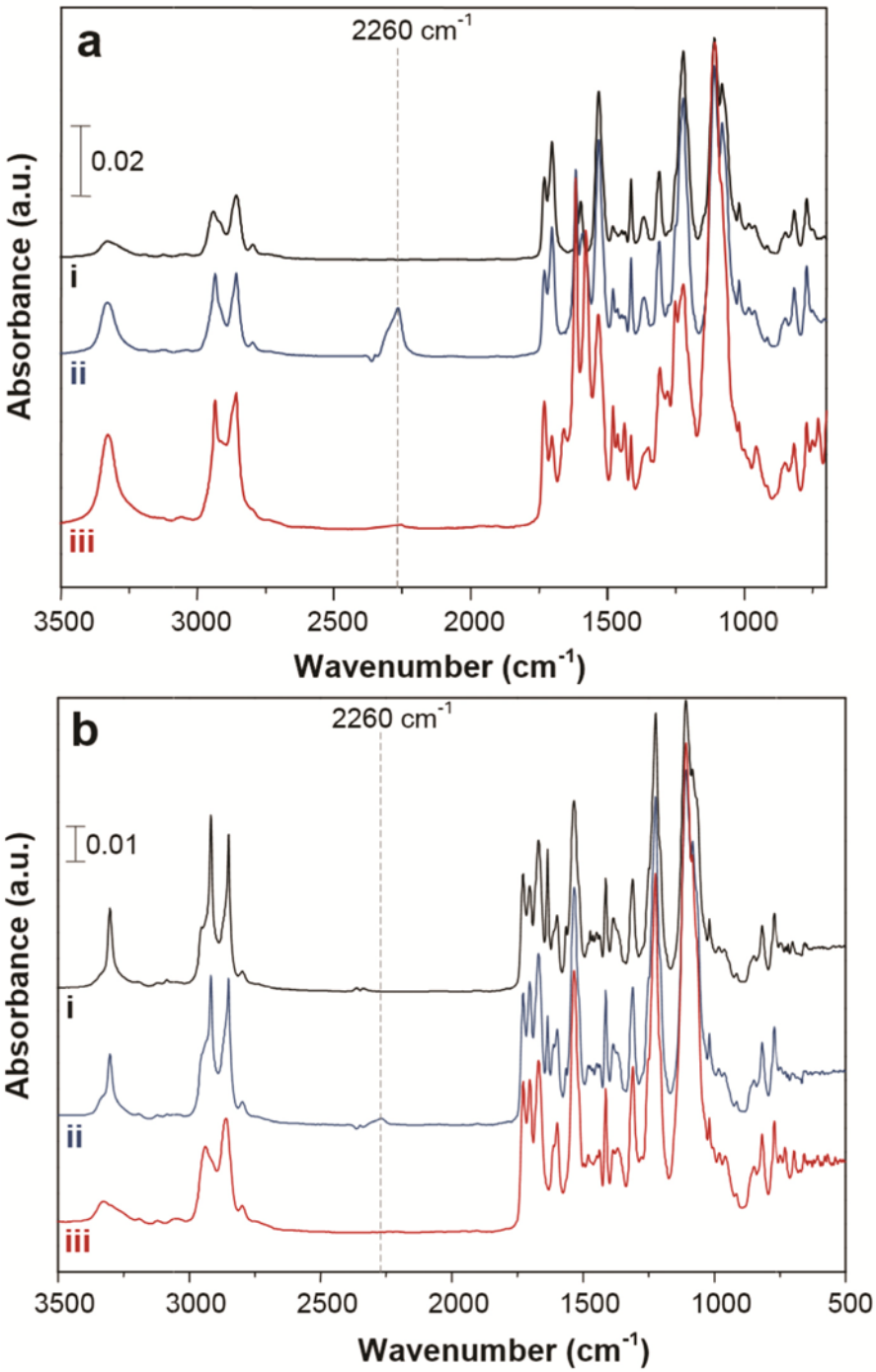


**Figure 4.4.** Attenuated reflection infrared spectroscopy of (a) polyurethane (PU) coated on the luminal surface of ePTFE grafts and (b) thin solvent cast PU films. Representative spectra given for (i) PU, (ii) PU subjected to isocyanate activation with hexamethylene diisocyanate, and (iii) PU modified with a heterobifunctional $NH_2$-$PEG_{11}$-triphenylphosphine linker.

### 4.2.2. Chemical Modification of ePTFE Grafts

Amine-reactive isocyanate groups were generated on PU coated grafts using a rotary reactor, which facilitated uniform mixing of reagents (Figure 4.5) [182]. PU coated grafts were incubated for 1 h with hexamethylene diisocyanate (HDI) in the presence of triethylamine (TEA) at 50 °C , as demonstrated elsewhere [373]. ATR-IR spectroscopy detected a distinct peak at 2260 $cm^{-1}$ corresponding to –N=C=O (Figure 4.4). A heterobifunctional linker comprised of a poly(ethylene glycol) (PEG) spacer with amino ($–NH_2$) and triphenylphosphine (TPP) end groups ($NH_2–PEG_{11}–TPP$) was used to derivatize accessible surface isocyanates (Scheme 1), as confirmed by loss of the –N=C=O peak by ATR spectroscopy (Figure 4.4).

Consistent with this finding, X-ray photoelectron spectroscopy (XPS) revealed a sharp decrease in the C (285eV) to O (532eV) ratio (Figure 4.6a-c and Table 4.1) and the presence of distinct phosphorous peaks (P*2p* at 133eV and P*2s* at 200eV) (Figure 4.6c). The absence of fluorine peaks (Figure 5a-c) further confirmed complete coverage of ePTFE by the PU thin film. High resolution C 1*s* XPS (Figure 4.6d-f and Table 4.1) revealed a dramatic increase in N–C=O (289.0eV) intensity and increased ether carbon content (C–O, 286.4eV) after immobilization of the PEG linker. These observations confirm the initial generation of reactive isocyanates followed by the display of TPP moieties on the luminal surface of PU-coated ePTFE grafts.

**Table 4.1.** Elemental analysis of modified ePTFE grafts by XPS.

| Substrate | Survey XPS | | | | High Resolution C 1*s* XPS | | |
|---|---|---|---|---|---|---|---|
| | C (%) | O (%) | N (%) | C/O Ratio | C–C (%) | C–O (%) | O–C=O N–C=O (%) |
| PU [a] | 81 | 17 | 1.6 | 4.8 | 65 | 13 | 1.1 |
| PU–NCO [b] | 86 | 13 | 0.70 | 6.6 | 74 | 6.0 | 9.2 |
| PU–TPP [c] | 70 | 24 | 4.6 | 2.9 | 50 | 45 | 2.8 |

[a] Bare polyurethane (PU); [b] isocyanate activated PU; [c] PU–NCO reacted with $NH_2$–$PEG_{11}$–TPP linker

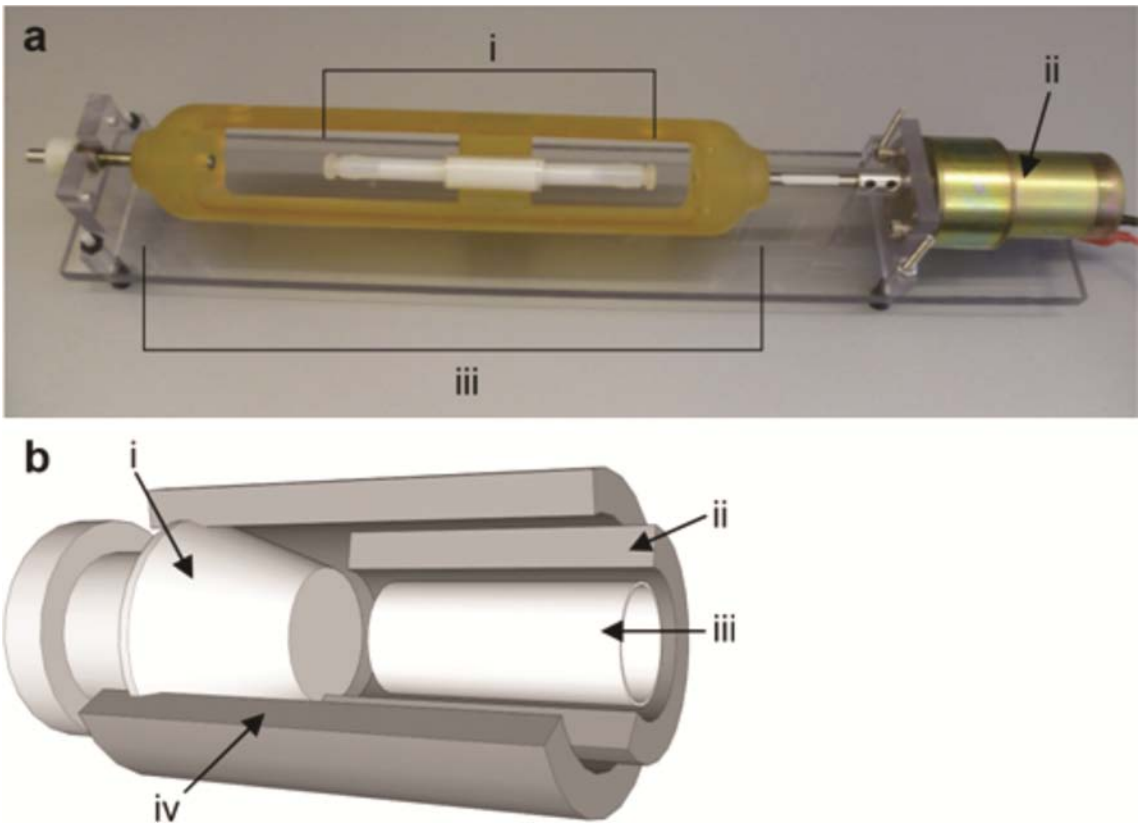


**Figure 4.5.** Reactor setup for chemical derivatization of PU modified ePTFE grafts. (a) 4 mm i.d. ePTFE grafts were chemically modified using a custom reactor design comprising (i) reactor housing for ePTFE graft and a (ii) DC motor that is coupled to a (iii) form-fitting rotator clamp for graft reactors to facilitate rotation along the axial length of grafts. (b) Inner construction of reactor housing for ePTFE graft comprising (i) barbed Kynar plugs to seal both ends of tubular reaction vessel; (ii) inner 5 mm i.d., 7 mm o.d. Teflon tube; (iii) 4 mm i.d. ePTFE graft; (iv) outer 7 mm i.d., 9 mm o.d. Teflon tube.

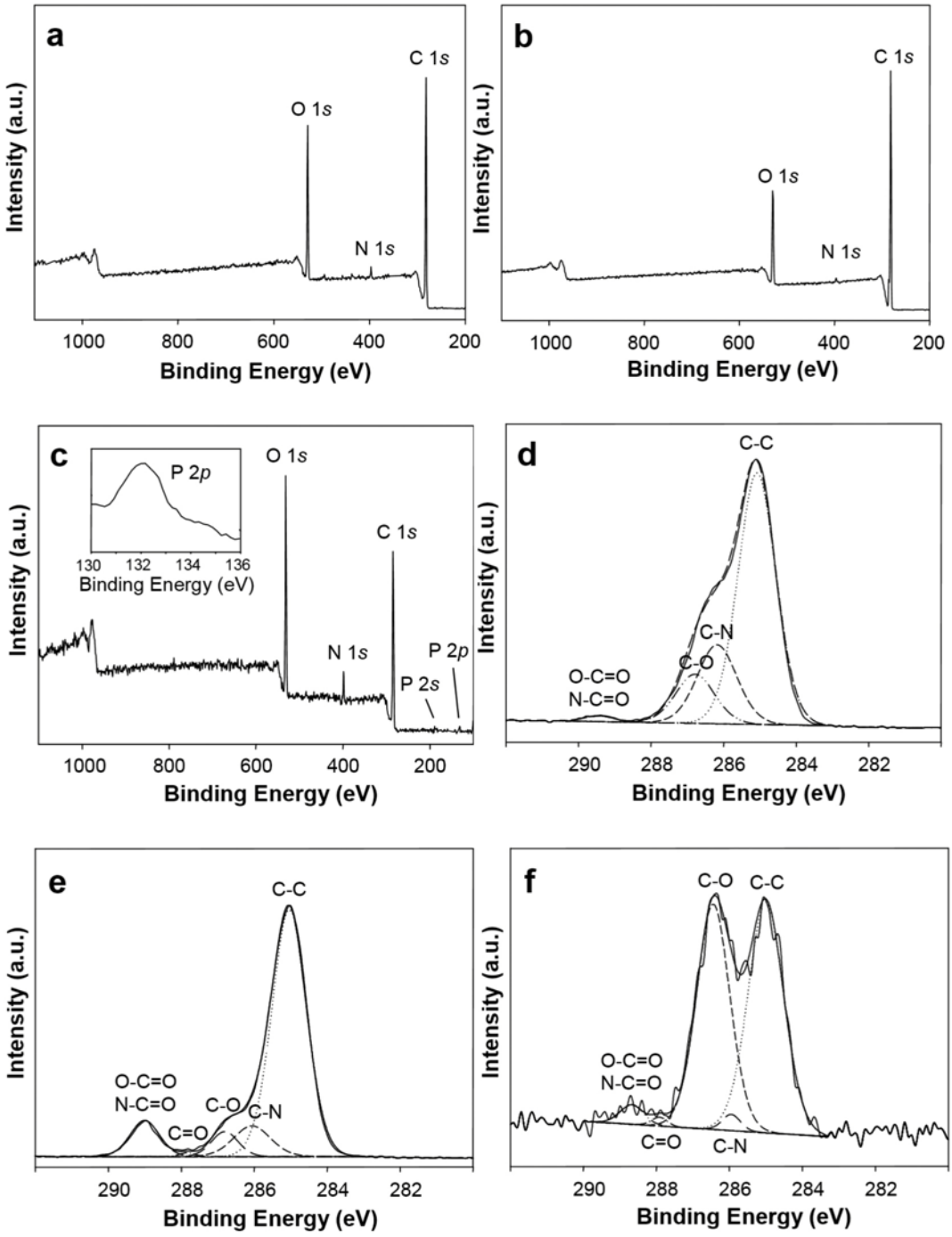


**Figure 4.6.** Survey and high resolution X-ray photoelectron spectroscopy (XPS) of PU modified ePTFE grafts. Survey XPS were performed on the ePTFE graft lumen following (a) surface coating with PU, (b) subsequent isocyanate modification, and (c) $NH_2$–$PEG_{11}$–TPP linker immobilization. Corresponding high resolution C 1*s* XPS were performed on the ePTFE graft lumen following (d) surface coating with PU, (e) subsequent isocyanate modification, and (f) $NH_2$–$PEG_{11}$–TPP linker immobilization.

### 4.2.3. Staudinger Ligation of Azide Probe on ePTFE

A fluorescent azide probe was used to initially assess the specificity of small molecule immobilization by Staudinger Ligation [374]. Rhodamine B and its azide analogue tetramethylrhodamine 5-carbonyl azide (Rh-$N_3$) were reacted in parallel with PU films functionalized with TPP. Following extensive rinsing in methanol, it was evident that only Rh-$N_3$ was covalently immobilized to TPP modified PU films (Figure 4.7a). This result was semi-quantitatively corroborated by UV-Vis spectroscopy (Figure 4.7b), and verified visually on PU-coated ePTFE grafts (Figure 4.7c).

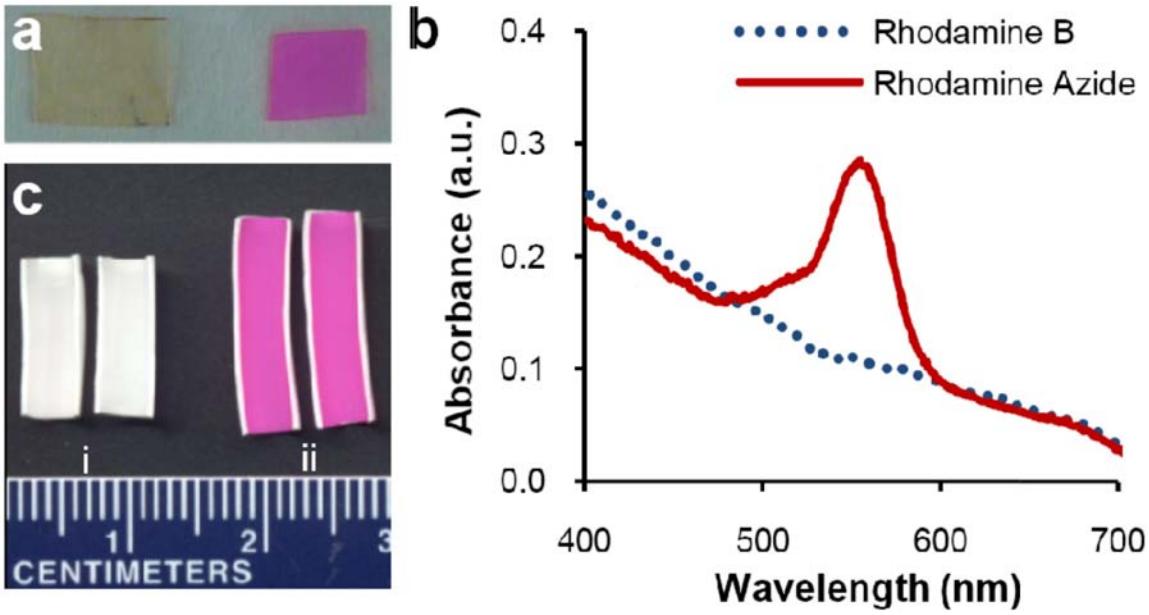


**Figure 4.7.** Feasibility of immobilizing azide probes by Staudinger Ligation on polyurethane films. (a) Visual confirmation of solvent cast PU films derivatized with TPP and reacted with either (left) rhodamine B or (right) rhodamine azide. (b) Solvent cast thin PU films activated with TPP anchor groups were reacted with either rhodamine B or rhodamine azide and analyzed by UV-Vis spectroscopy. (c) En face examination of TPP modified grafts following reaction with (i) rhodamine B or (ii) rhodamine azide and rinsing with methanol.

### 4.2.4. Immobilization of Thrombomodulin

TPP modified grafts were exposed to recombinant TM expressing either a single C-terminal azide moiety (TM-$N_3$) or a native methionine (TM-methionine). Following a phosphate buffered saline (PBS, pH 7.4) rinse for 24 h, the capacity to activate PC was assessed *in vitro*. Grafts reacted with TM-$N_3$ afforded a 30-fold increase in their capacity to activate aPC as compared to grafts incubated with TM-methionine (~0.4 vs ~12 ng aPC $cm^{-2}$ $min^{-1}$, $p<0.01$; Figure 4.8a). The density of covalently bound TM was measured using a horseradish peroxidase (HRP) conjugated antibody that recognizes the human TM $EGF_{5–6}$ domain. Surface density of TM-$N_3$ was ~170 fmol/$cm^2$ after subtracting background binding of antibody to unmodified PU (Figure 4.8b) [375]. The aPC generating capacity reported herein is greater than that previously reported for random immobilization strategies [364, 367]. Since the minimum aPC flux required to inhibit thrombosis has not been established, predicting *in vivo* performance is not feasible.

Biostability was assessed by subjecting TM-modified grafts to PBS at a shear rate of 500 $s^{-1}$ and 37 °C for 24 h, as well as to an additional 2 week period in PBS at 37 °C. Catalytic activity remained nearly constant indicating that covalently immobilized TM-$N_3$ was unaffected by short-term exposure to arterial shear, as well as extended incubation under physiologically relevant pH and temperature conditions (Figure 4.8c). Notably, random amine-crosslinking techniques used to immobilize TM on ePTFE resulted in a 50 % reduction in surface activity following exposure to mechanical shear for 7 hours at 37 °C [376]. Others have reported a ~30 % reduction in activity when TM modified surfaces were subjected to static incubation in PBS at 37 °C for 4 weeks [359].

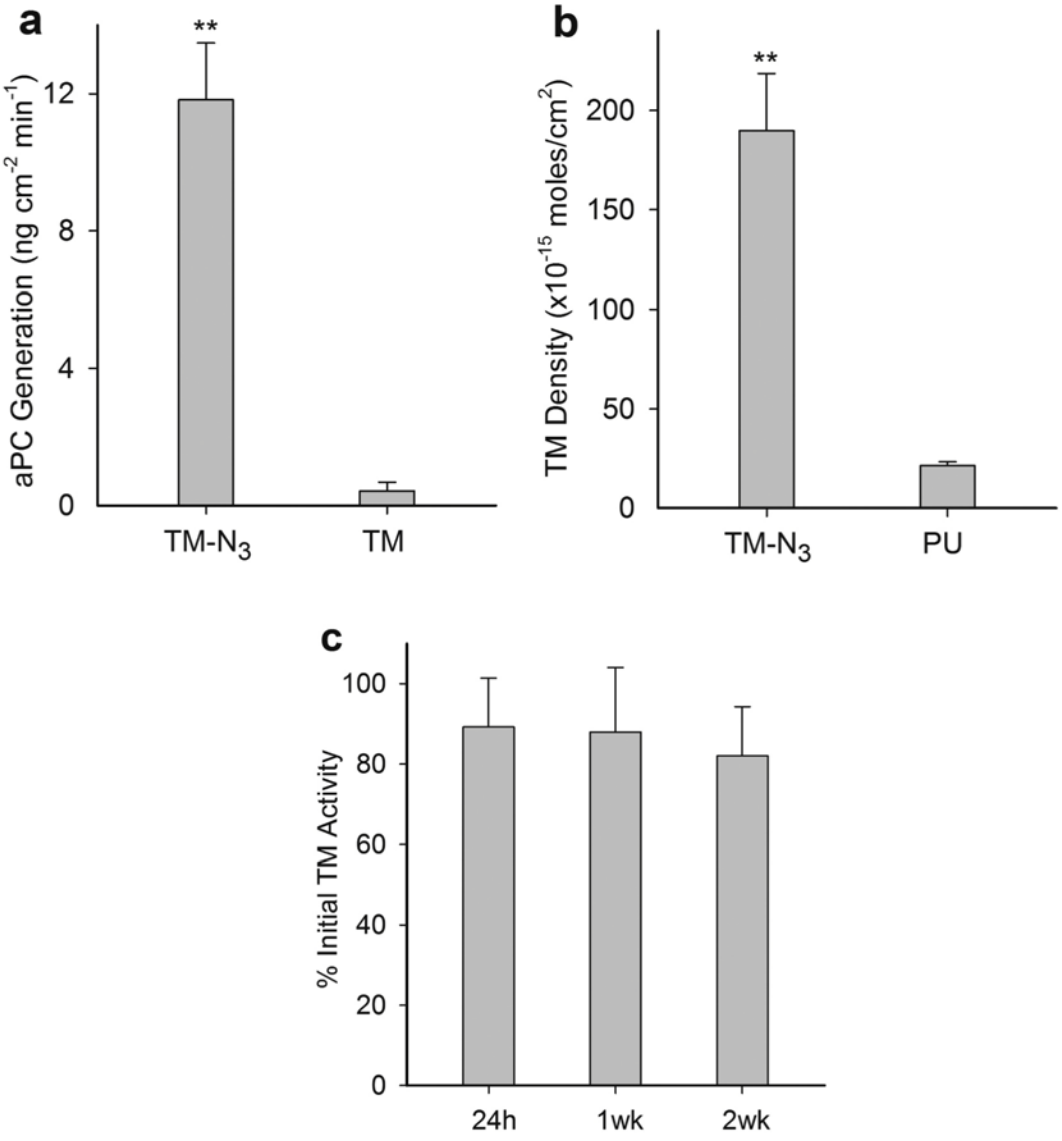


**Figure 4.8.** Measurement of thrombomodulin (TM) cofactor activity to generate aPC, TM surface density, and stability of immobilized TM on modified ePTFE grafts. (a) Catalytic activity of TPP modified ePTFE grafts reacted with recombinant TM expressing a C-terminal azide moiety (TM-$N_3$) or TM containing its native C-terminal methionine. (b) Surface density of TM on grafts was quantified using a TM antibody and compared with background binding of antibody to bare PU coated ePTFE. (c) Graft activity measured as a percentage of initial levels following 24 h of mechanical shear at 500 $s^{-1}$ at 37 °C and subsequent 2-week incubation in PBS at 37 °C. Data represents mean ± standard deviation for $n \geq 3$ samples. Statistical difference ($p < 0.01$) versus control is denoted by a double asterisk.

### 4.2.5. *In Vivo* Performance of ePTFE Grafts Modified with Thrombomodulin

The *ex vivo* femoral arteriovenous shunt model provides a means to assess the thrombogenicity of blood contacting materials under dynamic arterial flow conditions, particularly when implanted in sub-human primates, such as the baboon, whose hemostatic system closely resembles that of man [377-380]. Platelet binding to PU coated PTFE grafts (4 mm i.d.) was assessed using an arteriovenous perfusion chamber and compared to responses observed to unmodified Dacron grafts (Figure 4.9) [195, 378]. Cumulative platelet deposition on PU coated ePTFE was substantially lower than on Dacron grafts (0.0082 vs 1.5 billion/$cm^2$).

Since the level of platelet deposition on PU coated ePTFE grafts is too low to gauge the therapeutic efficacy of immobilized TM, we explored thrombus growth in a perfusion system in which a test graft was interposed between a collagen coated ePTFE graft, as a thrombogenic source, and a distal expansion chamber (Figure 4.10) [377, 378]. TM modified ePTFE grafts reduced platelet deposition in the distal expansion chamber by nearly 50% when compared to unmodified PU coated grafts ($n=4$, $p < 0.05$). Since thrombin is an important physiological agonist for platelet activation [344], the measured reduction of platelet deposition in the distal expansion chamber suggests that substantial levels of aPC are generated from the TM modified surface. In addition to attenuating thrombosis, local generation of aPC may influence the healing characteristics of implanted grafts, as late prosthetic graft failure has been attributed to progressive intimal hyperplasia, a process exacerbated by thrombin and platelet derived pro-inflammatory factors [345, 381].

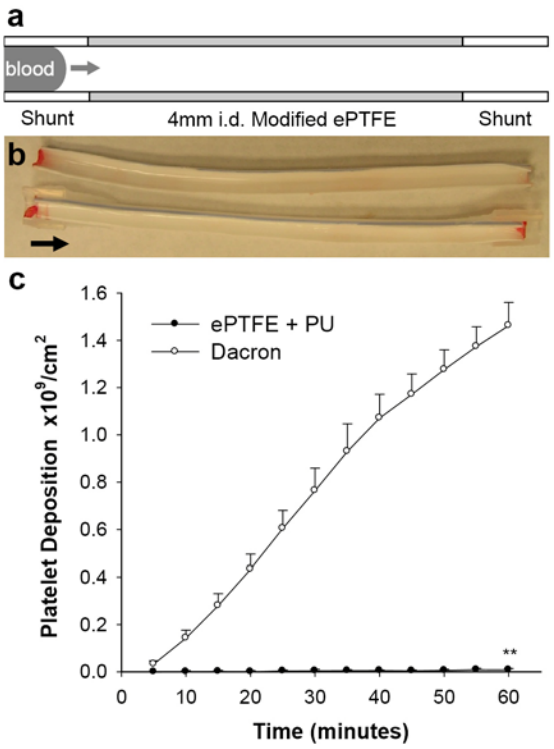


**Figure 4.9.** Real time platelet deposition on modified ePTFE grafts in the absence of an upstream thrombus source in the baboon shunt model. (a) Shunt configuration for testing thrombogenicity of 4 mm i.d. tubular materials. (b) Representative photo of a 7 cm length bare PU coated ePTFE graft split in half lengthwise following 1 h perfusion at 100 mL/min; Arrow points in direction of blood flow. (c) Comparison of platelet deposition on bare PU coated 4 mm i.d. ePTFE (ePTFE + PU) with plain 4 mm i.d. Dacron grafts. Each data point represents mean ± standard deviation for $n \geq 3$ samples. Statistical difference ($p < 0.01$) is denoted by double asterisk.

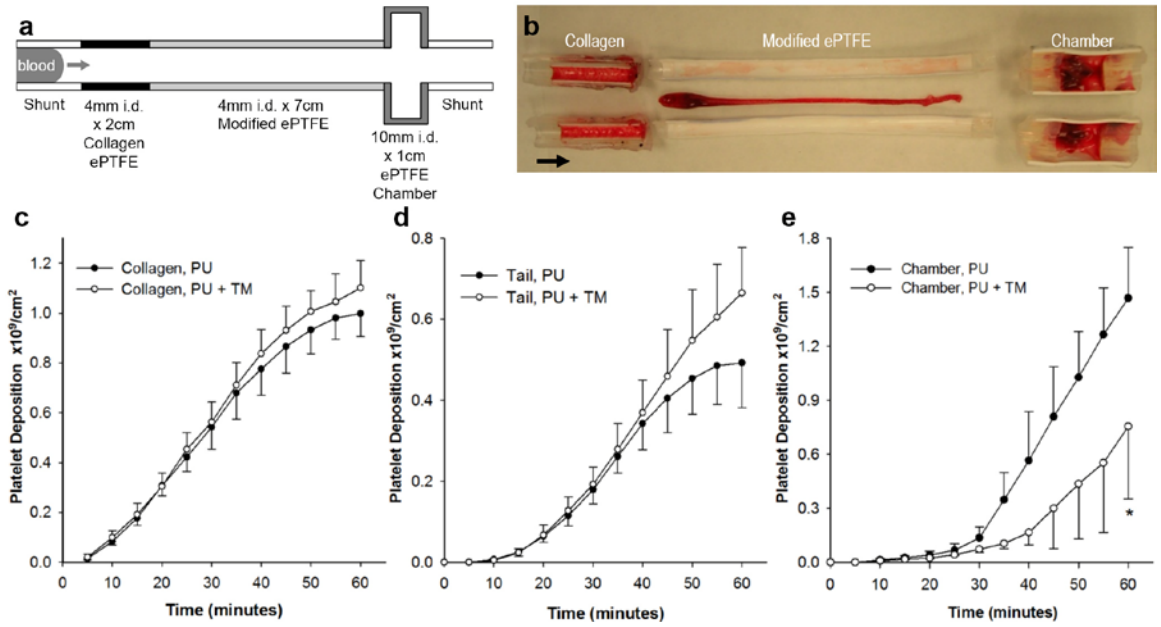


**Figure 4.10.** The biological function of TM modified ePTFE grafts was evaluated using a three-compartment thrombogenic device inserted into chronic arteriovenous shunts in baboons. (a) A 2 cm x 4 mm inner diameter (i.d.) segment of collagen coated ePTFE serving as a thrombin source was connected upstream of a 7 cm x 4 mm i.d. segment of test graft, and the therapeutic function of aPC generated *in situ* was detected in a 1 cm x 10 mm i.d. distal expansion chamber. Arrow points in direction of blood flow. (b) Representative photograph of the entire chamber assembly that tested a 7 cm TM modified ePTFE graft split in half lengthwise following perfusion for 1 h at 100 mL/min. Arrow points in direction of blood flow. Real-time platelet deposition (c) in the upstream collagen coated 4 mm i.d. ePTFE segment; (d) in the thrombus tail developing distal to collagen coated ePTFE; and (e) in the 10 mm i.d. expansion chamber distal to TM modified ePTFE grafts (PU + TM) compared with bare PU coated ePTFE controls. Each data point represents mean ± standard deviation of 4 independent studies. Statistical difference ($p < 0.05$) is denoted by single asterisk.

## 4.3. Conclusions

We have presented a biomimetic surface engineering approach that combines molecular engineering and orthogonal chemistry strategies to site-specifically functionalize clinical vascular prostheses with recombinant human TM that exhibit biocatalytic activity and biostability *in vitro*. Moreover, we have devised and tested a robust, clinically relevant *in vivo* model of vascular graft thrombosis in non-human primates that facilitated evaluation of the therapeutic function of bioactive TM surface assemblies. The data presented herein indicate that biologically active TM surface assemblies reduces the thrombogenic properties of blood contacting surfaces despite the presence of an upstream thrombin generating stimulus. The modular nature of heterobifunctional linker design, combined with recent advances in chemoselective techniques to modify peptides and proteins [382, 383], will undoubtedly expand the utility of bioenzyme surface assemblies to a range of clinically important host-material interfaces.

## 4.4. Methods

### 4.4.1. Expression of TM-$N_3$ and TM-methionine

All reagents were purchased from Sigma-Aldrich, St Louis and used without further purification unless otherwise noted. Expression and purification of recombinant TM-methionine and TM-$N_3$ are similar to a previous report [384]. A fresh LB agar plate was streaked with methionine auxotrophic cells containing the appropriate TM vector and incubated at 37 °C overnight. Next, a single cell colony was inoculated into 50 ml of Novagen media supplemented with 0.4% glucose and 50 μg/ml ampicillin (Calbiochem) and cultured at 37 °C, 225 RPM, for 16 h. 25 ml of fully grown starter culture (OD600 =

1.20) was added per 500 ml of Novagen media (Overnight Express Autoinduction System, Novagen) supplemented with 0.4% glucose and 50 μg/ml ampicillin, and cultured at 37 °C, 225 RPM. Upon cell growth to OD600 = ~0.9, IPTG was added at a final concentration of 1mM to induce TM-methionine expression. After 4 h at 37 °C, the cells were sedimented by centrifugation for 25 min at 1650 RCF at 4 °C. Alternatively, TM-$N_3$ was generated by spinning down the initial OD600 = 0.9 cells culture to obtain a cell pellet which is resuspended in fresh Novagen media lacking methionine. After incubation at 37 °C, 225 RPM for 20 minutes for cells to exhaust residual methionine from the media, azidohomoalanine was added at a final concentration of 100 mg/L culture, and IPTG was added at a final concentration for 1 mM, the expression was induced for 4 h at 37 °C, 225 RPM.

The collected cell pellets were stored at 4C overnight and their periplasmic proteins extracted by osmotic shock protocol. Cell pellets were warmed to room temperature and re-suspended in 40 ml/g cells of 0.5 M Sucrose, 0.03 M Tris-HCl (pH 8.0) at a final pH of 8.0 per gram of cells. Suspended cells were evenly distributed into round bottom centrifuge tubes (60 mL per tube). 120 μL of 500 mM sucrose was added to each tube to achieve final 1mM EDTA concentration and incubate with gentle shaking for 10 minutes at RT. The cell suspension was centrifuged at 3,500x RCF for 10 min at 10 °C, and the supernatant was decanted. The cell pellet was rapidly resuspended in 25 ml/g cell pellet ice-cold, distilled water (40 mL per tube is sufficient) for 10 minutes, and the cell suspension was centrifuged at 3,500x RCF for 10 min at 4 °C. 35ml of supernatant was removed per tube immediately and transferred to clean round bottom centrifuge tubes. These were clarified by further centrifugation at 25,000x RCF for 25

min at 4°C, and sterilized using a 0.22 µm filtration system. Anti-FLAG immunoaffinity chromatography (Sigma) was performed on the clarified supernatant per manufacturer's instructions. SDS-PAGE analysis, and total protein quantification were performed using standard Bradford assay (Biorad) following protocols from the manufacturer.

### 4.4.2. Synthesis of $NH_2$–$PEG_{11}$–TPP

$NH_2$–$PEG_{11}$–TPP was synthesized by reaction of *O*-(2-aminoethyl)-*O'*-[2-(Boc-amino)ethyl]decaethylene glycol with a pentafluorophenyl ester of triphenylphosphine 3 shown in Figure 3.11 (TPP) [374] in $CH_2Cl_2$ and 3 equiv 2,6-lutidine at 25 °C for 12 h, followed by removal of the Boc protecting group using $CF_3COOH$ and purification by column chromatography.

Synthesis of Iodo-derivative 2

A solution of $NaNO_2$ (0.90 g, 13 mmol) in 5 ml of $H_2O$ was added dropwise to a solution of 1-methyl-2-aminoterephthalate (**1** Aldrich # 393673) (2.5 g, 12.8 mmol) in 25 ml of cold concentrated HCl. The mixture was stirred for 30 min at room temperature and then filtered through glass wool into a solution of KI (10 g, 60.2 mmol) in 15 mL of $H_2O$. The dark red solution was stirred for 1 hour and then diluted with $CH_2Cl_2$ (200 ml) and washed with saturated $Na_2SO_3$ (2 x 20 ml). The organic layer was washed with water (2 x 20 ml) and saturated NaCl (1 x 20 ml). The combined aqueous layers were back extracted with $CH_2Cl_2$ (40 ml). The combined organic layers were dried over $Na_2SO_4$ and concentrated. The crude product was dissolved in a minimum amount of MeOH and $H_2O$ was added until the solution appeared slightly cloudy. Cooling to 4 °C and subsequent filtration afforded 2.8 g (70%) of a yellow solid.

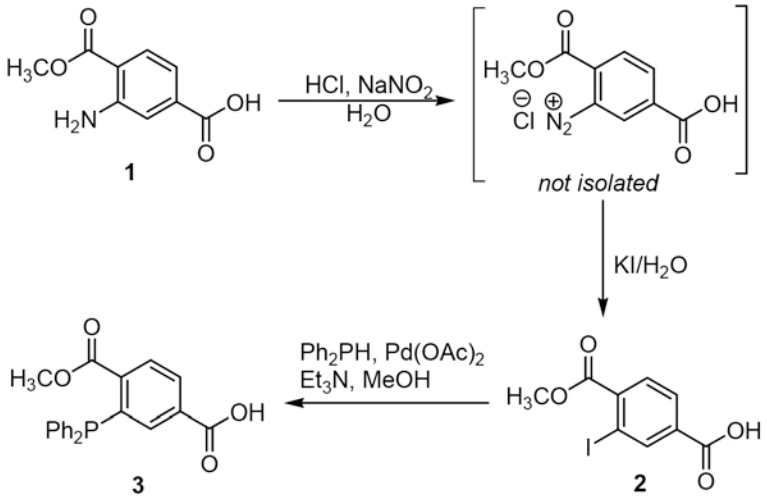


**Figure 4.11.** Synthesis of triphenylphosphine 3

Synthesis of triphenylphosphine 3

To a flame-dried flask was added **2** (300 mg, 1.00 mmol), dry MeOH (3 ml), triethylamine (0.3 ml, 2 mmol), and palladium acetate (2.2 mg, 0.010 mmol). While stirring under an atmosphere of Ar, diphenylphosphine (0.17 ml, 1.0 mmol) was added to the flask by means of a syringe. The resulting solution was heated at reflux overnight, and then allowed to cool to room temperature and concentrated. The residue was dissolved in 250 ml of a 1:1 mixture of $CH_2Cl_2/H_2O$ and the layers were separated. The organic layer was washed with 1 M HCl (1 x 10 ml) and concentrated. The crude product was dissolved in a minimum amount of methanol and an equal amount of $H_2O$ was added. The solution was cooled to 4 $^oC$ for 2 hours and the resulting solid was collected by filtration. The pure product 3 (Figure 4.11) was isolated. $^1$H-NMR ($CDCl_3$, 400 MHz) $\delta$ 3.75 (s, 3H), 7.28-7.35 (m, 11H), 7.63-7.67 (m, 1.5 Hz, 1H), 8.04-8.07 (m, 1.5 Hz,1H). HRMS (ESI): Calculated for $C_{21}H_{18}O_4P$: 365.0943 $[M+H]^+$; found 365.0923.

Synthesis of PFP-activated ester of triphenylphosphine

The triarylphosphine derivative **3** was converted to the corresponding PFP activated ester **4** in Figure 4.12.

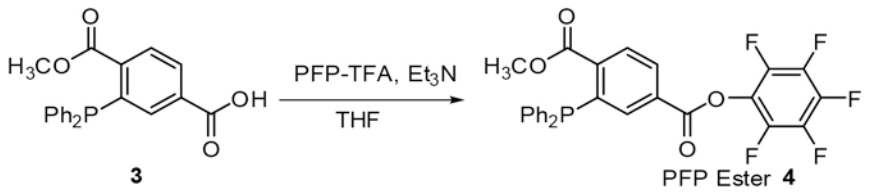


**Figure 4.12.** Synthesis of PFP activated ester **4**

Synthesis of PFP-active ester 4

Triarylphosphine **3** (300 mg, 0.82 mmol) was dissolved in THF (6.4 mL) under argon. Triethylamine (167 mg, 1.65 mmol) was added, followed by a drop-wise addition of pentafluorophenyl trifluoroacetate (Aldrich# 377074, 277 mg, 0.99 mmol) over a period of 2 minutes. The reaction was stirred at room temperature for 30 minutes and then concentrated. Purification by silica gel chromatography (1:1 ethyl acetate:hexanes) afforded phosphine-PFP **4** (300 mg, 69% yield) as a solid. IR (thin film): 1766, 1725, 1521, 1052 $cm^{-1}$. $^{1}H$ NMR (400 MHz, CDCl3): $\delta$ 3.68 (s, 3H), 7.38-7.32 (m, 10H), 7.71 (t, 1H, $J$ = 3.9), 8.08 (app t, 2H, $J$ = 3.0); $^{13}C$ NMR (75 MHz, CDCl3): *d* 15.29, 30.02, 52.76, 66.26, 125.24, 129.05, 129.50, 129.86, 130.29, 131.26, 132.18, 134.18, 136.71, 136.84, 138.23, 139.78, 141.60, 142.87, 142.94, 161.99, 166.75; HRMS (ESI): Calculated for $C_{27}H_{17}O_4PF_5$: 531.0779 $[M+H]^+$; found 531.0774. The activated ester **4** can be used for the amide coupling reaction with various PEG linkers to form the corresponding PEG-Phosphine derivatives.

Synthesis of $NH_2$–$PEG_{11}$–TPP Linker

PFP active ester **4** when reacted with amino-d$PEG_{12}$-*t*-boc-amine **5**, an amide bond formation takes place to afford the compound **6**. Subsequent removal of Boc group by reaction with TFA provided the desired $NH_2$–$PEG_{11}$–TPP **7**. The chemical scheme and experimental procedure are outlined in Figure 4.13 below. PFP-ester **4** (312 mg, 0.587 mmol) and amino-$PEG_{12}$- *t*-boc-amine **5** (Aldrich# 77090, 315 mg, 0.489 mmol) were dissolved in 4 mL of $CH_2Cl_2$ and 2,6-lutidine (204 ul, 3 equiv.) was added under argon at room temperature. The resulting mixture was stirred for 12 h at room temperature. Solvent was evaporated under vacuum and the residue was purified by column chromatography to afford the product **6** as pale yellow oil.

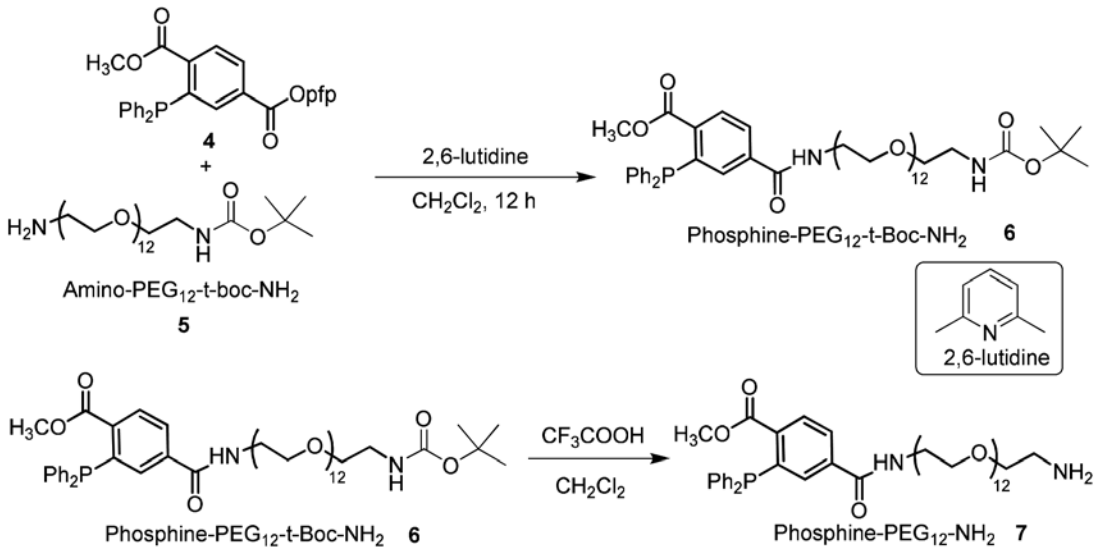


**Figure 4.13.** Synthesis of $NH_2$–$PEG_{11}$–triphenylphosphine

Removal of Boc group

To the stirred solution of compound **6** in $CH_2Cl_2$ (0.7 ml/1 mmol) was added $CF_3COOH$ (0.7 ml/1 mmol). The resultant mixture was stirred at room temperature for 4 h. After this time, the volatiles were removed under vacuum and the crude product was

dissolved in $CH_2Cl_2$, washed with $NaHCO_3$, brine and dried ($Na_2SO_4$). Purification by column chromatography afforded the desired product in 79-81% yield in 2 steps. $^1H$ NMR (400 MHz, $CDCl_3$): $\delta$ 8.10 (dd, 1H, J = 3.6, 8), 7.83 (dd, 1H, J = 1.6, 8.4), 7.39-7.28 (m, 11H), 6.81 (m, 1H), 3.80 (brs, 2H), 3.76 (s, 3H), 3.70-3.49 (m, 46H), 2.97 (t, 2H, J = 5.2). HRMS (ESI): Calculated for $C_{45}H_{68}N_2O_{14}P$: 891.4408 $[M+H]^+$; found 891.4396.

### 4.4.3. Modification of ePTFE Grafts

A 5% w/v solution of Elasthane 80A (Polymer Tech, Berkeley) in *N*,*N*-dimethylformamide (DMF) was prepared by dissolving pellets with vigorous shaking for 24 hours at room temperature. The PU solution was extravasated through 4 mm i.d. ePTFE thin wall vascular grafts (Bard, Tempe) that is clamped shut at one end by forcing the solution through the graft pores using a 3 ml standard Luer lock syringe. Following extravasation, the coated graft segment was drained of excess PU solution and dried under vacuum at 60 °C for 20 min by hanging the graft segment on a rack using alligator clips. Additional PU was deposited in multiple flow-through/drying cycles over the base layer, and dried overnight under vacuum at 60 °C. The final coating should appear shiny and clear and completely covers the luminal surface of the ePTFE graft.

PU coated graft segments were inserted into tubular reactors as depicted in Figure 4.5 and rotated at 500rpm for surface reactions. Each reactor was fabricated using acetone/ethanol cleaned tubing parts obtained from McMaster Carr. To ensure complete sealing, barbed plugs were inserted at the ends of the reactor chamber one end at a time. To modify the PU coating on grafts, HDI (16% v/v) and TEA (4% v/v) solution in anhydrous toluene was added to the chamber and rotated at 50 °C for 1 h. After this step,

the graft was removed from the chamber and rinsed in anhydrous toluene for 6 h with 1 exchange of fresh wash toluene. Isocyanate activated grafts were then reacted in the same reactor setup constructed with fresh parts with $NH_2$–$PEG_{11}$–TPP linker (10 mg/mL) and TEA (1% v/v) in anhydrous toluene at 40 °C overnight, rinsed with toluene for 6 h, and dried under vacuum at 25 °C overnight. TPP activated grafts were reacted with a 1 mg/mL dilution of tetramethylrhodamine-5-carbonyl azide (Invitrogen, Carlsbad) in 1:4 tert-butanol/PBS at 37 °C for 24 h followed by rinsing in multiple exchanges of methanol for 24 h, or reacted with 20 µM TM-$N_3$ in PBS at 37 °C for 24 h and rinsed with 50ml PBS in a Falcon tube under constant rotation for 24 h. Grafts coated with PU and activated with TPP were reacted with rhodamine B or TM-methionine as controls.

### 4.4.4. Modification of Polyurethane Films

Thin clear PU films were solvent cast by drying 12.5 % w/v Elasthane 80A in DMF for 24 h at 60 °C on an acetone/ethanol cleaned glass Petri dish under vacuum. The films were removed with a razor and cut into rectangular test samples. Films were subjected to isocyanate, TPP, and rhodamine reactions in a glass vial. Briefly, PU films were immersed in dry toluene solution containing HDI (16 % v/v) and TEA (4 % v/v) at 50 °C for 1 h and rinsed in toluene for 6 h. The films were then immersed in dry toluene containing 10mg/mL $NH_2$–$PEG_{11}$–TPP linker and 1 % TEA and toluene at 40 °C overnight, rinsed with toluene for 6 h, and dried under vacuum at 25 °C overnight. TPP activated films were reacted with 1 mg/mL tetramethylrhodamine-5-carbonyl azide (Invitrogen, Carlsbad) in 1:4 tert-butanol/PBS at 37 °C for 24 h followed by rinsing in multiple exchanges of methanol under vigorous shaking for 24 h.

Rhodamine modified thin films were characterized by UV-Vis spectroscopy (Cary 50 Bio UV-visible spectrophotometer, Varian) using a jig built in-house. An adaptor for the UV-Vis spectrometer was redesigned to hold the film segment in place between two quartz slide pieces. UV-Vis spectroscopy was performed on plain solvent cast PU films, PU films modified with TPP, and TPP modified films reacted with either rhodamine-azide or control rhodamine B.

### 4.4.5. Surface Analysis

An in-lens field-emission SEM (ISI DS-130F Schottky Field Emission SEM) operated at 10 kV was used to examine the graft luminal surface. Graft samples were first prepared by cutting with a razor blade to expose the luminal surface as well as the cross section of the graft wall, and sputter coated with gold.

Light microscopy images of serial thin sections of modified grafts were used to determine PU thickness. Samples were prepared by manually cutting graft segments into ~ 0.5 mm thick rings, which were mounted on a glass slide and imaged by standard light microscopy. Due to the opaqueness of the ePTFE graft component, visualization of the clear PU coating was achieved by focusing the image at the surface of the coating.

ATR-IR spectra were acquired using a FTS-4000 FT-IR spectrometer (Bio-Rad, Hercules) equipped with a wide-band MCT detector, collected with 100 scans at 2 $cm^{-1}$ resolution. XPS data were recorded on an Axis Ultra X-ray photoelectron spectrometer (Kratos Analyticals, UK) equipped with a monochromatized Al Kα X-ray source.

### 4.4.6. TM Graft Cofactor Activity Assay

A 4 mm graft segment was cut using a clean razor blade from the fabricated TM grafts, and incubated in 200 µL of 0.2 µM human protein C (Calbiochem, Gibbstown), 5

mM calcium chloride, and 2 nM human α-thrombin (Haematologic Technologies, Essex Junction) in Tris buffer (20 mM Tris, 100 mM NaCl, pH 7.5) with 0.1% bovine serum albumin (BSA) at 37 °C for 1 h, and quenched with 2 IU/mL human anti-thrombin III (American Diagnostica, Stamford) for 5 min. The generation of aPC was quantified using 0.2 mM of an enzymatically digestible chromogenic substrate, Spectrozyme PCa (American Diagnostica). TM activity was assayed after grafts were exposed for 24 h to PBS at 37 °C and 500 $s^{-1}$ shear, as well as after incubation in PBS with 0.02% sodium azide at 37 °C over a two week period.

### 4.4.7. Determination of TM Surface Density

All assay reactions were run in a 96-well plate, per manufacturer's instructions (American Diagnostica, Stamford). Moles of $EGF_{5-6}$ domains bound to test grafts were calculated by a standard curve generated by ELISA using known concentrations of TM provided by the manufacturer. At the end of each assay, graft segments were flattened between glass slides and scanned at 600 dpi using a HP ScanJet 5370C scanner and the reactive area of each test sample was measured using ImageJ software. Representative images of graft samples tested are provided in Fig. 4.14.

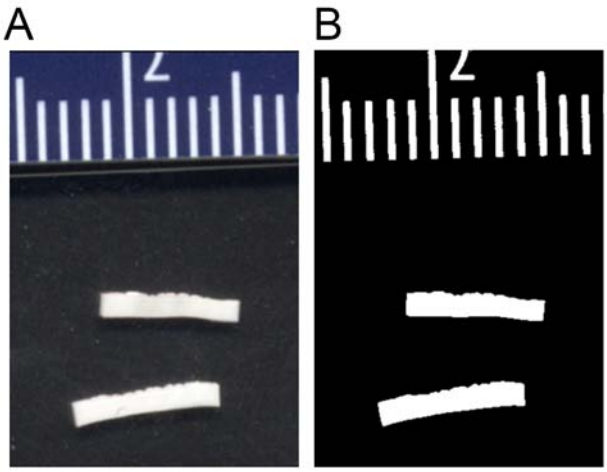


**Figure 4.14.** Representative image of graft segments used for measuring TM surface density. (A) 600dpi image generated using a scanner; (B) ImageJ software was used to convert images to 8-bit and the threshold was adjusted to 165 for area measurement.

### 4.4.8. *In Vivo* Baboon Arteriovenous Shunt Model

*In vivo* functional capacity of TM modified ePTFE grafts were evaluated as previously described [195, 378]. All studies were approved by the Institutional Animal Care and Use Committee at Oregon Health and Science University. Grafts were interposed into a permanent Silastic arteriovenous shunt that had been surgically implanted between the femoral artery and vein in male Baboons (*Papio papio*). Circulating platelet concentrations averaged ~300,000 platelets/μL. Ketamine hydrochloride (10 mg/kg intramuscularly) was given as a preanesthetic agent, and the operation was performed under general 1% halothane anesthesia. Mean blood flow rate through the shunt was measured continuously using a Doppler ultrasonic flow meter and held constant by an external screw clamp at 100 mL/min.

Autologous platelets were radiolabeled one day prior to shunt study with Indium-111 oxine and re-injected into the baboon. Forty-five milliliters of whole blood were initially withdrawn into syringes containing 5 mL of 3.8% sodium citrate anticoagulant.

The blood was centrifuged at 160 RCF for 15 min and the platelet rich plasma (PRP) transferred to a 50 mL sterile tube to which was added PGE1 to a final concentration of 4 ng/mL PRP and centrifuged at 1500 RCF for 25 min. The platelet pellet was resuspended in plasma to a platelet concentration of $1\times10^{10}$ and 1000 μCi of indium-111 tropolone ($^{111}InCl_3$, Amersham Co.) was added to the platelet suspension. Following 10 min incubation at room temperature, 3 mL of platelet-poor plasma was added and the platelets were incubated for an additional 2 min. A small aliquot was removed to determine labeling efficiency and the PRP was centrifuged at 1500g for 10 min to remove excess $^{111}In$. The platelets were resuspended in 5 mL of reserved plasma and reinjected into the baboon. Platelet function is not altered by this technique, when studied by either thrombin stimulated platelet release of $^{14}C$ serotonin or by morphological studies of dense body distribution. Platelet labeling efficiency ranged between 80% and 90%.

Platelet deposition in the individual compartments of the shunt assembly was measured over a 60-minute perfusion period using a high sensitivity 99Tc collimator and scintillation camera (GE 400T, General Electric) imaging of the 172 keV $^{111}In$ g photon peak at 5-min intervals [195]. Immediately before imaging, a 5 min image was acquired of a 3 mL blood sample (blood standard). Images were obtained continuously with data storage at 5 min intervals.

Deposited $^{111}In$-platelet activity was calculated by subtracting the blood standard activity from all dynamic study images. Data were converted, at each time point, to total platelet deposition per unit test surface, as follows:

$$\frac{Platelets}{area} = \frac{[measured\ activity\ (cpm) - \ background\ activity\ (cpm)] \times platelets/ml}{blood\ specific\ activity\ (\frac{cpm}{ml})}$$

where

$$blood\ specific\ activity$$

$$= \frac{[blood\ std\ (cpm) - \ background\ activity\ (cpm)] \times (^{111}In\ fraction\ in\ platelets)}{vol\ of\ blood\ std\ (ml)}$$

### 4.4.9. Statistical Analysis

Two-tailed student's *t*-test assuming unequal variances was used to test for statistical significance between the means of two groups.

# CHAPTER 5

# IMMOBILIZATION OF ACTIVELY THROMBORESISTANT ASSEMBLIES ON STERILE BLOOD CONTACTING SURFACES

In this Chapter, we describe our efforts to optimize the production of azide-tagged thrombomodulin (TM), as well as surface chemistry schemes that would enable the site-specific immobilization of TM in a manner that facilitates terminal sterilization of medical device surfaces. Through this process we developed a general method to conjugate a single azide motif to the C-terminus of TM using the bacteria transpeptidase Sortase A. This approach facilitates expression of TM without the use of non-natural azido-tagged amino acid analogues, and is compatible with eukaryotic expression systems typically used in the biopharmaceutical industry. Moreover, we developed a surface modification strategy whereby sterically strained cyclooctyne motifs covalently immobilized on the luminal surface of 4 mm i.d. ePTFE grafts retained their capacity undergo [3+2] cycloaddition with azide-tagged TM after ethylene oxide sterilization, the current industry standard used in sterilization of synthetic vascular grafts. We demonstrated for the first time the superior efficacy of TM to reduce the level of local platelet deposition than commercial heparin modified grafts using a novel A-V shunt model in nonhuman primates, which more closely mimics the thrombotic stresses encountered during and immediately after surgical implantation.

## 5.1. Introduction

All artificial organ systems and medical devices that operate in direct contact with blood elicit activation of coagulation and platelets with long-term use [11, 12], often

necessitating antithrombotic therapies that carry significant cost and bleeding risk [1, 2]. Since the clinical inception of fabric grafts in 1952, none of the existing synthetic arterial substitutes perform comparably to autologous conduits in small-caliber (< 6 mm) revascularization procedures central to the field of cardiac, vascular, and plastic surgery [3]. Poor clinical outcomes are driven by blood-material and tissue-material interactions that include rapid thrombotic occlusion, restenosis due to biomechanical mismatch, as well as impaired reendothelialization due to a persistent foreign body response to synthetic materials many years after implantation [4]. Despite advances in tissue engineering approaches that have yielded biomaterials that mimic the bulk properties of native tissue and promote healing [5-7], a generally accepted blood compatible material does not exist [8].

Physiological onset of thrombosis hinges on the generation of thrombin, a central mediator that amplifies the intrinsic coagulation cascade, crosslinks fibrin, and activates platelets [9, 10]. Biomimetic surface engineering approaches that reconstitute the natural mechanism of endothelial cells to attenuate thrombin production, such as heparin and thrombomodulin, have yielded promising results [8, 11, 12]. First demonstrated in 1963 [13], heparin immobilization has been hypothesized to mimic the antithrombin activity of cell surface heparan sulfate proteglycans (HSPG) expressed by the endothelium [14]. The physiological role of heparin, produced primarily by mast cells, in hemostasis remains unclear [15] as the majority of anticoagulantly active HSPG is not in direct contact with flowing blood [16] and knock-out mice lacking the specific pentasaccharide sequence that inhibits thrombin do not exhibit a procoagulant phenotype [17]. In contrast, thrombomodulin (TM) is a major vasculoprotective molecule localized on the

endothelial cell surface, and overwhelming evidence indicates that defects therein increase the risk of inflammatory disorders and thromboembolism [18]. TM sequesters thrombin's prothrombotic activity and accelerates thrombin's ability to activate protein C (APC) by 1000-fold, which inhibits upstream proteases necessary for amplifying thrombin production and represents the primary physiological mechanism by the endothelium to regulate hemostasis [19].

Clinical implementation of strategies reported to date on the immobilization TM has been primarily limited by two main factors: the inherent reduction in activity associated with schemes that non-specifically react with free amino, carboxyl, or thiol motifs contained near the catalytically active site [230, 233, 358-360, 376, 385], and the necessity for terminal sterilization by industry standards, which mainly comprise ethylene oxide and radiation that may disrupt the chemical structure and activity of surface-bound biomolecules [386-388]. We were first to demonstrate a bioorthogonal strategy to site-specifically tether recombinant human TM via a single C-terminal azide motif by Staudinger Ligation on the luminal surface of 4 mm i.d. expanded poly(tetrafluoroethylene) (ePTFE) grafts, and validated the biological activity of TM to reduce thrombosis in a nonhuman primate model [389]. However, auxotrophic incorporation of a single non-canonical azido-alanine in TM is difficult to implement at industry scales, and restricts the scope of suitable candidate enzymes for surface immobilization to those with a single C-terminal methionine. In this work, we first optimized the production of TM-$N_3$ using a general enzymatic transpeptidation approach with an evolved mutant of *S. Aureus* sortase A (SrtA) exhibiting 140-fold higher catalytic activity than wild-type. We then demonstrated a surface chemistry platform using strain-

promoted [3+2] cycloaddition that facilitates terminal sterilization by ethylene oxide, and validated the superior *in vivo* thromboresistant characteristics of thrombomodulin compared with commercially available heparin modified ePTFE grafts.

## 5.2. Results and Discussion

### 5.2.1. Sortase-catalyzed Tagging of Thrombomodulin with Azide

As a replacement for auxotrophic incorporation of non-canonical azide-tagged amino acids to produce TM-$N_3$, we first benchmarked a site-specific protein labeling system using the *S. Aureus* sortase A (SrtA). SrtA is a calcium-dependent cysteine transpeptidase that anchors proteins containing a C-terminal LPXTG motif (where X denotes any amino acid) by breaking the threonine-glycine bond and forming a new amide bond with the nucleophilic group of the pentaglycine portion of lipid II [390-392]. However, the low catalytic activity of wild type (WT) SrtA ($k_{cat}/K_{m\ LPETG} \sim 200\ M^{-1}\ s^{-1}$) has necessitated high molar excess of enzyme and long reaction times [393]. Recently, the development of a general yeast display system has facilitated directed evolution of WT SrtA to generate a pentamutant SrtA variant (5' SrtA) which exhibited 140-fold increase in catalytic activity [394]. We hypothesized that the incorporation of a small LPETG motif at the C-terminus of TM would not affect its catalytic activity, and would facilitate the tagging of pentaglycine modified probes that contain bioorthogonal handles such as biotin, as outlined Figure 5.1 below.

In our initial effort, we expressed a recombinant human TM fragment containing the minimal fragment for antithrombotic activity (TM456) [235, 395] and a single C-terminal LPETG motif ($TM_{LPETG}$) in the periplasm of *E Coli* (Figure 5.2), and purified by immunoaffinity chromatography. $TM_{LPETG}$ exhibited no difference in its catalytic

activity to generate activated protein C in the presence of thrombin and calcium relative to previous batches of TM456 generated in our lab [235]. Detailed sequence of the $TM_{LPETG}$ and mutations are provided in the methods section.

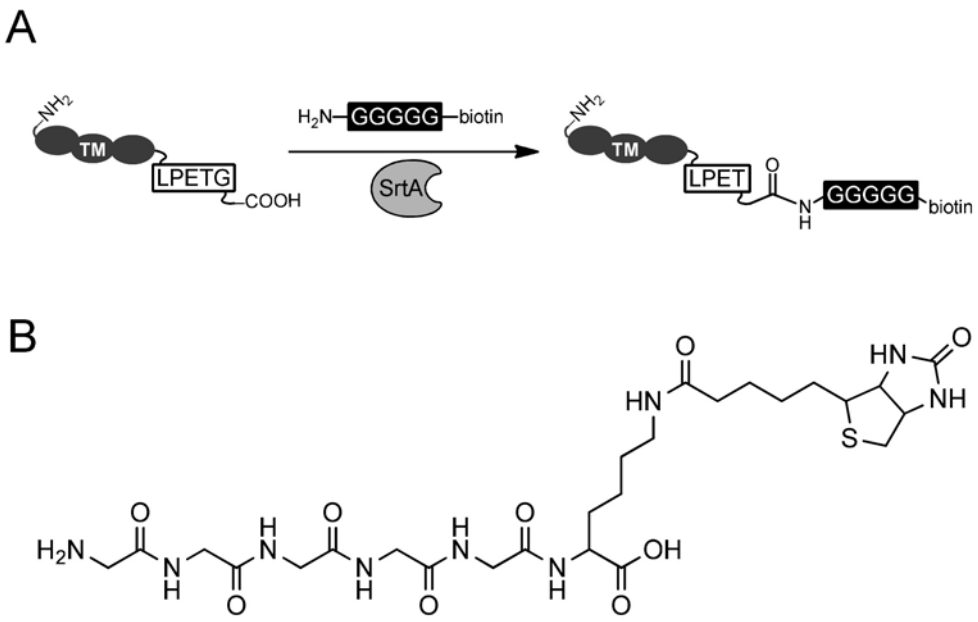


**Figure 5.1.** (A) Sortase catalyzed transpeptidation of biotinylated pentaglycine peptide to the C-terminus of thrombomodulin (TM). (B) Chemical structure of the $NH_2$-$Gly_5$-Lys-biotin peptide.

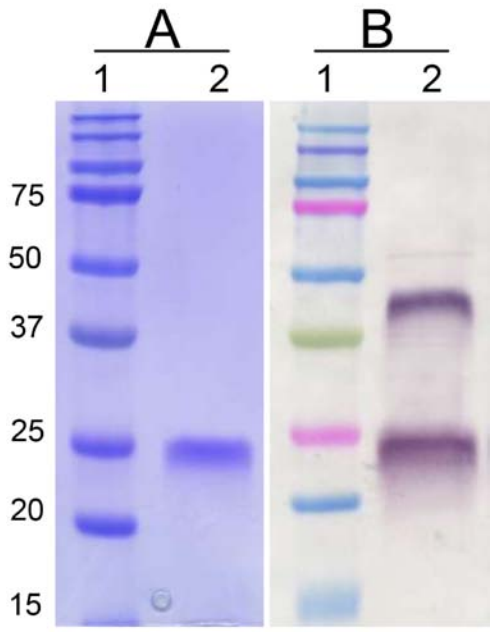


**Figure 5.2.** (A) SDS-PAGE gel tracking of FLAG-tagged $TM_{LPETG}$ purification by anti-FLAG immunoaffinity chromatography. Lanes: 1 – MW markers, 2 – $TM_{LPETG}$. (B) Western blot of purified $TM_{LPETG}$ using an antibody that recognizes TM456. Lanes: 1 – MW markers, 2 – $TM_{LPETG}$.

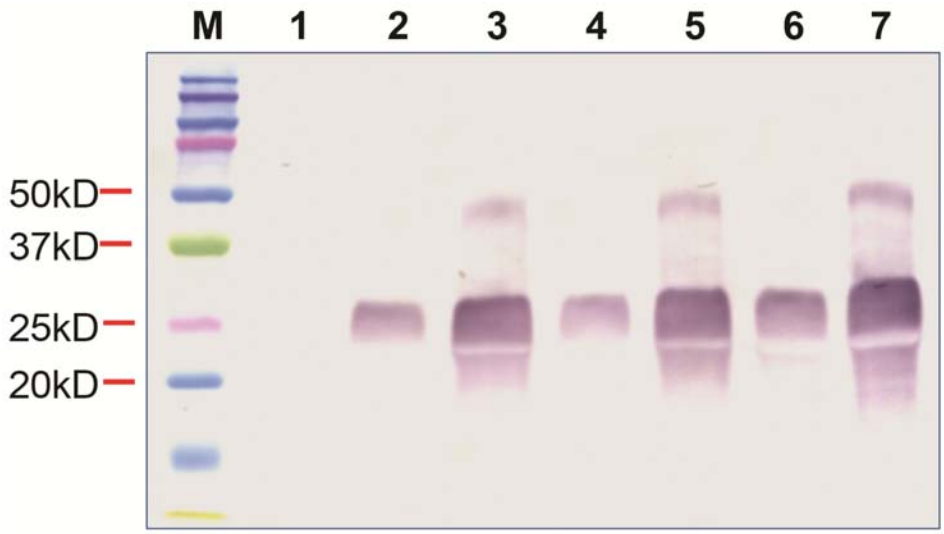


| Lane | TM | SrtA | GGG-biotin | Rxn Time |
|---|---|---|---|---|
| **1** | 1 | 0 | 100 | 20h |
| **2** | 1 | 2 | 10 | 2h |
| **3** | 1 | 2 | 10 | 20h |
| **4** | 1 | 2 | 100 | 2h |
| **5** | 1 | 2 | 100 | 20h |
| **6** | 1 | 5 | 100 | 2h |
| **7** | 1 | 5 | 100 | 20h |

**Figure 5.3.** Sortase catalyzed transpeptidation of $TM_{LPETG}$ with $NH_2$-$(Gly)_5$-Lys-biotin (GGG-biotin) nucleophiles. Top: western blot analysis to detect presence of biotin using streptavidin-AP conjugate; bottom: molar ratios of the $TM_{LPETG}$, WT SrtA, and biotin nucleophile as well as reaction times.

To confirm the sortase-catalyzed transpeptidation of nucleophiles to site-specifically label $TM_{LPETG}$, we synthesized a $NH_2$-$(Gly)_5$-Lys-biotin probe. As a starting point, we tested the ligation of $TM_{LPETG}$ with 2 or 5 molar equivalents WT SrtA and 10 or 100 molar equivalents of $NH_2$-$(Gly)_5$-Lys-biotin reacted for 2 or 20 hours (Figure 5.3).

We observed that 10 molar equivalents of $NH_2$-$(Gly)_5$-Lys-biotin and 2-fold molar excess sortase relative to $TM_{LPETG}$ was required to achieve maximal transpeptidation. Increasing the quantity of $NH_2$-$(Gly)_5$-Lys-biotin further did not improve yields, which may be due to the high specificity of the sortase enzyme towards the oligoglycine nucleophiles ($K_m$). However, due to the low catalytic activity of wild-type sortase ($k_{cat}$), a total reaction time of 20 hours appeared necessary to achieve maximal labeling yields, despite simultaneously increasing the amount of sortase to 5-fold and the nucleophile to 100-fold excess relative to $TM_{LPETG}$. Therefore, it appears that a 2-fold molar excess sortase, 10-fold molar excess oligoglycine nucleophile, and 20 hour reaction time are required to maximize yields.

As shown in Figure 5.4, during the course of these studies, we unexpectedly observed that the 5' SrtA catalyzed ligation of a commercially available $NH_2$-$PEG_3$-biotin with nearly equal efficiency as $NH_2$-$(Gly)_5$-Lys-biotin peptide, at the reaction conditions where the nucleophiles were in 100-fold molar excess relative to $TM_{LPETG}$.

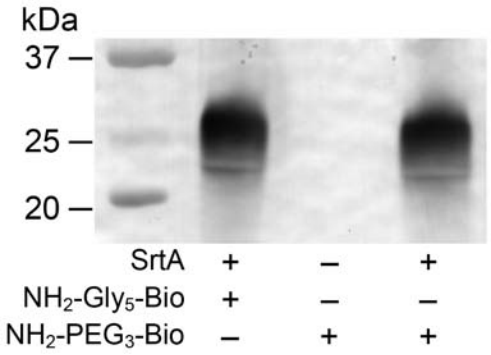


**Figure 5.4.** Sortase catalyzed transpeptidation of pentaglycine and alkyl-amine nucleophiles tagged with biotin. Western blot analysis of $TM_{LPETG}$ reacted with either pentaglycine-biotin or $NH_2$-$PEG_3$-biotin.

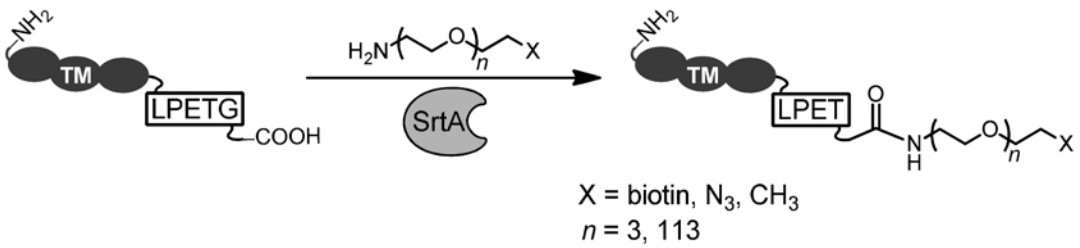


**Figure 5.5.** Sortase catalyzed transpeptidation of alkyl-amine nucleophiles.

Simple alkyl-amine nucleophiles have previously been shown to be suitable, though less efficient, nucleophile substrates for wild-type SrtA [393], and in general they have been regarded as a non-specific side product of transpeptidation involving oligoglycine nucleophiles. Due to their synthetic simplicity, ligation of simple PEG-amines afforded by 5' SrtA may provide a versatile and general approach to modify a range of biomolecules containing a C-terminal LPETG motif. We validated this approach by first demonstrating the capacity of 5'SrtA to ligate a commercial $NH_2$-$PEG_3$-$N_3$ to $TM_{LPETG}$, to generate a single C-terminal azide motif, which successfully reacted with a Biotinylated dibenzocyclooctyne (DBCO) probe as visualized by western blotting (Figure 5.6) as well as biotin quantification assay which showed ~10-fold increase in the fraction of TM tagged with azide compared with auxotrophic incorporation of azidohomoalanine.

Next, we optimized the reaction conditions to tag $TM_{LPETG}$ with azide by performing reactions with a 5kDa PEG-amine, which would result in an increase in the molecular weight of the $TM_{LPETG}$ upon forming the TM-PEG conjugate. By running parallel reactions using wild type and 5' SrtA and measuring the formation of TM-PEG conjugate on a SDS-PAGE gel, we were able to verify the substantially higher reactivity afforded by 5' SrtA to PEGylate $TM_{LPETG}$ with a 5kDa PEG-amine, which appeared to reach ~80% completion after only 2h, compared with WT SrtA under the same conditions (Figure 5.7).

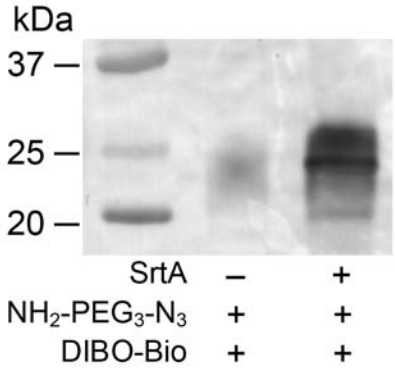


**Figure 5.6.** Strain-promoted [3+2] cycloaddition of dibenzocyclootyne-biotin (DIBO-bio) with azide-tagged TM generated by SrtA-catalyzed transpeptidation of $NH_2$-$PEG_3$-$N_3$.

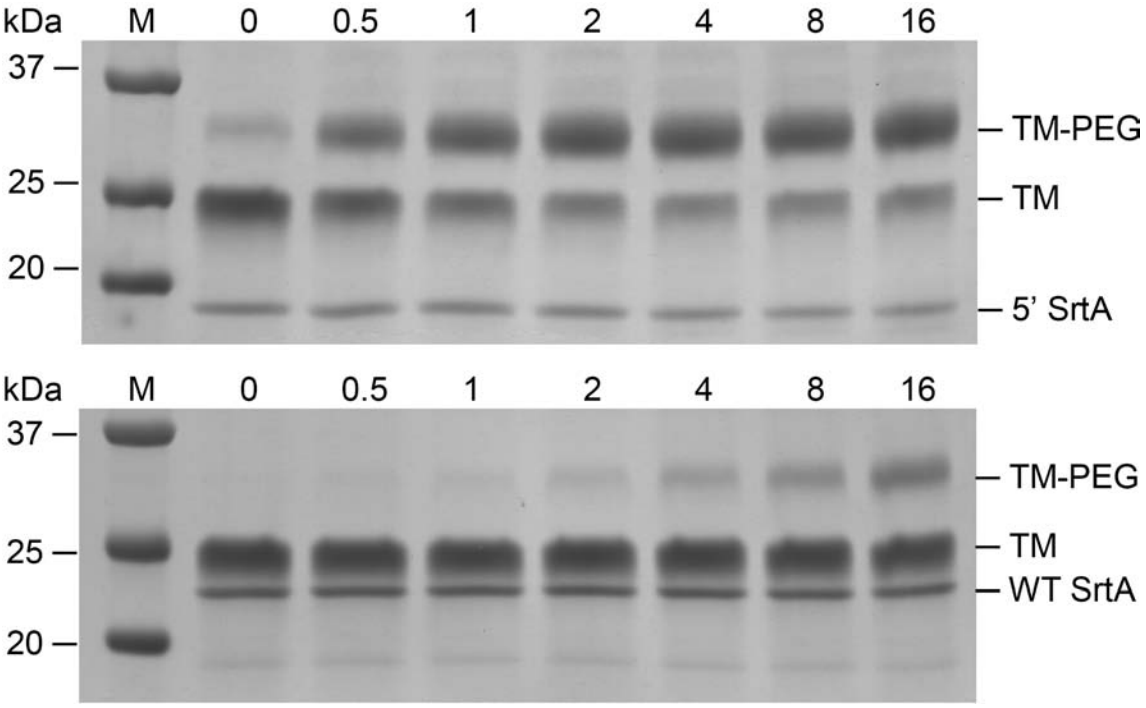


**Figure 5.7.** SDS-PAGE gel tracking of pentamutant (5') or wild-type (WT) S. Aureus sortase A (SrtA) catalyzed transpeptidation of an amine-$PEG_{113}$ (MW 5kDa) to thrombomodulin expressing a C-terminal LPETG peptide motif ($TM_{LPETG}$) over a 16 hour time period.

Further supporting the superior performance of 5' SrtA in transpeptidation reactions involving alkylamine nucleophiles, it was found that the efficiency of $TM_{LPETG}$ PEGylation with PEG-amines was improved slightly when the molar excess of WT SrtA used in these studies by 20-fold, but still required 24h reaction time to reach the same level achieved by 5' SrtA after 2 h (Figure 5.8). These results support the use of 5' SrtA as a highly active transpeptidase to covalently modify the C-terminus of $TM_{LPETG}$ with alkylamine nucleophiles, which are synthetically simpler to generate than pentaglycine peptides. Moreover, we have demonstrated a rapid and straightforward approach to site-specifically PEGylate $TM_{LPETG}$. Due to the short length of the sortase recognition motif LPETG and fast reaction times afforded by 5' SrtA, a feasible future direction would be translating this technique for PEGylation of a broad range of protein therapeutics in the biopharmaceutical industry is to tailor stability and half-life characteristics.

We next optimized the reaction concentrations of the amine nucleophiles required to achieve maximal transpeptidation after 2 h reaction time. $TM_{LPETG}$ was reacted with 0.1 molar excess 5' SrtA and either 1-fold, 10-fold, or 100-fold molar excess 5kDa PEG-amine for 2h. These studies show that the 100-fold molar excess of alkyl-amine nucleophiles was a requisite reaction parameter in this approach, as 1 and 10 molar equivalents of 5kDa PEG-amine did not facilitate significant levels of the transpeptidation TM-PEG product (Figure 5.9).

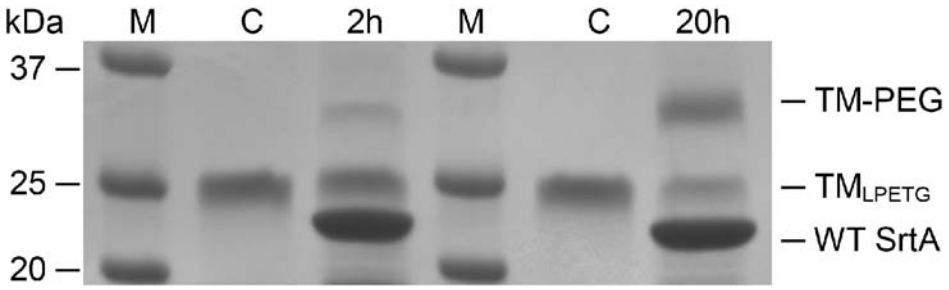


**Figure 5.8.** SDS-PAGE gel tracking of wild-type (WT) S. Aureus sortase A (SrtA) catalyzed transpeptidation of an amine-$PEG_{113}$ (MW 5kDa) to thrombomodulin expressing a C-terminal LPETG peptide motif ($TM_{LPETG}$) for 2 h or 20 h reaction time. Notations: C – controls with only $TM_{LPETG}$, M – molecular weight markers.

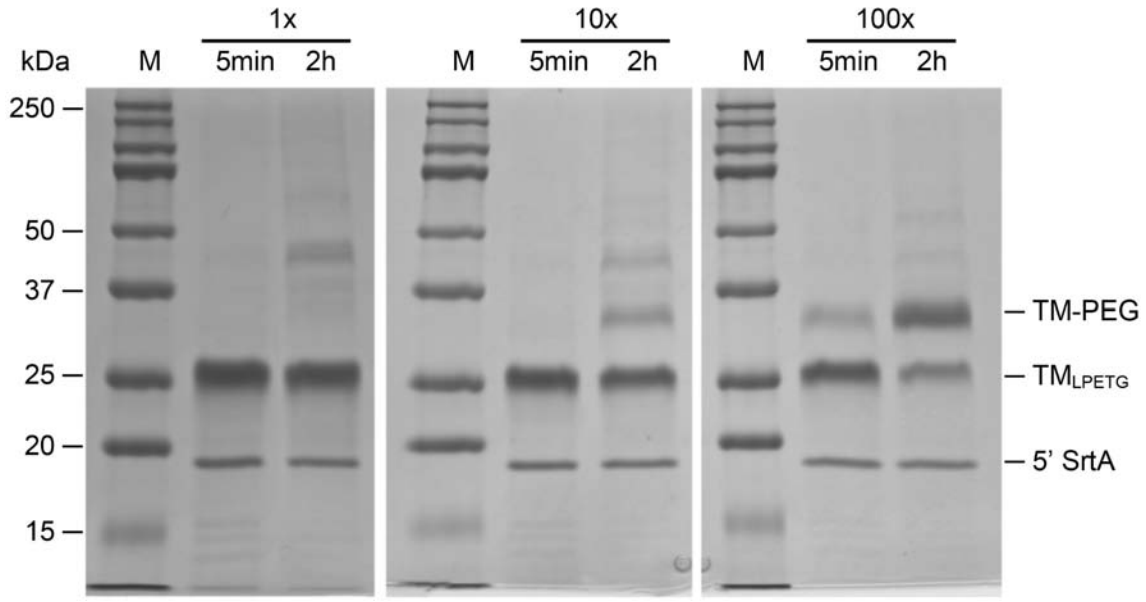


**Figure 5.9.** SDS-PAGE gel tracking of pentamutant *S. Aureus* sortase A (5' SrtA)-catalyzed transpeptidation of 1x, 10x, or 100x molar excess amine-$PEG_{113}$ (MW 5kDa) relative to thrombomodulin expressing a C-terminal LPETG peptide motif ($TM_{LPETG}$) for 5 min or 2h reaction time. Notations: M – molecular weight markers.

We observed the formation of slight quantities of higher molecular weight proteins, as evident by staining at ~40kDa, when lower quantities of alkylamine nucleophiles were present. This minor product may be due to 5' SrtA catalyzed conjugation of $TM_{LPETG}$ to either the ε-amine of lysine residues or the N-terminal amine present on $TM_{LPETG}$ or 5' SrtA. A 100-fold molar excess of alkylamine nucleophiles appears to minimize these side reactions.

The high molar excess of required nucleophiles may be due to the high $K_{m, GGG}$ = 2,900 μM exhibited by 5' SrtA, which was about 20 times higher than WT SrtA [394]. We do not anticipate this will be a significant hurdle in our studies, as the high molar excess of unreacted biotin or azide tagged PEG-amine probes can be easily removed by established dialysis methods due to their small molecular weight (< 1 kDa). While sortase-catalyzed transpeptidation with primary amines on the LPETG tagged protein to form protein-protein conjugates does occur, this is highly inefficient perhaps due to steric hindrance or suboptimal pKa, which both influence the nucleophilic resolution of the sortase acyl-intermediate. The His-tagged 5' SrtA was removed by applying the crude reaction mixture on a metal-affinity column (Figure 5.10)

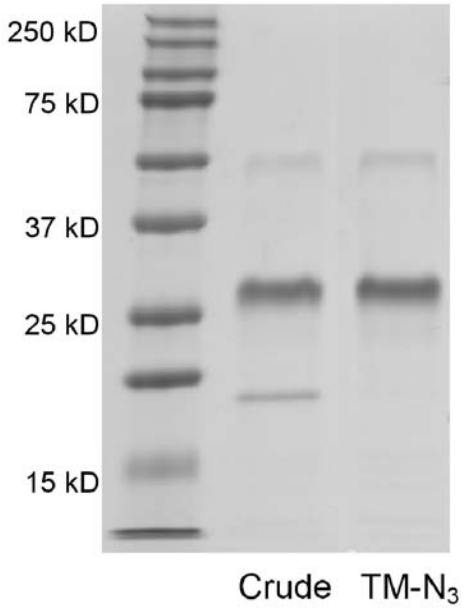


**Figure 5.10.** SDS-PAGE gel tracking of the removal of 5' SrtA (~17kD) from the crude reaction mixture after reaction of $TM_{LPETG}$ with $NH_2$-PEG-$N_3$.

### 5.2.2. Immobilization of Azide Tagged Molecules by Copper-free Click Chemistry

We next focused our efforts to optimize the surface chemistry to tether TM-PEG-$N_3$ to the luminal surface of small-diameter ePTFE grafts. Since terminal sterilization of modified surfaces is a crucial enabling step in the clinical translation of our approach, we transitioned away from Staudinger Ligation due to the tendency of triphenylphosphines to degrade by air oxidation [396]. Emerging copper-free strain promoted [3+2] cycloaddition is increasingly utilized in as a bioorthogonal chemistry method in biological applications [397]. Optimization of strain promoted cyclooctynes has yielded variants that exhibit substantially higher reaction kinetics than Staudinger Ligation, while maintaining similar levels of bioorthogonality [398]. DBCO has been among the most well characterized alkynes suitable for strain promoted [3+2] cycloaddition and has been commercialized for cell imaging applications [399]. We synthesized a DBCO-$PEG_{11}$-$NH_2$ linker that enabled the functionalization of the luminal surface of 4 mm i.d. ePTFE vascular grafts as well as thin solvent-cast polyurethane films with DBCO anchor groups using an approach reported previously [389] and outlined in Figure 5.11.

We hypothesized that DBCO modified substrates could be sterilized with ethylene oxide without affecting its reactivity with azide-tagged biomolecules, and as a first step, we tested the conjugation of rhodamine-azide (Rh-$N_3$) to thin polyurethane films modified with DBCO. Using a similar sequential surface modification approach as outlined in Figure 5.11 for polyurethane coatings, we modified thin polyurethane films with DBCO and performed standard ethylene oxide (EtO) sterilization protocol, and reacted films with azide tagged rhodamine as a colorimetric readout. UV-vis absorbance of modified films was measured using an adaptor built in house, which showed that EtO

sterilization did not diminish the quantity of immobilized Rh-$N_3$ (Figure 5.12), and moreover, non-specific reactivity with rhodamine B was minimal.

Next, we quantitatively determined the stability of the cyclooctyne modified surfaces and further demonstrated the broader applicability of this surface engineering platform to attach azide-$PEG_3$-biotin on ePTFE grafts modified with cyclooctyne. We developed a streptavidin-HRP based quantification system to measure the surface density of biotin on small ePTFE segments, which corroborated our qualitative findings with rhodamine-azide by demonstrating no significant change in the immobilized biotin surface density on ePTFE grafts surfaces subjected to ethylene oxide sterilization (Figure 5.13). The combination of these results show that terminal ethylene oxide treatment is a viable method to sterilize cyclooctyne modified surfaces without reducing their capacity to immobilize azide-tagged biomolecules.

Covalent immobilization of TM-$N_3$ was validated on 4 mm i.d. ePTFE grafts modified with DBCO. Non-specific reaction of DBCO with $TM_{LPETG}$ was minimal, and EtO sterilization did not diminish the activity of subsequently immobilized TM-$N_3$ (Figure 5.14A), as measured by the capacity of TM grafts to generate activated protein C in the presence of thrombin, protein C, and calcium. TM grafts exhibited ~15 ng aPC $cm^{-2}$ $min^{-1}$ activity, or about 25% higher than previous levels generated by Staudinger Ligation of TM-$N_3$ [389]. Using azide tagged rhodamine as a colorimetric readout, we confirmed the uniformity and specificity of the copper-free cycloaddition reaction on ePTFE grafts modified with DBCO (Figure 5.14B).

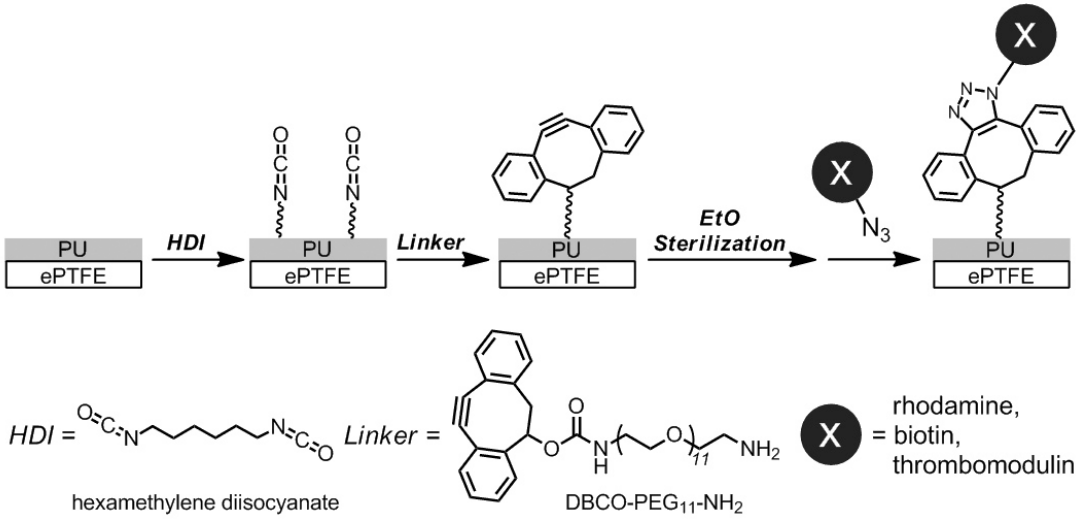


**Figure 5.11.** Surface reaction scheme to modify the lumen of expanded poly(tetrafluoroethylene) vascular grafts with dibenzocyclooctyne (DBCO) that facilitates strain-promoted [3+2] cycloaddition to immobilize any azide-modified molecules such as biotin, thrombomodulin, and rhodamine.

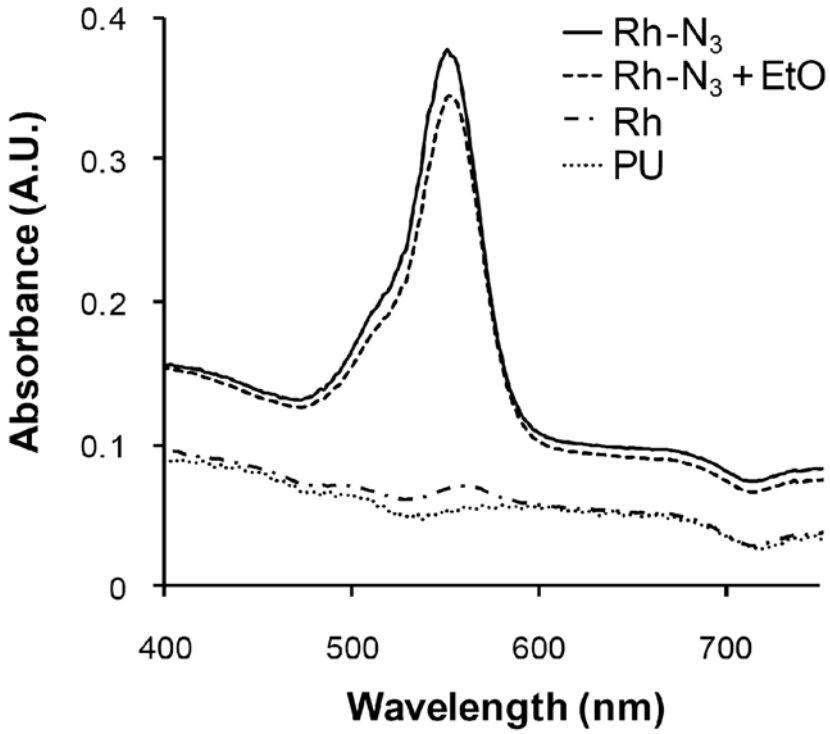


**Figure 5.12.** UV-vis spectroscopy of polyurethane (PU) films functionalized with dibenzocyclooctyne (DBCO) and reacted with rhodamine-azide (Rh-$N_3$) or rhodamine B (Rh) either with or without ethylene oxide (EtO) treatment.

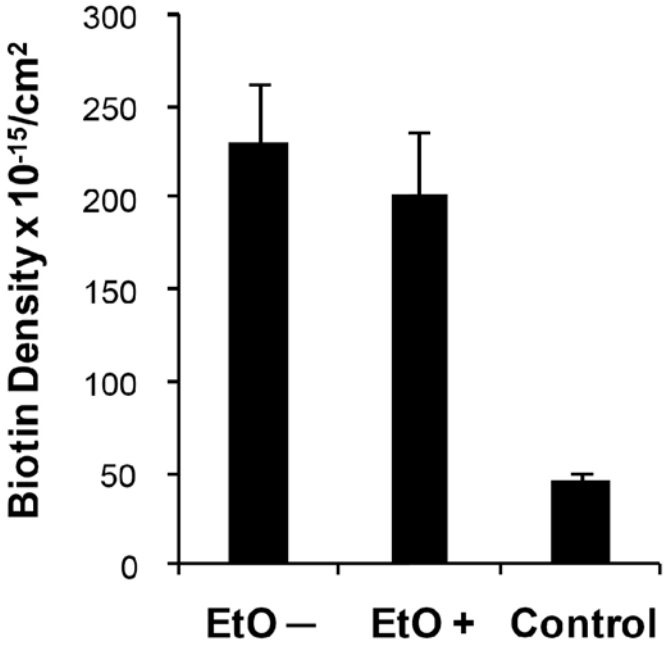


**Figure 5.13.** Surface density of biotin-$PEG_3$-$N_3$ immobilized on EtO treated and non-treated expanded poly(tetrafluoroethylene) (ePTFE) grafts modified with DBCO.

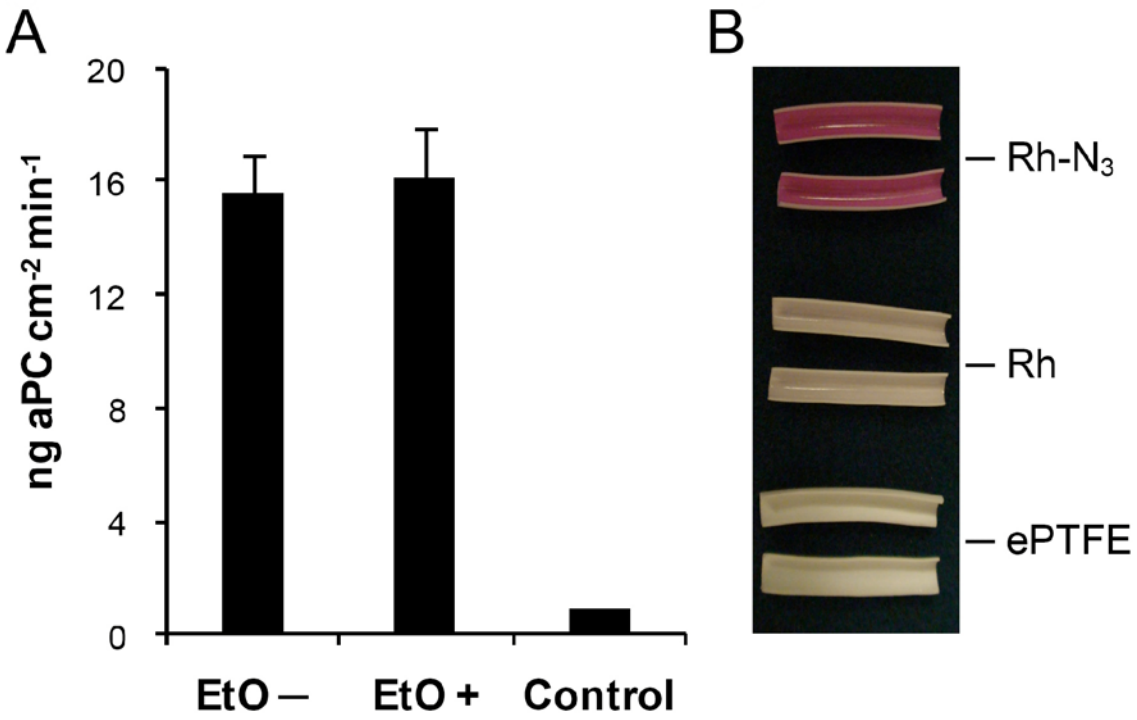


**Figure 5.14.** (A) Surface bioactivity of thrombomodulin to produce activated protein C (aPC) immobilized on EtO treated and non-treated ePTFE grafts modified with DBCO. (B) Visual assessment of Rh-$N_3$ or Rh immobilization on DBCO functionalized ePTFE grafts.

### 5.2.3. Biological Function of Modified ePTFE Grafts to Resist Thrombosis

Next, we tested the functional capacity of TM modified ePTFE grafts to inhibit thrombosis *in vivo*. Chronic arteriovenous shunt models in baboons, whose hemostatic systems most closely mirror that of man [400], are routinely used to assess the thrombogenicity of blood contacting materials under dynamic flow *in vivo*. We have previously demonstrated a multi-compartment shunt configuration that inserted an upstream prothrombotic graft segment that served as a source of thrombin generation to test the therapeutic function of aPC generated in a downstream TM graft segment [389]. Due to the presence of tissue injury at the graft anastomosis which express highly thrombogenic tissue factor and collagen motifs [401], this shunt configuration (Figure 5.15) may be more representative of the *in vivo* thrombogenic stress exerted on implanted graft materials. Thrombogenicity of materials was evaluated by radioscintigraphy measuring the real-time deposition of radio-labeled autologous platelets on the luminal surface of plain ePTFE, TM modified ePTFE, as well as commercial heparin modified ePTFE.

In our model, an upstream segment of Dacron served as a thrombogenic stress source, which was prone to platelet deposition as evident by steady accumulation over a 1 h perfusion period (Figure 5.16A). In this model, TM modified 4 mm i.d. ePTFE graft segments significantly reduced the deposition of platelets on the plain ePTFE graft surface by nearly 80% (Figure 5.16B), which was significantly greater than the ~50% reduction in platelet deposition on commercial heparin modified ePTFE relative to plain ePTFE graft. These results support our hypothesis that a surface TM assembly attenuates thrombogenesis at a blood-contacting interface. In our previous surface chemistry

platform where TM-$N_3$ generated by incorporation of azidohomoalanine was site specifically immobilized by Staudinger Ligation, no change in platelet deposition was observed downstream of a thrombogenic graft source [389]. This may be a consequence of the ~25% improvement in the catalytic activity of the TM grafts generated by the copper-free click immobilization approach over Staudinger Ligation [389].

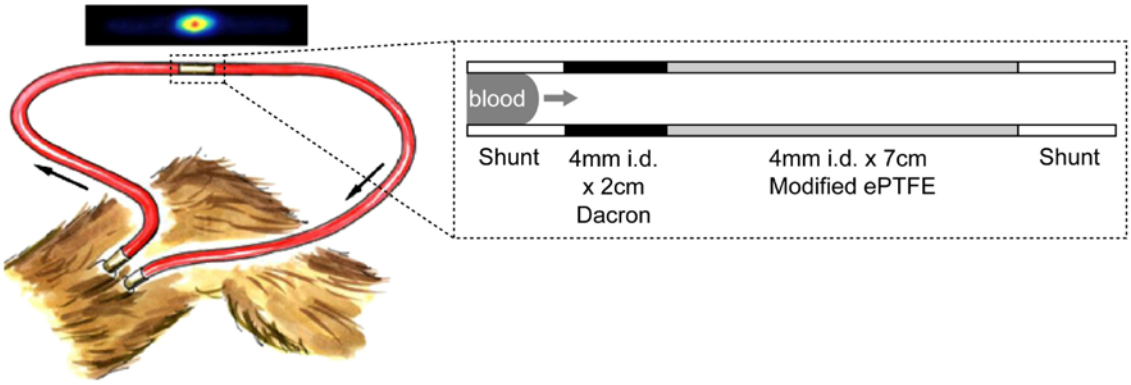


**Figure 5.15.** Baboon arteriovenous shunt model and the 2-compartment test bed to measure the real time deposition of platelets on modified expanded poly(tetrafluoroethylene) (ePTFE) grafts in the presence of an upstream prothrombotic Dacron segment. Arrow points in the direction of blood flow.

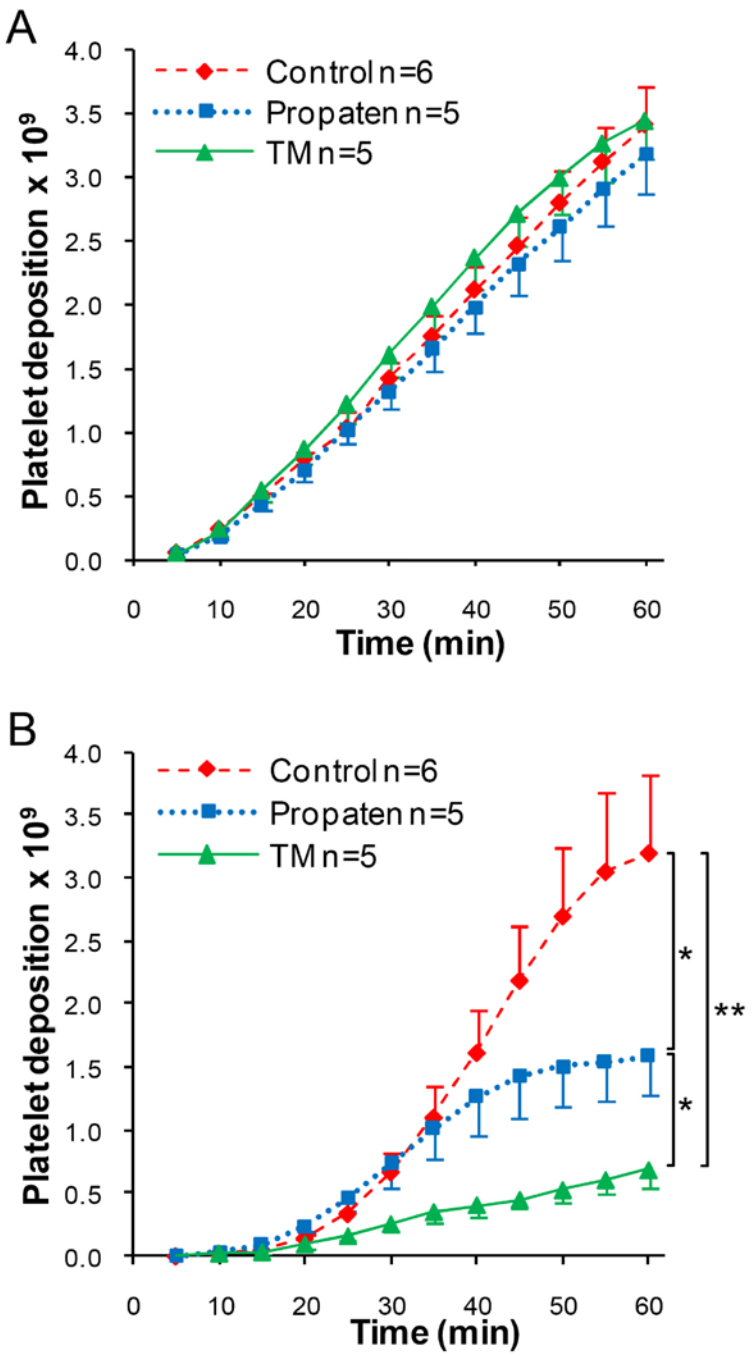


**Figure 5.16.** (A) Quantity of platelets deposited over a 1 h perfusion period on the Dacron segment. (B) Quantity of platelets deposited over a 1 h perfusion period on plain ePTFE controls, heparin modified Propaten grafts, and TM modified grafts. Notations: * $p < 0.05$, ** $p < 0.01$.

Although minimal deposition of platelets has been observed in the past on heparin modified ePTFE in a primate A-V shunt model [402], this model lacked the upstream Dacron segment which provided a more robust test bed in our model as it is more representative of tissue trauma and injury at the anastomosis. However, due to the complexities involved in the activation of thrombosis *in vivo*, the impact on long term patency and performance of small diameter vascular grafts from the reduction in platelet deposition afforded by TM immobilization will need to be evaluated in surgically implanted bypass configurations in relevant animal models.

## 5.3. Conclusions

In summary, we have described a surface engineering platform that enables the attachment of biologically active enzymes on terminally sterilized materials, and demonstrated the superior *in vivo* thromboresistant efficacy of a TM film compared with current commercial heparin coatings on the luminal surface of small diameter commercial ePTFE grafts. Although further studies are required to evaluate the impact of our surface engineering strategy on long term durability, we anticipate the combination of our approach to attenuate acute thrombosis with emerging development in bioactive surface modifications that induce spontaneous endothelialization [403] would produce a new generation of blood-compatible materials to improve the performance of implantable devices and artificial organ systems.

## 5.4. Methods

### 5.4.1. Generation of $TM_{LPETG}$

The minimal fragment of human thrombomodulin, the epidermal growth factor-like domains 4 – 6 (TM456) was cloned into the Sigma pFLAG ATS expression vector. Amino acid changes relative to the native TM456 sequence is colored red:

$TM_{LPETG}$ (15.2 kDa)

MKKTAIAIAVALAGFATVAQADYKDDDDKVKLVEPVDPCFRANC

EYQCQPLNQTSYLCVCAEGFAPIPHEPHRCQLFCNQTACPADCDP

NTQASCECPEGYILDDGFICTDIDECENGGFCSGVCHNLPGTFECIC

GPDSALAGQIGTDCGGGGSGGGGSLPETGG

Note that highlighted in blue and underlined is the OmpA tag that facilitates transport of $TM_{LPETG}$ to the periplasmic space of E Coli to optimize folding, this sequence is cleaved in final mature $TM_{LPETG}$. The FLAG peptide sequence is DYKDDDDK at the N-terminus. It has been previously demonstrated that the conversion of the internal methionine residue to leucine maximizes the stability of TM [404]. A second mutation was made to convert the internal RH sequence, which is an active trypsin cleavage site, to GQ. The additional sequence at the C-terminus includes a GGGGSGGGGS spacer and the LPETG sortase recognition motif. An extra glycine was added at the C-terminus as this was previously demonstrated to maximize sortase activity.

Following transformation of chemically competent cells, a fresh LB agar plate was streaked with methionine auxotrophic cells containing the appropriate TM vector and incubated at 37 ºC overnight. Next, a single cell colony was inoculated into 50ml of Novagen media supplemented with 0.4 % glucose and 50 µg/ml ampicillin and cultured at 37 ºC, 225 RPM, for 16 h. 25 ml of fully grown starter culture (OD600 = 1.20) was

added per 500 ml of Novagen media supplemented with 0.4 % glucose and 50 µg/ml ampicillin, and cultured at 37 ºC, 225 RPM. Upon cell growth to OD600 = ~0.9, IPTG was added at a final concentration of 1mM to induce $TM_{LPETG}$ expression, and the culture was incubated for an additional 4 h at 37 ºC, 225 RPM. Cell cultures were centrifuged at 4,000x RCF at 4 ºC for 10 minutes and stored at 4 ºC.

Standard osmotic shock protocol was performed on stored cell pellets to extract the crude periplasmic proteins. Cell pellets were first warmed to room temperature and re-suspended in 40 ml/g cells of 0.5 M Sucrose, 0.03 M Tris-HCl (pH 8.0) at a final pH of 8.0 per gram of cells. Suspended cells were evenly distributed into round bottom centrifuge tubes (60 mL per tube). 120 µL of 500 mM sucrose was added to each tube to achieve final 1 mM EDTA concentration and incubate with gentle shaking for 10 minutes at RT. The cell suspension was centrifuged at 3,500x g for 10 min at 10 °C, and the supernatant was decanted. The cell pellet was rapidly resuspended in 25 ml/g cell pellet ice-cold, distilled water (40mL per tube is sufficient) for 10 minutes, and the cell suspension was centrifuged at 3,500x RCF for 10 min at 4 °C. 35 ml of supernatant was removed per tube immediately and transferred to clean round bottom centrifuge tubes. These were clarified by further centrifugation at 25,000x RCF for 25 min at 4 °C, and sterilized using a 0.22 µm filtration system. Anti-FLAG immunoaffinity chromatography (Sigma) was performed on the clarified supernatant per manufacturer's instructions. SDS-PAGE analysis, and total protein quantification were performed using standard Bradford assay (Bio-Rad) protocols from the manufacturer.

### 5.4.2. Bacterial Expression of 5' Sortase and Wild-type Sortase

The amino acid sequence of the wild-type sortase and 5' sortase is provided below:

Wild-type sortase with N-terminal His-tag (19.5 kDa):

MASSHHHHHHDYDIPTTENLYFQGSQAKPQIPKDKSKVAGYIEIPDADIKE
PVYPGPATPEQLNRGVSFAEENESLDDQNISIAGHTFIDRPNYQFTNLKAA
KKGSMVYFKVGNETRKYKMTSIRDVKPTDVGVLDEQKGKDKQLTLITCD
DYNEKTGVWEKRKIFVATEVK

5' sortase with C-terminal His-tag (17.9 kDa) and mutations highlighted in red:

MQAKPQIPKDKSKVAGYIEIPDADIKEPVYPGPATREQLNRGVSFAEENES
LDDQNISIAGHTFIDRPNYQFTNLKAAKKGSMVYFKVGNETRKYKMTSIR
NVKPTAVEVLDEQKGKDKQLTLITCDDYNEETGVWETRKIFVATEVKLE
HHHHHH

*E. coli* BL21 transformed with pET29 wild-type sortase or 5' sortase expression plasmids were cultured at 37 °C and 225 RPM in LB media supplemented with 50 µg/mL kanamycin. Upon OD600 = 0.8, IPTG was added to a final concentration of 0.4 mM and protein expression was induced for 3 h at 30 °C. The cells were harvested by centrifugation and resuspended in lysis buffer (50 mM Tris pH 8.0, 300 mM NaCl supplemented with 1 mM MgCl2, 2 units/mL DNAseI (NEB), 260 nM aprotinin, 1.2 µM leupeptin, and 1 mM PMSF). Cells were lysed by sonication on ice and the clarified supernatant was purified by column chromatography using Cobalt Talon Resin (Clontech Laboratories) following the manufacturer's instructions. Fractions that were >95 % purity, as judged by SDS-PAGE, were consolidated and dialyzed against Tris-buffered

saline (25 mM Tris pH 7.5, 150 mM NaCl) using PD-10 columns (GE Healthcare) and stored as 5 mg/ml stocks at 4 °C.

### 5.4.3. Sortase-catalyzed Transpeptidation

$TM_{LPETG}$ was reacted with 0.1 or 2 molar equiv WT or 0.1 molar equiv 5' SrtA and 1, 10, or 100 molar equiv $NH_2$-$PEG_{5kDa}$ (Nektar) at room temperature. At various reaction time points, a 2 µg aliquot was removed and frozen at -80 °C. Upon completion of the study, all aliquots were thawed at room temperature and incubated at 100 °C in 1x reducing buffer (Fisher Scientific), and run on a 12 % Tris PAGE gel (Biorad) and visualized by Coommassie staining. The stained gels were dried and scanned at 1200 dpi on an Epson Perfection 1660 photo scanner, and quantification of the extent of TM-PEG formation relative to unreacted $TM_{LPETG}$ was performed using the Gel Analyzer function in ImageJ software.

To generate TM-$PEG_3$-$N_3$ using sortase catalyzed transpeptidation, $TM_{LPETG}$ was reacted with 0.1 molar equivalent 5' SrtA and 100 molar excess $NH_2$-$PEG_3$-$N_3$ (Sigma) for 2 h at room temperature. The crude reaction mixture was run through a chromatography column containing Cobalt Talon Resin, and the flow through was collected and dialyzed against TBS buffer (20 mM Tris pH 7.5, 100 mM NaCl). Following 2 days of dialysis with regular buffer exchanges approximately every 8 h, the final reaction mixture was concentrated and the final yield determined by total protein quantification per manufacturer's protocol (Bio-Rad).

The extent of azide tagging of $TM_{LPETG}$ was determined by incubating the final reaction mixture with excess DBCO-biotin (Invitrogen) overnight at 37 °C. Unreacted DBCO-biotin was removed by 2x sequential dialysis using Zeba Spin Desalting Columns

with a 7 kDa MWCO (Fisher Scientific). Final concentration of the dialyzed reaction mixture was determined by total protein quantification per manufacturer's protocol (Bio-Rad). The extent of biotinylation of TM-$N_3$ by DBCO-biotin was determined using a fluorescent biotin quantification kit per manufacturer's instructions (Fisher Scientific).

### 5.4.4. Synthesis of $NH_2$-$PEG_{11}$-CyO

The activated cyclooctyne was synthesized according to a previously published protocol. $NH_2$-$PEG_{11}$-CyO was synthesized by reaction between the activated cyclooctyne and t-Boc-N-amido-dPEG11-amine (Quanta BioDesign, Powell) followed by TFA deprotection as detailed previously.

### 5.4.5. Modification of ePTFE Grafts

Following conformal coating of the luminal surface of 4 mm i.d. ePTFE grafts with a 50 µm thick polyurethane coating as detailed elsewhere, grafts where incubated with 16 % v/v hexamethylene diisocyanate and 4 % v/v triethylamine in anhydrous toluene for 1 h at 50 °C. Following rinsing in toluene, grafts were reacted with $NH_2$-$PEG_{11}$-CyO at 5 mg/ml in anhydrous toluene with 1 % v/v DMSO for 16 h at 40 °C, then rinsed in toluene and dried under vacuum for 24 h at RT.

Ethylene oxide sterilization was carried out by the Beth Israel Deaconess Medical Center. For rhodamine binding studies, CyO modified ePTFE grafts were reacted 1mg/ml tetramethylrhodamine-5-carbonyl azide in 1:4 tert-butanol/TBS at 37 °C for 24 h followed by rinsing in methanol for 2 days. For TM binding studies, CyO modified ePTFE grafts were reacted with 20 µM TM-$PEG_3$-$N_3$ in TBS at 37 °C for 24 h and rinsed with TBS for 24 h. For biotin binding studies, CyO modified ePTFE grafts were reacted with biotin-PEG-$N_3$ in TBS at 37 °C for 24 h followed by rinsing in TBS for 24 h.

### 5.4.6. Modification of Polyurethane Films

Thin clear PU films were solvent cast by drying 12.5 % w/v Elasthane 80A in DMF for 24 h at 60 °C under vacuum. Films were subjected to isocyanate, TPP, and rhodamine reactions using identical conditions as graft substrates, and characterized by UV-Vis spectroscopy (Cary 50 Bio UV-visible spectrophotometer, Varian) using an adaptor built in house that comprises two quartz slides to sandwich the modified PU films.

### 5.4.7. Graft aPC Generation Assay

A 4 mm segment was incubated in 200 µL of 0.2 µM protein C (Calbiochem, Gibbstown), 5 mM calcium chloride, and 2 nM α-thrombin (Haematologic Technologies, Essex Junction) in Tris buffer (20 mM Tris, 100 mM NaCl, pH 7.5) with 0.1 % bovine serum albumin at 37 °C for 1 h, and quenched with human anti-thrombin III (American Diagnostica, Stamford) at 120 µg/mL final concentration for 5min. The concentration of aPC was determined using Spectrozyme PCa (American Diagnostica) at 0.2 mM and extrapolating the rate of absorbance at 405 nm increase with a standard curve. TM activity was assayed after coated grafts were exposed to 24 h of 500 $s^{-1}$ shear with PBS at 37 °C generated by a peristaltic flow loop, and after grafts were incubated in PBS over two weeks at 37 °C.

### 5.4.8. *In Vivo* Baboon Arteriovenous Shunt Model

Chronic exteriorized Silastic tubings were implanted in male baboons as described previously [27, 29]. All studies were approved by the Institutional Animal Care and Use Committee at Oregon Health and Science University. Mean blood flow rate through the shunt was measured continuously using a Doppler ultrasonic flow meter

and held constant by an external screw clamp at 100 ml/min. Autologous platelets were radiolabeled one day prior to shunt study with Indium-111 oxine and re-injected into the baboon [29]. Platelet deposition on test surfaces was measured over a 60-minute perfusion period using a high sensitivity 99Tc collimator and scintillation camera (GE 400T, General Electric) imaging of the 172 keV 111In g photon peak at 5-min intervals. Thrombogenic devices were assembled and inserted into shunts similar to previous configurations [27] and detailed below.

### 5.4.9. Preparation of Thrombosis Test Devices

The device consists of 3 parts: (1) 2 cm, 4 mm i.d. Dacron segment, (2) a test segment of 4 mm i.d. thin wall ePTFE control graft of 7 cm length, or 4 mm i.d. TM or Propaten heparin coated graft of identical length, (3) 1 cm, 10 mm i.d. chamber constructed from ePTFE graft material.

A 4 mm i.d. Teflon rod was inserted into a 6in. length of 4 mm silicone tubing until it protrudes about 3 cm beyond the silicone. A thin bead of undiluted silicone glue was placed around the silicone tubing edge and a 2 cm Dacron segment was slid onto the rod into the glue until some of the glue squeezes out. More glue was placed around the joined section and smoothed out. This joint was cured for several hours and covered with thin diluted silicone glue, and then cured overnight.

Test graft segments were glued to the Dacron section in the next step. First, a 3-4 mm sleeve of silicone tubing 4.76 mm i.d. / 7.94 mm o.d. was cut, and slid over one end of the test segment. A bead of silicone glue (undiluted) was placed on the other end of the Dacron segment with the rod still extending through the Dacron. The test segment was then slid onto the rod and pushed into the glue, and the small tubing ring was slipped

onto the rod over the test segment until it fits snugly next to the Dacron segment. More thick glue was placed around this joint and smoothed out, and another thin bead of thick glue was placed next to the silicone ring around the test segment. This setup was let cure for several hours, and the whole Dacron segment was covered with thin glue and cured overnight, and the rod was then removed.

The expansion chamber parts were prepared by cutting a 2 cm length of 10 mm i.d. ePTFE graft using a new razor blade, and the center 1 cm section was marked by placing small dots circumferentially around the outside of the graft segment and set aside.

A 4 mm i.d. silicone tubing was inserted into another silicone tubing of 6.35 mm i.d. and 9.53 mm o.d. tubing about 7 mm deep. Both tubing were cut about 5 mm from the end of the larger diameter tube. The 4 mm i.d. tubing that is protruding about 5mm from the large tubing end was cut to leave a 1 cm section. A short 4 mm Teflon rod was inserted from the blunt end onto the just prepared section protruding about 5mm, and a 304 mm segment of silicone tubing 4.76 mm i.d. and 7.94 mm o.d. was slipped over the free end of the test section of ePTFE. A bead of glue was placed on the end of the short segment on the rod and slipped on the ePTFE section over the rod butting the ends, and then the sleeve was slipped onto the rod to form a seal. More thick glue was placed around this joint and smoothed out. A thin bead of thick glue was placed on the ePTFE graft next to the sleeve to form a seal, and cured for several hours. Next thin glue was spread carefully in a line around the 9.53 mm o.d. tubing about 2 mm from the end. The expansion chamber segment prepared earlier was slipped over this section up to the dotted line, and sealed with thin glue and dried overnight.

The Teflon rod was removed and 10 µL of Chronolog collagen (1 mg/mL) was placed on the inside of the chamber on the silicone tubing and let dry. The other side of the chamber was prepared by inserting a 4 mm i.d. silicone tubing into a 6.35 mm i.d. and 9.53 mm o.d. tubing about 7 mm deep, and both tubing were cut about 5mm from the end of the larger diameter tube in a similar fashion as described above. A line of thin glue was placed around the 9.53 mm o.d. large tubing and inserted into the open end of the expansion chamber up to the marked end leaving a 1 cm chamber section. Thin glue was used to seal the joint and this was cured overnight, and the device was then inserted into the A-V shunt.

**5.4.10. Statistical Analysis**

Two-tailed student's t-test assuming unequal variances was used to test for statistical significance between the means of two groups.

# CHAPTER 6

# A RECHARGEABLE SURFACE ENGINEERING PLATFORM ENABLED BY DIRECTED EVOLUTION OF *STAPHYLOCOCCUS AUREUS* SORTASE A

Enzyme immobilization has shaped the development of modern industrial catalysis and bioprocess engineering, and is revolutionizing the design of medical device, diagnostics, and artificial organ systems. Long term performance of bioactive surface enzyme assemblies is limited due to degradation in the operating environment by stresses that include, among others, oxidation, hydrolysis, and proteolysis. In this work, we present a bioinspired surface engineering platform utilizing reversible sortase-catalyzed transpeptidation to regenerate immobilized enzymes by a repeatable charge/strip cycle. The enhanced activity and bioorthogonality of a mutant sortase generated by directed evolution was an enabling step in facilitating the *in vivo* immobilization and removal of biomolecules on medical catheters deployed in mice. These findings establish a new reversible enzyme immobilization paradigm, which may broadly impact the performance characteristics of solid-supported enzymes as components in emerging biomedical technologies or industrial bioprocesses.

## 6.1 Introduction

Medical devices in blood contacting applications such as extracorporeal support systems, vascular access, and permanent implants are prone to life threatening complications initiated by maladaptive host biological responses at the blood-material interface [346, 405]. Immobilization of bioactive molecules and drug eluting assemblies on implantable devices has yielded promising combination products that mitigate

thrombotic cascades and detrimental inflammation [11], enhance device integration and regeneration of healthy tissue [5, 403], and inhibit microbial colonization [406]. Clinical translation of these strategies for permanent implants has been constrained, in part, by the limited therapeutic duration afforded by a finite surface reservoir of bioactive agents, as well as degradation of surface components following exposure to the physiological environment [70, 407]. Efforts to improve biostability and bioactivity have included the manipulation of surface properties such as hydrophilicity, charge, and topography [408], immobilization chemistry [409, 410], as well as rational and evolutionary protein engineering [411]. Despite advances in these areas, a surface coating for implantable devices that reliably retains biological activity for a commercially and clinically viable time scale have not been developed. As a potential workaround, systemic delivery of bioactive therapeutic payloads that target the blood contacting surface of the implant facilitates *in situ* regeneration of bioactivity. This concept has been explored extensively in alternate clinical applications such as targeted drug delivery [412, 413], molecular imaging [414], and minimally invasive cell therapy [415]. In the present study, we report for the first time a highly specific, covalent, and rapidly "rechargeable" surface engineering platform that enables regeneration of depleted or degraded biomolecules at a blood-material interface *in vivo*.

Current techniques to covalently modify surfaces with bioactive compounds have largely involved bioconjugate techniques that link nucleophilic motifs such as amines, thiols, and hydroxyls to their partner electrophiles [416]. Abundant presentation of these motifs in the complex chemical landscape of biological systems reduces the efficiency of targeting payloads for regenerating these device surfaces [417]. Recent advances in rapid

and highly bioorthogonal chemistries, notably Staudinger Ligation and copper-free click cycloaddition [418], have facilitated coupling of azide-tagged targets in living systems. These irreversible bond-forming reactions would increase the complexity of regenerating the covalent chemical anchor sites *in vivo*. Our platform is inspired by the *Staphylococcus Aureus* sortase A (SrtA), a calcium dependent cysteine transpeptidase which catalyzes covalent ligation of a specific "sorting motif" LPXTG (where X denotes any amino acid) on substrate proteins to oligoglycine nucleophiles [419]. Due to the synthetic simplicity of incorporating oligoglycine and LPXTG motifs on biomolecules, as well as the very limited occurance of sorting motifs in native proteins, SrtA-catalyzed transpeptidation is increasingly used in a range of biotechnology applications including protein purification, labeling, as well as immobilization on solid supports as reviewed elsewhere [393, 420]. However, the low catalytic activity of wild type (WT) SrtA necessitates high molar excess of the enzyme as well as long incubation times to approach reaction completion, thereby, limits the effectiveness of this system [393]. We show that an evolved pentamutant SrtA (5'SrtA) variant which exhibited 140-fold higher LPETG-ligation activity than WT SrtA [394] was a critical enabling technology for *ex vivo* and *in vivo* modification of oligoglycine modified surfaces. We demonstrate the superior capacity of 5' SrtA over WT SrtA to catalyze multiple cycles of rapid assembly of LPETG tagged recombinant human thrombomodulin (TM) on pentaglycine modified surfaces (Figure 6.1), as well as regeneration of the pentaglycine motifs by stripping the immobilized TM using 5'SrtA and triglycine (GGG) peptide (Figure 6.2). The performance of this rechargeable surface engineering platform was further validated *in vivo* by 5'SrtA-catalyzed reversible modification of cannulated catheters in mice.

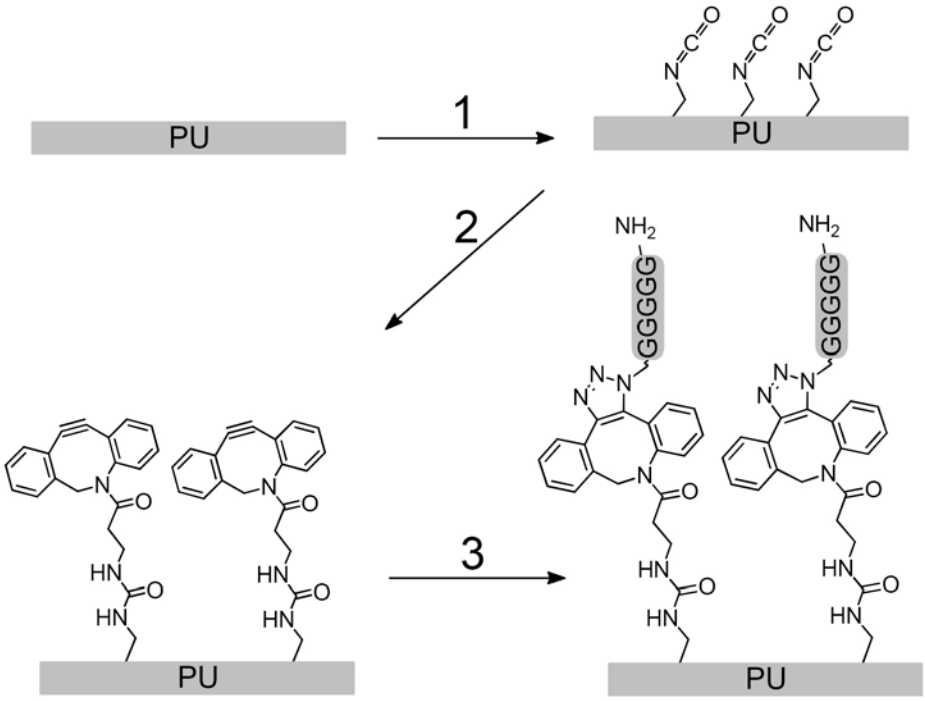


**Figure 6.1.** Reaction scheme to modify polyurethane with pentaglycine (GGGGG) peptide motifs. (1) hexamethylene diisocyanate / triethylamine; (2) DBCO-amine / triethylamine; (3) $NH_2$-GGGGG-$N_3$

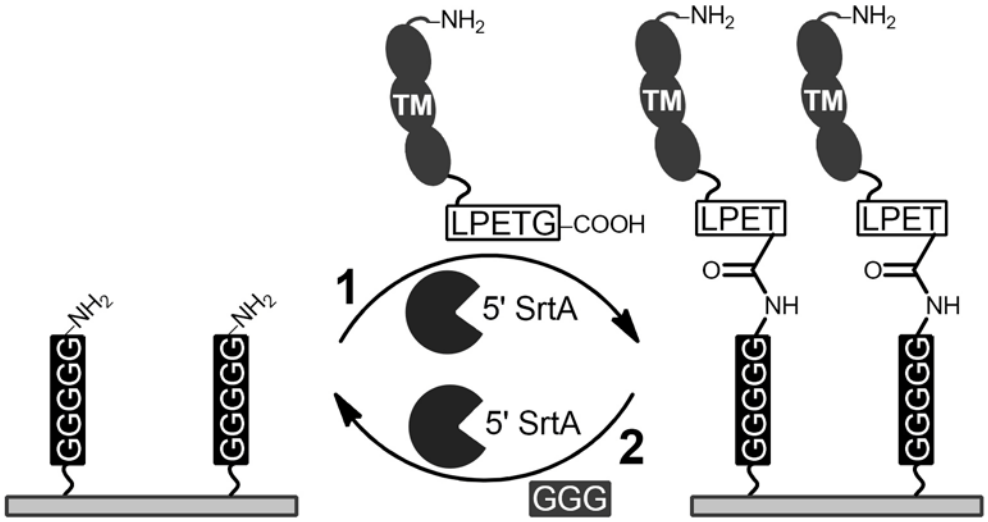


**Figure 6.2.** Reaction scheme to charge and strip pentaglycine (GGGGG) modified surfaces with LPETG-tagged thrombomodulin (TM). (1) $TM_{LPETG}$ / SrtA; (2) GGG / SrtA.

## 6.2. Results and Discussion

### 6.2.1. Reversible Assembly of $TM_{LPETG}$ on Model Surfaces

In order to demonstrate the rechargeable surface assembly of biologically active enzymes, we have expressed and purified a C-terminal LPETG tagged recombinant human thrombomodulin fragment ($TM_{LPETG}$), which represents a major physiological anticoagulant mechanism localized on the endothelial cell lining [19, 356]. Blood-contacting materials functionalized with TM by our lab and others exhibited resistance to thrombosis *in vitro* and *in vivo* [228, 230-233, 358-360, 421]. 5' SrtA was generated by directed evolution using a yeast display system as described previously [394]. 5'SrtA enhanced the covalent immobilization density of $TM_{LPETG}$ on model pentaglycine modified surfaces by ~10-fold compared to WT SrtA under the same reaction conditions (Figure 6.3A). Further increasing the quantity of WT SrtA used in these reactions by 20-fold was only able to achieve 40% of the benchmark immobilization density achieved by 5'SrtA. By shifting the reaction equilibrium using excess triglycine peptide in solution, the immobilized $TM_{LPETG}$ could be stripped off by 5'SrtA to regenerate the pentaglycine surface anchors. On the model pentaglycine surfaces, 5'SrtA dramatically improved the surface stripping efficiency compared with WT SrtA, achieving nearly complete removal of immobilized TM (Figure 6.3B). After 1 hour reaction time, 5'SrtA-catalyzed immobilization of $TM_{LPETG}$ approached ~50% of levels achieved after 16 hours of reaction (Figure 6.4). The rapid kinetics of 5'SrtA-catalyzed immobilization approached that of avidin-biotin mediated immobilization of biotinylated TM in a parallel reaction. Following SrtA-catalyzed stripping to regenerate pentaglycine anchor motifs on model surfaces, additional recharging using 5' SrtA and fresh $TM_{LPETG}$ was demonstrated

without significant decreases in the surface density. This charge/strip cycle of $TM_{LPETG}$ can be repeated at least 10 times (Figure 6.5).

To assess the feasibility of translating our platform for *in vivo* surface modification, the reaction media was switched to whole blood diluted to 50% with 5'SrtA, $TM_{LPETG}$, and heparin without additional calcium. Following 1 hour reaction at 37 ºC, we observed a decrease in surface coupling efficiency of 5'SrtA, which required a 5-fold greater concentration to generate similar surface densities as the Tris buffer system. The TM surface density levels achieved by 5'SrtA were ~20-fold higher relative to WT SrtA under identical conditions (Figure 6.6). Increasing the molar excess of WT SrtA 20-fold yielded ~60% of the benchmark surface density generated by 5' SrtA. These results highlight the impact of rapid kinetics and substrate specificity afforded by 5' SrtA to modify surfaces in the presence of extremely heterogeneous whole blood components.

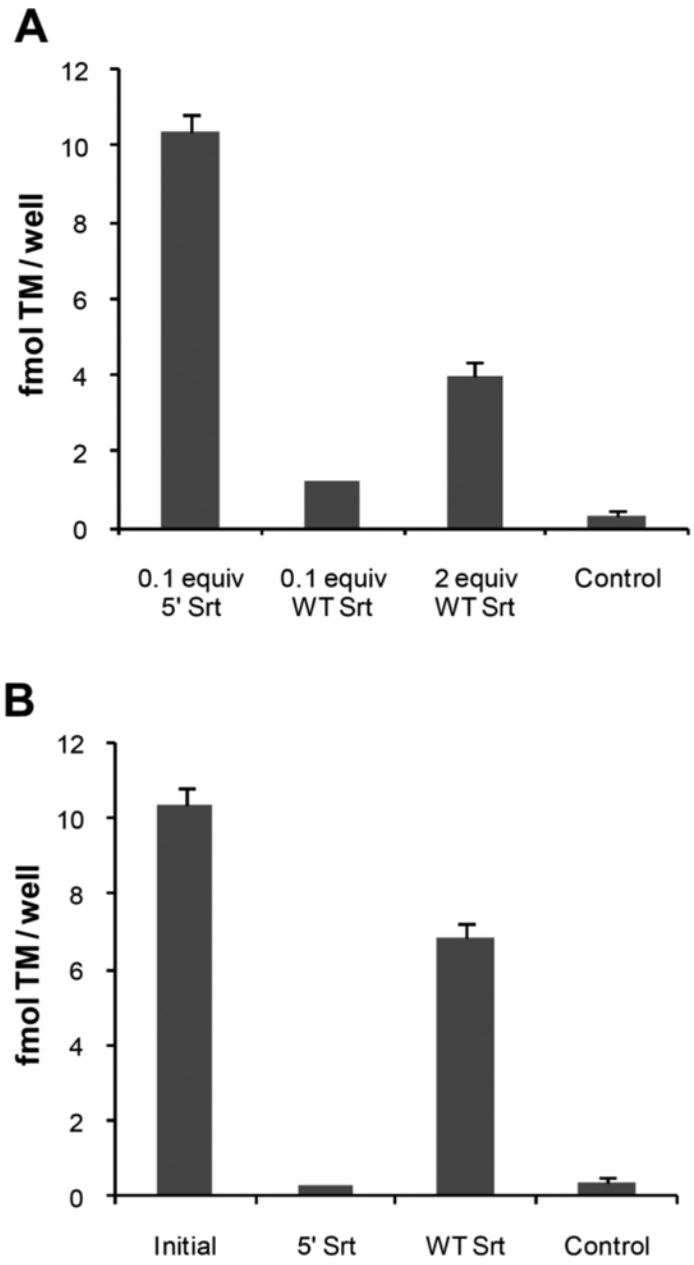


**Figure 6.3**. Sortase-catalyzed rechargeable assembly of LPETG labeled thrombomodulin ($TM_{LPETG}$) on pentaglycine modified model surfaces. (A) Immobilization of 1μM $TM_{LPETG}$ on pentaglycine coated microwells using 0.1 molar equivalents evolved 5' sortase, 0.1 and 2 molar equivalents wild-type (WT) sortase, or no sortase as a negative control. (B) Following immobilization of 1μM $TM_{LPETG}$ on pentaglycine coated microwells using 0.1 molar equivalents evolved 5' sortase, removal of bound TM was carried out using 20 μM of either evolved 5' sortase or WT sortase with 1mM triglycine.

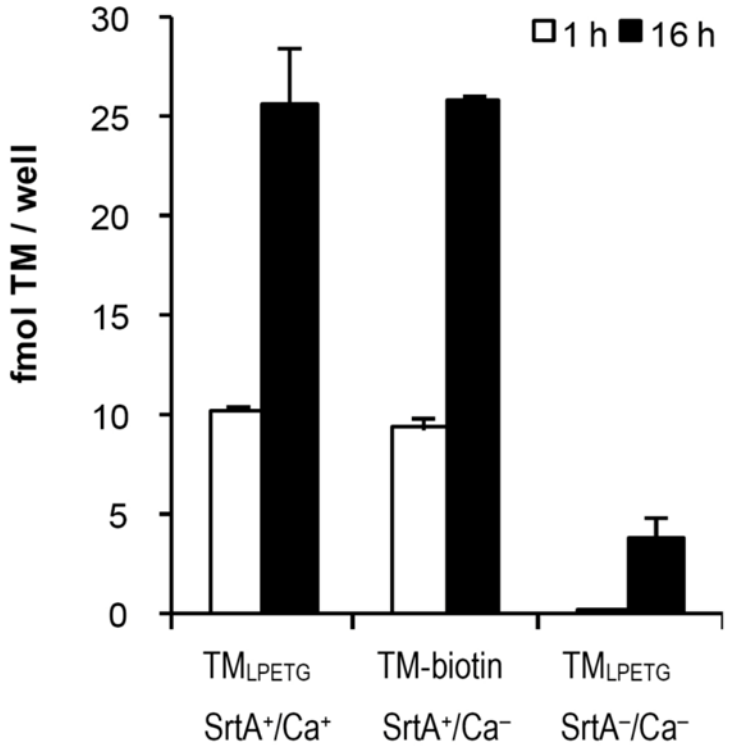


**Figure 6.4.** Sortase-catalyzed binding of $TM_{LPETG}$ on pentaglycine modified model surfaces following 1 and 16 hour reaction were compared with the binding of TM-biotin directly on streptavidin coated microwells. In parallel, $TM_{LPETG}$ was incubated in microwells without sortase as a negative control.

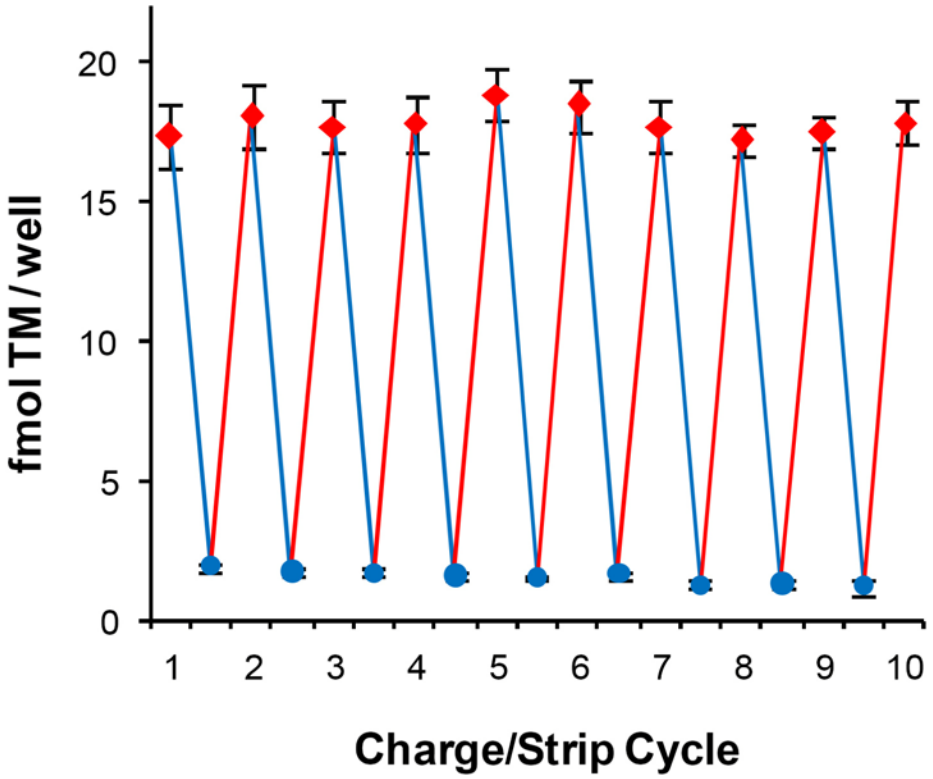


**Figure 6.5.** Sequential 5' sortase-catalyzed charging (filled red diamonds) and stripping (filled blue circles) cycles of $TM_{LETPG}$ performed on model pentaglycine surfaces.

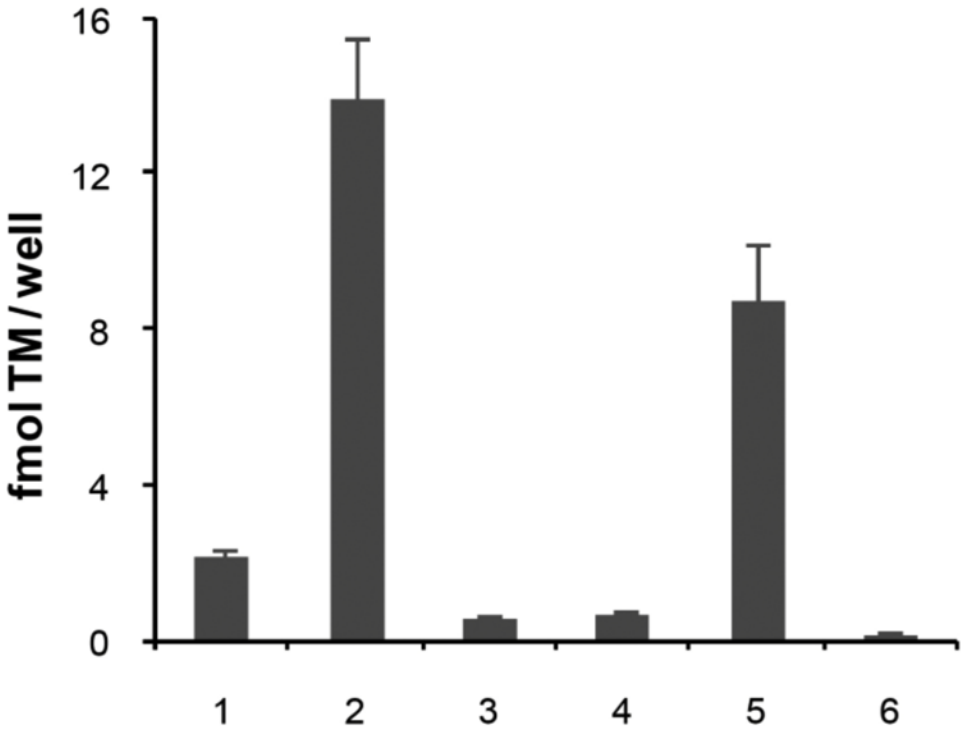


**Reaction conditions**

| Cond | [$TM_{LPETG}$] (μM) | [Sortase] (μM) | Sortase |
|---|---|---|---|
| 1 | 1 | 0.1 | 5’ |
| 2 | 5 | 0.5 | 5’ |
| 3 | 1 | 2 | WT |
| 4 | 5 | 0.5 | WT |
| 5 | 5 | 10 | WT |
| 6 | 5 | – | – |

**Figure 6.6.** Direct sortase-catalyzed assembly of $TM_{LPETG}$ in 50% v/v heparinized whole blood (20 U heparin/mL blood) at 37°C for 1 hour without additional calcium. Evolved and wild-type (WT) sortases were tested at 2 different $TM_{LPETG}$ concentrations as well as $TM_{LPETG}$/sortase ratios, as summarized in the table of reaction conditions.
.

### 6.2.2. Sortase-catalyzed Modification of Catheters *In Vivo*

Recharge of oligoglycine modified catheters deployed in mice with LPETG-tagged probes was tested as a proof-of-concept. We modified polyurethane catheters with pentaglycine anchor motifs using a sequential scheme similar to a previous report (Figure 6.1) [389]. Free isocyanate motifs were first generated on the catheters by reacting hexamethylene diisocyanate with the polyurethane, and subsequently converted to dibenzylcyclooctyne (DBCO) anchor sites using a commercial amino-DBCO linker. Commercial rhodamine-azide was used as a test probe to verify the azide-reactivity of DBCO modified catheters (Figure 6.7). We then reacted $NH_2$-GGGGG-$N_3$ to DBCO modified catheters to display the pentaglycine motifs for SrtA-catalyzed transpeptidation. Optimal reaction parameters that maximize SrtA-catalyzed charging and stripping of catheters were first determined *ex vivo* by fluorescent detection of a biotin-LPETG probe using Cy3-labeled streptavidin (Figure 6.8 – 6.10). Using these optimal reaction conditions as a starting point, we performed deployment of pentaglycine-modified catheters in the vena cava of mice and verified the *in vivo* capacity of 5'SrtA-catalyzed transpeptidation to reversibly immobilize LPETG-tagged probes (Figure 6.11A). Immobilization of biotin-LPETG on GGG-catheters for 1 hour following remote IV delivery through the penile vein was verified using streptavidin-Cy3 and fluorescent imaging (Figure 6.11B). Removal of LPETG-tagged Alexa Fluor 750, a near IR fluorescent probe, by remote IV delivery of GGG peptide and 5'SrtA was monitored by real time fluorescent *in vivo* imaging, which showed a surface depletion half life of approximately 50 minutes (Figure 6.12). Local delivery of reagents for

charging/stripping GGG modified catheters was demonstrated using biotin-LPETG probes under similar conditions (Figure 6.13).

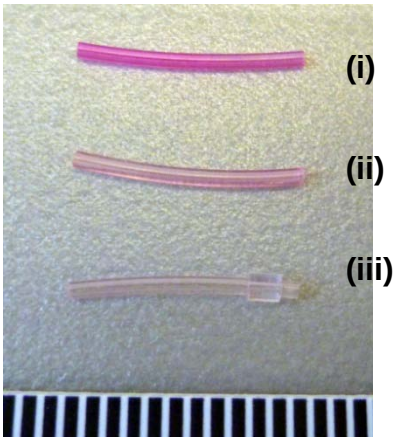


**Figure 6.7**. Verification of the presence of dibenzocyclooctyne (DBCO) motifs on the surface of polyurethane catheters following modification. (i) DBCO catheters reacted with rhodamine azide; (ii) plain catheter reacted with rhodamine azide; (iii) DBCO modified catheter reacted with rhodamine B.

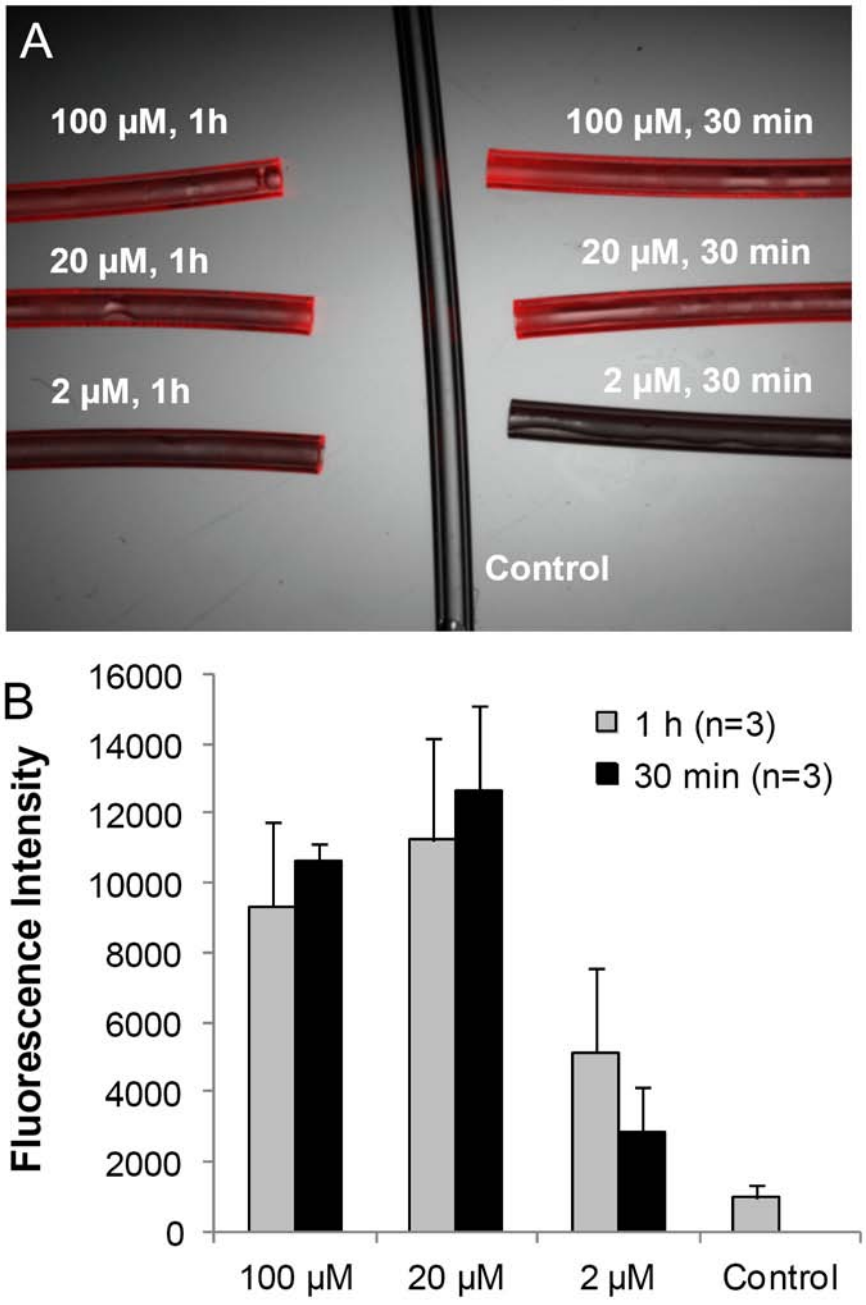


**Figure 6.8**. (A) Merged fluorescent and bright field microscopy of polyurethane catheters modified with pentaglycine motifs, and reacted with various concentrations of biotin-LPETG peptide for 30 minutes or 1 hour. Pentamutant sortase was kept at a constant 0.1 molar equivalent ratio relative to biotin-LPETG. Cy3-streptavidin was incubated at 0.1mg/ml with catheters for 30 minutes to assess the surface density of biotin. (B) Fluorescence intensity was measured using Image J and expressed as mean ± std. dev. for 3 individual catheter segments per reaction condition.

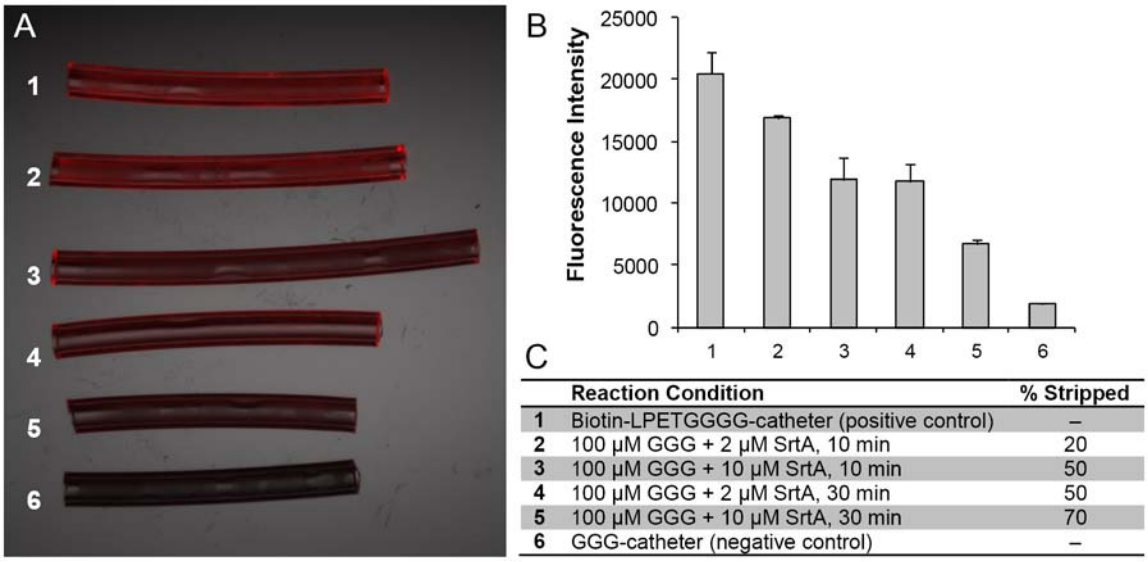


C

| | Reaction Condition | % Stripped |
|---|---|---|
| 1 | Biotin-LPETGGGG-catheter (positive control) | – |
| 2 | 100 μM GGG + 2 μM SrtA, 10 min | 20 |
| 3 | 100 μM GGG + 10 μM SrtA, 10 min | 50 |
| 4 | 100 μM GGG + 2 μM SrtA, 30 min | 50 |
| 5 | 100 μM GGG + 10 μM SrtA, 30 min | 70 |
| 6 | GGG-catheter (negative control) | – |

**Figure 6.9.** (A) Merged fluorescent and bright field microscopy of polyurethane catheters modified with pentaglycine motifs, reacted with biotin-LPETG, and finally with various concentrations of GGG peptide and 5' SrtA as summarized in (C). Cy3-streptavidin was incubated at 0.1mg/ml with catheters for 30 minutes to assess the surface density of biotin. (B) Fluorescence intensity was measured using Image J and expressed as mean ± std. dev. for 3 individual catheter segments per reaction condition.

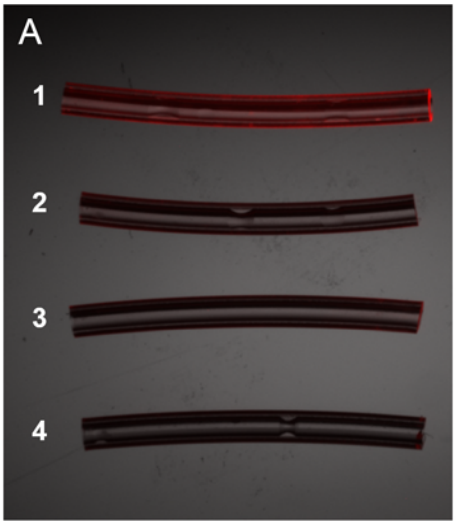


B

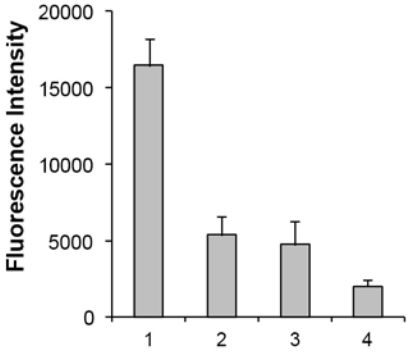


C

| | Reaction Condition | % Stripped |
|---|---|---|
| 1 | Biotin-LPETGGGG-catheter (positive control) | – |
| 2 | 1 mM GGG + 20 μM SrtA, 10 min | 80 |
| 3 | 1 mM GGG + 20 μM SrtA, 30 min | 80 |
| 4 | GGG-catheter (negative control) | – |

**Figure 6.10.** (A) Merged fluorescent and bright field microscopy of polyurethane catheters modified with pentaglycine motifs, reacted with biotin-LPETG, and finally with various concentrations of GGG peptide and 5' SrtA as summarized in (C). Cy3-streptavidin was incubated at 0.1mg/ml with catheters for 30 minutes to assess the surface density of biotin. (B) Fluorescence intensity was measured using Image J and expressed as mean ± std. dev. for 3 individual catheter segments per reaction condition.

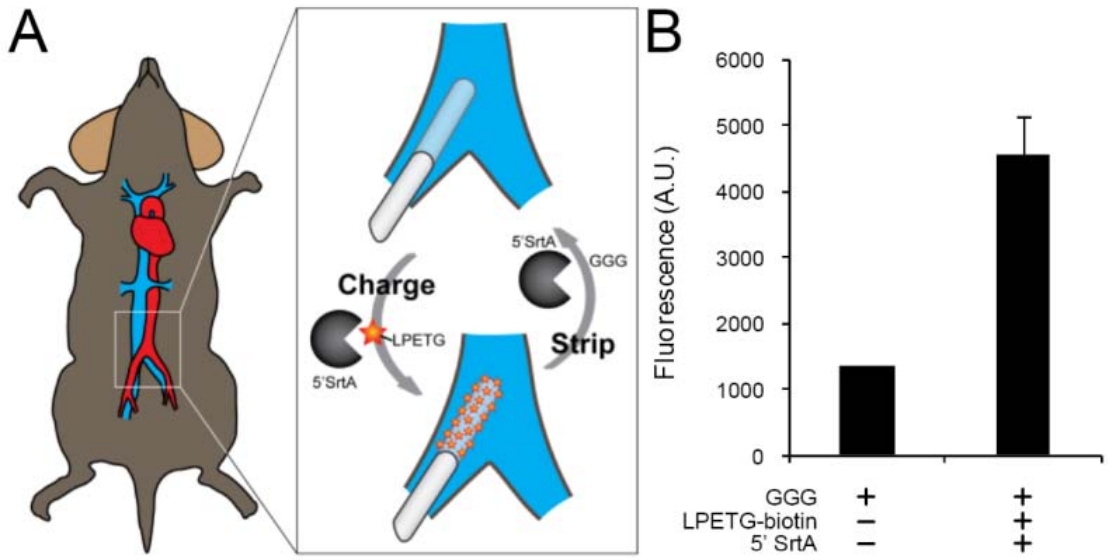


**Figure 6.11.** Sortase-catalyzed reversible covalent assembly of LPETG labeled probes on pentaglycine modified catheters deployed *in vivo*. (A) A 1 F catheter modified with GGG peptide was inserted into the iliac vein and deployed ~1 cm into the inferior vena cava of heparinized C57BL/6 mice. Administration of all reagents was carried out directly through the catheter or remotely through the penile vein. (B) Charge reaction was tested by remote IV delivery of biotin-LPETG peptide (50 µg) and 5' SrtA (70 µg) for 1 h, and assessed using streptavidin-Cy3.

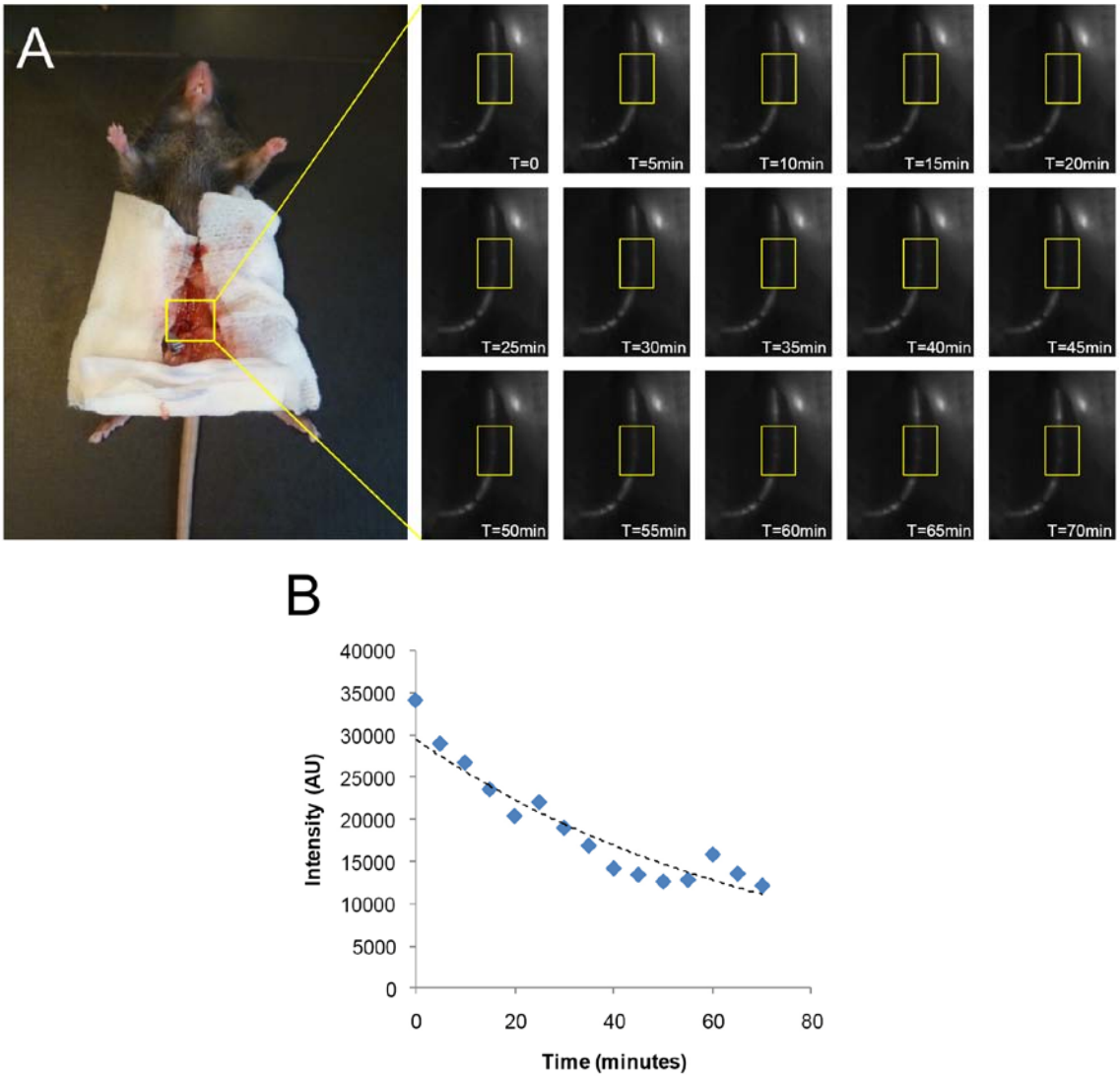


**Figure 6.12**. Catheters modified with GGG peptide and conjugated with LPETG labeled Alexa Fluor 750 was stripped using remote IV delivery of triglycine (400 µg) and 5'SrtA (700 µg). (A) The NIR fluorescent signal from the modified catheter was monitored using the Maestro multi-spectral fluorescence imaging system, and (B) quantitative image analysis was performed to evaluate the fluorescent signal intensity of the modified catheters.

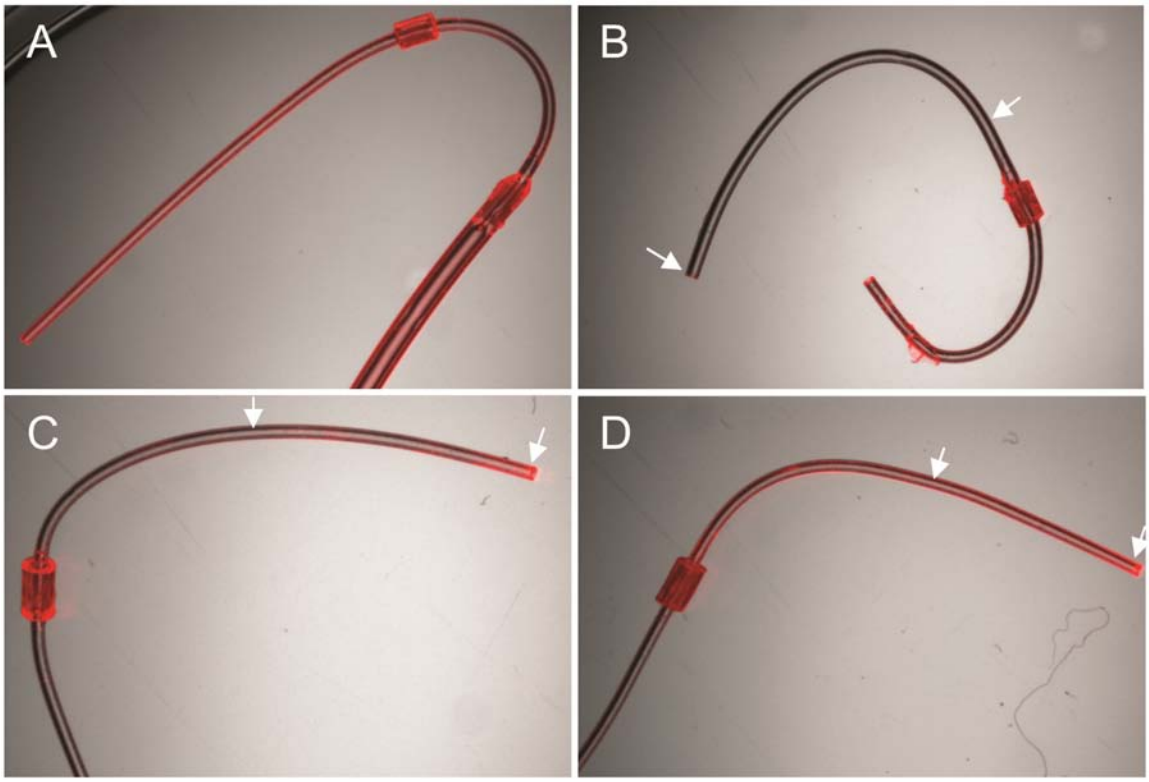


**Figure 6.13.** Fluorescent imaging of cannulated catheters subjected to *in vivo* modification by sortase-catalyzed transpeptidation. Biotin-LPETG probes were used to functionalize GGG modified catheters via transpeptidation, and streptavidin-Cy3 was used to detect the presence of biotin. (A) A fully biotinylated catheter, (B) a biotinylated catheter deployed in a mouse with intravenous injection of 400µg triglycine and 700µg 5' SrtA, (C) a GGG modified catheter deployed in a mouse with intravenous injection of 50µg biotin-LPETG and 70µg 5' SrtA, (D) a GGG modified catheter deployed in a mouse with intravenous injection of 250µg biotin-LPETG and 350µg 5' SrtA. Arrows bracket the insertion length of the catheter into the mouse vena cava.

## 6.3. Conclusions

Immobilization of TM at blood-contacting interfaces may be a key step in the development of a new generation of blood compatible synthetic materials[11, 389]. In particular, we have recently demonstrated in a clinically relevant baboon shunt model of acute graft thrombosis the superior efficacy of immobilized TM to reduce deposition of platelets, compared with commercial heparin modified grafts. Long term bioactivity of TM films may be depleted over time by the harsh *in vivo* environment. A two-step strip/recharge cycle to regenerate immobilized TM may be a potential strategy to extend the life time of bioactive films *in vivo*. We conclusively showed the enhanced efficacy of the evolved sortase variant 5'SrtA over WT SrtA in our demonstration of reversible immobilization of TM *in vitro*. Notably, the covalent bond-forming kinetics of 5'SrtA-catalyzed transpeptidation was similar to avidin-biotin binding interactions.

Although we demonstrated the robust regenerative capacity of pentaglycine surfaces over repeated strip/recharge cycles without reducing the fresh TM surface densities *in vitro*, the efficacy of 5'SrtA will likely decrease over time *in vivo* as suggested by the reduced immobilization efficiency of 5'SrtA in whole blood. Transpeptidation efficiency *in vivo* may be reduced by competitive surface adsorption of blood constituents that sterically hinder access to the LPETG sorting motif, and possibly competitive substrate competition due to presence of alkylamine nucleophiles that also react with SrtA [422]. Further enhancement of the catalytic activity and specificity of 5'SrtA by directed evolution under serum conditions as well as at 37 ºC are underway to overcome these limitations.

The animal model used in this study was intended as a proof of concept system to validate the reversible 5'SrtA's catalyzed transpeptidation *in vivo*, and does not fully recapitulate the operative time and conditions of clinical procedures. Although remote IV delivery of reagents was tested to validate our approach, local recharging strategies may maximize the concentration at the catheter site and thereby shorten the reaction times observed *in vivo*. Moreover, by isolating the site of reaction, the likelihood of systemic exposure to 5'SrtA will be minimized. The immunogenicity of systemically delivered sortase is unknown and would require further evaluation.

In summary, we have determined that SrtA-catalyzed transpeptidation of LPETG-tagged agents on pentaglycine modified surfaces enables the capacity to engineer highly specific, covalent, and rapidly rechargeable surfaces that can undergo regeneration of depleted or degraded biomolecules at a blood-material interface. An evolved SrtA (5'SrtA) was a critical enabling technology in the demonstration of this concept both *in vitro* as well as *in vivo*. Due to the facile incorporation of the LPETG and oligoglycine tags to therapeutic payload, as well as the relatively ease to introduce oligoglycine functionalities onto medical device surfaces, we anticipate this strategy may be applied to stripping and regenerating any of a number of potential film constituents that display finite stability or activity.

## 6.4. Methods

### 6.4.1. Peptides

Synthesis of $NH_2$-GGGGG-$N_3$, $NH_2$-GGGGG-biotin, biotin-LPETG, and $NH_2$-LPETG was performed off-site (Genscript, Piscataway), and LPETG tagged Alexa Fluor

750 was synthesized using $NH_2$-LPETG and Alexa Fluor 750 succinimidyl ester per manufacturer's instructions (Invitrogen, Carlsbad).

### 6.4.2. Expression of $TM_{LPETG}$ and Sortase Variants

Detailed DNA sequence, bacterial expression and purification of $TM_{LPETG}$ and sortase variants are provided in the methods section of Chapter 5. Briefly, the DNA sequence encoding for the human thrombomodulin epidermal growth factor like domains 4 – 6 was cloned into pFLAG ATS expression vector (Sigma). BL21 *E Coli* (Sigma) were transformed with expression plasmid and grown in minimal M9 media supplemented with 19 amino acids and 100 µg/ml ampicilin at 37 ºC until $OD_{600}$ reaches ~0.8. IPTG was added to a final concentration of 1mM, the protein expression was induced for 4 hours at 37 ºC. Following cell harvest by centrifugation, the periplasmic protein crude was obtained by osmotic shock as detailed elsewhere, and $TM_{LPETG}$ was purified by anti-FLAG immunoaffinity chromatography following manufacturer instructions (Sigma). Fractions >95% purity as judged by SDS-PAGE were dialyzed against Tris buffer (20 mM Tris, 100 mM NaCl, pH 7.5). $TM_{LPETG}$ activity was similar to previous TM variants developed in our lab which match the full length TM activity.

### 6.4.3. Immobilization of $TM_{LPETG}$ on Model Substrates

Direct sortase-mediated immobilization of $TM_{LPETG}$ on pentaglycine surfaces was tested in streptavidin coated 96-well microplates (Pierce, Rockford). $NH_2$-GGGGG-biotin was incubated at 200 µM for 1 hour in each well, and washed with TBS (20 mM Tris, 100 mM NaCl, pH 7.5) with 0.05 % Tween 20. 1 µM $TM_{LPETG}$ was immobilized by 0.1 µM or 2 µM SrtA for 1 hour at room temperature. Stripping of immobilized TM was performed using 20 µM SrtA and 1 mM triglycine peptide (Sigma). SrtA-catalyzed

assembly of $TM_{LPETG}$ in heparinized whole blood (20 U/ml freshly drawn blood obtained from healthy volunteer by venipuncture) diluted 50% v/v with normal saline containing the appropriate SrtA, $TM_{LPETG}$, or GGG reagents was carried out at 37 °C for 1 hour without additional calcium. The surface density of bound $TM_{LPETG}$ was determined per manufacturer's instructions (American Diagnostica, Stamford). Moles of $EGF_{5-6}$ domains bound to each microwell were calculated by a standard curve generated by ELISA kit using known concentrations of TM provided by the manufacturer.

### 6.4.4. Modification of Catheters *In Vitro*

Polyurethane mouse arterial catheters (SAI Infusion) with a 1F tip were modified with DBCO anchor motifs. Catheters were first reacted with 16% v/v hexamethylene diisocyanate (HDI) and 4% v/v triethylamine (TEA) in toluene at 50 °C for 1 h and rinsed in toluene for 6 h. Isocyanate activated catheters were reacted with 1 mg/ml DBCO-amine linker (Click Chemistry Tools, Scottsdale) and TEA (1% v/v) in toluene at 40 °C overnight, rinsed with toluene for 6 h, and dried under vacuum at 25 °C overnight. DBCO activated catheters were reacted with 1 mg/ml tetramethylrhodamine -5-carbonyl azide (Invitrogen, Carlsbad) in 1:4 tert-butanol/PBS at 37 °C for 24 h followed by rinsing in methanol for 24 h to confirm surface cyclooctyne reactivity. DBCO activated catheters were reacted with $NH_2$-GGGGG-$N_3$ at 37 °C overnight, and rinsed in TBS buffer (20 mM Tris pH 7.5, 100 mM NaCl). Pentaglycine modified catheters were incubated with biotin-LPETG or LPETG-labeled Alexa Fluor 750 peptide (2 µM to 100 µM) and 0.1 molar equivalents of 5' SrtA with relative to the LPETG probe concentration for 30 minutes or 1 hour, and rinsed for 4 hours in TBS. Biotinylated catheters were incubated in 0.1 mg/ml streptavidin-Cy3 in TBS with 0.05% Tween 20 for

30 min, and rinsed overnight in TBS. Imaging of catheters was carried out using the Zeiss Discovery V20 Stereo Microscope, and quantitative image analysis by ImageJ was performed to compare the fluorescence intensity between samples.

### 6.4.5. Deployment of Catheters in Mice

Modified polyurethane mouse arterial catheters (SAI Infusion) with a 1F tip were first perfused with 2U of heparin, then clamped shut at the infusion end. The procedure begins with opening the mouse abdomen and tying off one branch of the femoral vein with a suture. Next, both the vena cava and the remaining branch of the femoral vein was clamped approximately 1cm from the aortofemoral bifurcation. A separate suture was placed closer to bifurcation to provide support for the catheter, which was deployed approximately 0.5cm deep into the vena cava followed by releasing of the clamps. The catheter was then delivered 1 – 1.5 cm deep into the vena cava.

### 6.4.6. Dosing of Reagents in Mice

A 200µl dose of sortase, LPETG tagged probe, and 20U of heparin was injected intravenously into the mouse circulation through the catheter. The dosage required for a mouse blood volume of 2 ml was calculated using the optimized concentrations of sortase, GGG peptide, and biotin-LPETG from *in vitro* catheter modification studies. After reaction, the catheter was removed and incubated in streptavidin-Cy3 (30 min) and washed with buffer (2 h). Fluorescent and brightfield microscopy images were merged to detect biotin groups on the catheter surface. A Maestro Multi-Spectral *in vivo* fluorescence imaging system with near-IR filter sets was used to detect the Alexa Fluor 750 modified catheters deployed in the mouse vena cava. Images were taken using a

monochromatic 12-bit camera, and analyzed using ImageJ to quantitatively compare the level of fluorescence signal on the catheters.

### 6.4.7. Statistical Analysis

Two-tailed student's *t*-test assuming unequal variances was used to test for statistical significance between the means of two groups.

# CHAPTER 7

# CONCLUSIONS AND FUTURE DIRECTIONS

## 7.1. Conclusions

Synthetic conduits in modern arterial reconstructive or bypass surgery based on Teflon and Dacron polymers have largely remained unchanged since their inception half a century ago, and their incompatibility in small-diameter (< 6 mm id) applications such as coronary and lower extremity arterial bypass has been well documented. Despite significant progress towards understanding the physiological elaboration of thrombotic cascades elicited by synthetic materials, as well as efforts to functionalize the surface of implantable devices with bioactive therapeutics, a generally accepted blood-compatible material does not exist. This status quo has necessitated the use of pharmaceutical antithrombotic therapies with substantial cost burdens and bleeding risks in order to prolong the life time of synthetic vascular grafts, as well as other implantable devices and artificial organ systems that operate in direct contact with blood.

In this dissertation, we developed surface engineering platforms inspired by natural mechanisms contained in the endothelial lining of the circulatory system that attenuate thrombosis. In contrast with heparin, thrombomodulin (TM) is the major endogenous inhibitor of thrombin production localized on the endothelial cell surface. We developed covalent chemical coupling strategies to immobilize TM on blood-contacting interfaces, and validated their capacity to inhibit platelet deposition in a clinically relevant baboon shunt model of acute graft thrombosis. Moreover, we

demonstrated a reversible chemoenzymatic approach to regenerate depleted surfaces, with the potential to extend the life time of biologically active films.

During the course of these studies, it became apparent that the highly modular nature of chemoenzymatic bond-forming reaction enabled by directed evolution of the calcium-dependent cysteine transpeptidase Sortase A could be broadly applied in site-specific bioconjugation as well as surface immobilization reactions. As such, the synthetic simplicity of incorporating LPXTG and oligoglycine sorting motifs would facilitate sortase-catalyzed covalent modification of a range of candidate biomolecules, such as bioenzymes, peptides, and polysaccharides. Consequently, the sortase-catalyzed bioconjugation schemes presented here have established the use of reversible chemoenzymatic bond-formation as a paradigm for future design of medical device, diagnostics, drug delivery, and artificial organ systems, as well as development of more efficient solid-supported catalysts in industrial bioprocess engineering operations.

In the first phase of this dissertation, we aimed to optimize surface modification strategies to maximize the surface density of anchor sites available for assembly of bioactive enzymes. Layer-by-layer assembly of polyelectrolytes has emerged as a powerful and facile method to generate nanoscale architectures on a broad range of substrates. We tested the application of this strategy to incorporate a reservoir of the highly negatively charged heparin as a film component. The exponential growth nature of these films may maximize the surface density of chemical handles for downstream functionalization. Film growth behavior of PEM films incorporating heparin was explored, and the growth of PEM films on quartz substrates and ePTFE were characterized. Importantly, we showed that simple hydrazone bond forming reactions

could covalently crosslink oxidized polysaccharide components to improve the stability of the films on quartz substrates, and preserve the primary amine sites on the polycations for bioconjugate coupling. These strategies were translated to modify the luminal surface of commercial ePTFE grafts, which yielded films of excellent uniformity and acceptable stability under sustained high shears. Fluorescent probes were conjugated to the primary amine on the polycation as a demonstration of the potential anchor site density that could be generated on the luminal surface of commercial ePTFE vascular grafts, and the outcomes reported here motivate future work to optimize the covalent immobilization of biomolecules on these films.

In the second phase of this dissertation, we hypothesized that the immobilization of active catalysts that inhibit generation of thrombin can be assembled on the luminal surface of synthetic vascular grafts to abrogate coagulation activation cascades. Thrombomodulin, a transmembrane cofactor for thrombin that catalyzes production of activated protein C, represents a major physiologically active mechanism on the endothelial cell surface to prevent undesirable thrombosis in the circulatory system. We successfully expressed a recombinant human TM fragment (TM456) that contains the minimal fragment necessary for catalytic activity, as well as a single C-terminal azide which was incorporated by auxotrophic expression in *E Coli* with the methionine analogue homoazidoalanine. Site-specific immobilization of TM-$N_3$ on the luminal surface of commercial 4 mm i.d. ePTFE vascular grafts was carried out by a sequential chemical modification procedure that yielded the requisite triphenylphosphine motifs necessary for bioorthogonal covalent conjugation to azide, otherwise known as Staudinger Ligation. Using this approach, we were able to demonstrate site-specific

immobilization of TM-$N_3$ surface assemblies, which exhibited minimal change in activity following 24 h of 500 $s^{-1}$ fluid shear at 37 °C, as well as after 2 additional weeks of incubation at 37 °C in PBS. These results indicate that the covalent linkage of TM-$N_3$ to the graft surface remains stable under prolonged exposure to *in vivo* arterial shear rates as well as physiological pH and temperature. Moreover, TM modified ePTFE grafts exhibited reduced capacity to elicit deposition of platelets compared with non-TM grafts in a multi-chamber A-V shunt model in nonhuman primates. These results indicate that the site-specific immobilization thrombomodulin reconstitutes its antithrombotic activity to the blood-contacting interface, and may represent an important paradigm in the future design of blood-compatible materials.

In the third phase of this work, we focused on improving the surface activity of TM modified grafts by optimizing both the surface coupling chemistry, as well as recombinant engineering of TM-$N_3$. Specifically, a substitute for auxotrophic expression to generate TM-$N_3$, which limits scalability and the selection of bioenzymes that could be immobilized, was optimized. Chemoenzymatic coupling schemes are highly specific and rapid, and the bond-forming reaction catalyzed by the calcium-dependent cysteine transpeptidase *S. Aureus* Sortase A has emerged as a powerful tool to covalently modify or immobilize proteins containing a short LPXTG "sorting motif". We successfully expressed a recombinant TM456 variant containing a C-terminal LPETG motif in *E Coli* as a proof of concept. Notably, this $TM_{LPETG}$ construct could be potentially expressed in eukaryotic systems to optimize folding and post-translational modification, and may be a key step in adapting our method to standard protein production methods in the biopharmaceutical industry. We unexpectedly discovered that a mutant sortase A (5'

SrtA) variant, which exhibited enhanced catalytic activity, facilitated efficient covalent coupling of simple PEG-amine nucleophiles when they are reacted in high molar excess relative to $TM_{LPETG}$. We confirmed this approach using both a 5kD PEG-amine as well as azido-$PEG_3$-amine, which provided an alternate route to generate a single C-terminal azide motif on TM for immobilization on medical device surfaces. Moreover, the luminal surface of ePTFE vascular grafts could be modified with dibenzocyclooctyne (DBCO) motifs, which facilitate copper-free [3+2] cycloaddition to conjugate azide-tagged TM. Following exposure to standard ethylene oxide treatment, immobilized DBCO motifs on the luminal surface of commercial vascular grafts retained their capacity to undergo [3+2] cycloaddition to bind azide-tagged TM as well as other biomolecules such as biotin and rhodamine. Therefore, copper-free click chemistry provides a potential route to enable the clinical translation of our platform to satisfy the requisite terminal sterilization procedures used in industrial medical device manufacturing processes. Notably, TM grafts fabricated using this platform significantly reduced platelet deposition compared with commercial heparin coated vascular grafts, as well as plain grafts *in vivo*. The non-human primate model we used to test the blood compatibility of heparin and TM modified materials was the first to incorporate a thrombotic stress source that is more characteristic of the anastomotic tissue injury that occurs during and after graft implantation.

Long term performance of bioactive surface enzyme assemblies is limited due to degradation in the operating environment by stresses that include, among others, oxidation, hydrolysis, and proteolysis. In the final phase of this work, we developed a reversible surface engineering approach that could extend the lifetime of TM activity on

surfaces, using a bioorthogonal covalent chemistry scheme that facilitates removal of activity-depleted TM and regenerating the surface with fresh bioactive TM. We hypothesized that by shifting the reaction equilibrium of sortase A (SrtA), a house-keeping calcium-dependent cysteine transpeptidase used to anchor cell surface proteins in *S. Aureus*, a two-step strip/charge cycle could be performed to regenerate immobilized TM. Although these efforts were limited by the low catalytic activity of wild-type SrtA, we demonstrated that a mutant SrtA which exhibited 140-fold higher catalytic activity enabled the rapid and repeatable recharging of TM surfaces *in vitro*. Significantly, we were able to demonstrate the *in vivo* application of this approach to modify catheters deployed in the mice. To our knowledge, these results are the first to demonstrate a covalent chemistry approach to repeatably regenerate the activity of enzyme surface assemblies by a rapid two-step cycle. The capacity to recharge solid surfaces *in situ* under a range of environmental conditions would prolong the lifetime of medical device, diagnostics, and artificial organ system designs, as well as solid supported enzymes in industrial bioprocess applications.

### 7.2. Future Directions

Our long term goal is to develop a small-diameter synthetic conduit that performs comparably or superior to autologous vessels in vascular reconstructive surgery. We anticipate this will involve the combination of advances in (1) material science and tissue engineering to generate scaffolds which match the mechanical attributes of the native artery and satisfy surgical requirements such as burst strength and suture retention, as well as industrial manufacturing specifications such as scalability, off-the-shelf availability, and sterility; and (2) surface engineering approaches to incorporate

therapeutic biomolecules that minimize deleterious short term inflammatory and thrombotic cascades, and promote the regeneration of cellular components of the native blood vessel, in particular, a confluent endothelial lining to maintain long term blood compatibility.

Our specific objective is to develop a surface engineering platform that maximizes the functional activity and duration of biologically active components critical to limiting the elaboration of inflammatory and thrombotic cascades, as well as promoting the regeneration of cellular and matrix components critical to restoring the surface characteristics of the native blood vessel. Towards this end, we propose three major areas for future exploration: (1) maximize the biological activity and manufacturing scalability of thrombomodulin using eukaryotic cell lines that conform to current industry standards for recombinant human protein production; (2) directed evolution of sortase A to generate a family of highly active and bioorthogonal variants that facilitate rapid surface modification *in vivo*, as well as assembly of heterofunctional surface components that combine the antithrombotic function of TM with bioactive factors that control inflammation and promote regeneration of the endothelial cell lining; and (3) development of conformal film coating strategies that maximize the surface density of anchor sites for immobilization of bioactive components, and minimize perturbation to the underlying architecture of the synthetic material component.

First, the production of recombinant $TM_{LPETG}$ will be optimized using appropriate expression systems at scales suitable for industry manufacturing. Soluble recombinant human thrombomodulin has been explored by a number of pharmaceutical companies (Recomodulin by Asahi Kasei Pharm, Tokyo, Japan; Solulin by Schering, Berlin,

Germany; rTM by Eli Lilly), and the production of TM has been primarily carried out in eukaryotic expression systems, such as mammalian and insect cell lines, that optimize the folding of the ~120 amino acid TM456 fragment which contains 9 disulfide bonds that are essential for biological activity. Currently, the periplasmic expression system in E Coli suffers from poor yield, due in part to the highly inefficient purification protocol that likely generates a mixture that includes a substantial portion of misfolded TM456. Moreover, it has been demonstrated that several post-translational modifications to TM may be essential for biological activity, and current *E Coli* expression systems generally lack the necessary cellular machinery to achieve these modifications. Therefore, a reasonable next step to maximize the activity of $TM_{LPETG}$ is to optimize the amino acid sequence of TM to recapitulate the post-translational modifications and express the final construct in eukaryotic systems that maximize yields and folding of the TM product.

Second, the general directed evolution system based on yeast display that was recently developed could be utilized to further evolve orthogonal sortase variants with altered substrate specificity and enhanced catalytic activity. Transpeptidation by sortase A is suitable for a broad range of candidate biomolecules due to the synthetic simplicity of incorporating a C-terminal LPETG tags on compounds such as TM, heparin, CD39, PEG, and other peptides. In addition, increasing the catalytic activity of the existing 5' SrtA may improve the stripping efficiency in our current surface recharge scheme. Specifically, mutant 5' SrtA libraries cloned in yeast cells will be subjected to evolutionary pressure to enhance the affinity for LPESG, LAETG, or LAESG substrates in the presence of competing LPETG peptide at 37C in serum, in order to enrich mutants for maximal activity under simulated *in vivo* conditions. The surviving sortase genes

from the first phase will be diversified by gene shuffling, and subjected to greater evolutionary pressure for overall catalytic activity, by increasing selection stringency, reducing substrate concentration, and shortening reaction time with each successive round. We postulate that these efforts will yield highly efficient transpeptidation catalysts that recognize unique peptide motifs. These evolved sortase variants may be a key step in generating multimeric and/or heterofunctional bioenzyme assemblies that synergize the activity of surface enzyme assemblies which resist platelet and coagulation activation cascades, as well as biofilm formation, to improve the durability of implantable medical devices that operate in contact with blood.

A final area for future research will be the optimization of conformal coatings strategies that are suitable for generating high densities of anchor motifs to immobilize desired biomolecules with minimal impact on the bulk material properties. This set of parameters may be essential in future effort to synergize bioactive surface properties with bulk properties that optimize both blood-material and tissue-material interactions. In this dissertation we have demonstrated the layer-by-layer assembly of polyelectrolyte multilayers on ePTFE grafts. Alternatively, generation of reactive chemical groups by high energy methods, such as plasma irradiation or electron beams, may provide highly stable anchor sites but must be engineered to minimize risk of degrading the structural integrity of the underlying material. Chemical vapor deposition methods could also be a viable strategy to generate thin conformal coatings for immobilization of biomolecules, however, the challenge of generating a uniform coating on the luminal surface of vascular grafts remains a major hurdle. Another option is the use of mussel adhesive peptides motifs to generate conformal films, though the stability of these strategies in the harsh

physiological environment has not been validated. The testing and optimization of these conformal surface modification strategies may ultimately yield a platform that is compatible with any number of synthetic or biological materials used in the construction of implantable medical devices and artificial organs.

In summary, future efforts to achieve our goal of developing a small-diameter synthetic arterial substitute will hinge on the optimization of 3 major areas: the bioactive therapeutic production (TM, heparin, CD39, etc), the surface coupling chemistry (copper-free click, sortase, etc), as well as the surface coating methodology (PEM, plasma, CVD, etc) to maximize the surface activity and duration, as well as adaptability across synthetic and tissue engineered materials.

## REFERENCES


1. Douketis JD, Berger PB, Dunn AS, Jaffer AK, Spyropoulos AC, Becker RC, *et al.* The perioperative management of antithrombotic therapy: American College of Chest Physicians Evidence-Based Clinical Practice Guidelines (8th Edition). *Chest* 2008, **133**(6 Suppl)**:** 299S-339S.

2. Tatterton M, Wilshaw SP, Ingham E, Homer-Vanniasinkam S. The use of antithrombotic therapies in reducing synthetic small-diameter vascular graft thrombosis. *Vascular and endovascular surgery* 2012, **46**(3)**:** 212-222.

3. Conte MS. The ideal small arterial substitute: a search for the Holy Grail? *FASEB J* 1998, **12**(1)**:** 43-45.

4. Zilla P, Bezuidenhout D, Human P. Prosthetic vascular grafts: wrong models, wrong questions and no healing. *Biomaterials* 2007, **28**(34)**:** 5009-5027.

5. Ma PX. Biomimetic materials for tissue engineering. *Advanced drug delivery reviews* 2008, **60**(2)**:** 184-198.

6. Place ES, Evans ND, Stevens MM. Complexity in biomaterials for tissue engineering. *Nature materials* 2009, **8**(6)**:** 457-470.

7. Crapo PM, Gilbert TW, Badylak SF. An overview of tissue and whole organ decellularization processes. *Biomaterials* 2011, **32**(12)**:** 3233-3243.

8. Ratner BD. The catastrophe revisited: blood compatibility in the 21st Century. *Biomaterials* 2007, **28**(34)**:** 5144-5147.

9. Qu Z, Chaikof EL. Interface between hemostasis and adaptive immunity. *Current opinion in immunology* 2010, **22**(5)**:** 634-642.

10. Furie B, Furie BC. Mechanisms of thrombus formation. *The New England journal of medicine* 2008, **359**(9)**:** 938-949.

11. Jordan SW, Chaikof EL. Novel thromboresistant materials. *J Vasc Surg* 2007, **45 Suppl A:** A104-115.

12. Li S, Henry JJ. Nonthrombogenic approaches to cardiovascular bioengineering. *Annual review of biomedical engineering* 2011, **13:** 451-475.

13. Gott VL, Whiffen JD, Dutton RC. Heparin Bonding on Colloidal Graphite Surfaces. *Science* 1963, **142**(3597)**:** 1297-1298.

14. Murugesan S, Xie J, Linhardt RJ. Immobilization of heparin: approaches and applications. *Current topics in medicinal chemistry* 2008, **8**(2)**:** 80-100.

15. Bishop JR, Schuksz M, Esko JD. Heparan sulphate proteoglycans fine-tune mammalian physiology. *Nature* 2007, **446**(7139)**:** 1030-1037.

16. de Agostini AI, Watkins SC, Slayter HS, Youssoufian H, Rosenberg RD. Localization of anticoagulantly active heparan sulfate proteoglycans in vascular endothelium: antithrombin binding on cultured endothelial cells and perfused rat aorta. *The Journal of cell biology* 1990, **111**(3)**:** 1293-1304.

17. HajMohammadi S, Enjyoji K, Princivalle M, Christi P, Lech M, Beeler D, *et al.* Normal levels of anticoagulant heparan sulfate are not essential for normal hemostasis. *The Journal of clinical investigation* 2003, **111**(7)**:** 989-999.

18. Conway EM. Thrombomodulin and its role in inflammation. *Seminars in immunopathology* 2012, **34**(1)**:** 107-125.

19. Esmon CT. The roles of protein C and thrombomodulin in the regulation of blood coagulation. *The Journal of biological chemistry* 1989, **264**(9)**:** 4743-4746.

20. Lloyd-Jones D, Adams RJ, Brown TM, Carnethon M, Dai S, De Simone G, *et al.* Heart disease and stroke statistics--2010 update: a report from the American Heart Association. *Circulation* 2010, **121**(7)**:** e46-e215.

21. Hirsch AT, Haskal ZJ, Hertzer NR, Bakal CW, Creager MA, Halperin JL, *et al.* ACC/AHA 2005 guidelines for the management of patients with peripheral arterial disease (lower extremity, renal, mesenteric, and abdominal aortic): executive summary. *J Am Coll Cardiol* 2006, **47**(6)**:** 1239-1312.

22. Voorhees A, Jaretski A, Blakemore A. The use of tubes constructed from Vinyon "N" cloth in bridging arterial defects. *Ann Surg* 1952, **135:** 332.

23. Edwards WS, Tapp JS. Chemically treated nylon tubes as arterial grafts. *Surgery* 1955, **38**(1)**:** 61-70.

24. Harrison JH. Synthetic materials as vascular prostheses. II. A comparative study of nylon, dacron, orlon, ivalon sponge and teflon in large blood vessels with tensile strength studies. *American journal of surgery* 1958, **95**(1)**:** 16-24.

25. Kakisis JD, Liapis CD, Breuer C, Sumpio BE. Artificial blood vessel: the Holy Grail of peripheral vascular surgery. *J Vasc Surg* 2005, **41**(2)**:** 349-354.

26. Walpoth BH, Bowlin GL. The daunting quest for a small diameter vascular graft. *Expert Rev Med Devices* 2005, **2**(6)**:** 647-651.

27. Abbott WM, Green RM, Matsumoto T, Wheeler JR, Miller N, Veith FJ, *et al.* Prosthetic above-knee femoropopliteal bypass grafting: Results of a multicenter randomized prospective trial. Above-Knee Femoropopliteal Study Group. *J Vasc Surg* 1997, **25**(1)**:** 19-28.

28. Noon G, DeBakey M. DeBakey Dacron Prosthesis and Filamentous Velour Graft. In: Sawyer PN, Kaplitt MJ (eds). *Vascular Grafts*. Appleton-Century-Crofts: New York, NY, 1978, pp 177-184.

29. Jonas RA, Ziemer G, Schoen FJ, Britton L, Castaneda AR. A new sealant for knitted Dacron prostheses: minimally cross-linked gelatin. *J Vasc Surg* 1988, **7**(3)**:** 414-419.

30. Scott SM, Gaddy LR, Sahmel R, Hoffman H. A collagen coated vascular prosthesis. *The Journal of cardiovascular surgery* 1987, **28**(5)**:** 498-504.

31. Cziperle DJ, Joyce KA, Tattersall CW, Henderson SC, Cabusao EB, Garfield JD, *et al.* Albumin impregnated vascular grafts: albumin resorption and tissue reactions. *The Journal of cardiovascular surgery* 1992, **33**(4)**:** 407-414.

32. De Mol Van Otterloo JC, Van Bockel JH, Ponfoort ED, Briet E, Brommer EJ, Hermans J, *et al.* Systemic effects of collagen-impregnated aortoiliac Dacron vascular prostheses on platelet activation and fibrin formation. *J Vasc Surg* 1991, **14**(1)**:** 59-66.

33. Shindo S, Motohashi S, Katsu M, Kaga S, Inoue H, Matsumoto M. Coated prostheses are associated with prolonged inflammation in aortic surgery: A cost analysis. *Artif Organs* 2008, **32**(3)**:** 183-187.

34. Prager M, Polterauer P, Bohmig HJ, Wagner O, Fugl A, Kretschmer G, *et al.* Collagen versus gelatin-coated Dacron versus stretch polytetrafluoroethylene in abdominal aortic bifurcation graft surgery: results of a seven-year prospective, randomized multicenter trial. *Surgery* 2001, **130**(3)**:** 408-414.

35. Prager MR, Hoblaj T, Nanobashvili J, Sporn E, Polterauer P, Wagner O, *et al.* Collagen- versus gelatine-coated Dacron versus stretch PTFE bifurcation grafts for aortoiliac occlusive disease: long-term results of a prospective, randomized multicenter trial. *Surgery* 2003, **134**(1)**:** 80-85.

36. Goldman M, McCollum CN, Hawker RJ, Drolc Z, Slaney G. Dacron arterial grafts: the influence of porosity, velour, and maturity on thrombogenicity. *Surgery* 1982, **92**(6)**:** 947-952.

37. Eiberg JP, Røder O, Stahl-Madsen M, Eldrup N, Qvarfordt P, Laursen A, *et al.* Fluoropolymer-coated Dacron versus PTFE grafts for femorofemoral crossover

bypass: randomised trial. *European Journal of Vascular and Endovascular Surgery* 2006, **32**(4)**:** 431-438.

38. Nunn DB, Freeman MH, Hudgins PC. Postoperative alterations in size of Dacron aortic grafts: an ultrasonic evaluation. *Ann Surg* 1979, **189**(6)**:** 741-745.

39. Pourdeyhimi B, Text C. A review of structural and material properties of vascular grafts. *Journal of biomaterials applications* 1987, **2**(2)**:** 163-204.

40. Nunn DB. Structural failure of Dacron arterial grafts. *Seminars in vascular surgery* 1999, **12**(1)**:** 83-91.

41. Wilson SE, Krug R, Mueller G, Wilson L. Late disruption of Dacron aortic grafts. *Annals of vascular surgery* 1997, **11**(4)**:** 383-386.

42. Van Damme H, Deprez M, Creemers E, Limet R. Intrinsic structural failure of polyester (Dacron) vascular grafts. A general review. *Acta chirurgica Belgica* 2005, **105**(3)**:** 249-255.

43. Soyer T, Lempinen M, Cooper P, Norton L, Eiseman B. A new venous prosthesis. *Surgery* 1972, **72**(6)**:** 864-872.

44. Campbell CD, Brooks DH, Webster MW, Bahnson HT. The use of expanded microporous polytetrafluoroethylene for limb salvage: a preliminary report. *Surgery* 1976, **79**(5)**:** 485-491.

45. Greisler HP. *New biologic and synthetic vascular prostheses*. R.G. Landes Co.: Austin, 1991.

46. Clowes AW, Kirkman TR, Reidy MA. Mechanisms of arterial graft healing. Rapid transmural capillary ingrowth provides a source of intimal endothelium and smooth muscle in porous PTFE prostheses. *Am J Pathol* 1986, **123**(2)**:** 220-230.

47. Lenz BJ, Veldenz HC, Dennis JW, Khansarinia S, Atteberry LR. A three-year follow-up on standard versus thin wall ePTFE grafts for hemodialysis. *J Vasc Surg* 1998, **28**(3)**:** 464-470; discussion 470.

48. Hamlin GW, Rajah SM, Crow MJ, Kester RC. Evaluation of the thrombogenic potential of three types of arterial graft studied in an artificial circulation. *Br J Surg* 1978, **65**(4)**:** 272-276.

49. Goldman M, Hall C, Dykes J, Hawker RJ, McCollum CN. Does 111indium-platelet deposition predict patency in prosthetic arterial grafts? *Br J Surg* 1983, **70**(10)**:** 635-638.

50. Allen BT, Mathias CJ, Sicard GA, Welch MJ, Clark RE. Platelet deposition on vascular grafts. The accuracy of in vivo quantitation and the significance of in vivo platelet reactivity. *Ann Surg* 1986, **203**(3)**:** 318-328.

51. Shepard AD, Gelfand JA, Callow AD, O'Donnell TF, Jr. Complement activation by synthetic vascular prostheses. *J Vasc Surg* 1984, **1**(6)**:** 829-838.

52. Griffiths GD, Nagy J, Black D, Stonebridge PA. Randomized clinical trial of distal anastomotic interposition vein cuff in infrainguinal polytetrafluoroethylene bypass grafting. *Br J Surg* 2004, **91**(5)**:** 560-562.

53. Panneton JM, Hollier LH, Hofer JM. Multicenter randomized prospective trial comparing a pre-cuffed polytetrafluoroethylene graft to a vein cuffed polytetrafluoroethylene graft for infragenicular arterial bypass. *Annals of vascular surgery* 2004, **18**(2)**:** 199-206.

54. Pinchuk L. A review of the biostability and carcinogenicity of polyurethanes in medicine and the new-generation of biostable polyurethanes. *Journal of Biomaterials Science-Polymer Edition* 1994, **6**(3)**:** 225-267.

55. Webb LX, Schmidt U. Vacuum therapy for wound management. *Unfallchirurg* 2001, **104**(10)**:** 918-926.

56. Uchida N, Kambic H, Emoto H, Chen JF, Hsu SH, Murabayshi S, *et al.* Compliance effects on small-diameter polyurethane graft patency. *Journal of Biomedical Materials Research* 1993, **27**(10)**:** 1269-1279.

57. Santerre JP, Labow RS, Duguay DG, Erfle D, Adams GA. Biodegradation evaluation of polyether and polyester-urethanes with oxidative and hydrolytic enzymes. *Journal of Biomedical Materials Research* 1994, **28**(10)**:** 1187-1199.

58. Zhang Z, Marois Y, Guidoin RG, Bull P, Marois M, How T, *et al.* Vascugraft(R) polyurethane arterial prosthesis as femoro-popliteal and femoro-peroneal bypasses in humans: Pathological, structural and chemical analyses of four excised grafts. *Biomaterials* 1997, **18**(2)**:** 113-124.

59. Brinton LA, Brown SL. Breast implants and cancer. *Journal of the National Cancer Institute* 1997, **89**(18)**:** 1341-1349.

60. Glickman MH, Stokes GK, Ross JR, Schuman ED, Sternbergh WC, Lindberg JS, *et al.* Multicenter evaluation of a polyurethaneurea vascular access graft as compared with the expanded polytetrafluoroethylene vascular access graft in hemodialysis applications. *Journal of Vascular Surgery* 2001, **34**(3)**:** 465-473.

61. Farrar DJ. Development of a prosthetic coronary artery bypass graft. *The heart surgery forum* 2000, **3**(1)**:** 36-40.

62. Salacinski HJ, Tai NR, Carson RJ, Edwards A, Hamilton G, Seifalian AM. In vitro stability of a novel compliant poly(carbonate-urea) urethane to oxidative and hydrolytic stress. *Journal of Biomedical Materials Research* 2002, **59**(2)**:** 207-218.

63. Seifalian AM, Salacinski HJ, Tiwari A, Edwards A, Bowald S, Hamilton G. In vivo biostability of a poly(carbonate-urea)urethane graft. *Biomaterials* 2003, **24**(14)**:** 2549-2557.

64. Edwards A, Carson RJ, Szycher M, Bowald S. In vitro and in vivo biodurability of a compliant microporous vascular graft. *Journal of biomaterials applications* 1998, **13**(1)**:** 23-45.

65. Wilson GJ, MacGregor DC, Klement P, Dereume JP, Weber BA, Binnington AG, *et al.* The composite Corethane/Dacron vascular prosthesis. Canine in vivo evaluation of 4 mm diameter grafts with 1 year follow-up. *ASAIO transactions / American Society for Artificial Internal Organs* 1991, **37**(3)**:** M475-476.

66. Cinar B, Goksel OS, Yekeler I. Midterm results with the use of polycarbonate urethane heterografts for dialysis access. *The Tohoku journal of experimental medicine* 2005, **207**(3)**:** 233-238.

67. Helmus MN, Gibbons DF, Cebon D. Biocompatibility: meeting a key functional requirement of next-generation medical devices. *Toxicologic pathology* 2008, **36**(1)**:** 70-80.

68. Davi G, Patrono C. Platelet activation and atherothrombosis. *The New England journal of medicine* 2007, **357**(24)**:** 2482-2494.

69. Weiler H. Regulation of inflammation by the protein C system. *Crit Care Med* 2010, **38**(2 Suppl)**:** S18-25.

70. Banerjee I, Pangule RC, Kane RS. Antifouling Coatings: Recent Developments in the Design of Surfaces That Prevent Fouling by Proteins, Bacteria, and Marine Organisms. *Advanced Materials* 2011, **23**(6)**:** 690-718.

71. Olsen SM, Pedersen LT, Laursen MH, Kiil S, Dam-Johansen K. Enzyme-based antifouling coatings: a review. *Biofouling* 2007, **23**(5-6)**:** 369-383.

72. Talbert JN, Goddard JM. Enzymes on material surfaces. *Colloids and Surfaces B-Biointerfaces* 2012, **93:** 8-19.

73. Mateo C, Palomo JM, Fernandez-Lorente G, Guisan JM, Fernandez-Lafuente R. Improvement of enzyme activity, stability and selectivity via immobilization techniques. *Enzyme and Microbial Technology* 2007, **40**(6)**:** 1451-1463.

74. Sheldon RA. Enzyme immobilization: The quest for optimum performance. *Adv Synth Catal* 2007, **349**(8-9)**:** 1289-1307.

75. Worn A, Pluckthun A. Stability engineering of antibody single-chain Fv fragments. *Journal of molecular biology* 2001, **305**(5)**:** 989-1010.

76. Wu AM, Senter PD. Arming antibodies: prospects and challenges for immunoconjugates. *Nature Biotechnology* 2005, **23**(9)**:** 1137-1146.

77. Ruoslahti E, Bhatia SN, Sailor MJ. Targeting of drugs and nanoparticles to tumors. *J Cell Biol* 2010, **188**(6)**:** 759-768.

78. Massoud TF, Gambhir SS. Molecular imaging in living subjects: seeing fundamental biological processes in a new light. *Genes Dev* 2003, **17**(5)**:** 545-580.

79. Karp JM, Teol GSL. Mesenchymal Stem Cell Homing: The Devil Is in the Details. *Cell Stem Cell* 2009, **4**(3)**:** 206-216.

80. Hermanson GT. *Bioconjugate Techniques*. Academic Press: San Diego, 1996.

81. Stephan MT, Irvine DJ. Enhancing Cell therapies from the Outside In: Cell Surface Engineering Using Synthetic Nanomaterials. *Nano today* 2011, **6**(3)**:** 309-325.

82. Sletten EM, Bertozzi CR. From Mechanism to Mouse: A Tale of Two Bioorthogonal Reactions. *Accounts of Chemical Research* 2011, **44**(9)**:** 666-676.

83. Marraffini LA, DeDent AC, Schneewind O. Sortases and the art of anchoring proteins to the envelopes of gram-positive bacteria. *Microbiol Mol Biol Rev* 2006, **70**(1)**:** 192-+.

84. Popp MWL, Ploegh HL. Making and Breaking Peptide Bonds: Protein Engineering Using Sortase. *Angew Chem-Int Edit* 2011, **50**(22)**:** 5024-5032.

85. Mosnier LO, Zampolli A, Kerschen EJ, Schuepbach RA, Banerjee Y, Fernandez JA, *et al.* Hyperantithrombotic, noncytoprotective Glu149Ala-activated protein C mutant. *Blood* 2009, **113**(23)**:** 5970-5978.

86. Kaneider NC, Leger AJ, Agarwal A, Nguyen N, Perides G, Derian C, *et al.* 'Role reversal' for the receptor PAR1 in sepsis-induced vascular damage. *Nat Immunol* 2007, **8**(12)**:** 1303-1312.

87. McLaughlin JN, Patterson MM, Malik AB. Protease-activated receptor-3 (PAR3) regulates PAR1 signaling by receptor dimerization. *Proc Natl Acad Sci U S A* 2007, **104**(13)**:** 5662-5667.

88. Leger AJ, Jacques SL, Badar J, Kaneider NC, Derian CK, Andrade-Gordon P, *et al.* Blocking the protease-activated receptor 1-4 heterodimer in platelet-mediated thrombosis. *Circulation* 2006, **113**(9)**:** 1244-1254.

89. Vowinkel T, Wood KC, Stokes KY, Russell J, Tailor A, Anthoni C, *et al.* Mechanisms of platelet and leukocyte recruitment in experimental colitis. *Am J Physiol Gastrointest Liver Physiol* 2007, **293**(5)**:** G1054-1060.

90. Anthoni C, Russell J, Wood KC, Stokes KY, Vowinkel T, Kirchhofer D, *et al.* Tissue factor: a mediator of inflammatory cell recruitment, tissue injury, and thrombus formation in experimental colitis. *J Exp Med* 2007, **204**(7)**:** 1595-1601.

91. Friedman DJ, Kunzli BM, YI AR, Sevigny J, Berberat PO, Enjyoji K, *et al.* From the Cover: CD39 deletion exacerbates experimental murine colitis and human polymorphisms increase susceptibility to inflammatory bowel disease. *Proc Natl Acad Sci U S A* 2009, **106**(39)**:** 16788-16793.

92. Langer HF, Daub K, Braun G, Schonberger T, May AE, Schaller M, *et al.* Platelets recruit human dendritic cells via Mac-1/JAM-C interaction and modulate dendritic cell function in vitro. *Arterioscler Thromb Vasc Biol* 2007, **27**(6)**:** 1463-1470.

93. Zimmerli C, Lee BPL, Palmer G, Gabay C, Adams R, Aurrand-Lions M, *et al.* Adaptive Immune Response in JAM-C-Deficient Mice: Normal Initiation but Reduced IgG Memory. *J Immunol* 2009, **182**(8)**:** 4728-4736.

94. Kisucka J, Chauhan AK, Zhao BQ, Patten IS, Yesilaltay A, Krieger M, *et al.* Elevated levels of soluble P-selectin in mice alter blood-brain barrier function, exacerbate stroke, and promote atherosclerosis. *Blood* 2009, **113**(23)**:** 6015-6022.

95. Soga F, Katoh N, Inoue T, Kishimoto S. Serotonin activates human monocytes and prevents apoptosis. *J Invest Dermatol* 2007, **127**(8)**:** 1947-1955.

96. Leon-Ponte M, Ahern GP, O'Connell PJ. Serotonin provides an accessory signal to enhance T-cell activation by signaling through the 5-HT7 receptor. *Blood* 2007, **109**(8)**:** 3139-3146.

97. Lang PA, Contaldo C, Georgiev P, El-Badry AM, Recher M, Kurrer M, *et al.* Aggravation of viral hepatitis by platelet-derived serotonin. *Nat Med* 2008, **14**(7)**:** 756-761.

98. Cognasse F, Hamzeh-Cognasse H, Lafarge S, Delezay O, Pozzetto B, McNicol A, *et al.* Toll-like receptor 4 ligand can differentially modulate the release of cytokines by human platelets. *Br J Haematol* 2008, **141**(1)**:** 84-91.

99. Sprague DL, Elzey BD, Crist SA, Waldschmidt TJ, Jensen RJ, Ratliff TL. Platelet-mediated modulation of adaptive immunity: unique delivery of CD154 signal by platelet-derived membrane vesicles. *Blood* 2008, **111**(10)**:** 5028-5036.

100. Cognasse F, Hamzeh-Cognasse H, Lafarge S, Chavarin P, Cogne M, Richard Y, *et al.* Human platelets can activate peripheral blood B cells and increase production of immunoglobulins. *Exp Hematol* 2007, **35**(9)**:** 1376-1387.

101. Elzey BD, Schmidt NW, Crist SA, Kresowik TP, Harty JT, Nieswandt B, *et al.* Platelet-derived CD154 enables T-cell priming and protection against Listeria monocytogenes challenge. *Blood* 2008, **111**(7)**:** 3684-3691.

102. Iannacone M, Sitia G, Isogawa M, Whitmire JK, Marchese P, Chisari FV, *et al.* Platelets prevent IFN-alpha/beta-induced lethal hemorrhage promoting CTL-dependent clearance of lymphocytic choriomeningitis virus. *Proc Natl Acad Sci U S A* 2008, **105**(2)**:** 629-634.

103. Xu H, Zhang X, Mannon RB, Kirk AD. Platelet-derived or soluble CD154 induces vascularized allograft rejection independent of cell-bound CD154. *The Journal of clinical investigation* 2006, **116**(3)**:** 769-774.

104. Danese S, Scaldaferri F, Vetrano S, Stefanelli T, Graziani C, Repici A, *et al.* Critical role of the CD40 CD40-ligand pathway in regulating mucosal inflammation-driven angiogenesis in inflammatory bowel disease. *Gut* 2007, **56**(9)**:** 1248-1256.

105. Vaidyula VR, Rao AK, Mozzoli M, Homko C, Cheung P, Boden G. Effects of hyperglycemia and hyperinsulinemia on circulating tissue factor procoagulant activity and platelet CD40 ligand. *Diabetes* 2006, **55**(1)**:** 202-208.

106. Boden G, Vaidyula VR, Homko C, Cheung P, Rao AK. Circulating tissue factor procoagulant activity and thrombin generation in patients with type 2 diabetes: effects of insulin and glucose. *J Clin Endocrinol Metab* 2007, **92**(11)**:** 4352-4358.

107. Cui W, Wilson JT, Wen J, Angsana J, Qu Z, Haller CA, *et al.* Thrombomodulin improves early outcomes after intraportal islet transplantation. *Am J Transplant* 2009, **9**(6)**:** 1308-1316.

108. Light DB, Mclean K, inventors; Bayer Schering Pharma Aktiengesellschaft (Berlin, DE) assignee. Methods of using novel tissue factor targeted thrombomodulin fusion proteins as anticoagulants patent 7622122. 2009.

109. Stabler CL, Sun XL, Cui W, Wilson JT, Haller CA, Chaikof EL. Surface re-engineering of pancreatic islets with recombinant azido-thrombomodulin. *Bioconjug Chem* 2007, **18**(6)**:** 1713-1715.

110. Kappos L, Radue EW, O'Connor P, Polman C, Hohlfeld R, Calabresi P, *et al.* A placebo-controlled trial of oral fingolimod in relapsing multiple sclerosis. *The New England journal of medicine* 2010, **362**(5)**:** 387-401.

111. Cohen JA, Barkhof F, Comi G, Hartung HP, Khatri BO, Montalban X, *et al.* Oral fingolimod or intramuscular interferon for relapsing multiple sclerosis. *The New England journal of medicine* 2010, **362**(5)**:** 402-415.

112. Puneet P, Yap CT, Wong L, Lam Y, Koh DR, Moochhala S, *et al.* SphK1 regulates proinflammatory responses associated with endotoxin and polymicrobial sepsis. *Science* 2010, **328**(5983)**:** 1290-1294.

113. Jiang R, Weingart J, Zhang H, Ma Y, Sun XL. End-point immobilization of recombinant thrombomodulin via sortase-mediated ligation. *Bioconjug Chem* 2012, **23**(3)**:** 643-649.

114. Morelli AE, Thomson AW. Tolerogenic dendritic cells and the quest for transplant tolerance. *Nat Rev Immunol* 2007, **7**(8)**:** 610-621.

115. Shpacovitch V, Feld M, Hollenberg MD, Luger TA, Steinhoff M. Role of protease-activated receptors in inflammatory responses, innate and adaptive immunity. *J Leukoc Biol* 2008, **83**(6)**:** 1309-1322.

116. Jennings LK. Mechanisms of platelet activation: need for new strategies to protect against platelet-mediated atherothrombosis. *Thromb Haemost* 2009, **102**(2)**:** 248-257.

117. Yanagita M, Kobayashi R, Kashiwagi Y, Shimabukuro Y, Murakami S. Thrombin regulates the function of human blood dendritic cells. *Biochem Biophys Res Commun* 2007, **364**(2)**:** 318-324.

118. Li X, Syrovets T, Paskas S, Laumonnier Y, Simmet T. Mature dendritic cells express functional thrombin receptors triggering chemotaxis and CCL18/pulmonary and activation-regulated chemokine induction. *J Immunol* 2008, **181**(2)**:** 1215-1223.

119. Chen DX, Carpenter A, Abrahams J, Chambers RC, Lechler RI, McVey JH, *et al.* Protease-activated receptor 1 activation is necessary for monocyte chemoattractant protein 1-dependent leukocyte recruitment in vivo. *J Exp Med* 2008, **205**(8)**:** 1739-1746.

120. Rullier A, Gillibert-Duplantier J, Costet P, Cubel G, Haurie V, Petibois C, *et al.* Protease-activated receptor 1 knockout reduces experimentally induced liver fibrosis. *Am J Physiol Gastrointest Liver Physiol* 2008, **294**(1)**:** G226-235.

121. Ramelli G, Fuertes S, Narayan S, Busso N, Acha-Orbea H, So A. Protease-activated receptor 2 signalling promotes dendritic cell antigen transport and T-cell activation in vivo. *Immunology* 2010, **129**(1)**:** 20-27.

122. Rallabhandi P, Nhu QM, Toshchakov VY, Piao W, Medvedev AE, Hollenberg MD, *et al.* Analysis of proteinase-activated receptor 2 and TLR4 signal transduction - A novel paradigm for receptor cooperativity. *J Biol Chem* 2008, **283**(36)**:** 24314-24325.

123. Rivera J, Proia RL, Olivera A. The alliance of sphingosine-1-phosphate and its receptors in immunity. *Nat Rev Immunol* 2008, **8**(10)**:** 753-763.

124. Hannun YA, Obeid LM. Principles of bioactive lipid signalling: lessons from sphingolipids. *Nature Reviews Molecular Cell Biology* 2008, **9**(2)**:** 139-150.

125. Camerer E, Regard JB, Cornelissen I, Srinivasan Y, Duong DN, Palmer D, *et al.* Sphingosine-1-phosphate in the plasma compartment regulates basal and inflammation-induced vascular leak in mice. *The Journal of clinical investigation* 2009, **119**(7)**:** 1871-1879.

126. Niessen F, Schaffner F, Furlan-Freguia C, Pawlinski R, Bhattacharjee G, Chun J, *et al.* Dendritic cell PAR1-S1P3 signalling couples coagulation and inflammation. *Nature* 2008, **452**(7187)**:** 654-658.

127. Ledgerwood LG, Lal G, Zhang N, Garin A, Esses SJ, Ginhoux F, *et al.* The sphingosine 1-phosphate receptor 1 causes tissue retention by inhibiting the entry of peripheral tissue T lymphocytes into afferent lymphatics. *Nat Immunol* 2008, **9**(1)**:** 42-53.

128. Liu GW, Burns S, Huang GH, Boyd K, Proia RL, Flavell RA, *et al.* The receptor S1P(1) overrides regulatory T cell-mediated immune suppression through Akt-mTOR. *Nat Immunol* 2009, **10**(7)**:** 769-U132.

129. Niessen F, Furlan-Freguia C, Fernandez JA, Mosnier LO, Castellino FJ, Weiler H, *et al.* Endogenous EPCR/aPC-PAR1 signaling prevents inflammation-induced vascular leakage and lethality. *Blood* 2009, **113**(12)**:** 2859-2866.

130. Merrill EW, Salzman EW. Polyethylene oxide as a biomaterial. *Asaio J* 1983, **6:** 1.

131. Lee JH, Lee HB, Andrade JD. Blood compatibility of polyethylene oxide surfaces. *Prog Polym Sci* 1995, **20**(6)**:** 1043-1079.

132. Lyman D, Klein K, Brash J, Fritzinger B, Andrade JD, FS B. Platelet interaction with protein coated surfaces. *Thromb Diath Haemor Proc* 1970, **42:** 6.

133. Kim SW, Lee RG, Oster H, Coleman D, Andrade JD, Lentz DJ, *et al.* Platelet adhesion to polymer surfaces. *Transactions, American Society for Artificial Internal Organs* 1974, **B 20:** 449-455.

134. Lee ES, Kim SW. Adsorbed glycoproteins in platelet-adhesion onto polymer surfaces - significance of terminal galactose units. *Transactions, American Society for Artificial Internal Organs* 1979, **25:** 124-132.

135. Park K, Mosher DF, Cooper SL. Acute surface-induced thrombosis in the canine ex vivo model - importance of protein-composition of the initial monolayer and platelet activation *Journal of Biomedical Materials Research* 1986, **20**(5)**:** 589-612.

136. Ishikawa Y, Sasakawa S, Takase M, Osada Y. Effect of albumin immobilization by plasma polymerization on platelet activity. *Thrombosis Research* 1984, **35**(2)**:** 193-202.

137. Kang IK, Kwon BK, Lee JH, Lee HB. Immobilization of proteins on poly(methyl methacrylate) films. *Biomaterials* 1993, **14**(10)**:** 787-792.

138. Kamath KR, Demeo D, Park K. Albumin grafting on polymer surfaces by gamma-irradiation. *Abstracts of Papers of the American Chemical Society* 1993, **206:** 202-POLY.

139. Munro MS, Quattrone AJ, Ellsworth SR, Kulkarni P, Eberhart RC. Alkyl substituted polymers with enhanced albumin affinity. *Transactions, American Society for Artificial Internal Organs* 1981, **27:** 499-503.

140. Eberhart RC, Munro MS, Frautschi JR, Lubin M, Clubb FJ, Miller CW, *et al.* Influence of endogenous albumin binding on blood-material interactions. *Annals of the New York Academy of Sciences* 1987, **516:** 78-95.

141. Eberhart RC. Surface treatments to improve the albumin affinity and blood compatibility of polymers. *Ieee Engineering in Medicine and Biology Magazine* 1989, **8**(2)**:** 26-29.

142. Eberhart RC, Huo HH, Nelson K. Cardiovascular materials. *MRS Bulletin* 1991, **16**(9)**:** 50-54.

143. Frautschi JR, Eberhart RC, Hubbell JA. Alkylated cellulosic membranes with enhanced albumin affinity: Influence of competing proteins. *Journal of Biomaterials Science, Polymer Edition* 1995, **7**(7)**:** 563-575.

144. Nelson KD, Eisenbaumer R, Pomerantz M, Eberhart RC. High affinity polyethylene oxide for improved biocompatibility. *Asaio Journal* 1996, **42**(5)**:** M884-M889.

145. Guidoin RG, Awad J, Brassard A, Domurado D, Lawny F, Wetzer J, *et al.* Blood compability of silicone-rubber chemically coated with cross-linked albumin. *Biomaterials, Medical Devices and Artificial Organs* 1976, **4**(2)**:** 205-224.

146. Guidoin RG, King MW, Awad J, Martin L, Domurado D, Marois M, *et al.* Albumin coated and critical-point dried polyester prostheses as substitutes in the thoracic aorta of dogs. *Transactions, American Society for Artificial Internal Organs* 1983, **29:** 290-295.

147. Kottkemarchant K, Anderson JM, Umemura Y, Marchant RE. Effect of albumin coating on the invitro blood compatibility of Dacron arterial prostheses. *Biomaterials* 1989, **10**(3)**:** 147-155.

148. Marois Y, Chakfe N, Guidoin R, Duhamel RC, Roy R, Marois M, *et al.* An albumin-coated polyester arterial graft: In vivo assessment of biocompatibility and healing characteristics. *Biomaterials* 1996, **17**(1)**:** 3-14.

149. AlKhaffaf H, Charlesworth D. Albumin-coated vascular prostheses: A five-year follow-up. *J Vasc Surg* 1996, **23**(4)**:** 686-690.

150. Kudo FA, Nishibe T, Miyazaki K, Flores J, Yasuda K. Albumin-coated knitted Dacron aortic prostheses. *International Angiology* 2002, **21**(3)**:** 214-217.

151. Gott VL, Koepke DE, Daggett RL, Zarnstorff W, Young WP. The coating of intravascular plastic prostheses with colloidal graphite. *Surgery* 1961, **50:** 382-389.

152. Gott VL. Heparin bonding on colloidal graphite surfaces. *Science* 1963, **142**(359)**:** 1297-&.

153. Olcott EL. Pyrolytic biocarbon materials. *J Biomed Mater Res* 1974, **8**(3)**:** 209-217.

154. Goldfarb D, Houk JA, Moore JL, Gain DL. Graphite-expanded polytetrafluoroethylene - improved small artery prosthesis. *Transactions, American Society for Artificial Internal Organs* 1977, **23:** 268-276.

155. Debski R, Borovetz H, Haubold A, Hardesty R. Polytetrafluoroethylene grafts coated with Ulti carbon. *Transactions, American Society for Artificial Internal Organs* 1982, **28:** 456-458.

156. Scott SM, Gaddy LR, Parra S. Pyrolytic carbon-coated vascular prostheses. *Journal of Surgical Research* 1980, **29**(5)**:** 395-405.

157. Tsuchida H, Cameron BL, Marcus CS, Wilson SE. Modified polytetrafluoroethylene - In-111 labeled platelet deposition on carbon-lined and high-porosity polytetrafluoroethylene grafts. *Journal of Vascular Surgery* 1992, **16**(4)**:** 643-650.

158. Arabi H, Mirzadeh H, Ahmadi SH, Amanpour S, Rabbani S, Abdi A. In vitro and in vivo hemocompatibility evaluation of graphite coated polyester vascular grafts. *International Journal of Artificial Organs* 2004, **27**(8)**:** 691-698.

159. Kapfer X, Meichelboeck W, Groegler FM. Comparison of carbon-impregnated and standard ePTFE prostheses in extra-anatomical anterior tibial artery bypass: A prospective randomized multicenter study. *European Journal of Vascular and Endovascular Surgery* 2006, **32**(2)**:** 155-168.

160. Tegoulia VA, Rao WS, Kalambur AT, Rabolt JR, Cooper SL. Surface properties, fibrinogen adsorption, and cellular interactions of a novel phosphorylcholine-containing self-assembled monolayer on gold. *Langmuir* 2001, **17**(14)**:** 4396-4404.

161. Lu JR, Murphy EF, Su TJ, Lewis AL, Stratford PW, Satija SK. Reduced protein adsorption on the surface of a chemically grafted phospholipid monolayer. *Langmuir* 2001, **17**(11)**:** 3382-3389.

162. Glasmastar K, Larsson C, Hook F, Kasemo B. Protein adsorption on supported phospholipid bilayers. *Journal of Colloid and Interface Science* 2002, **246**(1)**:** 40-47.

163. Andersson AS, Glasmastar K, Sutherland D, Lidberg U, Kasemo B. Cell adhesion on supported lipid bilayers. *J Biomed Mater Res A* 2003, **64A**(4)**:** 622-629.

164. Vermette P, Gauvreau V, Pezolet M, Laroche G. Albumin and fibrinogen adsorption onto phosphatidylcholine monolayers investigated by Fourier transform infrared spectroscopy. *Colloids and Surfaces B-Biointerfaces* 2003, **29**(4)**:** 285-295.

165. Winger TM, Ludovice PJ, Chaikof EL. Formation and stability of complex membrane-mimetic monolayers on solid supports. *Langmuir* 1999, **15**(11)**:** 3866-3874.

166. Kaladhar K, Sharma CP. Supported cell mimetic monolayers and their interaction with blood. *Langmuir* 2004, **20**(25)**:** 11115-11122.

167. Kaladhar K, Sharma C. Cell mimetic lateral stabilization of outer cell mimetic bilayer on polymer surfaces by peptide bonding and their blood compatibility. *Journal of Biomedical Materials Research Part A* 2006, **79A**(1)**:** 23-35.

168. Stine R, Pishko MV, Hampton JR, Dameron AA, Weiss PS. Heat-stabilized phospholipid films: Film characterization and the production of protein-resistant surfaces. *Langmuir* 2005, **21**(24)**:** 11352-11356.

169. Marra KG, Winger TM, Hanson SR, Chaikof EL. Cytomimetic biomaterials .1. In-situ polymerization of phospholipids on an alkylated surface. *Macromolecules* 1997, **30**(21)**:** 6483-6488.

170. Marra KG, Kidani DDA, Chaikof EL. Cytomimetic biomaterials .2. In-situ polymerization of phospholipids on a polymer surface. *Langmuir* 1997, **13**(21)**:** 5697-5701.

171. Orban JM, Faucher KM, Dluhy RA, Chaikof EL. Cytomimetic biomaterials. 4. In-situ photopolymerization of phospholipids on an alkylated surface. *Macromolecules* 2000, **33**(11)**:** 4205-4212.

172. Ross EE, Rozanski LJ, Spratt T, Liu SC, O'Brien DF, Saavedra SS. Planar supported lipid bilayer polymers formed by vesicle fusion. 1. Influence of diene monomer structure and polymerization method on film properties. *Langmuir* 2003, **19**(5)**:** 1752-1765.

173. Ross EE, Spratt T, Liu SC, Rozanski LJ, O'Brien DF, Saavedra SS. Planar supported lipid bilayer polymers formed by vesicle fusion. 2. Adsorption of bovine serum albumin. *Langmuir* 2003, **19**(5)**:** 1766-1774.

174. Kim HK, Kim K, Byun Y. Preparation of a chemically anchored phospholipid monolayer on an acrylated polymer substrate. *Biomaterials* 2005, **26**(17)**:** 3435-3444.

175. Iwasaki Y, Ishihara K. Phosphorylcholine-containing polymers for biomedical applications. *Analytical and bioanalytical chemistry* 2005, **381**(3)**:** 534-546.

176. Lewis AL, Stratford PW. Phosphorylcholine-coated stents. *Journal of long-term effects of medical implants* 2002, **12**(4)**:** 231-250.

177. Yoneyama T, Ishihara K, Nakabayashi N, Ito M, Mishima Y. Short-term in vivo evaluation of small-diameter vascular prosthesis composed of segmented poly(etherurethane)/2-methacryloyloxyethyl phosphorylcholine polymer blend. *J Biomed Mater Res* 1998, **43**(1)**:** 15-20.

178. Ishihara K, Fujita H, Yoneyama T, Iwasaki Y. Antithrombogenic polymer alloy composed of 2-methacryloyloxyethyl phosphorylcholine polymer and segmented polyurethane. *Journal of biomaterials science* 2000, **11**(11)**:** 1183-1195.

179. Yoneyama T, Sugihara K, Ishihara K, Iwasaki Y, Nakabayashi N. The vascular prosthesis without pseudointima prepared by anti thrombogenic phospholipid polymer. *Biomaterials* 2002, **23**(6)**:** 1455-1459.

180. Chen CY, Lumsden AB, Ofenloch JC, Noe B, Campbell EJ, Stratford PW, *et al.* Phosphorylcholine coating of ePTFE grafts reduces neointimal hyperplasia in canine model. *Annals of vascular surgery* 1997, **11**(1)**:** 74-79.

181. Chen C, Ofenloch JC, Yianni YP, Hanson SR, Lumsden AB. Phosphorylcholine coating of ePTFE reduces platelet deposition and neointimal hyperplasia in arteriovenous grafts. *Journal of Surgical Research* 1998, **77**(2)**:** 119-125.

182. Jordan SW, Faucher KM, Caves JM, Apkarian RP, Rele SS, Sun XL, *et al.* Fabrication of a phospholipid membrane-mimetic film on the luminal surface of an ePTFE vascular graft. *Biomaterials* 2006, **27**(18)**:** 3473-3481.

183. Chandy T, Das GS, Wilson RF, Rao GHR. Use of plasma glow for surface-engineering biomolecules to enhance bloodcompatibility of Dacron and PTFE vascular prosthesis. *Biomaterials* 2000, **21**(7)**:** 699-712.

184. Baumgartner HR, Muggli R, Tschopp TB, Turitto VT. Platelet-adhesion, release and aggregation in flowing blood: effects of surface properties and platelet-function. *Thromb Haemost* 1976, **35**(1)**:** 124-138.

185. Barnes MJ, Macintyre DE. Platelet-reactivity of isolated constituents of the blood-vessel wall. *Haemostasis* 1979, **8**(3-5)**:** 158-170.

186. Ito S, Ishimaru S, Wilson SE. Application of coacervated alpha-elastin to arterial prostheses for inhibition of anastomotic intimal hyperplasia. *Asaio Journal* 1998, **44**(5)**:** M501-M505.

187. Huang L, McMillan RA, Apkarian RP, Pourdeyhimi B, Conticello VP, Chaikof EL. Generation of synthetic elastin-mimetic small diameter fibers and fiber networks. *Macromolecules* 2000, **33**(8)**:** 2989-2997.

188. McPherson DT, Morrow C, Minehan DS, Wu JG, Hunter E, Urry DW. Production and purification of a recombinant elastomeric polypeptide, G-(VPGVG)19-VPGV, from Escherichia coli. *Biotechnol Prog* 1992, **8**(4)**:** 347-352.

189. Daniell H, Guda C, McPherson DT, Zhang X XJ, DW U. Hyperexpression of a synthetic protein-based polymer gene. *Methods Mol Biol* 1997, **63:** 359-371.

190. Trabbic-Carlson K, Setton LA, Chilkoti A. Swelling and mechanical behaviors of chemically cross-linked hydrogels of elastin-like polypeptides. *Biomacromolecules* 2003, **4**(3)**:** 572-580.

191. Nagapudi K, Brinkman WT, Leisen J, Thomas BS, Wright ER, Haller C, *et al.* Protein-based thermoplastic elastomers. *Macromolecules* 2005, **38**(2)**:** 345-354.

192. Lim DW, Nettles DL, Setton LA, Chilkoti A. In situ cross-linkinig of elastin-like polypeptide block copolymers for tissue repair. *Biomacromolecules* 2008, **9**(1)**:** 222-230.

193. Defife KM, Hagen KM, Clapper DL, Anderson JM. Photochemically immobilized polymer coatings: effects on protein adsorption, cell adhesion, and leukocyte activation. *Journal of Biomaterials Science, Polymer Edition* 1999, **10**(10)**:** 1063-1074.

194. Woodhouse KA, Klement P, Chen V, Gorbet MB, Keeley FW, Stahl R, *et al.* Investigation of recombinant human elastin polypeptides as non-thrombogenic coatings. *Biomaterials* 2004, **25**(19)**:** 4543-4553.

195. Jordan SW, Haller CA, Sallach RE, Apkarian RP, Hanson SR, Chaikof EL. The effect of a recombinant elastin-mimetic coating of an ePTFE prosthesis on acute thrombogenicity in a baboon arteriovenous shunt. *Biomaterials* 2007, **28**(6)**:** 1191-1197.

196. Clagett GP, Burkel WE, Sharefkin JB, Ford JW, Hufnagel H, Vinter DW, *et al.* Platelet reactivity in vivo in dogs with arterial prostheses seeded with endothelial cells. *Circulation* 1984, **69**(3)**:** 632-639.

197. Hess F, Steeghs S, Jerusalem R, Reijnders O, Jerusalem C, Braun B, *et al.* Patency and morphology of fibrous polyurethane vascular prostheses implanted in the femoral artery of dogs after seeding with subcultivated endothelial cells. *European journal of vascular surgery* 1993, **7**(4)**:** 402-408.

198. Pasic M, Muller-Glauser W, von Segesser L, Odermatt B, Lachat M, Turina M. Endothelial cell seeding improves patency of synthetic vascular grafts: manual versus automatized method. *Eur J Cardiothorac Surg* 1996, **10**(5)**:** 372-379.

199. Sugitachi A, Takagi K. Antithrombogenicity of immobilized urokinase: clinical application. *International Journal of Artificial Organs* 1978, **1**(2)**:** 88-92.

200. Aoshima R, Kanda Y, Takada A, Yamashita A. Sulfonated poly(vinylidene fluoride) as a biomaterial: Immobilization of urokinase and biocompatibility. *J Biomed Mater Res* 1982, **16**(3)**:** 289-299.

201. Kitamoto Y, Tomita M, Kiyama S, Inoue T, Yabushita Y, Sato T, *et al.* Antithrombotic mechanisms of urokinase immobilized polyurethane. *Thromb Haemost* 1991, **65**(1)**:** 73-76.

202. Lai ZF, Imamura T, Koike N, Kitamoto Y. Urokinase-immobilization suppresses inflammatory responses to polyurethane tubes implanted in rabbit muscles. *Journal of Biomedical Materials Research Part A* 2006, **76A**(1)**:** 81-85.

203. Sugitachi A, Takagi K. Antithrombogenicity of immobilized urokinase - Clinical application. *International Journal of Artificial Organs* 1978, **1**(2)**:** 88-92.

204. Lai ZF, Imamura T, Koike N, Kitamoto Y. Urokinase-immobilization suppresses inflammatory responses to polyurethane tubes implanted in rabbit muscles. *Journal of biomedical materials research* 2006, **76**(1)**:** 81-85.

205. vonSegesser LK. Heparin-bonded surfaces in extracorporeal membrane oxygenation for cardiac support. *Annals of Thoracic Surgery* 1996, **61**(1)**:** 330-335.

206. Hsu LC. Heparin-coated cardiopulmonary bypass circuits: current status. *Perfusion-Uk* 2001, **16**(5)**:** 417-428.

207. Hubbell JA. Pharmacological Modification of Materials. *Cardiovascular Pathology* 1993, **2**(3)**:** S121-S127.

208. Olsson P, Sanchez J, Mollnes TE, Riesenfeld J. On the blood compatibility of end-point immobilized heparin. *Journal of biomaterials science* 2000, **11**(11)**:** 1261-1273.

209. Tanzi MC. Bioactive technologies for hemocompatibility. *Expert Rev Med Devices* 2005, **2**(4)**:** 473-492.

210. Sperling C, Schweiss RB, Streller U, Werner C. In vitro hemocompatibility of self-assembled monolayers displaying various functional groups. *Biomaterials* 2005, **26**(33)**:** 6547-6557.

211. Huang LY, Yang MC. Hemocompatibility of layer-by-layer hyaluronic acid/heparin nanostructure coating on stainless steel for cardiovascular stents and its use for drug delivery. *Journal of Nanoscience and Nanotechnology* 2006, **6**(9-10)**:** 3163-3170.

212. Laredo J, Xue L, Husak VA, Ellinger J, Greisler HP. Silyl-heparin adsorption improves the in vivo thromboresistance of carbon-coated polytetrafluoroethylene vascular grafts. *American journal of surgery* 2003, **186**(5)**:** 556-560.

213. Laredo J, Xue L, Husak VA, Ellinger J, Singh G, Zamora PO*, et al.* Silyl-heparin bonding improves the patency and in vivo thromboresistance of carbon-coated polytetrafluoroethylene vascular grafts. *Journal of Vascular Surgery* 2004, **39**(5)**:** 1059-1065.

214. Li YL, Neoh KG, Kang ET. Plasma protein adsorption and thrombus formation on surface functionalized polypyrrole with and without electrical stimulation. *Journal of Colloid and Interface Science* 2004, **275**(2)**:** 488-495.

215. Chen H, Chen Y, Sheardown H, Brook MA. Immobilization of heparin on a silicone surface through a heterobifunctional PEG spacer. *Biomaterials* 2005, **26**(35)**:** 7418-7424.

216. Wang AF, Cao T, Tang HY, Liang XM, Black C, Salley SO, *et al.* Immobilization of polysaccharides on a fluorinated silicon surface. *Colloids and Surfaces B-Biointerfaces* 2006, **47**(1)**:** 57-63.

217. Keuren JFW, Wielders SJH, Driessen A, Verhoeven M, Hendriks M, Lindhout T. Covalently-bound heparin makes collagen thromboresistant. *Arteriosclerosis, Thrombosis, and Vascular Biology* 2004, **24**(3)**:** 613-617.

218. Luong-Van E, Grondahl L, Chua KN, Leong KW, Nurcombe V, Cool SM. Controlled release of heparin from poly(epsilon-caprolactone) electrospun fibers. *Biomaterials* 2006, **27**(9)**:** 2042-2050.

219. Larm O, Larsson R, Olsson P. A new non-thrombogenic surface prepared by selective covalent binding of heparin via a modified reducing terminal residue. *Biomaterials, medical devices, and artificial organs* 1983, **11**(2-3)**:** 161-173.

220. Pasche B, Elgue G, Olsson P, Riesenfeld J, Rasmuson A. Binding of antithrombin to immobilized heparin under varying flow conditions. *Artif Organs* 1991, **15**(6)**:** 481-491.

221. Elgue G, Blomback M, Olsson P, Riesenfeld J. On the mechanism of coagulation inhibition on surfaces with end point immobilized heparin. *Thromb Haemost* 1993, **70**(2)**:** 289-293.

222. Devine C, McCollum C. Heparin-bonded Dacron or polytetrafluorethylene for femoropopliteal bypass: Five-year results of a prospective randomized multicenter clinical trial. *Journal of Vascular Surgery* 2004, **40**(5)**:** 924-931.

223. Scharn DM, Dirven M, Barendregt WB, Boll APM, Roelofs D, van der Vliet JA. Human umbilical vein versus heparin-bonded polyester for femoro-popliteal bypass: 5-year results of a prospective randomized multicentre trial. *European Journal of Vascular and Endovascular Surgery* 2008, **35**(1)**:** 61-67.

224. Walluscheck KP, Bierkandt S, Brandt M, Cremer J. Infrainguinal ePTFE vascular graft with bioactive surface heparin bonding - First clinical results. *Journal of Cardiovascular Surgery* 2005, **46**(4)**:** 425-430.

225. Bosiers M, Deloose K, Verbist J, Schroe H, Lauwers G, Lansink W, *et al.* Heparin-bonded expanded polytetrafluoroethylene vascular graft for femoropopliteal and femorocrural bypass grafting: 1-year results. *J Vasc Surg* 2006, **43**(2)**:** 313-318.

226. Peeters P, Verbist J, Deloose K, Bosiers M. Results with heparin bonded polytetrafluoroethylene grafts for femorodistal bypasses. *Journal of Cardiovascular Surgery* 2006, **47**(4)**:** 407-413.

227. Kishida A, Ueno Y, Fukudome N, Yashima E, Maruyama I, Akashi M. Immobilization of human thrombomodulin onto poly(ether urethane urea) for developing antithrombogenic blood-contacting materials. *Biomaterials* 1994, **15**(10)**:** 848-852.

228. Kishida A, Ueno Y, Maruyama I, Akashi M. Immobilization of human thrombomodulin on biomaterials: evaluation of the activity of immobilized human thrombomodulin. *Biomaterials* 1994, **15**(14)**:** 1170-1174.

229. Kishida A, Akatsuka Y, Yanagi M, Aikou T, Maruyama I, Akashi M. In vivo and ex vivo evaluation of the antithrombogenicity of human thrombomodulin immobilized biomaterials. *Asaio J* 1995, **41**(3)**:** M369-374.

230. Vasilets VN, Hermel G, Konig U, Werner C, Muller M, Simon F, *et al.* Microwave CO2 plasma-initiated vapour phase graft polymerization of acrylic acid onto polytetrafluoroethylene for immobilization of human thrombomodulin. *Biomaterials* 1997, **18**(17)**:** 1139-1145.

231. Li JM, Singh MJ, Nelson PR, Hendricks GM, Itani M, Rohrer MJ, *et al.* Immobilization of human thrombomodulin to expanded polytetrafluoroethylene. *Journal of Surgical Research* 2002, **105**(2)**:** 200-208.

232. Sperling C, Konig U, Hermel G, Werner C, Muller M, Simon F, *et al.* Immobilization of human thrombomodulin onto PTFE. *Journal of Materials Science-Materials in Medicine* 1997, **8**(12)**:** 789-791.

233. Sperling C, Salchert K, Streller U, Werner C. Covalently immobilized thrombomodulin inhibits coagulation and complement activation of artificial surfaces in vitro. *Biomaterials* 2004, **25**(21)**:** 5101-5113.

234. Han HS, Yang SL, Yeh HY, Lin JC, Wu HL, Shi GY. Studies of a novel human thrombomodulin immobilized substrate: surface characterization and anticoagulation activity evaluation. *Journal of Biomaterials Science, Polymer Edition* 2001, **12**(10)**:** 1075-1089.

235. Cazalis CS, Haller CA, Sease-Cargo L, Chaikof EL. C-terminal site-specific PEGylation of a truncated thrombomodulin mutant with retention of full bioactivity. *Bioconjugate Chemistry* 2004, **15**(5)**:** 1005-1009.

236. Sun XL, Stabler CL, Cazalis CS, Chaikof EL. Carbohydrate and protein immobilization onto solid surfaces by sequential Diels-Alder and azide-alkyne cycloadditions. *Bioconjugate Chemistry* 2006, **17**(1)**:** 52-57.

237. Tseng PY, Jordan SW, Sun XL, Chaikof EL. Catalytic efficiency of a thrombomodulin-functionalized membrane-mimetic film in a flow model. *Biomaterials* 2006, **27**(13)**:** 2768-2775.

238. Feng J, Tseng PY, Faucher KM, Orban JM, Sun XL, Chaikof EL. Functional reconstitution of thrombomodulin within a substrate-supported membrane-mimetic polymer film. *Langmuir* 2002, **18**(25)**:** 9907-9913.

239. Seifert B, Romaniuk P, Groth T. Covalent immobilization of hirudin improves the haemocompatibility of polylactide-polyglycolide in vitro. *Biomaterials* 1997, **18**(22)**:** 1495-1502.

240. Phaneuf MD, Berceli SA, Bide MJ, Quist WC, LoGerfo FW. Covalent linkage of recombinant hirudin to poly(ethylene terephthalate) (Dacron): creation of a novel antithrombin surface. *Biomaterials* 1997, **18**(10)**:** 755-765.

241. Berceli SA, Phaneuf MD, LoGerfo PW. Evaluation of a novel hirudin-coated polyester graft to physiologic flow conditions: Hirudin bioavailability and thrombin uptake. *Journal of Vascular Surgery* 1998, **27**(6)**:** 1117-1127.

242. Phaneuf MD, Dempsey DJ, Bide MJ, Szycher M, Quist WC, LoGerfo FW. Bioengineering of a novel small diameter polyurethane vascular graft with covalently bound recombinant hirudin. *Asaio J* 1998, **44**(5)**:** M653-658.

243. Phaneuf MD, Szycher M, Berceli SA, Dempsey DJ, Quist WC, LoGerfo FW. Covalent linkage of recombinant hirudin to a novel ionic poly(carbonate) urethane polymer with protein binding sites: determination of surface antithrombin activity. *Artif Organs* 1998, **22**(8)**:** 657-665.

244. Wyers MC, Phaneuf MD, Rzucidlo EM, Contreras MA, LoGerfo FW, Quist WC. In vivo assessment of a novel Dacron surface with covalently bound recombinant hirudin. *Cardiovascular Pathology* 1999, **8**(3)**:** 153-159.

245. Tangelder MJD, Algra A, Lawson JA, Eikelboom BC, Tangelder MJD, Algra A, *et al.* Efficacy of oral anticoagulants compared with aspirin after infrainguinal bypass surgery (The Dutch Bypass Oral anticoagulants or Aspirin study): a randomised trial. *Lancet* 2000, **355**(9201)**:** 346-351.

246. Chandy T, Sharma CP. The antithrombotic effect of prostaglandin E1 immobilized on albuminated polymer matrix. *J Biomed Mater Res* 1984, **18**(9)**:** 1115-1124.

247. Joseph G, Sharma CP. Prostacyclin immobilized albuminated surfaces. *Journal of Biomedical Materials Research* 1987, **21**(7)**:** 937-945.

248. Aldenhoff YBJ, Pijpers AP, Koole LH. Synthesis of a new photoreactive derivative of dipyridamole and its use in the manufacture of artificial surfaces with low thrombogenicity. *Bioconjug Chem* 1997, **8**(3)**:** 296-303.

249. Aldenhoff YBJ, van der Veen FH, ter Woorst J, Habets J, Poole-Warren LA, Koole LH. Performance of a polyurethane vascular prosthesis carrying a dipyridamole (Persantin (R)) coating on its lumenal surface. *J Biomed Mater Res* 2001, **54**(2)**:** 224-233.

250. Aldenhoff YB, Koole LH. Platelet adhesion studies on dipyridamole coated polyurethane surfaces. *European cells & materials* 2003, **5:** 61-67; discussion 67.

251. Paul W, Sharma CP. Acetylsalicylic acid loaded poly(vinyl alcohol) hemodialysis membranes: Effect of drug release on blood compatibility and permeability. *Journal of Biomaterials Science, Polymer Edition* 1997, **8**(10)**:** 755-764.

252. Vasudev SC, Chandy T, Sharma CP. Development of chitosan/polyethylene vinyl acetate co-matrix: Controlled release of aspirin-heparin for preventing cardiovascular thrombosis. *Biomaterials* 1997, **18**(5)**:** 375-381.

253. Rodriguez G, Gallardo A, San Roman J, Rebuelta M, Bermejo P, Bujan J, *et al.* New resorbable polymeric systems with antithrombogenic activity. *Journal of Materials Science-Materials in Medicine* 1999, **10**(12)**:** 873-878.

254. Rodriguez G, Gallardo A, Fernandez M, Rebuelta M, Bujan J, Bellon J, *et al.* Hydrophilic polymer drug from a derivative of salicylic acid: Synthesis, controlled release studies and biological behavior. *Macromolecular Bioscience* 2004, **4**(6)**:** 579-586.

255. SanRoman J, Bujan J, Bellon JM, Gallardo A, Escudero MC, Jorge E, *et al.* Experimental study of the antithrombogenic behavior of Dacron vascular grafts coated with hydrophilic acrylic copolymers bearing salicylic acid residues. *Journal of Biomedical Materials Research* 1996, **32**(1)**:** 19-27.

256. Viscardi PJ, Page EA, Clark HG, Serafin D, Klitzman B. Iloprost in alginate decreases the thrombogenicity of expanded polytetrafluoroethylene. *Journal of Reconstructive Microsurgery* 1997, **13**(4)**:** 303-306.

257. Groves PH, Banning AP, Penny WJ, Newby AC, Cheadle HA, Lewis MJ. The effects of exogenous nitric oxide on smooth muscle cell proliferation following porcine carotid angioplasty. *Cardiovascular Research* 1995, **30**(1)**:** 87-96.

258. Kibbe M, Billiar T, Tzeng E. Inducible nitric oxide synthase and vascular injury. *Cardiovasc Res* 1999, **43**(3)**:** 650-657.

259. Keefer LK. Nitric oxide (NO)- and nitroxyl (HNO)-generating diazeniumdiolates (NONOates): emerging commercial opportunities. *Current topics in medicinal chemistry* 2005, **5**(7)**:** 625-636.

260. Smith DJ, Chakravarthy D, Pulfer S, Simmons ML, Hrabie JA, Citro ML, *et al.* Nitric oxide-releasing polymers containing the [N(O)NO](-) group. *Journal of Medicinal Chemistry* 1996, **39**(5)**:** 1148-1156.

261. Pulfer SK, Ott D, Smith DJ. Incorporation of nitric oxide-releasing crosslinked polyethyleneimine microspheres into vascular grafts. *Journal of Biomedical Materials Research* 1997, **37**(2)**:** 182-189.

262. Taite LJ, Yang P, Jun HW, West JL. Nitric oxide-releasing Polyurethane-PEG copolymer containing the YIGSR peptide promotes endothelialization with decreased platelet adhesion. *Journal of Biomedical Materials Research Part B, Applied Biomaterials* 2008, **84B**(1)**:** 108-116.

263. Jun HW, Taite LJ, West JL. Nitric oxide-producing polyurethanes. *Biomacromolecules* 2005, **6**(2)**:** 838-844.

264. Mowery KA, Schoenfisch MH, Saavedra JE, Keefer LK, Meyerhoff ME. Preparation and characterization of hydrophobic polymeric films that are thromboresistant via nitric oxide release. *Biomaterials* 2000, **21**(1)**:** 9-21.

265. Batchelor MM, Reoma SL, Fleser PS, Nuthakki VK, Callahan RE, Shanley CJ, *et al.* More lipophilic dialkyldiamine-based diazeniumdiolates: Synthesis, characterization, and application in preparing thromboresistant nitric oxide release polymeric coatings. *Journal of Medicinal Chemistry* 2003, **46**(24)**:** 5153-5161.

266. Frost MC, Batchelor MM, Lee YM, Zhang HP, Kang YJ, Oh BK, *et al.* Preparation and characterization of implantable sensors with nitric oxide release coatings. *Microchemical Journal* 2003, **74**(3)**:** 277-288.

267. Fleser PS, Nuthakki VK, Malinzak LE, Callahan RE, Seymour ML, Reynolds MM, *et al.* Nitric oxide-releasing biopolymers inhibit thrombus formation in a sheep model of artcriovenous bridge grafts. *Journal of Vascular Surgery* 2004, **40**(4)**:** 803-811.

268. Jourd'heuil D, Hallen K, Feelisch M, Grisham MB. Dynamic state of S-nitrosothiols in human plasma and whole blood. *Free Radical Biology and Medicine* 2000, **28**(3)**:** 409-417.

269. Rafikova O, Rafikov R, Nudler E. Catalysis of S-nitrosothiols formation by serum albumin: The mechanism and implication in vascular control. *Proc Natl Acad Sci U S A* 2002, **99**(9)**:** 5913-5918.

270. Bohl KS, West JL. Nitric oxide-generating polymers reduce platelet adhesion and smooth muscle cell proliferation. *Biomaterials* 2000, **21**(22)**:** 2273-2278.

271. Oh BK, Meyerhoff ME. Spontaneous catalytic generation of nitric oxide from S-nitrosothiols at the surface of polymer films doped with lipophilic copper(II) complex. *Journal of the American Chemical Society* 2003, **125**(32)**:** 9552-9553.

272. Oh BK, Meyerhoff ME. Catalytic generation of nitric oxide from nitrite at the interface of polymeric films doped with lipophilic Cu(Il)-complex: a potential route to the preparation of thromboresistant coatings. *Biomaterials* 2004, **25**(2)**:** 283-293.

273. Duan XB, Lewis RS. Improved haemocompatibility of cysteine-modified polymers via endogenous nitric oxide. *Biomaterials* 2002, **23**(4)**:** 1197-1203.

274. Gappa-Fahlenkamp H, Duan X, Lewis RS. Analysis of immobilized L-cysteine on polymers. *J Biomed Mater Res A* 2004, **71**(3)**:** 519-527.

275. Hwang S, Meyerhoff ME. Organoditelluride-tethered polymers that spontaneously generate nitric oxide when in contact with fresh blood. *Journal of Materials Chemistry* 2008, **18**(15)**:** 1784-1791.

276. Herring M, Gardner A, Glover J. Single-staged technique for seeding vascular grafts with autogenous endothelium. *Surgery* 1978, **84**(4)**:** 498-504.

277. Zilla P, Fasol R, Deutsch M, Fischlein T, Minar E, Hammerle A, *et al.* Endothelial cell seeding of polytetrafluoroethylene vascular grafts in humans: a preliminary report. *J Vasc Surg* 1987, **6**(6)**:** 535-541.

278. Herring M, Smith J, Dalsing M, Glover J, Compton R, Etchberger K, *et al.* Endothelial seeding of polytetrafluoroethylene femoral popliteal bypasses: the failure of low-density seeding to improve patency. *J Vasc Surg* 1994, **20**(4)**:** 650-655.

279. Jensen N, Lindblad B, Bergqvist D. Endothelial cell seeded Dacron aortobifurcated grafts: platelet deposition and long-term follow-up. *The Journal of cardiovascular surgery* 1994, **35**(5)**:** 425-429.

280. Lindblad B, Wright SW, Sell RL, Burkel WE, Graham LM, Stanley JC. Alternative techniques of seeding cultured endothelial cells to ePTFE grafts of different diameters, porosities, and surfaces. *J Biomed Mater Res* 1987, **21**(8)**:** 1013-1022.

281. Graham LM, Vinter DW, Ford JW, Kahn RH, Burkel WE, Stanley JC. Cultured autogenous endothelial cell seeding of prosthetic vascular grafts. *Surgical forum* 1979, **30:** 204-206.

282. Zilla P, Deutsch M, Meinhart J, Puschmann R, Eberl T, Minar E*, et al.* Clinical in vitro endothelialization of femoropopliteal bypass grafts: an actuarial follow-up over three years. *J Vasc Surg* 1994, **19**(3)**:** 540-548.

283. Deutsch M, Meinhart J, Fischlein T, Preiss P, Zilla P. Clinical autologous in vitro endothelialization of infrainguinal ePTFE grafts in 100 patients: A 9-year experience. *Surgery* 1999, **126**(5)**:** 847-855.

284. Meinhart JG, Deutsch M, Fischlein T, Howanietz N, Froschl A, Zilla P. Clinical autologous in vitro endothelialization of 153 infrainguinal ePTFE grafts. *Annals of Thoracic Surgery* 2001, **71**(5)**:** S327-S331.

285. Laube HR, Duwe J, Rutsch W, Konertz W. Clinical experience with autologous endothelial cell-seeded polytetrafluoroethylene coronary artery bypass grafts. *Journal of Thoracic and Cardiovascular Surgery* 2000, **120**(1)**:** 134-141.

286. Seeger JM, Klingman N. Improved endothelial cell seeding with cultured cells and fibronectin-coated grafts. *The Journal of surgical research* 1985, **38**(6)**:** 641-647.

287. Kesler KA, Herring MB, Arnold MP, Glover JL, Park HM, Helmus MN*, et al.* Enhanced strength of endothelial attachment on polyester elastomer and polytetrafluoroethylene graft surfaces with fibronectin substrate. *J Vasc Surg* 1986, **3**(1)**:** 58-64.

288. Jarrell BE, Speicher L, Carabasi RA, Williams SK, Koolpe E, Greener D*, et al.* Use of an endothelial monolayer on a vascular graft prior to implantation - temporal dynamics and compatibility with the operating-room. *Annals of Surgery* 1986, **203**(6)**:** 671-678.

289. Anderson JS, Price TM, Hanson SR, Harker LA. Invitro endothelialization of small-caliber vascular grafts. *Surgery* 1987, **101**(5)**:** 577-586.

290. Greisler HP, Klosak JJ, Dennis JW, Karesh SM, Ellinger J, Kim DU. Biomaterial pretreatment with Ecgf to augment endothelial-cell proliferation. *Journal of Vascular Surgery* 1987, **5**(2)**:** 393-399.

291. Radomski JS, Jarrell BE, Williams SK, Koolpe EA, Greener DA, Carabasi RA. Initial adherence of human capillary endothelial cells to Dacron. *Journal of Surgical Research* 1987, **42**(2)**:** 133-140.

292. Mazzucotelli JP, Kleinsoyer C, Beretz A, Brisson C, Archipoff G, Cazenave JP. Endothelial cell seeding: Coating Dacron and expanded polytetrafluoroethylene vascular grafts with a biological glue allows adhesion and growth of human saphenous vein endothelial cells. *International Journal of Artificial Organs* 1991, **14**(8)**:** 482-490.

293. Steele JG, Johnson G, Mcfarland C, Dalton BA, Gengenbach TR, Chatelier RC, *et al.* Roles of serum vitronectin and fibronectin in initial attachment of human vein endothelial cells and dermal fibroblasts on oxygen-containing and nitrogen-containing surfaces made by radiofrequency plasmas. *Journal of Biomaterials Science, Polymer Edition* 1994, **6**(6)**:** 511-532.

294. Gosselin C, Vorp DA, Warty V, Severyn DA, Dick EK, Borovetz HS, *et al.* ePTFE coating with fibrin glue, FGF-1, and heparin: effect on retention of seeded endothelial cells. *Journal of Surgical Research* 1996, **60**(2)**:** 327-332.

295. Kaehler J, Zilla P, Fasol R, Deutsch M, Kadletz M. Precoating substrate and surface configuration determine adherence and spreading of seeded endothelial cells on polytetrafluoroethylene grafts. *Journal of Vascular Surgery* 1989, **9**(4)**:** 535-541.

296. Lin HB, Garciaecheverria C, Asakura S, Sun W, Mosher DF, Cooper SL. Endothelial-cell adhesion on polyurethanes containing covalently attached RGD-peptides. *Biomaterials* 1992, **13**(13)**:** 905-914.

297. Massia SP, Hubbell JA. Vascular endothelial-cell adhesion and spreading promoted by the peptide redv of the Iiics region of plasma fibronectin is mediated by integrin alpha-4-beta-1. *J Biol Chem* 1992, **267**(20)**:** 14019-14026.

298. Jun HW, West J. Development of a YIGSR-peptide-modified polyurethaneurea to enhance endothelialization. *Journal of Biomaterials Science, Polymer Edition* 2004, **15**(1)**:** 73-94.

299. Salacinski HJ, Tiwari A, Hamilton G, Seifalian AM. Cellular engineering of vascular bypass grafts: role of chemical coatings for enhancing endothelial cell attachments. *Medical and Biological Engineering and Computing* 2001, **39**(6)**:** 609-618.

300. Bowlin GL, Meyer A, Fields C, Cassano A, Makhoul RG, Allen C, *et al.* The persistence of electrostatically seeded endothelial cells lining a small diameter expanded polytetrafluoroethylene vascular graft. *Journal of biomaterials applications* 2001, **16**(2)**:** 157-173.

301. Fields C, Cassano A, Makhoul RG, Allen C, Sims R, Bulgrin J, *et al.* Evaluation of electrostatically endothelial cell seeded expanded polytetrafluoroethylene grafts in a canine femoral artery model. *Journal of biomaterials applications* 2002, **17**(2)**:** 135-152.

302. Ballermann BJ, Ott MJ. Adhesion and differentiation of endothelial cells by exposure to chronic shear-stress: A vascular graft model. *Blood Purification* 1995, **13**(3-4)**:** 125-134.

303. Isenberg BC, Williams C, Tranquillo RT. Endothelialization and flow conditioning of fibrin-based media-equivalents. *Annals of biomedical engineering* 2006, **34**(6)**:** 971-985.

304. Dichek DA, Anderson J, Kelly AB, Hanson SR, Harker LA. Enhanced in vivo antithrombotic effects of endothelial cells expressing recombinant plasminogen activators transduced with retroviral vectors. *Circulation* 1996, **93**(2)**:** 301-309.

305. Vonderleyen HE, Gibbons GH, Morishita R, Lewis NP, Zhang L, Nakajima M, *et al.* Gene-therapy inhibiting neointimal vascular lesion: In vivo transfer of endothelial cell nitric oxide synthase gene. *Proc Natl Acad Sci U S A* 1995, **92**(4)**:** 1137-1141.

306. Fujita Y, Hong-De Wu M, Ishida A, Shi Q, Walker M, Hammond WP, *et al.* Accelerated healing of dacron grafts seeded by preclotting with autologous bone marrow blood. *Annals of vascular surgery* 1999, **13**(4)**:** 402-412.

307. Bhattacharya V, McSweeney PA, Shi Q, Bruno B, Ishida A, Nash R, *et al.* Enhanced endothelialization and microvessel formation in polyester grafts seeded with CD34(+) bone marrow cells. *Blood* 2000, **95**(2)**:** 581-585.

308. Griese DP, Ehsan A, Melo LG, Kong DL, Zhang LN, Mann MJ, *et al.* Isolation and transplantation of autologous circulating endothelial cells into denuded vessels and prosthetic grafts. Implications for cell-based vascular therapy. *Circulation* 2003, **108**(21)**:** 2710-2715.

309. Tiwari A, Kidane A, Punshon G, Hamilton G, Seifalian AM. Extraction of cells for single-stage seeding of vascular-bypass grafts. *Biotechnology and Applied Biochemistry* 2003, **38:** 35-41.

310. Pasic M, Mullerglauser W, Vonsegesser LK, Lachat M, Mihaljevic T, Turina MI. Superior late patency of small-diameter Dacron grafts seeded with omental microvascular cells - an experimental-study. *Annals of Thoracic Surgery* 1994, **58**(3)**:** 677-684.

311. Jarrell BE, Williams SK, Stokes G, Hubbard FA, Carabasi RA, Koolpe E, *et al.* Use of freshly isolated capillary endothelial cells for the immediate establishment of a monolayer on a vascular graft at surgery. *Surgery* 1986, **100**(2)**:** 392-399.

312. Pasic M, Mullerglauser W, Odermatt B, Lachat M, Seifert B, Turina M. Seeding with omental cells prevents late neointimal hyperplasia in small-diameter Dacron grafts. *Circulation* 1995, **92**(9)**:** 2605-2616.

313. Greisler HP, Cziperle DJ, Kim DU, Garfield JD, Petsikas D, Murchan PM, *et al.* Enhanced endothelialization of expanded polytetrafluoroethylene grafts by fibroblast growth-factor type-1 pretreatment. *Surgery* 1992, **112**(2)**:** 244-255.

314. Greisler HP, Gosselin C, Ren DW, Kang SS, Kim DU. Biointeractive polymers and tissue engineered blood vessels. *Biomaterials* 1996, **17**(3)**:** 329-336.

315. Gray JL, Kang SS, Zenni GC, Kim DU, Kim PI, Burgess WH, *et al.* Fgf-1 affixation stimulates ePTFE endothelialization without intimal hyperplasia. *Journal of Surgical Research* 1994, **57**(5)**:** 596-612.

316. Doi K, Matsuda T. Enhanced vascularization in a microporous polyurethane graft impregnated with basic fibroblast growth factor and heparin. *Journal of Biomedical Materials Research* 1997, **34**(3)**:** 361-370.

317. Rotmans JI, Heyligers JMM, Verhagen HJM, Velema E, Nagtegaal MM, de Kleijn DPV, *et al.* In vivo cell seeding with anti-CD34 antibodies successfully accelerates endothelialization but stimulates intimal hyperplasia in porcine arteriovenous expanded polytetrafluoroethylene grafts. *Circulation* 2005, **112**(1)**:** 12-18.

318. Tang ZY, Wang Y, Podsiadlo P, Kotov NA. Biomedical applications of layer-by-layer assembly: From biomimetics to tissue engineering. *Advanced Materials* 2006, **18**(24)**:** 3203-3224.

319. Thierry B, Winnik FM, Merhi Y, Silver J, Tabrizian M. Bioactive coatings of endovascular stents based on polyelectrolyte multilayers. *Biomacromolecules* 2003, **4**(6)**:** 1564-1571.

320. Thierry B, Winnik FM, Merhi Y, Tabrizian M. Nanocoatings onto arteries via layer-by-layer deposition: toward the in vivo repair of damaged blood vessels. *J Am Chem Soc* 2003, **125**(25)**:** 7494-7495.

321. Tan Q, Ji J, Zhao F, Fan DZ, Sun FY, Shen JC. Fabrication of thromboresistant multilayer thin film on plasma treated poly (vinyl chloride) surface. *J Mater Sci Mater Med* 2005, **16**(7)**:** 687-692.

322. Tan Q, Ji J, Barbosa MA, Fonseca C, Shen J. Constructing thromboresistant surface on biomedical stainless steel via layer-by-layer deposition anticoagulant. *Biomaterials* 2003, **24**(25)**:** 4699-4705.

323. Yu DG, Lin WC, Lin CH, Yeh YH, Yang MC. Construction of antithrombogenic polyelectrolyte multilayer on thermoplastic polyurethane via layer-by-layer self-assembly technique. *J Biomed Mater Res B Appl Biomater* 2007, **83**(1)**:** 105-113.

324. Xie HG, Zheng JN, Li XX, Liu XD, Zhu J, Wang F, *et al.* Effect of surface morphology and charge on the amount and conformation of fibrinogen adsorbed onto alginate/chitosan microcapsules. *Langmuir* 2010, **26**(8)**:** 5587-5594.

325. Wilson JT, Cui W, Chaikof EL. Layer-by-layer assembly of a conformal nanothin PEG coating for intraportal islet transplantation. *Nano Lett* 2008, **8**(7)**:** 1940-1948.

326. Ladam G, Schaaf P, Decher G, Voegel J, Cuisinier FJ. Protein adsorption onto auto-assembled polyelectrolyte films. *Biomol Eng* 2002, **19**(2-6)**:** 273-280.

327. Salloum DS, Schlenoff JB. Protein adsorption modalities on polyelectrolyte multilayers. *Biomacromolecules* 2004, **5**(3)**:** 1089-1096.

328. Chuang TW, Masters KS. Regulation of polyurethane hemocompatibility and endothelialization by tethered hyaluronic acid oligosaccharides. *Biomaterials* 2009, **30**(29)**:** 5341-5351.

329. Boontheekul T, Kong HJ, Mooney DJ. Controlling alginate gel degradation utilizing partial oxidation and bimodal molecular weight distribution. *Biomaterials* 2005, **26**(15)**:** 2455-2465.

330. Bouhadir KH, Lee KY, Alsberg E, Damm KL, Anderson KW, Mooney DJ. Degradation of partially oxidized alginate and its potential application for tissue engineering. *Biotechnol Prog* 2001, **17**(5)**:** 945-950.

331. Wu NQ, Pan CY, Zhang BJ, Rao YP, Yu D. Preparation and properties of a thermo-sensitive hydrogel based on oxidized sodium alginate. *Acta Polym Sin* 2007(6)**:** 497-502.

332. Lee KY, Bouhadir KH, Mooney DJ. Controlled degradation of hydrogels using multi-functional cross-linking molecules. *Biomaterials* 2004, **25**(13)**:** 2461-2466.

333. Alves NM, Picart C, Mano JF. Self Assembling and Crosslinking of Polyelectrolyte Multilayer Films of Chitosan and Alginate Studied by QCM and IR Spectroscopy. *Macromolecular Bioscience* 2009, **9**(8)**:** 776-785.

334. Huang CJ, Chang FC. Using Click Chemistry To Fabricate Ultrathin Thermoresponsive Microcapsules through Direct Covalent Layer-by-Layer Assembly. *Macromolecules* 2009, **42**(14)**:** 5155-5166.

335. Wilson JT, Krishnamurthy VR, Cui W, Qu Z, Chaikof EL. Noncovalent cell surface engineering with cationic graft copolymers. *J Am Chem Soc* 2009, **131**(51)**:** 18228-18229.

336. Krishnamurthy VR, Wilson JT, Cui W, Song X, Lasanajak Y, Cummings RD, *et al.* Chemoselective immobilization of peptides on abiotic and cell surfaces at controlled densities. *Langmuir* 2010, **26**(11)**:** 7675-7678.

337. Etienne O, Picart C, Taddei C, Haikel Y, Dimarcq JL, Schaaf P, *et al.* Multilayer polyelectrolyte films functionalized by insertion of defensin: a new approach to protection of implants from bacterial colonization. *Antimicrob Agents Chemother* 2004, **48**(10)**:** 3662-3669.

338. Etienne O, Gasnier C, Taddei C, Voegel JC, Aunis D, Schaaf P, *et al.* Antifungal coating by biofunctionalized polyelectrolyte multilayered films. *Biomaterials* 2005, **26**(33)**:** 6704-6712.

339. Zhang J, Chua LS, Lynn DM. Multilayered thin films that sustain the release of functional DNA under physiological conditions. *Langmuir* 2004, **20**(19)**:** 8015-8021.

340. Ikada Y. Surface modification of polymers for medical applications. *Biomaterials* 1994, **15**(10)**:** 725-736.

341. Nel AE, Madler L, Velegol D, Xia T, Hoek EMV, Somasundaran P, *et al.* Understanding biophysicochemical interactions at the nano-bio interface. *Nature materials* 2009, **8**(7)**:** 543-557.

342. Jordan SW, Chaikof EL. Novel thromboresistant materials. *J Vasc Surg* 2007, **45 Suppl A:** A104-115.

343. Gorbet MB, Sefton MV. Biomaterial-associated thrombosis: roles of coagulation factors, complement, platelets and leukocytes. *Biomaterials* 2004, **25**(26)**:** 5681-5703.

344. Furie B, Furie BC. Mechanisms of thrombus formation. *N Engl J Med* 2008, **359**(9)**:** 938-949.

345. Qu Z, Chaikof EL. Interface between hemostasis and adaptive immunity. *Curr Opin Immunol* 2010, **22**(5)**:** 634-642.

346. Anderson JM, Rodriguez A, Chang DT. Foreign body reaction to biomaterials. *Semin Immunol* 2008, **20**(2)**:** 86-100.

347. Gott VL, Whiffen JD, Dutton RC. Heparin Bonding on Colloidal Graphite Surfaces. *Science* 1963, **142:** 1297-1298.

348. de Agostini AI, Watkins SC, Slayter HS, Youssoufian H, Rosenberg RD. Localization of anticoagulantly active heparan sulfate proteoglycans in vascular endothelium: antithrombin binding on cultured endothelial cells and perfused rat aorta. *J Cell Biol* 1990, **111**(3)**:** 1293-1304.

349. Liaw PC, Becker DL, Stafford AR, Fredenburgh JC, Weitz JI. Molecular basis for the susceptibility of fibrin-bound thrombin to inactivation by heparin cofactor ii in the presence of dermatan sulfate but not heparin. *J Biol Chem* 2001, **276**(24)**:** 20959-20965.

350. Lahann J, Klee D, Pluester W, Hoecker H. Bioactive immobilization of r-hirudin on CVD-coated metallic implant devices. *Biomaterials* 2001, **22**(8)**:** 817-826.

351. Hashi CK, Derugin N, Janairo RR, Lee R, Schultz D, Lotz J, *et al.* Antithrombogenic modification of small-diameter microfibrous vascular grafts. *Arterioscler Thromb Vasc Biol* 2010, **30**(8)**:** 1621-1627.

352. Freitas SC, Barbosa MA, Martins MC. The effect of immobilization of thrombin inhibitors onto self-assembled monolayers on the adsorption and activity of thrombin. *Biomaterials* 2010, **31**(14)**:** 3772-3780.

353. Ito Y, Liu LS, Matsuo R, Imanishi Y. Synthesis and nonthrombogenicity of polymer membrane with surface-graft polymers carrying thrombin inhibitor. *J Biomed Mater Res* 1992, **26**(8)**:** 1065-1080.

354. Salvagnini C, Gharbi S, Boxus T, Marchand-Brynaert J. Synthesis and evaluation of a small library of graftable thrombin inhibitors derived from (L)-arginine. *Eur J Med Chem* 2007, **42**(1)**:** 37-53.

355. Gouzy MF, Sperling C, Salchert K, Pompe T, Streller U, Uhlmann P, *et al.* In vitro blood compatibility of polymeric biomaterials through covalent immobilization of an amidine derivative. *Biomaterials* 2004, **25**(17)**:** 3493-3501.

356. Esmon CT. Regulation of blood coagulation. *Biochim Biophys Acta* 2000, **1477**(1-2)**:** 349-360.

357. Goddard JM, Hotchkiss JH. Polymer surface modification for the attachment of bioactive compounds. *Prog Polym Sci* 2007, **32**(7)**:** 698-725.

358. Kishida A, Ueno Y, Maruyama I, Akashi M. Immobilization of human thrombomodulin onto biomaterials. Comparison of immobilization methods and evaluation of antithrombogenicity. *ASAIO J* 1994, **40**(3)**:** M840-845.

359. Wu B, Gerlitz B, Grinnell BW, Meyerhoff ME. Polymeric coatings that mimic the endothelium: combining nitric oxide release with surface-bound active thrombomodulin and heparin. *Biomaterials* 2007, **28**(28)**:** 4047-4055.

360. Yeh HY, Lin JC. Bioactivity and platelet adhesion study of a human thrombomodulin-immobilized nitinol surface. *J Biomater Sci Polym Ed* 2009, **20**(5-6)**:** 807-819.

361. Jonkheijm P, Weinrich D, Schroder H, Niemeyer CM, Waldmann H. Chemical Strategies for Generating Protein Biochips. *Angew Chem Int Edit* 2008, **47**(50)**:** 9618-9647.

362. Sletten EM, Bertozzi CR. Bioorthogonal chemistry: fishing for selectivity in a sea of functionality. *Angew Chem Int Edit* 2009, **48**(38)**:** 6974-6998.

363. Watzke A, Kohn M, Gutierrez-Rodriguez M, Wacker R, Schroder H, Breinbauer R, *et al.* Site-selective protein immobilization by Staudinger ligation. *Angew Chem Int Edit* 2006, **45**(9)**:** 1408-1412.

364. Kalia J, Abbott NL, Raines RT. General method for site-specific protein immobilization by Staudinger ligation. *Bioconjug Chem* 2007, **18**(4)**:** 1064-1069.

365. David R, Richter MP, Beck-Sickinger AG. Expressed protein ligation. Method and applications. *European Journal of Biochemistry* 2004, **271**(4)**:** 663-677.

366. Suzuki K, Kusumoto H, Deyashiki Y, Nishioka J, Maruyama I, Zushi M, *et al.* Structure and expression of human thrombomodulin, a thrombin receptor on endothelium acting as a cofactor for protein C activation. *EMBO J* 1987, **6**(7)**:** 1891-1897.

367. Soellner MB, Dickson KA, Nilsson BL, Raines RT. Site-specific protein immobilization by Staudinger ligation. *Journal of the American Chemical Society* 2003, **125**(39)**:** 11790-11791.

368. Parkinson JF, Nagashima M, Kuhn I, Leonard J, Morser J. Structure-function studies of the epidermal growth factor domains of human thrombomodulin. *Biochem Biophys Res Commun* 1992, **185**(2)**:** 567-576.

369. Kiick KL, Saxon E, Tirrell DA, Bertozzi CR. Incorporation of azides into recombinant proteins for chemoselective modification by the Staudinger ligation. *Proc Natl Acad Sci U S A* 2002, **99**(1)**:** 19-24.

370. Dargaville TR, George GA, Hill DJT, Whittaker AK. High energy radiation grafting of fluoropolymers. *Prog Polym Sci* 2003, **28**(9)**:** 1355-1376.

371. Klee D, Hocker H. *Polymers for biomedical applications: Improvement of the interface compatibility*, vol. 149. Springer-Verlag Berlin: Berlin, 1999.

372. Lamba NMK, Woodhouse KA, Cooper SL, Lelah MD. *Polyurethanes in biomedical applications*. CRC Press: Boca Raton, 1998.

373. Freijlarsson C, Wesslen B. Grafting of polyurethane surfaces with poly(ethylene glycol). *J Appl Polym Sci* 1993, **50**(2)**:** 345-352.

374. Saxon E, Armstrong JI, Bertozzi CR. A "traceless" Staudinger ligation for the chemoselective synthesis of amide bonds. *Org Lett* 2000, **2**(14)**:** 2141-2143.

375. Weisel JW, Nagaswami C, Young TA, Light DR. The shape of thrombomodulin and interactions with thrombin as determined by electron microscopy. *J Biol Chem* 1996, **271**(49)**:** 31485-31490.

376. Li JM, Singh MJ, Nelson PR, Hendricks GM, Itani M, Rohrer MJ, *et al.* Immobilization of human thrombomodulin to expanded polytetrafluoroethylene. *J Surg Res* 2002, **105**(2)**:** 200-208.

377. Cadroy Y, Maraganore JM, Hanson SR, Harker LA. Selective inhibition by a synthetic hirudin peptide of fibrin-dependent thrombosis in baboons. *Proc Natl Acad Sci U S A* 1991, **88**(4)**:** 1177-1181.

378. Hanson SR, Griffin JH, Harker LA, Kelly AB, Esmon CT, Gruber A. Antithrombotic effects of thrombin-induced activation of endogenous protein C in primates. *J Clin Invest* 1993, **92**(4)**:** 2003-2012.

379. Hanson SR, Sakariassen KS. Blood flow and antithrombotic drug effects. *Am Heart J* 1998, **135**(5, Supplement 1)**:** S132-S145.

380. Byrom MJ, Bannon PG, White GH, Ng MK. Animal models for the assessment of novel vascular conduits. *J Vasc Surg* 2010.

381. McNamara CA, Sarembock IJ, Gimple LW, Fenton JW, Coughlin SR, Owens GK. Thrombin Stimulates Proliferation of Cultured Rat Aortic Smooth-muscle Cells by a Proteolytically Activated Receptor. *Journal of Clinical Investigation* 1993, **91**(1)**:** 94-98.

382. Chen I, Ting AY. Site-specific labeling of proteins with small molecules in live cells. *Current Opinion in Biotechnology* 2005, **16**(1)**:** 35-40.

383. Hackenberger CPR, Schwarzer D. Chemoselective Ligation and Modification Strategies for Peptides and Proteins. *Angew Chem Int Edit* 2008, **47**(52)**:** 10030-10074.

384. Cazalis CS, Haller CA, Sease-Cargo L, Chaikof EL. C-terminal site-specific PEGylation of a truncated thrombomodulin mutant with retention of full bioactivity. *Bioconjug Chem* 2004, **15**(5)**:** 1005-1009.

385. Sperling C, Konig U, Hermel G, Werner C, Muller M, Simon F, *et al.* Immobilization of human thrombomodulin onto PTFE. *J Mater Sci Mater Med* 1997, **8**(12)**:** 789-791.

386. Allison DG. A review: taking the sterile out of sterility. *Journal of applied microbiology* 1999, **87**(6)**:** 789-793.

387. Lambert BJ, Mendelson TA, Craven MD. Radiation and ethylene oxide terminal sterilization experiences with drug eluting stent products. *AAPS PharmSciTech* 2011, **12**(4)**:** 1116-1126.

388. Mendes GC, Brandao TR, Silva CL. Ethylene oxide sterilization of medical devices: a review. *American journal of infection control* 2007, **35**(9)**:** 574-581.

389. Qu Z, Muthukrishnan S, Urlam MK, Haller CA, Jordan SW, Kumar VA, *et al.* A Biologically Active Surface Enzyme Assembly that Attenuates Thrombus Formation. *Adv Func Mat* 2011, **21**(24)**:** 4736-4743.

390. Ton-That H, Liu G, Mazmanian SK, Faull KF, Schneewind O. Purification and characterization of sortase, the transpeptidase that cleaves surface proteins of Staphylococcus aureus at the LPXTG motif. *Proc Natl Acad Sci U S A* 1999, **96**(22)**:** 12424-12429.

391. Huang X, Aulabaugh A, Ding W, Kapoor B, Alksne L, Tabei K, *et al.* Kinetic mechanism of Staphylococcus aureus sortase SrtA. *Biochemistry* 2003, **42**(38)**:** 11307-11315.

392. Frankel BA, Kruger RG, Robinson DE, Kelleher NL, McCafferty DG. Staphylococcus aureus sortase transpeptidase SrtA: insight into the kinetic mechanism and evidence for a reverse protonation catalytic mechanism. *Biochemistry* 2005, **44**(33)**:** 11188-11200.

393. Proft T. Sortase-mediated protein ligation: an emerging biotechnology tool for protein modification and immobilisation. *Biotechnology letters* 2010, **32**(1)**:** 1-10.

394. Chen I, Dorr BM, Liu DR. A general strategy for the evolution of bond-forming enzymes using yeast display. *Proc Natl Acad Sci U S A* 2011, **108**(28)**:** 11399-11404.

395. Fuentes-Prior P, Iwanaga Y, Huber R, Pagila R, Rumennik G, Seto M, *et al.* Structural basis for the anticoagulant activity of the thrombin-thrombomodulin complex. *Nature* 2000, **404**(6777)**:** 518-525.

396. Lin FL, Hoyt HM, van Halbeek H, Bergman RG, Bertozzi CR. Mechanistic investigation of the staudinger ligation. *J Am Chem Soc* 2005, **127**(8)**:** 2686-2695.

397. Sletten EM, Bertozzi CR. Bioorthogonal chemistry: fishing for selectivity in a sea of functionality. *Angewandte Chemie* 2009, **48**(38)**:** 6974-6998.

398. Jewett JC, Bertozzi CR. Cu-free click cycloaddition reactions in chemical biology. *Chemical Society reviews* 2010, **39**(4)**:** 1272-1279.

399. Ning X, Guo J, Wolfert MA, Boons GJ. Visualizing metabolically labeled glycoconjugates of living cells by copper-free and fast huisgen cycloadditions. *Angewandte Chemie* 2008, **47**(12)**:** 2253-2255.

400. Myers DD, Jr. Nonhuman primate models of thrombosis. *Thromb Res* 2012, **129 Suppl 2:** S65-69.

401. Furie B, Furie BC. Mechanisms of disease: Mechanisms of thrombus formation. *N Engl J Med* 2008, **359**(9)**:** 938-949.

402. Lin PH, Chen C, Bush RL, Yao Q, Lumsden AB, Hanson SR. Small-caliber heparin-coated ePTFE grafts reduce platelet deposition and neointimal hyperplasia in a baboon model. *J Vasc Surg* 2004, **39**(6)**:** 1322-1328.

403. de Mel A, Jell G, Stevens MM, Seifalian AM. Biofunctionalization of biomaterials for accelerated in situ endothelialization: a review. *Biomacromolecules* 2008, **9**(11)**:** 2969-2979.

404. Wood MJ, Helena Prieto J, Komives EA. Structural and functional consequences of methionine oxidation in thrombomodulin. *Biochimica et biophysica acta* 2005, **1703**(2)**:** 141-147.

405. Leung LLK, Myles T, Nishimura T, Song JJ, Robinson WH. Regulation of tissue inflammation by thrombi n-activatable carboxypeptidase B (or TAFI). *Mol Immunol* 2008, **45**(16)**:** 4080-4083.

406. Scatena M, Liaw L, Giachelli CM. Osteopontin: a multifunctional molecule regulating chronic inflammation and vascular disease. *Arterioscler Thromb Vasc Biol* 2007, **27**(11)**:** 2302-2309.

407. Seier AM, Renkl AC, Schulz G, Uebele T, Sindrilaru A, Iben S, *et al.* Antigen-Specific Induction of Osteopontin Contributes to the Chronification of Allergic Contact Dermatitis. *Am J Pathol* 2010, **176**(1)**:** 246-258.

408. Schulz G, Renkl AC, Seier A, Liaw L, Weiss JM. Regulated osteopontin expression by dendritic cells decisively affects their migratory capacity. *J Invest Dermatol* 2008, **128**(10)**:** 2541-2544.

409. Murugaiyan G, Mittal A, Weiner HL. Increased osteopontin expression in dendritic cells amplifies IL-17 production by CD4+ T cells in experimental autoimmune encephalomyelitis and in multiple sclerosis. *J Immunol* 2008, **181**(11)**:** 7480-7488.

410. Shinohara ML, Kim JH, Garcia VA, Cantor H. Engagement of the type I interferon receptor on dendritic cells inhibits T helper 17 cell development: Role of intracellular osteopontin. *Immunity* 2008, **29**(1)**:** 68-78.

411. Chen MY, Chen GJ, Nie H, Zhang X, Niu XY, Zang YCQ, *et al.* Regulatory effects of IFN-beta on production of osteopontin and IL-17 by CD4(+) T Cells in MS. *Eur J Immunol* 2009, **39**(9)**:** 2525-2536.

412. Hur EM, Youssef S, Haws ME, Zhang SY, Sobel RA, Steinman L. Osteopontin-induced relapse and progression of autoimmune brain disease through enhanced survival of activated T cells. *Nat Immunol* 2007, **8**(1)**:** 74-83.

413. Steinman L. A molecular trio in relapse and remission in multiple sclerosis. *Nat Rev Immunol* 2009, **9**(6)**:** 440-447.

414. Han MH, Hwang SI, Roy DB, Lundgren DH, Price JV, Ousman SS, *et al.* Proteomic analysis of active multiple sclerosis lesions reveals therapeutic targets. *Nature* 2008, **451**(7182)**:** 1076-1081.

415. Cao C, Gao Y, Li Y, Antalis TM, Castellino FJ, Zhang L. The efficacy of activated protein C in murine endotoxemia is dependent on integrin CD11b. *The Journal of clinical investigation* 2010.

416. Du XY, Zabel BA, Myles T, Allen SJ, Handel TM, Lee PP, *et al.* Regulation of chemerin bioactivity by plasma carboxypeptidase N, carboxypeptidase B (activated thrombin-activable fibrinolysis inhibitor), and platelets. *The Journal of biological chemistry* 2009, **284**(2)**:** 751-758.

417. Albanesi C, Scarponi C, Pallotta S, Daniele R, Bosisio D, Madonna S, *et al.* Chemerin expression marks early psoriatic skin lesions and correlates with plasmacytoid dendritic cell recruitment. *J Exp Med* 2009, **206**(1)**:** 249-258.

418. Parolini S, Santoro A, Marcenaro E, Luini W, Massardi L, Facchetti F, *et al.* The role of chemerin in the colocalization of NK and dendritic cell subsets into inflamed tissues. *Blood* 2007, **109**(9)**:** 3625-3632.

419. Graham KL, Zabel BA, Loghavi S, Zuniga LA, Ho PP, Sobel RA, *et al.* Chemokine-like receptor-1 expression by central nervous system-infiltrating leukocytes and involvement in a model of autoimmune demyelinating disease. *J Immunol* 2009, **183**(10)**:** 6717-6723.

420. Cash JL, Hart R, Russ A, Dixon JP, Colledge WH, Doran J, *et al.* Synthetic chemerin-derived peptides suppress inflammation through ChemR23. *J Exp Med* 2008, **205**(4)**:** 767-775.

421. Kulig P, Zabel BA, Dubin G, Allen SJ, Ohyama T, Potempa J, *et al.* Staphylococcus aureus-derived staphopain B, a potent cysteine protease activator of plasma chemerin. *J Immunol* 2007, **178**(6)**:** 3713-3720.

422. Parthasarathy R, Subramanian S, Boder ET. Sortase A as a novel molecular "stapler" for sequence-specific protein conjugation. *Bioconjug Chem* 2007, **18**(2)**:** 469-476.